Applications of Nonuniform Sampling in Wideband Multichannel Communication Systems

Bashar Ibrahim Ahmad

School of Electronics and Computer Science

Applications of Nonuniform Sampling in Wideband Multichannel Communication Systems

Bashar Ibrahim Ahmad

A thesis submitted in partial fulfilment of the requirements of the University of Westminster for the degree of Doctor of Philosophy

July 2011

"It can scarcely be denied that the supreme goal of all theory is to make the irreducible basic elements as simple and as few as possible without having to surrender the adequate representation of a single datum of experience."

Albert Einstein

Abstract

This research is an investigation into utilising randomised sampling in communication systems to ease the sampling rate requirements of digitally processing narrowband signals residing within a wide range of overseen frequencies. By harnessing the aliasing suppression capabilities of such sampling schemes, it is shown that certain processing tasks, namely spectrum sensing, can be performed at significantly low sampling rates compared to those demanded by uniform-sampling-based digital signal processing. The latter imposes sampling frequencies of at least twice the monitored bandwidth regardless of the spectral activity within. Aliasing can otherwise result in irresolvable processing problems, as the spectral support of the present signal is *a priori* unknown. Lower sampling rates exploit the processing module(s) resources (such as power) more efficiently and avoid the possible need for premium specialised high-cost DSP, especially if the handled bandwidth is considerably wide.

A number of randomised sampling schemes are examined and appropriate spectral analysis tools are used to furnish their salient features. The adopted periodogram-type estimators are tailored to each of the schemes and their statistical characteristics are assessed for stationary, and cyclostationary signals. Their ability to alleviate the bandwidth limitation of uniform sampling is demonstrated and the smeared-aliasing defect that accompanies randomised sampling is also quantified.

In employing the aforementioned analysis tools a novel wideband spectrum sensing approach is introduced. It permits the simultaneous sensing of a number of non-overlapping spectral subbands constituting a wide range of monitored frequencies. The operational sampling rates of the sensing procedure are not limited or dictated by the overseen bandwidth antithetical to uniform-sampling-based techniques. Prescriptive guidelines are developed to ensure that the proposed technique satisfies certain detection probabilities predefined by the user. These recommendations address the trade-off between the required sampling rate and the length of the signal observation window (sensing time) in a given scenario. Various aspects of the introduced multiband spectrum sensing approach are investigated and its applicability highlighted.

Table of Contents

List of Figures

List of Tables

Acknowledgments

First and foremost, I would like to express my deepest gratitude to my supervisor, Dr. Andrzej Tarczynski, for his valuable and much appreciated guidance throughout the course of my research studies. His deep insight, enthusiasm, constant encouragement, friendliness and above all his willingness to help in each and every occasion were a valuable assets and crucial factors for the completion of my studies. His impact on my views on science and education goes beyond sampling and signal processing recalling all the general discussions we had. In addition to his impressive academic skills, Dr. Tarczynski is a truly honourable person with outstanding human qualities who is always willing to support whoever seeks his help. I am sincerely grateful for his help and efforts in securing funding for my studies and giving me the opportunity to do research under his supervision. I thank Dr. Anush Yardim (my second supervisor) for her advice.

Also, I thank all the lecturers and staff members at the school of Electronics and Computer Science among whom I spent the last seven years since I joined as an undergraduate student. They always provided encouragement and valuable support when I needed it. Many thanks to other fellow research students (Mustafa, Damla, Adam, Saumya and all the others) for the good times we had together. I have been truly blessed to cross paths with all these wonderful people.

I would like to thank the examination committee: Prof. Richard C. S. Morling (University of Westminster, London), Dr. Pier Luigi Dragotti (Imperial College, London) and Prof. Izzet Kale (University of Westminster, London) for their efforts in assessing this thesis.

Last but not least, I thank my parents and family for their unconditional care, love, encouragement and unremitting support despite being physically far from them. My father's determination and commitment to offer me and my siblings the opportunity to seek further education have been a constant source of inspiration. Many thanks to my uncle Naji

El Hajj for his financial support during my undergraduate studies without whom I could not have attended university in the UK. I would like to thank my two lovely nieces (Lana and Loulin) and nephew (Mustafa), not that they would particularly understand given their tender ages, for being a source of motivation. Many thanks to my uncle Eyad, his wife Salwa and my cousin Youssef who are/were truly a second family of mine in the UK. Many thanks go to my partner Sarah for her continuous support, encouragement and understanding over the last few years.

Associated Publications

Journal Papers

1. **B. I. Ahmad** and A. Tarczynski, "A SARS Method for Reliable Spectrum Sensing in Multiband Communication Systems", accepted, *to appear in IEEE Transactions on Signal Processing,* issue 99, 2011.
2. **B. I. Ahmad** and A. Tarczynski, "Spectral Analysis of Stratified Sampling: A Means to Perform Efficient Multiband Spectrum Sensing", accepted, *to appear in IEEE Transactions on Wireless Communications*, 2011.
3. **B. I. Ahmad** and A. Tarczynski, "Wideband Spectrum Sensing Technique Based on Random Sampling on Grid: Achieving Lower Sampling Rates", *Digital Signal Processing,* Elsevier, vol. 90, pp. 466-476, December 2010.
4. **B. I. Ahmad** and A. Tarczynski, "Reliable Wideband Multichannel Spectrum Sensing Using Randomized Sampling Schemes", *Signal Processing,* Elsevier, vol. 90, pp. 2232-2242, February 2010.

Conference Papers

1. **B. I. Ahmad** and A. Tarczynski, "A SARS Multiband Spectrum Sensing Method in Wideband Communication Systems Using RSG", *Proceedings of the 19th European Signal Processing Conference (EUSIPCO'11*), Barcelona*,* Aug 2011, pp. 1219-1223.
2. **B. I. Ahmad** and A. Tarczynski, "A Spectrum Sensing Method Based on Stratified Sampling", *Proceedings of the IEEE International Symposium on Circuits and Systems (ISCAS '11),* Rio De Janeiro, Brazil, May 2011, pp. 402-405.

3. M. Al-Ani, A. Tarczynski and **B. I. Ahmad**, " A Novel Fourier Transform Estimation Method Using Random Sampling", *Proceedings of the 19th European Signal Processing Conference (EUSIPCO'11*), Barcelona*,* August 2011, pp. 859-863.

4. **B. I. Ahmad** and A. Tarczynski, "The Effect of Cyclostationarity on A DASP-Based Spectrum Sensing Method", *Proceedings of the 9th International Conference on Sampling Theory and Its Applications*, Singapore, May 2011.

5. M. Al-Ani, A. Tarczynski and **B. I. Ahmad**, "The Effect of Missing Samples on the Quality of the Spectral Analysis", *Proceedings of the 9th International Conference on Sampling Theory and Its Applications*, Singapore, May 2011.

6. **B. I. Ahmad**, A. Tarczynski and M. Al-Ani, "A DASP Multiband Spectrum Sensing Method Based on Total Random Sampling on Grid Without Replacement", Invited paper, *Proceedings of the 9th International Conference on Sampling Theory and Its Applications (SAMPTA '11)*, Singapore, May 2011.

7. **B. I. Ahmad** and A. Tarczynski, "A DASP Approach to Wideband Multichannel Spectrum Sensing", *Proceedings of the 18th European Signal Processing Conference (EUSIPCO '10)*, Aalborg, Denmark, August 2010, pp. 865-869.

8. **B. I. Ahmad** and A. Tarczynski, "Spectrum Sensing in Multichannel Communication Systems Using Randomized Sampling", *Proceedings of the 17th European Signal Processing Conference (EUSIPCO'09)*, Glasgow, Scotland, August 2009, pp.1690-1695.

9. **B. I. Ahmad** and A. Tarczynski, "Evaluation of Several Reconstruction Methods of Band-limited Signals", *Proceedings of the IEEE International Conference on Signals, Circuits and Systems,* November 2008, pp.1-5.

Author Declaration

I declare that all the material contained in this thesis is my own work; and that to the best of my knoweldge the thesis does not contain any material previously published or written by another person except where due reference is made in the text.

Bashar I. Ahmad

Glossary

Acronyms and Abbreviations

ADC	Analogue to Digital Converter
ARS	Additive Random Sampling
AWGN	Additive White Gaussian Noise
BP	Band Pass
BPF	Bandpass Filter
CDF	Cumulative Distribution Function
CR	Cognitive Radio
DASP	Digital Alias-free Signal Processing
DFT	Discrete Fourier Transform
DSA	Dynamic Spectrum Access
DSP	Digital Signal Processing
DTFT	Discrete Time Fourier Transform
ED	Energy Detector
FFT	Fast Fourier Transform
FT	Fourier Transform
IID	Independent Identically Distributed
LP	Low Pass
LS	Least Squares
QAM	Quadrature Amplitude Modulation
MSE	Mean Squared Error
MSS	Multiband Spectrum Sensing
NBI	Narrowband Interference

PDF	Probability Density Function
PSK	Phase Shift Keying
PSD	Power Spectral Density
RF	Radio Frequency
ROC	Receiver Operating Characteristics
RSG	Random Sampling on Grid
SARS	Spectral Analysis of Randomized Sampling
SDF	Sample-point Density Function
SDR	Spectrum Dynamic Range
SNR	Signal-to-Noise Ratio
SS	Stratified Sampling
SSEP	Stratified Sampling with Equal Partitions
SSF	Spectrum Support Function
TRS	Total Random Sampling
WKS	Whittaker-Kotelnikov-Shannon
WSCE	Wide Sense Cycloergodic
WSCS	Wide Sense Cyclostationary
WSE	Wide Sense Ergodic
WSN	Wireless Sensor Network
WSS	Wide Sense Stationary

Special Notations, Operators and Functions

Scalar variables are denoted by lower case letters and vectors are denoted by bold upper case letters:

x	Scalar variable x
$\mathbf{X}$	Vector quantity

Operators

$E[x]$	Statistical expectation of x
$E[x\|y]$	Condition statistical expectation of x given y
σ_X	Standard deviation of random variable X

$\lfloor x \rfloor$	The largest integer less than or equal to x
$\Pr\{X\}$	Probability of a random variable X
arccotan(x)	Inverse cotangent of (x)
$\lvert x \rvert$	Absolute value or magnitude of x
Z^*	Conjugate of complex variable Z
*	Convolution
x >> y	"x" quantity is significantly greater than "y"
x << y	"x" quantity is significantly smaller than "y"

Special functions

Q-function $$Q(x) = \frac{1}{\sqrt{2\pi}} \int_x^{+\infty} e^{-\tau^2/2} d\tau$$

Rectangular function $$\text{rect}(x) = \begin{cases} 1 & \text{for } |x| \le 0.5 \\ 0 & \text{elsewhere} \end{cases}$$

Sinc function $$\text{sinc}(x) = \sin(\pi x)/\pi x$$

Principal Symbols

B	Width of the overseen frequency range(s) in Hertz
B_A	Joint width of L_A concurrently active subbands in Hertz
B_C	Width of an individual monitored subband in Hertz
B_R	Single sided bandwidth of the reconstruction filter in Hertz
B_W	Bandwidth of the baseband shaping filter(s) in Hertz
d_n	Time interval between two consecutive samples in seconds
f_g	Underlying uniform grid rate in Hertz for the RSG scheme
$f_{\min}$	Initial frequency of the monitored frequency range(s)
f_{Lndu}	Landau sampling rate in Hertz
$f_{\max}$	Highest frequency present in the signal in Hertz
f_{Nyq}	Nyquist sampling rate in Hertz

f_S	Symbol rate or baud rate in Hertz
f_{US}	Uniform sampling rate in Hertz
f_C	Carrier frequency in Hertz
$H_R(f)$	Frequency response of the reconstruction filter
$h_R(t)$	Impulse response of the reconstruction filter
K	Number of estimate averages
L	Total number of monitored spectral subbands
L_A	Maximum number of simultaneously active subbands at any time
$\mathbb{L}_A$	Set of L_A concurrently active channels with highest power levels
M	Number of simultaneously active subbands
$m_{0,k}$	Estimator's expected value at frequency point f_k for $\mathscr{H}_{0,k}$
$m_{1,k}$	Estimator's expected value at frequency point f_k for $\mathscr{H}_{1,k}$
N	Number of processed samples
N_g	Number of underlying uniform grid points for RSG
$P_{f,k}$	Probability of false alarm for the k-th channel
$P_{d,k}$	Probability of detection for the k-th subband
P_N	Power/variance of the present AWGN
P_S	Signal power
$R_X(t,t+\tau)$	Autocorrelation function of $X(t)$
$\mathbb{S}_n$	The time subinterval for the n-th sample point
$\lvert\mathbb{S}_n\rvert$	Width of the n-th stratum
t	Time instant in seconds
t_n	Position of the n-th sample point in seconds
T_0	Width of the signal analysis window in seconds
T_{obs}	Length of the signal observation window in seconds
T_g	Period separating two successive grid points in seconds for RSG
T_{US}	Uniform sampling period in seconds

T_S	Symbol period in seconds
$x(t)$	Continuous-time signal
$x_m(t)$	Incoming signal over the m-th channel
$x_{T,m}(t)$	Transmitted signal over the m-th subband
$x^d(t)$	Sampled signal
$X_W(f)$	Continuous-time windowed Fourier transform of $X(t)$
$X_W^d(f)$	Windowed Fourier transform of a sampled $X(t)$
$X_e(\not{t}_r, f)$	Spectrum estimator of a randomly sampled signal
$\hat{X}_e(f)$	K averaged $X_e(\not{t}_r, f)$ from non-overlapping signal windows
$y(t_n)$	Collected noisy samples of the received signal
$\not{\mathcal{H}}_{0,k}$	Hypothesis that signifies the idle state of the k-th spectral subband
$\not{\mathcal{H}}_{1,k}$	Hypothesis that indicates the presence of an activity in the channel
$\Phi_X(f)$	Continuous-time power spectral density of signal
$\Phi_X^d(f)$	Powered spectral density of a uniformly sampled $X(t)$
§	Section, subsection or sub-subsection in the thesis
$\delta(t)$	Dirac delta
α	Average sampling rate in Hertz
μ	Energy of the used windowing function
$\sigma_{0,k}$	Estimator's standard deviation at frequency point f_k for $\not{\mathcal{H}}_{0,k}$
$\sigma_{1,k}$	Estimator's standard deviation at frequency point f_k for $\not{\mathcal{H}}_{1,k}$
μ_d	Energy of the discretised windowing function
β_n	Instantaneous sampling rate at t_n in Hertz
$\not{\mathcal{B}}$	Monitored frequency range(s) starting at f_{min} and is of width B
$\varepsilon_T(t)$	Truncation error of the reconstruction formulas
$\not{\mathcal{F}}\{x(t_1,t_2,\ldots t_N),t_n\}$	Fourier Transform of with respect to t_n, $\int_{-\infty}^{+\infty} x(t_1,t_2,\ldots t_N)e^{-j2\pi f t_n}dt_n$
$\not{\mathcal{N}}(m,\sigma^2)$	Normal distribution of mean m and variance σ^2

$p_n(t)$	Probability density function of the n-th sample point
$p_{SDF}(t)$	Sample-point density function
$\mathcal{P}_X(f)$	Continuous-time periodogram of the random process $X(t)$
t_r	Initial time of the r-th signal analysis window in seconds
$\mathcal{S}(t)$	Sampling signal
$\mathcal{T}_r$	r-th signal analysis window $\mathcal{T}_r = [t_r, t_r + T_0]$
Δ_k	Maximum allowed probability of false alarm for the k-th subband
ℓ_k	Minimum sought probability of detection for the k-th channel
γ_k	Hypothesis testing threshold for the k-th subband
e	One-sided Chebychev's inequality parameter, positive integer

Chapter 1

Introduction

In today's information driven societies, wireless communication applications are viewed as indispensible essentials. The overwhelming demand on wireless data transfer services has led to new communication paradigms emerging on a regular basis, creating new formidable challenges to systems designers. It is envisioned that Digital Signal Processing (DSP) will be a key element/player in accommodating the additional flexibility and features requested by the communication systems/services of the future. However, uniform sampling limitations can hamper, in some cases, the DSP opportunities of taking an earlier and more principal role in the information treatment chain. This is particularly severe when handling high frequency wideband signals at the data receiver end. Consequently, alternative sampling and processing techniques and methodologies are sought.

This research is an investigation into the utilisation of nonuniform sampling in multichannel communication systems. It is shown that such a sampling approach has the ability to resolve a number of persistent digital signal processing problems in certain scenarios. This chapter highlights the impetus of this work, defines the problem tackled and outlines the adopted methodology. It also states the focus and scope of this research along with its original contributions.

1.1 Motivation

Traditional/classical DSP uses uniformly distributed sampling grids to collect data of the processed signals. Uniform sampling brings undeniable numerous benefits to the users, with simplicity of the signal processing algorithms being among the most popular ones. On the other hand, the use of uniform sampling is always accompanied by burdensome

aliasing effects that prevent the user from accomplishing virtually any DSP task if the processed frequency range is wider than half of the sampling rate. Even if the bandwidth of a multiband signal is less than the abovementioned limit, undesirable aliasing may still be present, obstructing the user from handling a given DSP problem.

Some signal processing tasks require dealing with fairly narrowband signals placed somewhere within overseen frequency ranges at *a priori* unknown positions. Examples of such scenarios can be found in instrumentation (e.g. when narrowband or multiband signals with unknown centre frequencies are acquired and analysed, as in spectrum analysers) and in communication systems (e.g. when many transmitters that use various carrier frequencies communicate with a single receiver). Digitally processing such signals is not an issue when the ranges are relatively narrow as sufficiently high uniform sampling rates can be applied. It becomes more problematic if the processed bandwidth is considerably wide imposing uniform sampling rates possibly higher than the currently available Analogue to Digital Converters (ADCs) can cope with. Such signal processing tasks are still often tackled with analogue techniques or, if digital technology is to be deployed, the data acquisition hardware has to resort to specialised solutions. This will increase the implementation cost of the system. Ultimately, with the ever-expanding trend of higher rates and more reliable as well as complex data services, i.e. wider bandwidth requirements, the DSP solutions have two routes to take: 1) faster more complex computationally capable hardware and 2) cleverer, more tactful sampling and processing strategies (whenever applicable). Here the second option is pursued and its aspects as well as possible benefits are explored.

Nonuniform randomised sampling and processing, i.e. randomised signal processing, is an alternative approach that offers economically effective solutions to many digital signal processing problems in wide frequency range(s) [1-7]. It relies on combining carefully designed sampling schemes and appropriate signal processing algorithms to mitigate the effects of aliasing. Nonuniform sampling is introduced intentionally to provide additional flexibility and opportunities. It allows sampling narrowband signal(s) residing within wide frequency ranges at significantly low rates, easing the sampling rate requirements of the digital signal processing block(s). The usage of lower sampling rates (well below the uniform sampling ones) means lower quantity of collected data. This can lead to considerable savings in the processing power, which implies more power efficient systems.

New emerging communication paradigms and applications have motivated our interest in the promising aspects and solutions of randomised signal processing. Below, two potential communication systems that call for the developed algorithms are highlighted. At this point, we emphasise that the processing techniques provided in this research are not tailored or do not target a particular application/system with its specific requirements. They are generic and can be adapted to a given scenario whenever their benefits are apparent and can be realised.

Cognitive Radio (CR)

The current spectrum allocation policies adopted by governments give exclusive rights to legacy users and services to operate over predetermined spectrum bands. Any attempt by an unlicensed service to use subscribed spectrum band(s) is not permitted and is regarded as a violation of the regulations. Since wireless application and services have been growing rapidly during the last two decades, spectrum limited resources are facing huge demands and becoming congested. Clearly, the current regulatory framework does not offer any solutions or flexibility to the growing spectrum scarcity problem. Recent surveys carried out by the Federal Communications Commission (FCC) in the United States, and similar agencies in other countries, indicated that the spectrum is hugely underutilised in a given time duration and/or in a certain geographical region [8-10]. For instance, a field spectrum measurement taken in New York City has shown that the maximum spectrum occupancy is only 13.1% from 30 MHz to 3 GHz [11]. This called for new spectrum management regulations to resolve the conflict between spectrum scarcity and its underutilisation.

The emerging Cognitive Radio (CR) technology aims at alleviating the spectrum scarcity predicament [10-13] and is a key part of the envisioned Dynamic Spectrum Access (DSA) paradigm. It ushers in a new form of radio that is aware of its environment and can opportunistically use the temporary vacant spectral bands (referred to as spectral holes) without causing harmful interference to an inactive primary/licensed user. Figure 1.1 exhibits the concept of spectral holes and the possibility of exploiting unutilised spectrum regions in a given time frame in a certain geographical region. Evidently, spectrum sensing has critical functionality in CR networks that allows unveiling the spectral holes for opportunistic access and precedes any action taken by the CR(s). This triggered an enormous interest in spectrum sensing techniques and their various aspects, e.g. [10, 14-

20]. Some of these methods are addressed in Chapter 4. Cognitive radios have to continuously scan the spectrum to identify any spectrum opportunities that may arise or the presence or reappearance of the primary user. In the latter case, it must switch its transmission to another vacant band to avoid clashing or interfering with the licensed user. Therefore, a reliable spectrum sensing routine of an affordable complexity is essential for CR technology.

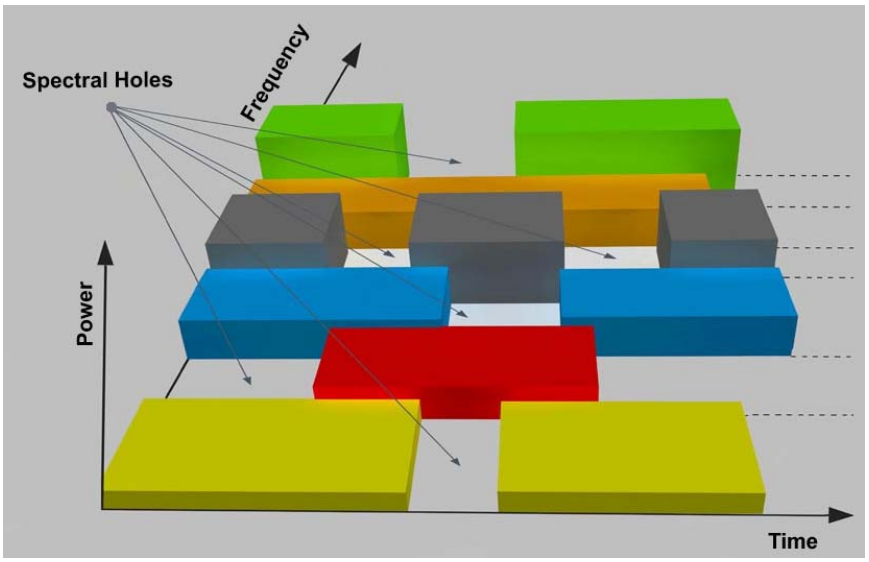

Figure 1.1: A graphical illustration of the activity of certain frequency bands over time and frequency. Some of these bands are inactive within a certain geographical region and at a certain time resulting in an underutilised spectrum.

The cognitive radio of the future will be capable of scanning a wide range of frequencies, i.e. in the order of several GHz [15, 17, 21-24]. Spectrum sensing regime over such wide bandwidths faces considerable technical challenges, especially in terms of developing reliable signal processing algorithms. A classical solution is to employ a bank of narrowband bandpass filters at the RF frontend to search one narrow frequency band at a time. Any of the classical detection methods can be used to determine the status of the subband in question, e.g. energy detector [25]. This approach requests an unfavourably large number of RF components whose parameters should be fine-tuned and preset. Alternatively, in order to simultaneously search multiple subbands, we need a wideband circuit utilising a single wideband RF front-end followed by premium high-speed acquisition device(s) and DSP. Such solutions typically involve spectrum estimation of the wideband incoming signal [15-20]. A major challenge lies in the prohibitively large sampling rates imposed by conventional spectral estimation methods that operate at or

above the Nyquist rate. Ultimately, the bottleneck for deploying DSP for such tasks is the required wideband ADC running at excessively high sampling rates, e.g. several giga-samples per second [19, 23], accompanied with sufficiently fast DSP to accommodate the high rate of the data streaming.

On the other hand, the use of considerably low rate intentional nonuniform sampling with suitable spectral analysis tools permits the simultaneous scanning of the spectral subbands that form the overseen wide frequency range(s). This noticeably relaxes the stringent sampling requirements on the data acquisition module(s) and the subsequent signal processing involved. The randomised signal processing methodology is behind such benefits, as demonstrated in the rest of this thesis.

Wireless Sensor Networks (WSNs)

A WSN is a wireless network consisting of spatially distributed devices (sensors) cooperatively monitoring physical or environmental conditions such as vehicle tracking (e.g. [26]) , energy evaluation (e.g. [27]), water quality measurements (e.g. [28]) and many others. These networks are normally comprised of large numbers of sensor nodes. Each node has wireless communication capability and some level of intelligence for signal processing and data networking. In many WSN applications, the network can be placed in a remote area where direct access to the mains is not feasible. The nodes are battery powered and re-charging might not be practical. Among various sensor networks parameters, power consumption is believed to be among the most critical ones. The lifetime of any node in the network is determined by the battery life, thereby requiring the minimisation of power expenditure. Thus there are challenges to be faced in designing energy efficient DSP and communication algorithms [26].

Sensor networks have been under intensive research where various proprietary and standards-based networks have emerged. Several protocols, network topologies and data aggregation methods are used depending on the application [29, 30]. It is agreed upon that communication between the network components is the highest power consumer. Therefore, performing data aggregation locally or within an intermediate node would save power by reducing the number of distant transmissions. Let’s consider a particular setup and applications of WSNs. The network is arranged hierarchically such that groups of sensor nodes are controlled by distinct components which have more computational and

communication resources as well as decision-making capabilities. These components, called the control/master nodes/hubs, communicate to the base station, perform data aggregation and possibly receive data. They act as gateways between sensor nodes and the main base station. The sensor nodes only communicate with the master node in one direction. Figure 1.2 demonstrates the sensor network layout discussed.

Each of the sensor nodes can communicate to its corresponding control node over a certain dedicated bandwidth which is typically narrow depending on the kind of data exchange handled, e.g. few MHz as in [27] and [28]. As a result the bandwidth monitored by the control node is made up of a number of non-overlapping subbands that are each allocated to a given sensor. The master node has to sweep through the spectrum, identify who is communicating and process the data. If uniform sampling is used, the required sampling rates can be significantly high, especially if the number of nodes is very large. This entails processing large quantities of data demanding more of the scarce power resource.

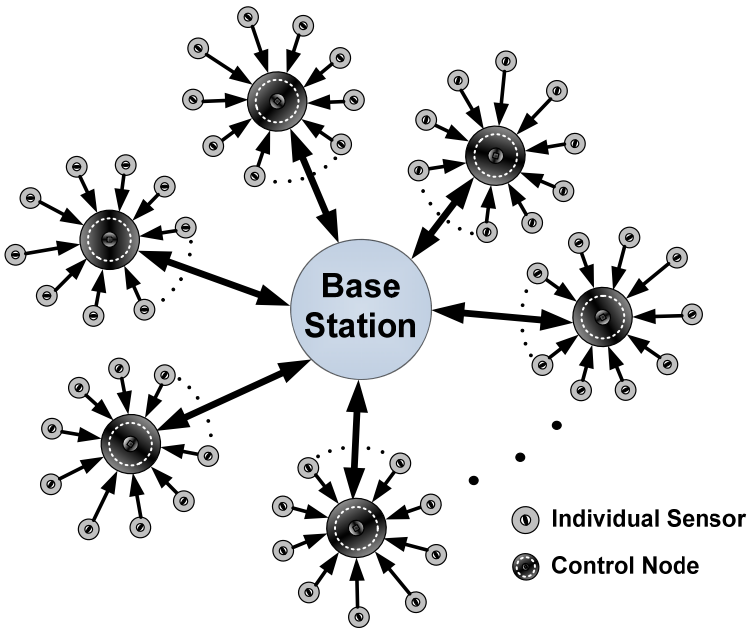

Figure 1.2: The layout of the discussed WSN (star topology). It comprises the base station and the control nodes which collect data from a number of sensing nodes.

In applications with occasional transmissions, e.g. disaster management or fire detection, the number of nodes reporting concurrently to the control node or the number of control nodes communicating with the base station is expected to be low. Accordingly, the spectrum utilisation can be assumed to be low. Nonuniform sampling can exploit such features, unlike uniform sampling, and use low sampling rates to effectively detect active

subband(s) and possibly recover the transmitted message(s). As a result, WSNs is a potential application area that can benefit from the algorithms devised in this research.

In summary, nonuniform randomised sampling demands lower sampling rates compared to uniform sampling when employed in wideband multichannel communication systems that are characterised by low spectrum occupancy. It is noted that the latter premise becomes critical only when signal reconstruction is sought as illustrated below. It is strongly believed that nonuniform sampling can bring new opportunities and numerous benefits to wideband communication systems in general and to the applications discussed above in particular. Although the developed algorithms here do not target a particular application, the provided solutions can encourage designers and researchers to consider applications and systems that heretofore were technically or economically unviable due to the classical DSP limitations.

1.2 Problem Formulation, Adopted Methodology, Focus and Aims

The wideband multichannel communication systems investigated here comprise L transmitters communicating with a single receiver over non-overlapping spectral subbands. These systems support heterogeneous wireless devices that may adopt different wireless technologies for their transmissions. The system subbands (alternatively called channels) are assumed to be contiguous and of equal width, i.e. B_C. The central frequencies of all channels are known, however no previous information is available on their activities or the characteristics of the incoming transmissions. Hence the range of frequencies monitored by the receiver is $\mathcal{B} = \left[f_{min}, f_{min} + B \right]$ where f_{min} is the initial frequency point in the range of interest, $B = LB_C$ is the total overseen bandwidth and $f_{\max} = f_{\min} + B$ is the highest frequency possibly present in the signal. The maximum number of simultaneously active subbands at any time is L_A, i.e. the joint width of the active channels never exceeds $B_A = L_A B_C$, and B_A / B is the maximum expected spectrum occupancy. The received multiband signal is: $x(t) = \sum_{m=1}^{M} x_m(t)$ where $M \le L_A$ is the unknown number of the concurrently active channels and $x_m(t)$ is the incoming transmission corresponding to the m-th active subband. Figure 1.3 demonstrates an example of the described system.

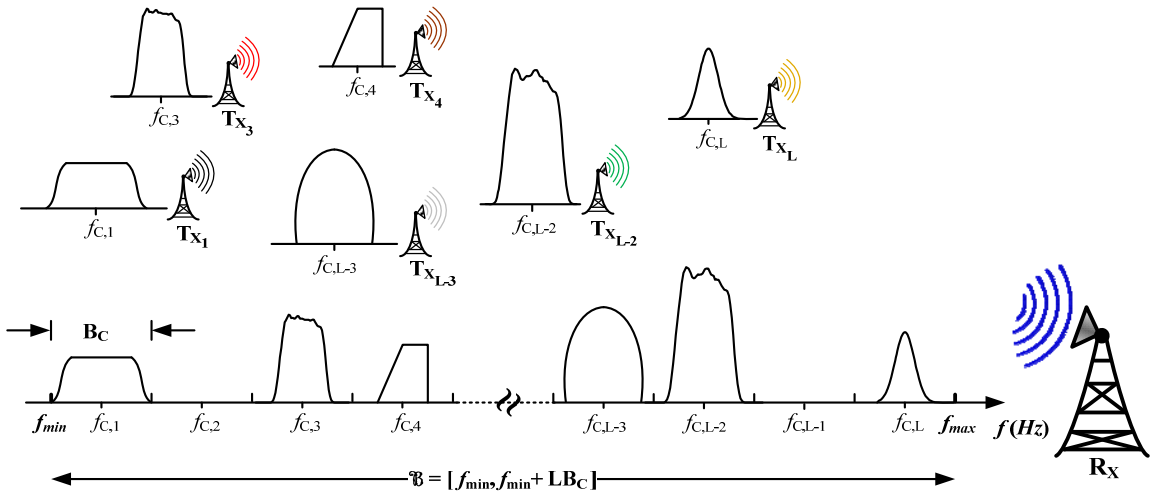

Figure 1.3: A number of transmitters operating over different carrier frequencies. The receiver deals with a number of concurrently active subbands constituting the multiband incoming signal. Six ($M = 6$) out of L monitored channels are simultaneously active.

Since the spectral support of the present multiband signal is *a priori* unknown, the use of classical DSP at the receiver would impose uniform sampling rates higher than Nyquist, i.e. $2f_{\max}$, or at least $2B$. The latter can be achieved if bandpass sampling is employed for the entire frequency range or the signal is down-converted to baseband before sampling [31]. If the examined bandwidth is wide (e.g. hundreds of MHz as in CRs) the sampling rate constraint demands specialised data acquisition hardware and high speed DSP. Traditionally to avoid such onerous requirements, the signal occupying a targeted subband is demodulated by multiplying the incoming signal by the channel's carrier frequency. This positions the targeted subband near/at the origin. Subsequently, the signal is filtered and sampled at rates proportion to the subband's bandwidth, e.g. $2B_C$ and not $2f_{\max}$ where $B_C << f_{\max}$. In the considered systems the positions of the active subbands are unknown and as a result the demodulation method cannot be efficiently utilised.

Capitalising on the potential of the randomised sampling to suppress the harmful aliasing phenomenon, we show here that we can survey the activity of the system subbands whilst operating at notably low-rate nonuniform sampling (well below the minimum permissible uniform sampling counterpart). This leads to exploiting the receiver (sensing device) resources such as power more effectively and avoiding the possible need for high-cost specialised fast hardware. After determining the status of all the channels (i.e. spectrum sensing) further processing can be requested, such as signal reconstruction to recover the

transmitted message (either fully or some of its characteristics). According to Landau [32], the minimum theoretical rate that allows the full reconstruction of the sampled signal is $2B_A$. Maintaining the sampling rate above, or arbitrarily close to Landau (if needed), does not undermine the benefits of the developed algorithms for low spectrum occupancy applications as $B_A << B$, e.g. in cognitive radio and some WSN applications. However, for uniform sampling, the sampling rate is directly proportional to $B >> B_A$ albeit B_A/B.

In this thesis, we focus on designing efficient reliable spectrum sensing algorithms illustrating that the operational sampling rates can be arbitrarily low for certain randomised sampling schemes. This stems from the fact that in some cases reconstructing the sampled signal might not be sought. For instance, in cognitive radio a dual-radio architecture is proposed [17, 33-35] where one radio chain is dedicated to spectrum monitoring and the other handles the data transmission/reception. The developed novel randomised-sampling-based spectrum sensing approach relies on the spectral analysis of the incoming signal. This permits the simultaneous sensing of all the channels in lieu of inspecting one subband at a time. Sensing methods that are based on nonparametric spectral analysis are recognised as low complexity efficient candidates for Multiband Spectrum Sensing (MSS) [13, 15-19]. This approach is adopted here, noting that overseeing the activity of the system subbands (spectrum sensing) does not require determining the detailed spectral shape(s) within the monitored wide bandwidth. Thus conventional spectral analysis techniques, whose aim is to estimate the signal's exact spectrum, can entail unnecessary complications. Accordingly, we utilise periodogram-type analysis tools to estimate a frequency representation of the signal. An exact estimation of the signal's spectrum, e.g. Power Spectral Density (PSD), is not the target and any frequency representation (e.g. biased windowed PSD) that facilitates detection is sufficient. We adopt estimators for a number of investigated randomised sampling schemes and study their behaviours as well as adequacy for the tackled problem, i.e. MSS and not PSD estimation. The aim of this research is not only to demonstrate the capability of the introduced randomised-sampling-based multiband spectrum sensing, but also to provide the user with prescriptive practical recommendations for using the developed approach. This includes answering: how fast to sample or how long to observe the incoming signal for in a given scenario. It is noted that the simplicity and low computational complexity are among the main merits of the proposed sensing method compared to other MSS techniques. Given the scope of this

study, some adverse system conditions related to communication systems, for example interference, channel modelling and propagation loss, are not analysed in this thesis.

1.3 Summary of Contributions

The original contributions of this research can be summarised by:

Chapter 3

- Developing the analytical expressions for the statistical characteristics of adopted periodogram-type estimators for a number of randomised sampling schemes and wide sense stationary signals. The examined schemes are Total Random Sampling (TRS), Random Sampling on Grid (RSG) and Stratified Sampling with Equal Partitions (SSEP). Those formulas capture the capability of randomised sampling to suppress the aliasing phenomenon within a wide range of frequencies. They also determine the accuracy of the estimation process where the adopted spectral analysis tools are unbiased estimators of detectable frequency representations of the incoming signal albeit the used sampling rates, i.e. suitable means for the pursued low rate spectrum sensing routine.
- Analysing quantitatively the levels of smeared-aliasing* for the studied randomised sampling schemes. This includes measuring the variations of the smeared-aliasing level of SSEP in the vicinity of the strong signal spectral components.
- Providing analytical expressions for the spectrum dynamic range for each of the TRS, RSG and SSEP schemes. General guidelines on the number of required sample points are presented to guarantee particular dynamic range values.

Chapter 4

- Analysing the impact of processing cyclostationary communication signals on the performances of the periodogram-type estimators:

* When a bandlimited signal is periodically sampled, the spectrum of the discrete-time data consists of scaled replicas of the spectrum of the continuous-time signal appearing at multiples of the sampling rate. With nonuniform sampling, the spectrum of the sampled data includes that of the underlying continuous-time signal plus a wideband bias-like component (see Figure 2.4). The latter represents the smeared-aliasing phenomenon whose level is dependent on the characteristics of the sampling scheme.

- The adopted estimators continue to be suitable tools for the spectrum sensing task. Their expected values contain detectable spectral components related to the present transmissions and are independent of the position of the time analysis window at certain frequency points.
- The estimation accuracy can notably deteriorate at selected frequencies that are related to the nature and parameters of the modulation scheme employed at the transmitter, e.g. the carrier frequency and the symbol rate.

Chapter 5

- The development of a novel randomised-sampling-based multiband spectrum sensing technique. It permits using significantly low sampling rates compared to the uniform sampling approaches utilising the aforementioned adopted spectral analysis tools; the rates can be arbitrarily low for some randomised sampling schemes.
- Demonstrating that the varying smeared-aliasing feature of stratified sampling imposes a limit on the minimum operational randomised sampling rate for the multiband spectrum sensing pursuit.
- Reliability guidelines are derived to ensure that the proposed spectrum sensing technique meets the sought detection probabilities in a given scenario. They depict the trade-offs between the needed sampling rate and the length of the signal observation window for each of the TRS, RSG and SSEP schemes.

1.4 Notations

This section lists the definitions of a selected number of crucial notions repetitively used in the following chapters.

Fourier Transform and Windowed Fourier Transform

Fourier Transform (FT) of a continuous-time waveform $x(t)$ is defined by:

$$X(f) = \int_{-\infty}^{+\infty} x(t) e^{-j2\pi ft} dt$$

and subsequently:

$$x(t) = \int_{-\infty}^{+\infty} X(f) e^{j2\pi ft} df \, .$$

In case the waveform is analysed within a finite time window $\mathcal{T}_r = [\not{t}_r, \not{t}_r + T_0]$ starting at the time instant $\not{t}_r$ and is of width T_0, we have:

$$X_W(\not{t}_r, f) = \int_{\not{t}_r}^{\not{t}_r + T_0} x(t) w(t) e^{-j2\pi ft} dt = \int_{-\infty}^{+\infty} x(t) w(t) e^{-j2\pi ft} dt$$

where $w(t)$ is the windowing function of width T_0 and aligned with $\mathcal{T}_r$.

A Bandlimited Signal and its Bandwidth

A signal is bandlimited to $f_{\max}$ if its FT or PSD diminishes for $|f| > f_{\max}$. Consequently, it has a bandwidth of $2f_{\max}$. This is well understood for Low Pass (LP) signals whilst the confusion normally arises for Bandpass (BP) and Multiband (MB) signals. In this case, we adopt the engineering notion where the single-sided bandwidth B_{eff} of a BP/MB signal is the sum of the magnitude of the set of positive frequency range(s) where the signal has nonzero spectral components (see Figure 1.4). For the LP case $B_{eff} = f_{\max}$.

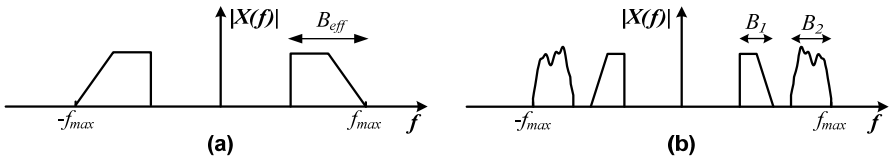

Figure 1.4: Spectrum. (a) BP signal and (b) MB signal $B_{eff} = B_1 + B_2$.

Spectral Support Function

The spectral support is a concept that exhibits the position(s)/location(s) of the processed signal spectral activity. It is a binary function that takes two values: $SSF(f) = 1$ if the spectrum of the signal is nonzero at f and $SSF(f) = 0$ otherwise. It describes the presence or absence of the signal's spectral components at certain frequencies without giving any indication of the spectrum characteristics, e.g. magnitude or shape.

Autocorrelation Function and Power Spectral Density

The autocorrelation function of a real continuous-time stochastic process is defined by: $R_X(t, t+\tau) = E[x(t)x(t+\tau)]$ where τ is the time-shift. Power Spectral Density (PSD) is

defined as the FT of $R_X(t,t+\tau)$ with respect to τ. For wide sense stationary processes, both the autocorrelation function and PSD are independent of time. Similar terminology applies to discrete-time processes. All the PSDs in the sequel are double sided.

1.5 Thesis Outline

After highlighting the scope, objectives and contributions of this research in the current introductory chapter, Chapter 2 provides a brief overview of the sampling theory in its uniform and nonuniform branches. Selected topics that are believed to be relevant to the theme of this research are discussed, including randomised sampling and its processing. This chapter lays the foundation for the work that follows in the thesis.

In Chapter 3, we state the aim behind conducting spectral estimation and discuss the related work in the literature. Spectrum estimators for a number of studied randomised sampling schemes are then introduced and their characteristics are examined for wide sense stationary signals. The detailed derivations of the developed analytical expressions are included in Appendix A, B and C. Whereas in Chapter 4, the impact of processing cyclostationary signals on the behaviour of the adopted estimators is evaluated and the detailed calculations are presented in Appendix D.

The spectrum sensing problem is formulated in Chapter 5 discussing existing sensing methods. A novel multiband spectrum sensing approach is proposed utilising the periodogram-type estimators analysed in Chapters 3 and 4. Reliability guidelines are developed to ensure that the proposed technique for each of TRS, RSG and SSEP schemes meet the detection probabilities specified by the user.

Finally, the overall contributions of this research are summarised in Chapter 6 addressing the potential future work related to the results presented in this thesis.

Acronyms, abbreviations, notations, special functions or operators and principle symbols are given in the preface section of this document.

Chapter 2

Sampling of Bandlimited Signals

Although collecting the signal samples (i.e. the first step towards processing the signal digitally) in a uniform periodic manner is the widely utilised and known form of sampling, it is not the only possible technique. In some scenarios, e.g. in the studied multichannel communication systems, resorting to intentional nonuniform random sampling can provide additional flexibility and opportunities that are unavailable with uniform sampling due to the latter's aliasing limitation. Before engaging in the analysis and deployment of randomised sampling, we give a general overview of the sampling theory in its uniform and nonuniform branches. The aim is not to give a review of the entire field since it has a vast history and various comprehensive reviews already exist for the sampling theory in general, e.g. [36-44], as well as for nonuniform sampling in particular, e.g. [1, 2, 6, 45-47], containing extensive bibliographies on related topics. We present the material that is believed to be most relevant to this research and serves as preliminaries for the analysis as well as discussions in the following chapters.

2.1 Sampling Process and Spectrum of Sampled Data

Any sampling process, which converts a continuous-time signal $x(t)$ into its discrete-time representation $x^d(t)$, is a multiplication operation described by:

$$x^d(t) = x(t)\mathscr{S}(t). \tag{2.1}$$

The sampling signal $\mathscr{S}(t)$ comprises an infinite series of Dirac delta pulses and is given by (see Figure 2.1):

$$\mathcal{S}(t) = \sum_{n=-\infty}^{+\infty} \delta(t - t_n) \tag{2.2}$$

where t_n's are the sample points along the time axis. For uniform sampling, the sampling instants are equidistant and separated by the sampling period T_{US}, i.e. $t_n = nT_{US}$. The multiplication in (2.1) translates into a convolution operation in the frequency domain and the spectrum of the sampled waveform is:

$$X^d(f) = X(f) * \mathcal{F}\{\mathcal{S}(t), t\} \tag{2.3}$$

where $X(f) = \mathcal{F}\{x(t), t\} = \int_{-\infty}^{+\infty} x(t) e^{-j2\pi ft} dt$, $\mathcal{F}\{.,t\}$ is the Fourier Transform (FT) with respect to t and $*$ denotes the convolution operation. In (2.3) signals $x(t)$ and $\mathcal{S}(t)$ are assumed to be of a deterministic nature and their FTs exist.

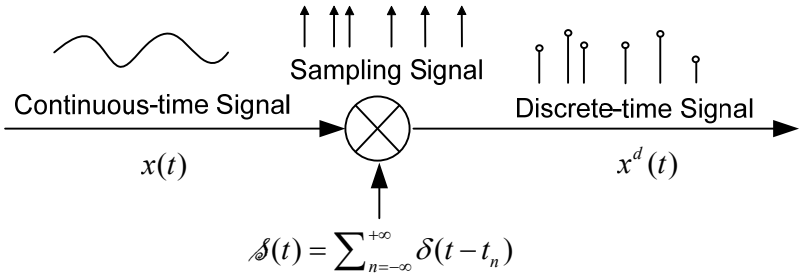

Figure 2.1: An ideal sampler.

Many communication signals can be modelled as random stationary or cyclostationary processes. The FT of one or more of their realisations or waveforms is random. Additionally, stationary and cyclostationary signals are not absolutely integrable, i.e. $\int_{-\infty}^{+\infty} |x(t)| dt \not< \infty$, and hence do not have a direct FT frequency representation [48]. Similar arguments apply to a randomised sampling signal which is a stochastic process. Power Spectral Density (PSD) is an alternative frequency representation that is normally utilised to describe the spectral content of random signals. From §1.4, the PSD is: $\Phi_X(t, f) = \mathcal{F}\{R_X(t, t+\tau), \tau\}$ where $R_X(t, t+\tau) = E[x(t)x(t+\tau)]$ is the signal's autocorrelation function. For Wide Sense Stationary (WSS) processes, $R_X(t, t+\tau) = R_X(\tau)$ and $\Phi_X(f) = \int_{-\infty}^{+\infty} R_X(\tau) e^{-j2\pi f\tau} d\tau$. As a result, the spectrum of the sampled signal is given by:

$$\Phi^d(f) = \Phi_X(f) * \Phi_S(f) \tag{2.4}$$

where $\Phi_S(f)$ is the PSD of the sampling process presumed to be WSS.

Typically, the ensemble average, i.e. $E[.]$, is obtained from the time averages by assuming that the processed wide sense stationary or Wide Sense Cyclostationary (WSCS) signals are Wide Sense Ergodic (WSE) and Wide Sense Cycloergodic (WSCE) respectively [3, 48-50]. This stems from the fact that any practical system has access to a finite number of the signal's realisations. For instance, Peebles [48, p. 189] states that:

"Ergodicity is a very restrictive form of stationarity and it may be difficult to prove that it constitutes a reasonable assumption in any physical situation. Nevertheless, we shall often assume a process is ergodic to simplify problems. In the real world, we are usually forced to work with only one sample function of a process and therefore must, like it or not, derive mean value, correlation functions, etc., from the time waveform. By assuming ergodicity, we may infer the similar statistical characteristics of the process. It must be remembered that all our theory only serves to model real-world condition. Therefore, what difference do our assumptions really make provided the assumed model does truly reflect real conditions?"

and Hayes [49, p.93] enunciates:

"In most applications determining whether or not a given process is ergodic is not practical. Therefore, whenever a solution to a problem requires knowledge of the mean, the autocorrelation or some other ensemble average, the process is typically assumed to be ergodic and time averages are used to estimate these ensemble averages. Whether or not this assumption is appropriate will be determined by the performance of the algorithm that uses these estimates".

Accordingly, for WSE processes we have:

$$m_X = E[x(t)] = \lim_{T_0 \to +\infty} \frac{1}{2T_0} \int_{-T_0}^{T_0} x(t)dt \tag{2.5}$$

$$R_X(\tau) = E[x(t)x(t+\tau)] = \lim_{T_0 \to +\infty} \frac{1}{2T_0} \int_{-T_0}^{T_0} x(t)x(t+\tau)dt. \tag{2.6}$$

The reader is referred to Garden [51] and Papoulis [52] where the ergodicity property is carefully treated and rigorously analysed.

2.2 Classical DSP and Uniform Sampling

Digital signal processing is deployed in a vast range of areas including telecommunication, digital control, biomedical sciences and many others. It introduced evolutionary changes to those fields benefiting from a well established theory and algorithms developed throughout the last 10 decades. The majority of widely used digital signal processing is uniform sampling based, i.e. classical DSP (a term used throughout the thesis). This is due to the simplicity of algorithms that can be defined in such environments. One might rightly think that handling well defined uniformly distributed data samples is easier than contending with randomly/irregularly spread ones whose positions are specified in a probabilistic sense. Martin in [2, p. 13] presented an interesting discussion pointing out that neither uniform nor nonuniform sampling technique is universally superior in terms of performance and/or the ease of applicability. Each should be evaluated in light of the problem tackled and its requirements. Generally, relating the samples to their underlying continuous process (i.e. reconstruction), going back and forth between time and frequency domain (duality) via processing algorithms (e.g. FFT and filtering/convolution) can be more challenging for nonuniform sampling compared to uniform. Nevertheless, the aliasing defect in the latter imposes limitations on the nature of the processed signals. This makes the uniform sampling approach less attractive in terms of feasibility and/or cost viability in certain scenarios.

Below, we start with the classical uniform sampling theory and its famous reconstruction formula. As the focus of this research is exploiting the salient features of nonuniform sampling, the elaboration on the sampling theory is kept concise and mostly informative.

2.2.1 Introduction to WKS Sampling Theorem

According to Whittaker-Kotelnikov-Shannon (WKS) sampling theorem or reconstruction formula, a bandlimited continuous-time signal $x(t)$ can be represented by:

$$x(t) = \sum_{n=-\infty}^{+\infty} x(nT_{US})\text{sinc}(f_{US}t - n) \tag{2.7}$$

where $f_{US} \geq 2f_{\max}$ is the uniform sampling rate, $T_{US} = 1/f_{US}$ and $f_{\max}$ is the highest frequency present in the signal. The rate $f_{Nyq} = 2f_{\max}$ is known by *Nyquist sampling rate*

following the contribution of Nyquist in [53]. Some books refer to WKS simply as Shannon who introduced the sampling theorem in the form known nowadays [54]. An excellent historical review of the development of the sampling theorem and interpolation in general is given in [55].

The significance of (2.7) is that a bandlimited signal can be uniquely determined by its equidistant samples via an explicit formula. The bandlimited constraint implies:

$$x(t) = \int_{-\infty}^{+\infty} X(f) e^{j2\pi ft} df = \int_{-f_{\max}}^{f_{\max}} X(f) e^{j2\pi ft} df \,. \tag{2.8}$$

WKS, named the cardinal series in some references such as [43], has been proved in several ways in the open literature, e.g. [2, p. 21] and [43, p.35]. We represent the one that is referred to as the "*physical interpretation*" in [43].

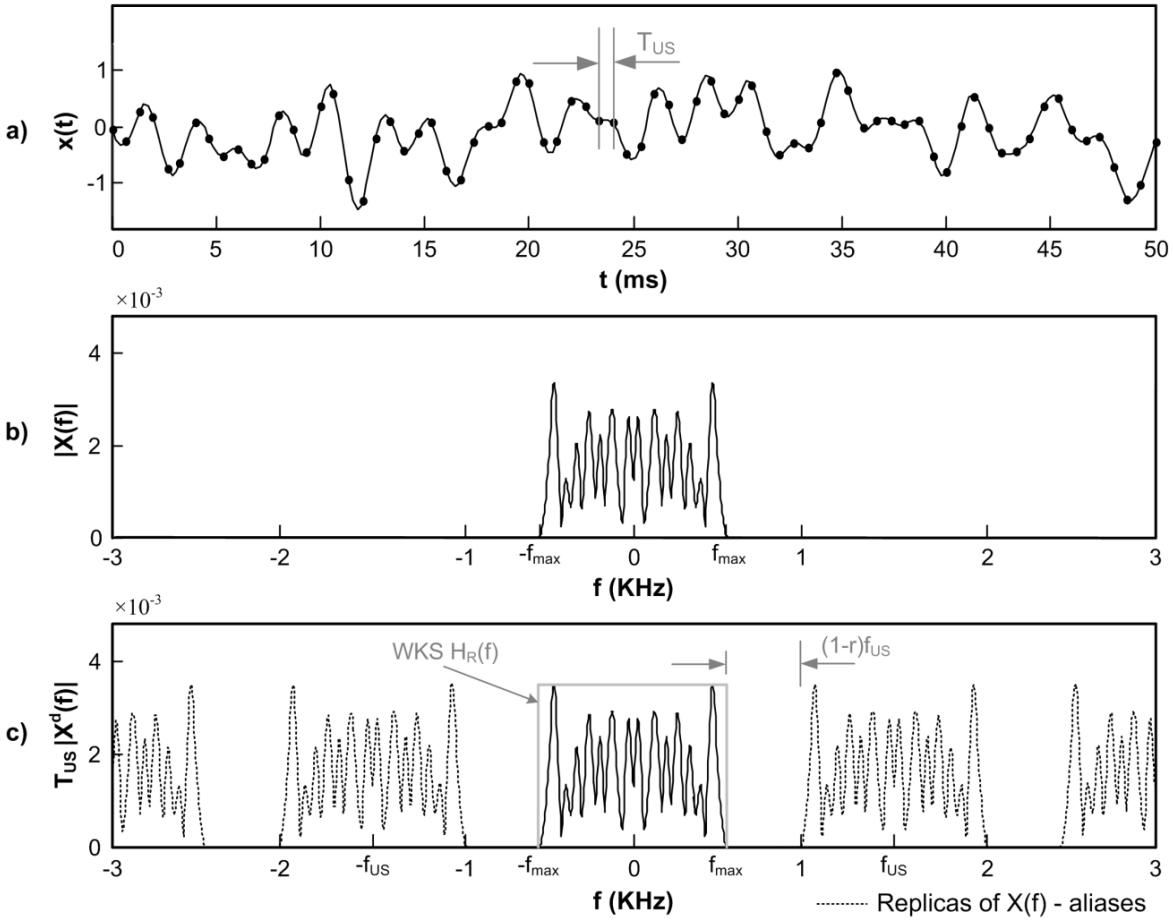

Figure 2.2: Spectrum of a uniformly sampled signal ($r = 0.667$). a) Continuous baseband bandlimited signal $x(t)$ of $f_{\max} = 500$ Hz, b) the magnitude FT of $x(t)$ from the observation window in (a) and c) the magnitude spectrum of the sampled signal such that $f_{US} = 3f_{\max}$.

We assume that the processed signal is of a determinstic nature. Utilising the Fourier expansion of the periodic sampling signal $\mathcal{S}(t)$ and noting that uniform sampling is inherently deterministic, we obtain: $\mathcal{F}\{\mathcal{S}(t),t\} = f_{US}\sum_{n=-\infty}^{+\infty}\delta(f-nf_{US})$. The FT of (2.1) then yields:

$$X^d(f) = X(f) * f_{US}\sum_{n=-\infty}^{+\infty}\delta(f-nf_{US}) = f_{US}\sum_{n=-\infty}^{+\infty}X(f-nf_{US}). \tag{2.9}$$

From (2.9), it can be seen that the sampled signal contains scaled replicas (aliases) of the original signal at multiples of the sampling frequency f_{US}. The Nyquist rate requirement ($f_{US} \geq f_{Nyq}$) ensures that the shifted images of $X(f)$ in the spectrum of $x^d(t)$ do not overlap. Subsequently, the underlying continuous-time signal can be restored from its uniformly distributed samples by using an ideal low-pass filter whose frequency response is described by:

$$H_R(f) = \begin{cases} T_{US} & |f| \leq f_{\max} \\ 0 & |f| > f_{\max} \end{cases} \tag{2.10}$$

e.g. see Figure 2.2. Thus (2.7) is proven by performing the filtering operation in the time domain.

Below, the impact of limiting the number of captured samples is addressed and some of the WKS extensions that are relevant to the theme of this research are discussed.

2.2.2 Truncation Error and WKS Extensions

In practice, no technical device is able to capture and store data for an infinite duration of time as requested by WKS theorem in (2.7). The latter has to be truncated to encompass a finite set of N samples collected within a time analysis window $\mathcal{T}_r = [t_r, t_r + T_0]$. This introduces an error and it becomes important to know how accurate a signal reconstruction is when obtained from a truncated formula. Specifically, the magnitude of the error:

$$\varepsilon_T(t) = x(t) - \sum_{n=-N/2}^{N/2-1} x(nT_{US})\mathrm{sinc}(tf_{US} - n). \tag{2.11}$$

Assessing the truncation error (2.11) is generally not a straightforward task since it depends on a large number of unknown signal samples. It has been noticed long ago that

the truncated WKS formula can provide poor reconstruction quality. There is an extensive literature on estimating the error $\varepsilon_T(t)$ dating back to the 1960's in an attempt to quantify its upper bound, e.g. [56-62]. Various analysis tools have been deployed for this purpose such as complex variables in conjunction with inequalities from theory of functions (e.g. [56, 60, 62]), real variable considerations (e.g. [58]) and bounds on linear systems (see [39, 44] for reviews). It is noted that the majority of the derived truncation error bounds are strictly upper bounds. This is a clear message that discarding an infinite number of samples does not necessarily lead to an infinite truncation error. Intuitively, $\varepsilon_T(t)$ rises quicker at/outside the boarders of the $\mathcal{T}_r$ samples interval as in the case with extrapolation.

Several methods, e.g. [61] and [62], have essentially improved the convergence of the truncated sampling theorem, i.e. lower truncation error for a given N, by using reconstruction filters with particular shapes. They exploit the flexibility offered by oversampling the signal which is typical in practical systems, i.e. $f_{\max} = rf_{US}/2$ such that $0 < r < 1$ (see Figure 2.2). From (2.9), the continuous-time signal can be reconstructed by passing the sampled signal through a filter whose frequency response is given by:

$$H_R(f) = \begin{cases} T_{US} & \text{when } |f| \le f_{\max} \\ 0 & \text{when } |f| > f_{US} - f_{\max} \\ \text{arbitrary} & \text{when } f_{\max} \le |f| \le f_{US} - f_{\max}. \end{cases} \tag{2.12}$$

The single-sided bandwidth B_R of the reconstruction filter can range from $f_{\max}$ to $f_{US} - f_{\max}$. Oversampling, i.e. the presence of an unoccupied band, gives freedom in shaping the reconstruction filter (2.12). This leads to an infinite number of possibilities in designing different reconstructions where all the relevant formulas reduce to:

$$x(t) = \sum_{n=-N/2}^{N/2-1} x(nT_{US}) h_R(t - nT_{US}) \tag{2.13}$$

where $h_R(t)$ is the impulse response of the filter described by (2.12). Figure 2.3 shows the maximum of $\mathscr{E}_n = \sup_{t \in \mathcal{T}_r}(|\varepsilon_T(t)|)/A$ for $n = 1, 2, \ldots 3000$ attained from time-limited independent realisations of a wide sense stationary signal bandlimited to $f_{\max} = 500\,\text{Hz}$. Bounded 25 uniformly collected signal samples, $f_{US} = 3f_{\max}$ and a varying $B_R/f_{\max}$ are considered. The depicted reconstruction filters which comply with (2.12) include: raised cosine as in [61]

and filters obtained from convolving rectangular shapes inspired by the self-truncating series enunciated by Helmes and Thomas in [62]. The frequency response of the latter filter is given by:

$$H_{R,m}(f) = T_{US}(B_R + f_{\max})\,\mathrm{rect}\left(\frac{f}{B_R + f_{\max}}\right) * \left\{\mathrm{rect}\left(\frac{mf}{B_R - f_{\max}}\right)\right\}^m \tag{2.14}$$

where m is the number of the convolutions. According to [62], $m = N(1-r)\pi / e$ achieves the lowest truncation error bound, e is the exponential function. The filter in (2.14) that uses this value of m is denoted by $H_{R,st}$. Figure 2.3 clearly demonstrates the capability of other reconstruction methods that utilise the available empty spectral bands of the oversamples signal to achieve higher rates of convergence compared to WKS. In [63], an experimental study is carried out on the performance of (2.13) for various reconstruction filters in absence as well as presence of noise.

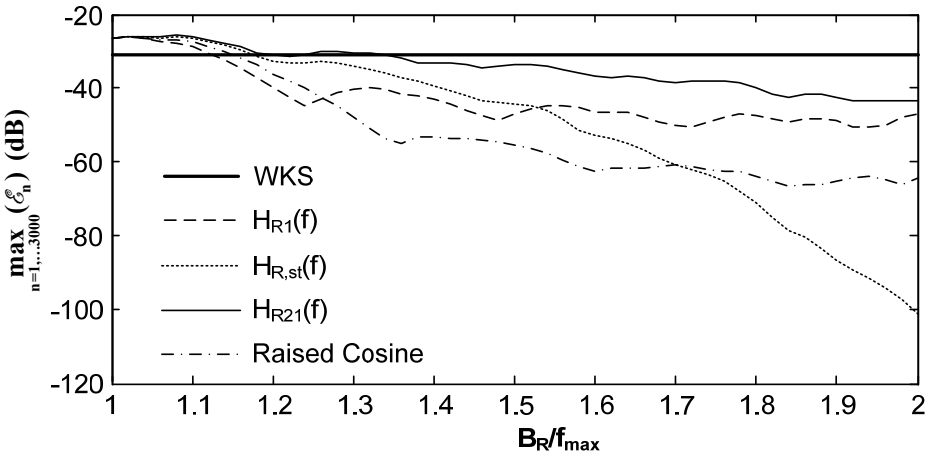

Figure 2.3: Truncation error of a number of reconstruction methods of an oversampled signals where $f_{\max} = 500\,\mathrm{Hz}$, $f_{US} = 3f_{\max}$ and a varying reconstruction filter bandwidth B_R.

Whilst (2.13) represents straightforward variants of (2.7) under the condition $f_{US} > 2f_{\max}$, a substantial part of the sampling theory literature has been devoted to generalising the WKS theorem and extending it. The sampling theorem in the form represented above is tailored to 1-D bandlimited signals that are of a lowpass/baseband nature and is confined to the uniform sampling environment. WKS extensions include: bandpass, multiband and random signals in addition to irregular sampling patterns and many others. The review paper by Jerri [44] in the 70's followed by Unser's [39] in 2000 which was recently complemented by Eldar [36] citing the emerging compressive sensing trend are encyclopaedic surveys

outlining the developments in the sampling theory; they also contain extensive bibliographies. The extension of the sampling theorem to bandpass and multiband signals, which are of an interest in the studied communication systems, are considered in §2.2.4.

2.2.3 Aliasing in Uniform Sampling

The WKS theorem gives sufficient conditions for signal reconstruction; however it produces erroronous results when aliasing occurs. Aliasing is classically associated with the fact that one sinusoid (or in fact any signal) is indistinguishable from the other at the sample points. According to (2.9), if the processed signal $x(t)$ has spectral components stretching outside the $[-0.5f_{US}, 0.5f_{US}]$ frequency region, the replicas/aliases of the underlying continuous-time signal given by: $f_{US}X(f-nf_{US})$, $n \in \mathbb{Z}$, will overlap. This is also known by the aliasing phenomenon. It arises from not satisfying the sampling rate condition of WKS and is attributed to the presence of displaced aliases of $f_{US}X(f)$ in the spectrum of the discretised signal $x^d(t)$.

More interestingly and departing from the above conventional definitions, aliasing in the frequency domain can be viewed in terms of being unable to unambiguously identify the spectral component(s) of the fundamental continuous-time signal from the spectrum of the sampled data. The spectrum of the sampled signal contains scaled identical images of the underlying analogue one shifted by multiples of the sampling frequency value (see Figure 2.2c). If the user does not have a previous knowledge of the incoming signal's spectral support, he/she would have no means to identify which of the aliases represent the original signal. Subsequently, the user is prone to mistakenly considering the wrong spectral component(s) of the sampled signal and processing it/them, e.g. for detection and/or reconstruction purposes. Evidently, if those replicas overlap, separating them is no longer feasible. This interpretation of aliasing is crucial and mostly relevant when handling Bandpass (BP) and Multiband (MB) signals, especially the ones with unknown spectral support as is the case with spectrum sensing.

Random processes, which can model communication signals, are of a paramount importance in this thesis. It is noted that the spectrum of a uniformly sampled random signal comprises scaled and shifted replicas of the underlying continuous one; spectrum in

this case refers to the signal's power spectral density. For example, from (2.4) the PSD of a uniformly sampled wide sense stationary signal is given by:

$$\Phi_X^d(f) = f_{US} \sum_{n=-\infty}^{+\infty} \Phi_X(f - nf_{US}) \tag{2.15}$$

where $\Phi_X(f)$ is the PSD of the continuous-time stochastic process. Similarly, aliasing is understood as the inseparability of $\Phi(f - nf_{US})$, $n \in \mathbb{Z}$, replicas due to unsuitably selected f_{US}. Therefore, uniform sampling DSP is inherently limited by using sufficiently high sampling rates in order to avoid the effects of aliasing. This prompts exploring other sampling options in order to mitigate such constraints.

2.2.4 Sampling Bandpass and Multiband Signals

A Bandpass signal is a bandlimited signal whose central frequency is not zero and resides in the frequency band $f \in [-f_U, -f_L] \cup [f_L, f_U]$ where $f_U > f_L$ and its single-sided bandwidth is $B_{eff} = f_U - f_L$. Such signals are commonly encountered in communication systems where a baseband signal is modulated over the carrier frequency f_C (typically $f_C >> B_{eff}$), e.g. in-phase and quadrature digital modulation. If baseband sampling is applied where $f_{US} \geq 2f_{\max}$, it would result in unnecessary excessive sampling rates. Alternatively, the uniform sampling frequency can be chosen prudently using the bandpass Figure 2.4). The latter represents the smeared-aliasing phenomenon whose level is dependent on the characteristics of the sampling sche

Bandpass sampling was first introduced by Feldman & Bennett [64] and Kohlenberg [65] as an expansion of WKS. Good reviews which highlight the main contributions to bandpass sampling are presented in [31], [66, p.32] and [67, p.35]. The uniform sampling rate that permits signal reconstruction and guarantees the absence of the aliasing effects depends mainly on f_U and B_{eff}. It is given by [31]:

$$f_{US} \geq \frac{2f_U}{\lfloor f_U / B_{eff} \rfloor} \tag{2.16}$$

where $\lfloor x \rfloor$ represents the largest integer less than or equal to x. It clearly specifies the minimum theoretically admissible uniform sampling rate as being $2B_{eff}$. In fact, the

equality condition in (2.16) is satisfied only for an integer band positioning, i.e. $f_L = nB_{eff}$ where $n \in \mathbb{N}$. The interpretation of f_{US} in (2.16) can be misleading as not all the sampling frequencies higher than the specified minimum are valid [31]. Several plots have been produced in the literature to graphically illustrate the permissible rates, e.g. in [31] and [66, p.39]. A refined guideline is provided in [31, 68] where:

$$\frac{2f_U}{\mathcal{K}} \le f_{US} \le \frac{2f_L}{\mathcal{K}-1} \tag{2.17}$$

and $\mathcal{K}$ is a positive integer not exceeding $\lfloor f_U / B_{eff} \rfloor$. Vaughan in [31] states that:

"*the theoretical minimum bandpass sampling rate is pathological in the sense that any engineering imperfections in an implementation will cause aliasing*".

Consequently, in [31] a guard band is suggested to circumvent critical choices of the sampling rates. The considered real signals are not assumed to have symmetrical spectrum component(s) around the carrier frequency(ies), i.e. not symmetrical double sided signals. As a result, attempts, e.g. Brown [69], to deploy rates as low as B_{eff} is not applicable.

A multiband signal is a bandlimited signal that is characterised by M disjointed spectral segments and whose single sided bandwidth is: $B_{eff} = \sum_{m=1}^{M} f_{U_m} - f_{L_m}$. Exploiting any redundancies in the spectrum of a multiband signal is trickier compared to the BP case, e.g. [70, 71]. We have to examine the class of all multiband signals whose bandwidth is B_{eff} and for each of these signals we check the minimum admissible uniform sampling rate. The smallest rate will be $2B_{eff}$ which is applicable to a small subset of the considered signals. Such rate is rarely achievable and is a special case rather than the rule since it requests the processed signal having a particular spectral support; this constraint is unreasonable in most practical cases. In summary, BP and MB sampling techniques have the potential to significantly minimise the uniform sampling rate of bandpass and multiband signals respectively by choosing the sampling frequencies wisely based on the spectral content of the signal. Nonetheless, those benefits intrinsically rely on *a priori* knowledge of the signal's exact spectral support. The lack of such knowledge, e.g. in the spectrum sensing problem tackled in this research, undermines the benefits of employing BP/MB sampling.

Before closing the uniform sampling part, we point out a fundamentally important result in the sampling theory. Landau in [32] showed that the theoretically minimum sampling rate that allows perfect reconstruction of a bandlimited signal is twice the actual bandwidth of the signal and is given by: $f_{Lndu} = 2B_{eff}$. The deployment of nonuniform sampling allows the sampling rates to arbitrarily approach the Landau rate, e.g. [72-74], without dictating the position and layout of the signal's spectral support as in uniform sampling. This entails designing sampling sequences that would lead to identifying the position(s) of the signal's spectral component(s) and reconstructing it. This has further encouraged researchers in the field to explore the possible use of nonconventional sampling schemes, i.e. nonuniform sampling.

2.3 Nonuniform Sampling and Randomised Signal Processing

Nonuniform sampling is a family of sampling techniques where the sampling points are separated by irregular intervals. The irregularity of the sampling points can be enforced by external factors that are beyond the control of the user such as:

- Inaccessibility of the measured signals at some time intervals or within certain time frames. This is common in astronomy [75-77], medical applications [78, 79], geophysical sciences [80, 81] and many others.
- Imperfections/deficiencies in the data acquisition hardware, for example losing samples from the uniform grid [82-84] or departure of samples from their nominal positions due to jitter [85, 86] and many other adverse effects.

Under such conditions the nonuniformity of the sampling instants is viewed as an inconvenience or a nuisance that necessitates the use of counter measures. Nevertheless, nonuniform sampling is sometimes intentionally introduced to offer new opportunities and flexibility that are unavailable in the uniform sampling environments. Hence the questions: why and when nonuniform is/becomes beneficial?

In this research, we explore processing digitally wide bandwidths where the spectral support of the present multiband signal is *a priori* unknown. The latter premise limits the ability of the bandpass or multiband sampling technique (described in §2.2.4) to offer any notable reduction on the needed sampling frequencies. The uniform sampling rate should

exceed at least twice the total monitored frequency range(s) regardless of the spectral activity within. If the aforementioned demands are not met, the aliasing phenomenon can cause irresolvable processing problems. Such stringent sampling rate requirements pose a principle restriction on the applicability of uniform sampling DSP to the examined scenario in terms of:

- The practicality of the imposed sampling frequencies, e.g. the technical feasibility and cost of the dedicated hardware solution if the currently available acquisition and processing module(s) cannot cope.
- The computational cost, e.g. the power consumption and memory obligations, that accompanies treating and storing relatively large quantities of collected data.

Thus despite the simplicity of the classical DSP and its plethora of existing algorithms, the uniform-sampling-based approaches can cease to be the most viable options for dealing with transmissions, typically narrowband signals, residing within a considerably wide frequency range at previously unknown locations.

Randomised sampling schemes, i.e. schemes with intentional irregular sampling intervals, offer the sought alternative to digital representation of analogue signals. They can be regarded as an alias repression measure which facilitates the use of remarkably low sampling rates. The utilisation of randomised sampling schemes along with appropriate algorithms to eliminate/suppress the effect of aliasing is a methodology referred to as Digital Alias-free Signal Processing (DASP). Few monographs on the topic exist, e.g. [1-7, 45]. DASP involves not only designing randomised sampling schemes but also devising suitable processing algorithms to harness their benefits, an endeavour we undertake in this research.

The sampling rates of randomised sampling are described by two notions: the average sampling rate $\alpha = N/T_0$ defines the samples density where N is the number of collected samples within the time analysis window $\mathcal{T}_r = [t_r, t_r + T_0]$ of duration T_0, and $\beta_n = 1/|t_n - t_{n-1}|$ is the instantaneous sampling frequency that depicts the inverse of the distance separating two successive sampling instants in $\{t_n\}_{n=1}^{N}$. Whilst DASP inherently relies on nonuniform sampling to alleviate the aliasing limitation, its benefits come at the expense of more specialised algorithms whose implementation in hardware can be a

challenging task (see e.g. [5, 6]). In answer to the last part of the question put forward at the beginning of this section: DASP methodology should be adopted only when uniform sampling DSP techniques are too costly to deploy, i.e. technically and/or economically.

At this stage other two pressing questions arise: How do we describe randomised sampling? What does alias-free sampling and processing mean? Below, the probabilistic description of randomised sampling, the general notion of alias-free processing and a selected number of sampling schemes are discussed.

2.3.1 Randomised Sampling and Stationary Point Processes

Sequences of randomised sampling instants $\{t_n\}$, $n \in \mathbb{Z}$, that occur along the time axis are commonly considered as point processes. The statistical characteristics of such random processes are essential and have been analysed in the early papers on randomised sampling, e.g. [87-89]. They mandate the properties of the sampling signal $\mathscr{S}(t)$ and subsequently those of the discretised signal $x^d(t)$ in (2.1). For instance, if the continuous-time signal $x(t)$ is WSS, a stationary $\mathscr{S}(t)$ would guarantee the wide sense stationarity of $x^d(t)$. The autocorrelation function and power spectral density of the sampled signal are time-invariant, i.e. $\Phi_X^d(f) = \Phi_X(f) * \Phi_S(f)$ as in (2.4) where $\Phi_X(f)$ and $\Phi_S(f)$ are the PSDs of $x(t)$ and $\mathscr{S}(t)$ respectively. This can significantly reduce the complexity of the spectral analysis. Apart from providing the latter simplification, the stationarity of $\mathscr{S}(t)$ is one of the criteria used in the literature, e.g. in [1, 3-6], to evaluate the alias suppression capability of a given sampling scheme; this is addressed in the next subsection. Below, we define certain statistical descriptions of randomised sampling and briefly discuss one of the sufficient conditions for a stationary $\mathscr{S}(t)$.

The sampling instants $\{t_n\}$ of a randomised sampling scheme are placed within the time analysis window based on their Probability Density Functions (PDFs), i.e. $\mathscr{p}_n(t)$ is for the n-th sample. For dependent sampling instants, t_n has a joint multidimensional PDF, i.e. $\mathscr{p}_n(t, t_{n-1}, t_{n-2}, \ldots, t_1)$, however customarily and for simplicity it is referred to as $\mathscr{p}_n(t)$, e.g. in [1, 3, 4, 6]. The probability of a sample instant belonging to a particular time-interval $\mathscr{S}$ is: $\Pr\{t_n \in \mathscr{S}\} = \int_{\mathscr{S}} \mathscr{p}_n(t)dt$. Another important statistical characteristic is the Sample-point Density Function (SDF) which is given by:

$$\not{p}_{SDF}(t) = \sum_{n=1}^{N} \not{p}_n(t) \,. \tag{2.18}$$

The SDF of an ideal infinite duration sampling signal is duly defined.

According to Bilinskis and Mikelsons [1], a sampling process is stationary if:

$$\not{p}_{SDF}(t) = \alpha \tag{2.19}$$

i.e. its sample-point density function is constant and equal to the average sampling rate for $-\infty \le t \le +\infty$. This implies that the probability of a sample occurring is the same everywhere on the time axis for a stationary sampling process. It is noted that for some sampling schemes a constant SDF might not be observed until after a certain time period, i.e. $\not{p}_{SDF}(t) = \alpha$ for $t \ge t_s$ where t_s is the elapse time. Experimental studies on the shapes of SDF for a number of randomised sampling techniques were conducted independently by Wojtiuk [3], Allay [4] and Qu [7]. Next, the notion of alias-free sampling which was linked in [1] to $\not{p}_{SDF}(t)$ is outlined.

2.3.2 Notion of Alias-free Sampling and Processing

The rational behind employing randomised sampling is to mitigate the aliasing phenomenon of uniform sampling where the spectrum of the sampled signal embodies displaced identical images/aliases of the underlying continuous-time signal (see §2.2.3). Alias-free sampling is a concept whose roots date back to the earliest papers on randomised sampling, e.g. [90]. As its name suggests, it encompasses sampling schemes geared to eliminate aliasing. This "*alias-free*" behaviour is typically related to the spectral analysis of a randomly sampled signal rather than signal reconstruction, e.g. estimating the process's power spectral density from its nonuniformly distributed samples as in [1, 3, 4, 90-94]. There are several criteria for assessing whether a particular sampling scheme is alias-free or not, and hence below we highlight the main contributions to this concept. The questions that are addressed here include: what makes a randomised sampling scheme alias-free? Does alias-free sampling or processing entails the total elimination of aliasing? How do we decide whether a sampling scheme is suitable for the pursued digital signal processing that is free from the limitations of aliasing?

2.3.2.1 Historical Perspective

The notion of alias-free sampling was first introduced by Shapiro and Silverman in [90]. They based their definition of the alias-free criterion on the autocorrelation sequence:

$$r(k)=E\left[x(t_n)x(t_{n+k})\right]=\int_{-\infty}^{+\infty} R_X(\tau)\not{p}_{\Delta_k}(\tau)d\tau \tag{2.20}$$

where $\not{p}_{\Delta_k}(\tau)$ is the PDF of $\Delta_k = t_{n+k} - t_n$ ($n \in \mathbb{Z}$, $k \in \mathbb{Z}$) and $R_X(\tau)$ is the autocorrelation function of the underlying continuous ergodic signal. In [90], the sampling scheme is deemed to be alias-free if there exists only one continuous process with a $R_X(\tau)$ that would yield $r(k)$ in (2.20). The alias-free feature implied that the exact PSD of the continuous stochastic process can be estimated from an infinite number of its irregularly distributed random samples captured at arbitrarily low rates. Additive Poisson and Bi-Poisson sampling schemes were found to be alias-free whilst Tri-Poisson, jittered sampling and additive random sampling based on uniform distribution of Δ_k are not. Beutler [91] extended Shapiro and Silverman concept to sampling schemes that are alias-free in relation to a family of spectra. A scheme being alias-free relative to the family of bandlimited signals $\mathbf{\Gamma}$ stipulates that no two processes that belong to $\mathbf{\Gamma}$ can have the same $r(k)$ sequence.

Masry [92-94] pointed out the deficiency in the alias-free definition in [90, 91]. He highlighted the fact that if a finite number of signal samples are available the Shapiro and Silverman criterion does not guarantee a consistent estimate of the power spectral density of the underlying continuous-time signal. He reformulated the definition in order to accommodate the latter practical constraint by proposing a covariance metric. He showed that additive Tri-Poisson sampling is alias-free which contradicts [90]. It is noted that the PSD estimation consistencies in [92-94] were attained under asymptotic assumptions, i.e. the number of the processed samples tends to infinity.

Most recently, Bilinskis and Mikelsons [1] enunciated a new criterion for alias-free sampling; a scheme is alias-free if it is stationary, i.e. it satisfies the condition in (2.19) they postulated. They showed that the spectrum of a randomly sampled signal approaches that of the underlying continuous-time one as the number of samples tends to infinity provided that the sampling scheme is stationary. This can be shown by simple analysis as

in [7]. For example, consider the problem of estimating the Fourier transform of a continuous-time deterministic signal from a set of its nonuniformly distributed samples. Using a nonuniform discrete-time Fourier transform defined by:

$$\tilde{X}(f) = \frac{1}{\alpha}\sum_{n=1}^{N} x(t_n) e^{-j2\pi f t_n} . \tag{2.21}$$

It can be noticed that: $x(t_n) = \int_{-\infty}^{+\infty} X(f) e^{-j2\pi f t_n} df$ where $X(f)$ is Fourier transform of the targeted signal. We can write:

$$E\left[\tilde{X}(f)\right] = \frac{1}{\alpha}\int_{-\infty}^{+\infty} X(\nu)\sum\nolimits_{n=1}^{N} E\left[e^{-j2\pi(f-\nu)t_n}\right] d\nu . \tag{2.22}$$

Since $E\left[e^{-j2\pi(f-\nu)t_n}\right] = \frac{1}{A_{p_n}}\int_{-\infty}^{+\infty} p_n(t) e^{-j2\pi(f-\nu)t} dt$, where A_{p_n} is a scaling factor that maintains $\int_{-\infty}^{+\infty} p_n(t) dt = 1$ for the n-th sample. The expression in (2.22) emerges as:

$$E\left[X_e(f)\right] = X(f) * \mathcal{F}\left\{p_{SDF}(t), t\right\} \tag{2.23}$$

where $\mathcal{F}\left\{p_{SDF}(t), t\right\}$ is the FT of the sample-point density function in (2.18). If $p_{SDF}(t)$ is constant and equal to α, i.e. $\mathcal{F}\left\{p_{SDF}(t), t\right\}$ is a Dirac delta, spectrum aliasing will be eradicated and $\tilde{X}(f)$ is an unbiased estimator of $X(f)$ regardless of the average sampling rate. However, such analysis demands sampling the signal for infinitely long periods. In [1] Bilinskis and Mikelsons noted that under the practical constraint of having a finite number of signal samples, i.e. (2.19) is not fulfilled for $-\infty \le t \le +\infty$, aliasing cannot be totally eliminated but rather suppressed by a finite amount [1]. This fact is taken into account when deciding on the criterion that best serves the purpose of resolving the problems tackled in this research, mainly low rate wideband spectrum sensing.

2.3.2.2 Adopted Criterion

Here, alias-free sampling and processing simply refers to the ability of the randomised sampling scheme and the deployed algorithms to attenuate spectrum aliasing in $x^d(t)$ within a wide frequency range(s) in lieu of totally eliminating it. As long as this

suppression permits the unambiguous identification of the spectral components of the analogue signal from that of the sampled one, the sampling process is conceived to be suitable for the pursued digital signal processing whose rates are not dictated by the processed bandwidths. Various randomised sampling schemes, despite violating the stationarity condition in (2.19), foster signal processing that is not limited by the aliasing phenomenon, i.e. digital alias-free signal processing. This is illustrated in Chapter 3.

At this juncture, we acknowledge that the widely used alias-free sampling and processing terms can be misleading as a nonuniformly sampled signal can never be completely free of aliasing for a finite number of samples. Although randomised sampling circumvent aliasing in its classical sense, it introduces what is commonly known by *smeared-aliasing* [3-6]. To demonstrate this phenomenon, Figure 2.4 displays the spectrum of a sampled bandpass wide sense stationary signal. The PSD of the continuous stochastic process is: $\Phi_X(f)=1$ if $f \in \pm[770,800]$ MHz and zero elsewhere. Uniform bandpass sampling with $f_{US}=95$ MHz which satisfies (2.17) and a randomised sampling scheme (namely total random sampling described in §2.3.3.1) with $\alpha=95$ MHz are utilised. The spectrum is attained via averaging a large number of a scaled periodogram-type estimates, i.e. $\left|\alpha\sum_{n=1}^{N}x(t_n)e^{-j2\pi ft_n}\right|^2$ where $N=950$. They are calculated from truncated independent realisations of the WSS process $x(t)$; this estimator is discussed in more details in the next chapter. Let's assume that the exact spectral support of the processed narrowband signal is unknown and that it resides somewhere in the frequency range $f \in \pm[0.5,1]$ GHz, i.e. a conservative spectral support. It is evident from Figure 2.4b that randomised sampling suppressed the spectrum aliases/replicas and smeared them (apart from the fundamental one) to create a white-noise like component present at all frequencies. It permitted distinguishing the spectral component of the underlying continuous signal in the wide range of observed frequencies, despite the used sampling rate. For the uniform sampling case depicted in Figure 2.4a, the user would have no indication which of the present identical spectral components represents the incoming signal. This clearly exhibits the alias suppression potential of randomised sampling. The shape of the smeared-aliasing is determined by the characteristics of the sampling scheme as shown in Chapter 3.

Martin [2, p.40] made a very important point regarding DASP techniques. He noted that alias-free sampling serves the purpose of analysing the signal's spectrum and is distinct

from signal reconstruction. This observation was confirmed by Wojtiuk experiments in [3]. He demonstrated that a sampling scheme with high aliasing suppression ability does not generally ensure superior signal reconstruction. Accordingly, the randomised sampling and processing adopted here serves the purpose of identifying the spectral support of the processed signal, i.e. spectrum sensing. Signal reconstruction is treated separately and can be considered after unveiling the locations of the active spectral bands.

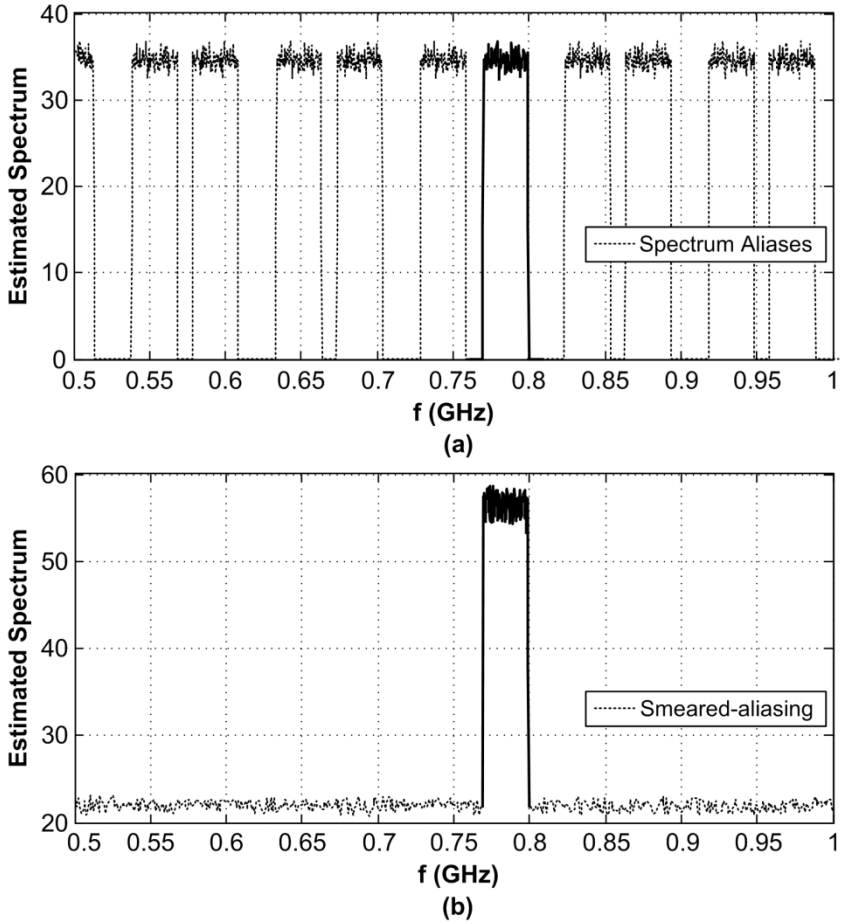

Figure 2.4: Estimated spectrum of a WSS signal from a finite set of its samples where $\Phi_X(f)=1$ if $f \in \pm[770,800]$ MHz and zero elsewhere. (a) Uniform bandpass sampling and $f_{US}=95$ MHz. (b) Total random sampling and $\alpha=95$ MHz.

2.3.3 Randomised Sampling Schemes

We emphasise that randomised sampling implies that the nonuniformity is introduced intentionally to enable alias-free processing. In this subsection, we describe a number of sampling schemes that are typically used to suppress the aliasing phenomenon, e.g. in [1-

6]. Apart from additive random sampling, these schemes are employed in the following chapters.

Sampling driven by the level of the processed signal, i.e. signal dependant sampling such as zero crossing and level crossing (e.g. [47, 95]), are excluded from the randomised schemes considered in this research. Besides, deterministic nonuniform sampling such as periodic nonuniform sampling is not analysed.

2.3.3.1 Total Random Sampling (TRS)

Total random sampling is viewed as a simple way of generating a set of N nonuniform samples within the finite signal analysis window $\mathcal{T}_r = [\mathcal{t}_r, \mathcal{t}_r + T_0]$, e.g. [96, 97]. Its concept is drawn from Monte-Carlo integration over a finite integral [98, 99]. All the sampling instants of TRS are Independent Identically Distributed (IID) random variables whose PDF $\mathcal{p}_n(t)$ takes non-zero values only within $\mathcal{T}_r$. For a uniform PDF across $\mathcal{T}_r$, we have:

$$\mathcal{p}_n(t) = \begin{cases} 1/T_0 & t \in \mathcal{T}_r \\ 0 & \text{elsewhere} \end{cases} \tag{2.24}$$

where $n = 1, 2, \ldots, N$. It can be easily seen from (2.24) that TRS ensures the stationarity of the scheme according to the sample-point density function criterion. Nonetheless, Allay in [4] showed that TRS is fit for DASP even if its SDF is not constant, e.g. for some PDF shapes other than (2.24).

2.3.3.2 Random Sampling on Grid (RSG)

Random sampling on grid selects randomly N samples out of the total N_g possible sample positions that can be in general arbitrarily distributed within $\mathcal{T}_r$ [100]. Here, these nominated time-locations are equally spaced. They form an underlying uniform grid whose sampling frequency and total number of samples are denoted by $f_g = 1/T_g$ and N_g respectively. Any of the grid points can be selected only once with equal probability. More precisely, it is RSG without replacement where $\binom{N_g}{N}$ possible distinct sampling sequences of length N exist. Figure 2.5 exhibits a realisation of a RSG sequence.

The sampling points of the RSG scheme are defined by: $t_n \in \mathcal{S}_1^d$ for $n = 1,2,\ldots N$ where $\mathcal{S}_1^d$ is the discrete sample space encompassing all the underlying uniformly distributed grid points, i.e. $0, kT_g, (k+1)T_g, \ldots N_g T_g$. Consequently, the PDF of the n-th collected sampling instants is given by:

$$p_n(t) = \frac{1}{N_g - n + 1} \sum_{\tau \in \mathcal{S}_n^d} \delta(t - \tau) \tag{2.25}$$

where $\mathcal{S}_{n+1}^d = \mathcal{S}_n^d - \{t_n\}$ is the set of "unused" grid points after selecting n sampling instants. For t_1 the entire sample space is considered, i.e. $\mathcal{S}_1^d$. The PDFs of the samples that follow depend on the precedent sample positions. Given the discrete nature of PDFs of random sampling on grid, its SPF is discrete and the stationarity condition (according to [1]) is not fulfilled. Nevertheless, it is shown in Chapter 3 that RSG is suitable for DASP provided an appropriately selected grid rate f_g. The random sampling on grid scheme can be viewed as a modification (special case) of TRS. It aims at accommodating the practical constraint enforced by the technological and physical factors of the acquisition device specifying a minimum distance between any two samples.

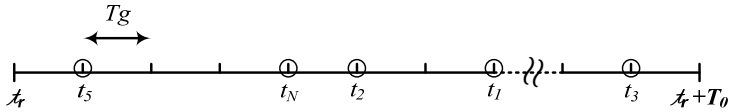

Figure 2.5: An RSG sampling sequence (circled instants are the selected grid points).

2.3.3.3 Stratified and Jittered Sampling

Stratified Sampling (SS) was proposed by Masry in [98, 101] as a scheme that permits estimating the spectrum of a deterministic continuous-time signal with high convergence rates. Generally, stratification divides the analysis window into $N_{\mathcal{S}}$ disjointed subintervals, i.e. $\mathcal{S}_1, \mathcal{S}_2, \ldots, \mathcal{S}_{N_{\mathcal{S}}}$ where $\bigcup_{n=1}^{N_{\mathcal{S}}} \mathcal{S}_n = \mathcal{T}_r$. The parameter N_n is the number of the collected samples in $\mathcal{S}_n$ such that $\sum_{n=1}^{N_{\mathcal{S}}} N_n = N$ is the total number of processed samples. Various methods exist for choosing the number of samples per subinterval/stratum, e.g. see [99].

In this research and similar to [98], each stratum contains one sample with a uniform PDF. The probability density functions of the N independent random samples are defined by:

$$p_n(t) = \begin{cases} \dfrac{1}{|\mathcal{S}_n|} & t \in \mathcal{S}_n \\ 0 & \text{elsewhere} \end{cases} \tag{2.26}$$

for $n = 1,2,\ldots,N$ where $|\mathcal{S}_n|$ is the width of the stratum. Choosing $|\mathcal{S}_n|$, e.g. to improve the spectrum estimation quality, demands *a priori* knowledge of the incoming signal [98, 101]. A practical approach is to assume equal strata, i.e. Stratified Sampling with Equal Partitions (SSEP). Figure 6 depicts a realisation of an SSEP sequence. Masry in [98, 101] showed that SS is adequate for DASP despite the fact it does not satisfy the stationarity condition for the majority of cases excluding SSEP.

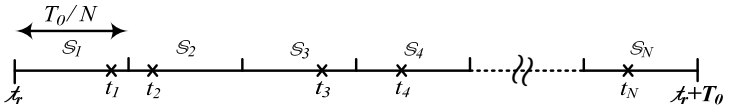

Figure 2.6: An SSEP sampling sequence (crosses are the sample points).

Another sampling scheme that is linked to SS is the widely distinguished Jittered Random Sampling (JRS). It is commonly expressed as the departure of the sampling instants from their nominal uniform sampling grid, e.g. due to imperfections in the data acquisition device(s). It is modelled by:

$$t_n = nT_{US} + \tau_n \tag{2.27}$$

for $n = 1,2,\ldots,N$ where T_{US} is the mean sample interval and τ_n's are zero mean IID random variables with a PDF $p_\tau(t)$ and variance σ^2. Thus the PDF of the n-th sample point is:

$$p_n(t) = p_\tau(t - nT_{US}). \tag{2.28}$$

Controlled/intentional jitter for alias-free processing has known characteristics and differs from the jitter introduced by the impairments of the sampling device. The latter is viewed as a nuisance which is either ignored or compensated for in later processing blocks. It can be noticed that if the PDF of τ_n has non-zero values within $[-0.5T_{US}, 0.5T_{US}]$ and zero elsewhere, JRS becomes a special case of stratified sampling.

From [3, 4], jittered random sampling is stationary if the jitter is uniformly distributed in the interval $[-0.5T_{US}, 0.5T_{US}]$ or τ_n distribution has a relatively high variance. Various analytical expressions for the power spectral density of JRS, i.e. $\Phi_S(f)$ in (2.4), are

derived in [2, 3, 42, 102]. All of them expose the fact that the power spectral density of a sampled WSS signal using JRS contains replicas of the PSD of the analogue signal shaped by the magnitude of the jitter characteristic function, i.e. $\left|\int_{-\infty}^{+\infty} \not{p}_{\tau}(t) e^{j2\pi ft} dt\right|$. Hence the ability of JRS to suppress aliasing is dependent on the PDF of the jitter. It was demonstrated in [3, 4] that the form of JRS where $\not{p}_{\tau}(t) = 1/T_{US}$ if $t \in [-0.5T_{US}, 0.5T_{US}]$ and zero elsewhere exhibits the scheme's maximum potential to attenuate (almost equally) all the undesirable spectrum aliases following sampling. This form of JRS presents itself as a legitimate DASP tool and is identical to the stratified sampling with equal partitions scheme.

2.3.3.4 Additive Random Sampling

Additive Random Sampling (ARS) was first introduced by Shapiro and Silverman [90] as an alias-free sampling scheme whose sampling instants are described by:

$$t_{n+1} = t_n + \tau_n \tag{2.29}$$

$n = 0,1,\ldots,N$. The τ_n's are IID random variables with a PDF given by $\not{p}_{\tau}(t)$ and a variance of σ^2. It is noted that the n-th sample point is the sum of n IID random variables and its PDF is given by:

$$\not{p}_n(t) = \overset{n}{*} \not{p}_{\tau}(t) \tag{2.30}$$

where $\overset{n}{*} \not{p}_{\tau}(t)$ denotes the n-fold convolutions of $\not{p}_{\tau}(t)$ with itself. This implies that the sample-point density function of ARS will be constant, i.e. the scheme becomes stationary, after a certain time period as the variance of the samples grows with the index n according to (2.30). The speed at which the stationarity condition in (2.19) is fulfilled depends on σ^2. This observations was confirmed by the analysis conducted in [1] and experimental results in [3, 4, 7]. Thus the ARS is asymptotically stationary, i.e. $\lim_{t\to\infty} \not{p}_{SDF}(t) = \alpha$.

In order to improve the speed at which ARS achieves stationarity given the typically finite analysis window, Correlated Additive Random Sampling (CARS) was proposed in [1]. In this case, the τ_n terms in (2.29) are deliberately made correlated. The correlation between two successive sampling instants is assessed by the correlation coefficient defined by: $\rho(\tau_n, \tau_{n+1}) = \left(E[\tau_n \tau_{n+1}] - 1/\alpha^2\right)/\sigma^2$ where $|\rho(\tau_n, \tau_{n+1})| \geq 1$. It dictates the speed at which the

variance of the sample points accumulates. If $\rho(\tau_n, \tau_{n+1}) > 0$, the variance of the sample points of CARS increases at faster rates compared to the ARS and vice versa. It is noted that the width of the signal analysis window $\mathcal{T}_r$ of ARS and CARS schemes varies from one sequence to another. In a practical scenario where N is finite, the T_0 and α are specified in a probabilistic sense, e.g. their mean values are examined. Additive random sampling is not studied here and is presented for completeness.

2.4 Summary

WKS theorem provides the sufficient condition under which a uniformly sampled signal can be perfectly reconstructed and therefore processed in the same way as if we had access to the whole waveform of the continuous-time signal. It demands:

- Sufficiently high sampling rates $f_{US} \geq 2f_{\max}$, i.e. above Nyquist rate. The use of rates lower than those recommended by WKS normally leads to a phenomenon called aliasing, where there is more than one signal within the class of analysed signals that have the same values at the sample points.

- An infinite number of the data samples, a request which cannot be met in practice. Truncating the reconstruction formula introduces an error whose upper bounds have been extensively studied in the literature. Variations of WKS with higher convergence rates can be deployed to minimise the truncation error. They represent one of the many extensions of the classical sampling theorem.

Uniform bandpass/multiband sampling techniques exploit the redundancies in the spectrum of BP/MB signals to avert aliasing. They permit the use of sampling rates well below Nyquist's, especially if $f_{\max} >> B_{eff}$. They inherently rely on a previous knowledge of the signal's exact spectral support which is not available in certain tasks. For example, in spectrum sensing only a conservative spectral support is known, i.e. the entire monitored bandwidth. Although the simplicity, availability of algorithms and ease of implementation are the key features of uniform sampling DSP, it is widely recognised that its foremost limitation is the imposed sampling rates. Violating the Nyquist or BP/MB sampling criterion, results in aliasing which introduces irresolvable processing problems.

2.4 Summary

Nonuniform randomised sampling poses as an alternative acquisition paradigm to uniform sampling; it is not limited by the aliasing phenomenon. Its ability to eliminate aliasing, i.e. alias-free sampling, has been measured by various criteria in the literature. This normally refers to the spectral analysis of the sampled signal not its reconstruction. Most importantly, not all DSP problems require the sampling scheme to completely eliminate spectrum aliasing which theoretically imposes an infinite number of signal samples collected at arbitrarily low rates. For instance, in the spectrum sensing endeavor it is sufficient to suppress spectrum aliasing within the overseen frequency range such that the spectral support of the present signal is unveiled. It is essential that we define the DSP problem to be solved; only then alias-free property can be analysed. In this context, we regard sampling schemes that permit revealing the activity of a number of monitored spectral subbands within in a wide range of surveyed frequencies as alias-free. This includes nonstationary schemes noting that the alias-free stationarity criterion cannot be fulfilled for a finite number of samples. It is natural to treat spectral analysis (e.g. aimed at spectrum sensing) and signal reconstruction (e.g. for extracting the feature(s) of the incoming signal) as two separate problems; the former precedes the latter in case both tasks are undertaken.

Finally, the randomised sampling and processing methodology, otherwise known as digital alias-free signal processing, offers additional opportunities that extend rather than contradict the theory and practice of the classical uniform sampling DSP. It is mostly applicable to digitally processing narrowband signals residing in a wide frequency range(s). Sampling alone is not sufficient to perform DASP; suitable algorithms should be devised to exploit the methodology leverages. Such algorithms are explored and analysed in the rest of the thesis. No claim is made on the superiority of randomised processing over classical DSP for all scenarios. In fact, the utilisation of uniform or nonuniform sampling techniques is based on which of them provides better results at the minimum technical/economical cost.

Chapter 3

Periodogram-type Estimators for Randomly Sampled Stationary Signals

The purpose of spectrum estimation in this research differs from that in many conventional spectral analysis tasks. In the latter cases, the problem of establishing the spectral characteristics of the processed signal, e.g. the distribution of the signal's power over frequency, is considered. Here, spectral analysis is utilised to facilitate conducting low rate wideband spectrum sensing harnessing the features/benefits of nonuniform randomised sampling. Determining the exact shape of the signal spectrum within the surveyed frequency range, e.g. Power Spectral Density (PSD), is not required. Accordingly, many traditional spectral analysis approaches become irrelevant and unnecessarily complicated. We seek a simple low complexity means that is suitable for the tackled problem, i.e. spectrum sensing and not PSD estimation.

This chapter commences by restating the considered problem and stressing the intention of the spectral analysis endeavour. Existing estimation techniques, starting with the uniform sampling ones, are then discussed. This sets the scene for introducing a number of periodogram-type estimators each tailored to a particular randomised sampling scheme. We refer to this type of analysis by Spectral Analysis of Randomised Sampling (SARS). The adequacy of the adopted estimators for the spectrum sensing task is investigated whilst the operational sampling rates are not only sub-Nyquist but also sub-Landau. It is noted that the simplicity and ease of implementation are the main merits of periodogram-type methods [2, 3, 5, 15, 49, 76, 103]. Numerical examples are deployed to exhibit and verify the accuracy of the developed analytical expressions.

3.1 Introduction

3.1.1 Problem Definition

The pursued Multiband Spectrum Sensing (MSS) involves overseeing the activity of a number of non-overlapping spectral subbands/channels occupying wide range(s) of frequencies (see §1.2). Spectrum estimation or analysis is deployed to concurrently sense the activity of the monitored channels. This is distinct from MSS techniques that examine one subband at a time using fined-tuned and preset bandpass filtering. The sensing device is assumed to have no previous knowledge of the location(s) of the active subband(s) and limited information, if any, about the characteristics of the incoming transmission(s). Consequently, the conventional uniform-sampling-based spectral analysis tools demand sampling rates that exceed at least twice the total monitored bandwidth. Otherwise, spectrum aliasing would result in irresolvable detection problems. Such rates can be prohibitively high, especially if the surveyed bandwidth is ultra-wide.

Here, spectral analysis methods that allow detecting the active subbands within a wide range of overseen frequencies are studied. They operate at substantially low sampling rates by utilising randomised sampling to mitigate the aliasing phenomenon (see §2.3.2). Subsequently, quantifying the statistical characteristics of the spectrum estimation from the finite set of captured signal samples becomes vital for assessing the suitability of the adopted estimators for the multiband spectrum sensing task (not PSD estimation). This entails evaluating their expected values and variances which give a clear indication of estimation accuracy as explained in §3.2. This is crucial for predicting the estimators' performances once employed in the detection routine. Since signal reconstruction is not sought, it is shown below that arbitrarily low nonuniform sampling rates can be used to estimate a detectable frequency representation of the received multiband signal.

3.1.2 Related Work

Spectral analysis has a plethora of application areas including astronomy, oceanography, interception, biomedical applications, speech analysis, finance, and many others. It has a long history and has been extensively studied [49, 104-106]. Here, we only address the techniques that are believed to be related to the work presented in this thesis.

In general spectrum estimation approaches can be divided into two groups:

- Nonparametric methods: they are independent of the processed signal. They generally rely on Fourier Transform (FT) analysis where Discrete-time Fourier Transform (DTFT) or optimised version of it, for example Fast Fourier Transform (FFT), is used to estimate the spectrum of the signal. Generally speaking, these techniques include periodogram and its various modifications [49, 105].
- Parametric methods: they are based on parametric models of the signal incorporating *a priori* available information into the estimation process. Such methods are useful when the mathematical model of the analysed signal is known, e.g. in voice recognition applications. Models that are commonly used include: autoregressive, moving average, autoregressive moving average and harmonic/exponential [49, 105].

Due to the limited information available about the incoming signal(s) in the considered systems, parametric techniques are excluded in the sequel. The nonparametric ones are more attractive as they are generally simpler and applicable to all signals. They are widely viewed as efficient low complexity tools for multiband spectrum sensing [13, 15-19]. Since the adopted SARS tool belongs to the family of periodograms, first we briefly discuss uniform sampling periodograms.

3.1.2.1 Uniform Sampling Periodogram

Periodogram is one of the most commonly known spectrum estimators and is defined by:

$$\mathscr{P}^N(f) = \frac{1}{N}\left|\sum_{n=1}^{N} x(nT_{US})e^{-j2\pi fnT_{US}}\right|^2 \tag{3.1}$$

where $x(t)$ is the random signal that is typically assumed to be Wide Sense Stationary (WSS). Whereas, N is the number of uniformly distributed samples captured at a rate of $f_{US} = 1/T_{US}$. Periodogram is an asymptotically unbiased estimator of the power spectral density of the processed signal, provided that f_{US} is equal or above the Nyquist rate. We have: $E\left[\mathscr{P}^N(f)\right] = \Phi_X^d(f) * \left|W(f)\right|^2 / N$ where $\Phi_X^d(f) = f_{US}\sum_{n=-\infty}^{+\infty}\Phi_X(f - nf_{US})$, $*$ denotes the convolution operation, $W(f)$ is the Fourier transform of the rectangular window limiting the signal analysis window and $\Phi_X(f)$ is the PSD of $x(t)$ [49]. It follows that for a finite number of samples a spectral leakage is introduced, producing a bias to the

estimate. The resolution of the estimated spectrum is determined by the length of the time window. Whereas, the variance of the estimator is of the same order of its expected value where $\text{var}\left\{\mathscr{P}^N(f)\right\} \approx \left[\Phi_X^d(f)\right]^2$ as N tends to infinity [49]. Hence (3.1) has a high level of uncertainty regardless of the number of collected samples.

Various tactics have been employed to enhance the periodogram performance. Bartlett [107] targeted reducing the periodogram variance, i.e. improving its accuracy, by averaging a K number of estimates calculated from non-overlapping signal windows. If the data within these segments are uncorrelated, the variance decays at a rate of $1/K$. Welch [108] modified Bartlett method by letting the signal segments overlap in an attempt to reduce the estimation variance for a finite set of available samples. With regards to the periodogram bias, the use of windowing functions (other than the rectangular one) gives a new lever to reduce the spectral leakage and the bias. A comprehensive reviews on windowing functions and their characteristics are given in [109, 110].

Other nonparametric spectral analysis tools aimed at more accurate PSD estimations exist, e.g. Blackman-Tukey [105] and multitaper method [111]. In general, the complications that can accompany such approaches, e.g. [111], are not all relevant to the tackled spectrum sensing problem. Despite the inaccuracy of the periodogram tool (in its various flavours), its popularity is attributed to its simplicity, low computational complexity and ease of implementation [2, 3, 5, 15, 49, 103]. Such features are desired here, where a simple spectral analysis technique that fosters low rate reliable wideband spectrum sensing is pursued.

3.1.2.2 Spectral Analysis of Nonuniformly Sampled Data

Spectral analysis of nonuniformly sampled data is a well known research area, e.g. see [76, 77, 104, 106]. One of the earliest and most popular analysis methods was proposed by Lomb [77] and Scargle [76] in the astronomical literature where the unavailability of measurements at certain time instants is an inherent problem. It is known by Lomb-Scargle or Least Squares (LS) periodogram. LS periodogram was motivated by detecting the presence of a sinusoidal signal contaminated with Additive White Gaussian Noise (AWGN). The irregular zero mean noisy observations $\left\{y(t_n)\right\}_{n=1}^N$ are represented by:

$$y(t_n) = a_f \cos\left(2\pi f t_n - \varphi_f\right) + b_f \sin\left(2\pi f t_n - \varphi_f\right) + \varepsilon_{n,f}. \tag{3.2}$$

The parameters a_f and b_f are selected as to minimise $\left\|\varepsilon_{n,f}\right\|_2 = \sum_{n=1}^{N}\left|\varepsilon_{n,f}\right|^2$. Using the standard LS solution, the reduction in the sum of the squares produces the LS periodogram defined by [77]:

$$\mathscr{P}_{LS}(f) = \frac{\sum_{n=1}^{N}\left[y(t_n)\cos\left(2\pi f t_n - \varphi_f\right)\right]^2}{2\sum_{n=1}^{N}\cos^2\left(2\pi f t_n - \varphi_f\right)} + \frac{\sum_{n=1}^{N}\left[y(t_n)\sin\left(2\pi f t_n - \varphi_f\right)\right]^2}{2\sum_{n=1}^{N}\sin^2\left(2\pi f t_n - \varphi_f\right)}. \tag{3.3}$$

It is similar to the classical uniform sampling periodogram in (3.1) for noiseless environments as: $\mathscr{P}^N(f) = \sum_{n=1}^{N}\left[x(t_n)\cos(2\pi f t_n)\right]^2/N + \sum_{n=1}^{N}\left[x(t_n)\sin(2\pi f t_n)\right]^2/N$ such that $t_n = nT_{US}$. We note the non-equidistant samples, the scaling factors and the phase-shift φ_f in (3.3). The latter two parameters are redundant and were introduced to simplify the analysis of $\mathscr{P}_{LS}(f)$, e.g. $\sum_{n=1}^{N}\cos^2\left(2\pi f t_n - \varphi_f\right) = 0.5N + 0.5\sum_{n=1}^{N}\cos\left(4\pi f t_n - 2\varphi_f\right) \approx 0.5N$ where the high frequency component is considered to have a negligible value and similarly $\sum_{n=1}^{N}\sin^2\left(2\pi f t_n - \varphi_f\right) \approx 0.5N$. This facilitates attaining the rates of successful/false detection of sinusoid(s) using (3.3), see Scargle [76] for more details.

New techniques that offer more accurate estimation by utilising more advanced mathematical tools compared to the LS periodogram keep unfolding. For example, the recent iterative adaptive approach [112] uses weighted least squares fitting criterion yielding more accurate estimation results than the LS one. An excellent recent review of the emerging and existing nonuniform sampling spectral analysis methods is presented in [106]. Although periodograms have a poor quality of estimation compared to other means, they are simple and quick techniques that enable detecting the presence of the targeted signals in a noisy environment [76, 77]. It is a sensible attitude adopted by Scargle in his defence of using periodograms, i.e. it is fit for the purpose. This resonates with the theme of this research where spectrum estimators that permit detection rather than exact estimation of the underlying signal spectrum are sought.

The aforementioned approaches consider arbitrary sampling, i.e. the user has no control/influence over the samples layout/distribution. On the other hand, the sampling studied in this research is randomised where the sampling process is prescribed by the user (see §2.3.3). Several spectrum estimation methods that deal with randomised sampling

schemes exist, e.g. [96, 98, 101], where the processed finite energy signals are of deterministic nature. They focus on estimating the signal's windowed Fourier transform defined by:

$$X_W(\mathcal{t}_r, f) = \int_{\mathcal{t}_r}^{\mathcal{t}_r+T_0} x(t)w(t)e^{-j2\pi ft}dt \tag{3.4}$$

from a finite set of N irregular samples collected within the time analysis window $\mathcal{T}_r = [\mathcal{t}_r, \mathcal{t}_r + \mathcal{T}_r]$ where $w(t)$ is the windowing function. Targeting (3.4) in lieu of the signal's exact FT, i.e. $X(f) = \int_{-\infty}^{+\infty} x(t)e^{-j2\pi ft}dt$, was referred to the impracticality of requesting an infinitely long time analysis window [96, 98, 101]. Masry [98, 101] improved the accuracy of estimating the spectrum in (3.4) by deploying sampling schemes other than the total random sampling in the original paper by Tarczynski [96]. Whilst [96, 98, 101] prompted our interest in the use of randomised sampling techniques, the signals handled here are random processes (either stationary or cyclostationary). Consequently, the required analysis fundamentally differs from that in [96, 98, 101].

Although the earliest papers on randomised sampling [90-92] treated the problem of estimating the PSD of wide sense stationary signals, they did not resolve the predicament of the estimator's accuracy for a finite number of samples. This issue was partially addressed by Masry in [93, 94, 104, 113] where the expressions for the estimator's bias and variance are provided under the assumption that the number of processed samples tends to infinity. In this research, the estimation of the signal's exact power spectral density is not the objective and an estimate of a frequency representation (not necessarily the exact PSD) that allows detecting the active spectral subbands is sufficient. We examine the statistical characteristics of the performed spectral analysis, such as the estimators' accuracies, from a finite set of samples in contrary to [92-94, 104, 113] where asymptotic consistency expressions are given. Besides, randomised sampling methods other than the ones investigated in [90-94, 104, 113] are studied.

Wojtiuk [3] has put a remarkable effort into assessing the PSD of randomly sampled data assuming that the processed and sampling signals are ergodic. The PSD of the sampled signal is given by: $\Phi_X^d(f) = \Phi_X(f) * \Phi_S(f)$ where $\Phi_S(f)$ is the power spectral density of an infinitely long ideal sampling signal. Wojtiuk derived the analytical expressions of $\Phi_S(f)$ and $\Phi_X^d(f)$ for a number of schemes, namely additive random sampling and

jittered random sampling. He cited other existing expressions for these schemes noting the discrepancies in the final formulas, e.g. by Martin [2], Marvasti [45] and Shapiro & Silverman [90]. However, Wojtiuk claimed that his expressions are the only ones verified by measured/simulated spectra by using the periodogram in (3.1) from a finite number of nonuniformly distributed samples. The response, characteristics and most importantly the accuracy of the estimation process were not scrutinised in [3] in order to validate the conducted measurements/simulations. Here, spectrum estimators are proposed and their behaviours are assessed for a finite set of samples captured at relatively low rates. An important observation can be made from the formulas provided in [3]. The PSD of the sampled signal is never equal to that of the underlying continuous-time one for a finite sampling frequency. This implies that aliasing is not completely eliminated by randomly sampling the incoming signal. It is suppressed based on the characteristics of the sampling scheme. This deficiency does not necessarily hinder the usefulness of the randomised sampling for the pursued spectrum sensing as shown in this chapter.

3.2 The Adopted Periodogram-type Estimator and its Accuracy

The adopted periodogram-type estimators of a detectable frequency representation of the received simultaneous transmissions are defined by:

$$X_e(\mathcal{t}_r, f) = \mathcal{G}\left|\sum_{n=1}^{N} y(t_n)w(t_n)e^{-j2\pi ft_n}\right|^2 \tag{3.5}$$

where $\mathcal{G}$ is a constant dependent on the sampling scheme. Whereas, N is the number of the captured samples at the irregular time instants $\{t_n\}_{n=1}^{N}$ within the time analysis window $\mathcal{T}_r$ starting at $\mathcal{t}_r$ and is of width T_0. The windowing function $w(t)$ is aligned with $\mathcal{T}_r$. It is noted that periodograms have retained their popularity in recent spectrum sensing studies such as [17, 18, 20, 114-118].

The incoming multiband signal $x(t)$ is assumed to be zero mean and wide sense stationary. It is contaminated with zero mean AWGN with variance P_N, i.e. $y(t_n) = x(t_n) + n(t_n)$ for $n = 1,2,\ldots,N$ are the collected samples of the received signal. Although communication signals are known to be of a cyclostationary nature, phase randomisation is a widely adopted technique to stationarise the process whenever its cyclic frequency is not of an

interest [49-51]. Assuming pseudostationarity of such signals within a short time analysis window is another technique that is commonly used, e.g. [16, 114]. This premise brings notable simplifications to the analysis of such stochastic processes.

Martin [2, p.38] and Scargle [76] listed the deficiencies of the periodogram spectral analysis tool in nonuniform sampling environments, namely spectral leakage, aliasing and inconsistency. Nevertheless, in this research we deploy several measures to combat such drawbacks and appropriate periodograms to the handled problem, i.e. spectrum sensing and not PSD estimation. They include:

- Windowing: a windowing function $w(t)$ is introduced to minimise the spectral leakage originating from the use of a time analysis window of finite length.
- Randomised sampling: selected sampling schemes are employed to enable the suppression of spectrum aliasing, permitting the detection of the signal(s) presence.
- Estimate averaging: a number of (3.5) estimates calculated from a number of signal windows are averaged to improve the estimator's performance, e.g. [49, 107, 108].

The appropriateness of (3.5) for the detection task is determined by its expected value, in other words: is $X_e(\not{t}_r, f)$ an unbiased estimator of a detectable spectrum representation of the transmitted signal(s)? Even if the answer is positive, the estimator's accuracy for a single realisation of $x(t)$ should be examined. To ensure that the spectrum sensing is accomplished whilst meeting some predefined detection probabilities (such as success rates), the estimation process should be completed with certain level of confidence. Chebychev's double-sided inequality states that:

$$\Pr\left\{\left|X-\bar{X}\right| \geq \kappa\sigma_X\right\} \leq 1/\kappa^2 \tag{3.6}$$

where X is a random variable, $\bar{X} = E[X]$, σ_X^2 is the variable's variance and $\kappa > 0$ [103]. Hence the discrepancy in the estimation process given by:

$$\Lambda(\not{t}_r, f) = \left|E\left[X_e(\not{t}_r, f)\right] - X_e(\not{t}_r, f)\right| \tag{3.7}$$

is directly related to the standard deviation of (3.5). The difference in (3.7) should be controlled by restraining the estimator's variance in order to predict/achieve the sought response of the sensing procedure.

Therefore, the variance gives a clear indication of the estimator's accuracy. As mentioned in §3.1.2, the standard deviation of a periodogram-type estimator is known to be of the same order as its expected value [49]. To reduce this uncertainly, we average a K number of the $X_e(\mathcal{t}_r, f)$ estimates calculated over K signal windows, i.e. $\sum_{r=1}^{K} X_e(\mathcal{t}_r, f) \big/ K$. This evokes shifting $\mathcal{T}_r$ and the repositioning/aligning of $w(t)$.

Evidently, the behaviour of (3.5) is governed by a number of factors including:

1) The randomised sampling scheme and its characteristics
2) The power of the present signal and noise
3) The width of the analysis window and the windowing function
4) The nature of the processed random signals, e.g. stationary or nonstationary
5) The number of averaged spectrum estimates

In this chapter, we consider the first two points and the processed signal is assumed to be wide sense stationary in order to focus on the features of SARS and its suitability for detecting the present spectral components. In Chapter 4 we explore the impact of processing cyclostationary signals on $X_e(\mathcal{t}_r, f)$, whilst the effects of T_0 and estimate averaging are addressed in Chapter 5.

In the following sections, the statistical characteristics of (3.5) for the total random sampling, random sampling on grid and stratified/jittered sampling schemes are derived.

3.3 Total Random Sampling (TRS)

The properties of the TRS scheme were outlined in §2.3.3. We consider the form of total random sampling where the PDF of the sample points is uniformly distributed within the time analysis window $\mathcal{T}_r$, i.e. $p_n(t) = 1/T_0$ for $t \in \mathcal{T}_r$ and zero elsewhere. Its periodogram-type estimator is defined by:

$$X_{e,TRS}(\mathcal{t}_r, f) = \frac{N}{(N-1)\mu} \left| \frac{T_0}{N} \sum_{n=1}^{N} y(t_n) w(t_n) e^{-j2\pi f t_n} \right|^2 \tag{3.8}$$

where

$$\mu = \int_{\mathcal{t}_r}^{\mathcal{t}_r + \mathcal{T}_r} w^2(t) dt \tag{3.9}$$

is the energy of the windowing function.

3.3.1 Estimator's Expected Value and Accuracy for TRS

Since the sample points $\{t_n\}_{n=1}^{N}$ in (3.8) are Independent Identically Distributed (IID) random variables, it can be shown that (see Appendix A):

$$E\left[X_{e,TRS}(\mathcal{t}_r,f)\middle|x(t)\right]=\frac{N}{(N-1)\mu\alpha}\left[\int_{\mathcal{t}_r}^{\mathcal{t}_r+T_0}x^2(t)w^2(t)dt+\mu P_N\right]+\frac{1}{\mu}\left|X_W(\mathcal{t}_r,f)\right|^2 \quad (3.10)$$

where the average sampling rate is $\alpha = N/T_0$ and P_N is the power of the present AWGN. This leads to:

$$C_{TRS}(f)=E\left[X_{e,TRS}(\mathcal{t}_r,f)\right]=\frac{N}{(N-1)\alpha}\left(P_S+P_N\right)+\frac{1}{\mu}\Phi_X(f)*\left|W(f)\right|^2 \quad (3.11)$$

where $P_S=E\left[x^2(t)\right]$ is the signal power and $E\left[\left|X_W(\mathcal{t}_r,f)\right|^2\right]=\Phi_X(f)*\left|W(f)\right|^2$ is the scaled expected value of a classical continuous-time periodogram [49] such that:

$$W(f)=\int_{-\infty}^{+\infty}w(t)e^{-j2\pi ft}dt\,. \quad (3.12)$$

It can be noticed from (3.11) that the estimator's expected value is time-invariant and is independent of $\mathcal{t}_r$. The bias of the estimator in terms of the windowed signal PSD, i.e. the first term in (3.11), is constant and frequency independent. Assuming that the analysis period T_0 is long enough, the windowed PSD forms an identifiable feature. Consequently, $C_{TRS}(f)$ comprises a detectable component $\Phi_X(f)*\left|W(f)\right|^2/\mu$ plus a constant offset $N(P_S+P_N)/\left[(N-1)\alpha\right]$. The $NP_S/\left[(N-1)\alpha\right]$ term represents the phenomenon previously referred to as *smeared-aliasing* originating from the irregularly spaced samples. It is a white-noise-like component present at all frequencies for the TRS scheme. Therefore, $X_{e,TRS}(\mathcal{t}_r,f)$ given by (3.8) is an unbiased estimator of $C_{TRS}(f)$ which is a detectable frequency representation of the incoming signal regardless of the sampling rate. Despite the fact that the constant offset in (3.11) does not have a visible effect on the detectable feature(s) of $C_{TRS}(f)$, it causes a deterioration in the spectrum dynamic range as discussed in §3.6.

Although $X_{e,TRS}(\mathcal{t}_r,f)$ is an unbiased estimator of $C_{TRS}(f)$, it will be an adequate tool for assessing the activity of the monitored subbands only if the difference:

$\Lambda_{TRS}(\not{t}_r, f) = \left| C_{TRS}(f) - X_{e,TRS}(\not{t}_r, f) \right|$ in (3.7) is small. Below, we present the variance expression for $X_{e,TRS}(\not{t}_r, f)$ in order to quantify its accuracy in light of (3.6) (the detailed derivations are shown in Appendix A). The variance is defined by:

$$\sigma^2_{e,TRS}(f) = \text{var}\left\{ X_{e,TRS}(\not{t}_r, f) \right\} = \left[\frac{N}{(N-1)\mu} \right]^2 \text{var}\left\{ \left| \frac{T_0}{N} \sum_{n=1}^{N} y(t_n) w(t_n) e^{-j2\pi f t_n} \right|^2 \right\} \quad (3.13)$$

and is independent of $\not{t}_r$ which is omitted thereafter to simplify the notation. First let,

$$\left| X_{WS}(f) \right|^2 = \left| \frac{T_0}{N} \sum_{n=1}^{N} y(t_n) w(t_n) e^{-j2\pi f t_n} \right|^2 = \tilde{R}^2_{WS}(f) + \tilde{I}^2_{WS}(f) \quad (3.14)$$

where $\tilde{R}_{WS}(f)$ and $\tilde{I}_{WS}(f)$ represent the real and imaginary parts of $X_{WS}(f)$. Each of the zero mean $\tilde{R}_{WS}(f)$ and $\tilde{I}_{WS}(f)$ consist of the sum of N independent identically distributed random variables $\forall f$. According to the Central Limit Theorem (CLT), they can be approximated by normal distribution for sufficiently large N [52], i.e. $\tilde{R}_{WS}(f) \sim \mathcal{N}\left(E\left[\tilde{R}_{WS}(f) \right], \sigma^2_{\tilde{R}_{WS}}(f) \right)$ and $\tilde{I}_{WS}(f) \sim \mathcal{N}\left(E\left[\tilde{I}_{WS}(f) \right], \sigma^2_{\tilde{I}_{WS}}(f) \right)$. In practice, moderate N values suffice for such an approximation [48, 52], e.g. $N \geq 30$ is perceived as sufficient in [15, 52, 114]. This normality requirement is reasonable as the number of the processed samples typically exceeds the aforementioned limit. It is shown in Appendix A that $\tilde{R}_{WS}(f)$ and $\tilde{I}_{WS}(f)$ are dependent for certain frequencies. Nonetheless, they can be replaced with independent ones without altering (3.8) in order to ascertain that (3.14) and subsequently (3.8) have approximately a chi-squared distribution with two degrees of freedom. We can write: $\left| X_{WS}(f) \right|^2 = \left| X_{WS}(f) e^{j\theta_{TRS}(f)} \right|^2 = R^2_{WS}(f) + I^2_{WS}(f)$, where $R_{WS}(f)$ and $I_{WS}(f)$ are the phase-shifted uncorrelated versions of $\tilde{R}_{WS}(f)$ and $\tilde{I}_{WS}(f)$ respectively such that:

$$R_{WS}(f) = T_0 \sum_{n=1}^{N} y(t_n) w(t_n) \cos\left(2\pi f t_n - \theta_{TRS}(f) \right) / N \quad (3.15)$$

$$I_{WS}(f) = T_0 \sum_{n=1}^{N} y(t_n) w(t_n) \sin\left(2\pi f t_n - \theta_{TRS}(f) \right) / N \,. \quad (3.16)$$

Using the characteristics of un-normalised chi-squared distribution [103], we get:

$$\sigma^2_{e,TRS}(f) = \mathrm{var}\left\{X_{e,TRS}(\mathcal{t}_r, f)\right\} = 2\left[\frac{N}{(N-1)\mu}\right]^2 \left[\sigma^4_{R_{WS}}(f) + \sigma^4_{I_{WS}}(f)\right] \tag{3.17}$$

where

$$\sigma^2_{R_{WS}}(f) = E\left[R^2_{WS}(f)\right] = \frac{(P_S + P_N)E_{WC}(f)}{\alpha} + \frac{N-1}{N}\lambda_R(f) \tag{3.18}$$

$$E_{WC}(f) = \int_{\mathcal{t}_r}^{\mathcal{t}_r+T_0}\left[w(t)\cos\left(2\pi ft - \theta_{TRS}(f)\right)\right]^2 dt \tag{3.19}$$

$$\lambda_R(f) = \int_{\mathcal{T}_r}\int_{\mathcal{T}_r} R_X(t_1 - t_2)w(t_1)w(t_2)\cos\left(2\pi ft_1 - \theta_{TRS}(f)\right)\cos\left(2\pi ft_2 - \theta_{TRS}(f)\right)dt_1 dt_2 \tag{3.20}$$

$$\sigma^2_{I_{WS}}(f) = E\left[I^2_{WS}(f)\right] = \frac{(P_S + P_N)E_{WS}(f)}{\alpha} + \frac{N-1}{N}\lambda_I(f) \tag{3.21}$$

$$E_{WS}(f) = \int_{\mathcal{t}_r}^{\mathcal{t}_r+T_0}\left[w(t)\sin\left(2\pi ft - \theta_{TRS}(f)\right)\right]^2 dt \tag{3.22}$$

$$\lambda_I(f) = \int_{\mathcal{T}_r}\int_{\mathcal{T}_r} R_X(t_1 - t_2)w(t_1)w(t_2)\sin\left(2\pi ft_1 - \theta_{TRS}(f)\right)\sin\left(2\pi ft_2 - \theta_{TRS}(f)\right)dt_1 dt_2 \tag{3.23}$$

such that $R_X(\tau) = E\left[x(t)x(t+\tau)\right]$ is the autocorrelation function of the WSS process. The introduced phase-shift $\theta_{TRS}(f)$ is defined by:

$$\theta_{TRS}(f) = 0.5\mathrm{arccot}\left(\frac{E\left[\tilde{R}^2_{WS}(f)\right] - E\left[\tilde{I}^2_{WS}(f)\right]}{2\zeta_{TRS}(f)}\right). \tag{3.24}$$

It can be easily seen that $E\left[\tilde{R}^2_{WS}(f)\right]$ and $E\left[\tilde{I}^2_{WS}(f)\right]$ are identical to (3.18) and (3.21) respectively such that $\theta_{TRS}(f)$ is discarded from their corresponding terms. Whereas,

$$\zeta_{TRS}(f) = \frac{(P_S + P_N)\int_{\mathcal{T}_r} w^2(t)\cos(2\pi ft)\sin(2\pi ft)dt}{\alpha} + \frac{N-1}{N}\lambda_{RI}(f) \tag{3.25}$$

$$\lambda_{RI}(f) = \int_{\mathcal{T}_r}\int_{\mathcal{T}_r} R_X(t_1 - t_2)w(t_1)w(t_2)\cos(2\pi ft_1)\sin(2\pi ft_2)dt_1 dt_2\ . \tag{3.26}$$

From (3.17)-(3.23), it can be recognised that the value of $\sigma^2_{e,TRS}(f)$ declines as α increases; in particular the parts related to the first term in each of (3.18) and (3.21). They debilitate upon increasing the sampling rate enhancing the accuracy of the estimator where there is no spectral activity related to the processed signal. On the other hand, a substantial

part of $\sigma^2_{e,TRS}(f)$ incorporating $\lambda_R(f)$ and $\lambda_I(f)$ is unaffected by the sampling rate and is concentrated at the active spectral subbands. As N tends to infinity, the estimator's variance $\sigma^2_{e,TRS}(f)$ does not diminish analogous to the uniform sampling periodogram in (3.1). A K number of $X_{e,TRS}(t_r, f)$ estimates are averaged, a measure we explore in Chapter 5, to control the possible perturbations/anomalies in the $C_{TRS}(f)$ estimation. The two parameters α and K are the available means to curb $\Lambda_{TRS}(f)$ and ensure that the estimation/sensing procedure is performed with a certain level of confidence.

Below, we give numerical examples to demonstrate the accuracy of the developed analytical expressions for the total random sampling scheme.

3.3.2 Numerical Examples on TRS

Consider a multiband system operating over $L = 20$ disjointed contiguous spectral subbands occupying the frequency range $f_{\min} = 1.45\,\text{GHz}$ and $f_{\min} + B = 1.55\,\text{GHz}$, i.e. the monitored frequency range is $\mathcal{B} = [f_{\min}, f_{\min} + B]$. The width of each of the system subbands is $B_C = 5\,\text{MHz}$ and their joint width (the processed bandwidth) is $B = 100\,\text{MHz}$. If no previous knowledge of the activity of the system subbands is available, a low valid uniform sampling rate that would avoid spectrum aliasing with $\mathcal{B}$ is 222 MHz (using bandpass sampling technique). If the signal is down-converted *a priori* to sampling, the admissible uniform sampling rates are $f_{US} \geq 200\,\text{MHz}$. Alternatively, an average sampling rate of $\alpha = 65\,\text{MHz}$ is selected for the TRS scheme. A signal analysis window of width $T_0 = 10\,\mu\text{s}$ is used where a Blackman windowing function is utilised. AWGN is present and the Signal-to-Noise Ratio (SNR) is $-1\,\text{dB}$. The PSD of the continuous-time incoming multiband signal is depicted in Figure 3.1. Figure 3.2a shows $C_{TRS}(f) = E\left[X_{e,TRS}(t_r, f)\right]$ defined in (3.11) and the statistical mean obtained from 10,000 independent experiments. Whilst, Figure 3.2b exhibits the estimator's variance $\sigma^2_{e,TRS}(f)$ as given in (3.17)-(3.26) and the Mean Squared Error (MSE) attained from the aforementioned experiments.

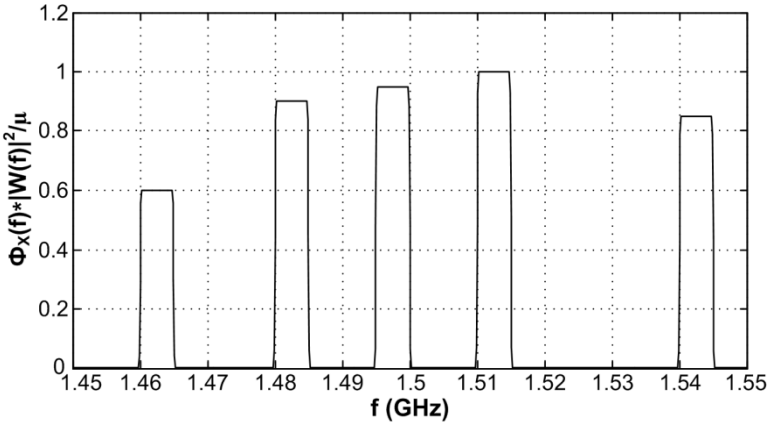

Figure 3.1: The PSD of the transmitted test signal.

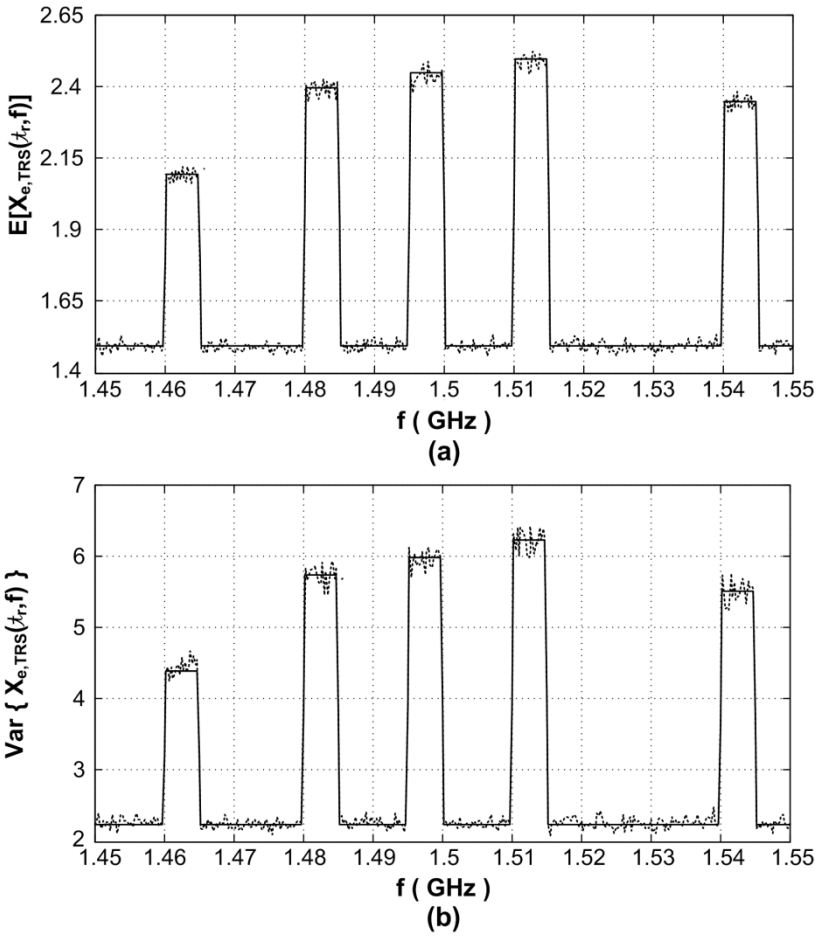

Figure 3.2: The mean and variance of the TRS estimator from the derived analytical formulas (solid lines) and simulations (dotted lines). (a) $C_{TRS}(f)$ from equation (3.11) and the statistical/experimental mean. (b) Estimator's variance from equations (3.17)-(3.26) and the MSE.

Both Figures 3.2a and 3.2b confirm that there is good match between the theoretical analysis and simulations which vindicates the accuracy of derived formulas. This implies

that the normality assumption did not have a noticeable effect on the results. It is clear from Figure 3.2a that $C_{TRS}(f)$ is an adequate spectrum representation for the detection pursuit. If uniform sampling was deployed at a similar rate, the spectrum of the sampled signal would include identical displaced replicas of the spectral components of the underlying continuous-time one. They would emerge within $\mathscr{B}$ and be indistinguishable from those of the analogue signal. For example, a copy of the component with the central frequency $f_C = 1.5425\,\text{GHz}$ would appear at $1.4775\,\text{GHz}$ if $f_{US} = 65\,\text{MHz}$. In this case, identifying the active subbands is feasible only if the signal spectral support is known. On the other hand, TRS suppressed aliasing in its classical sense and allowed detecting the presence of an activity in the corresponding subbands with a notably low sampling rate. This demonstrates the ability of the TRS scheme in conjunction with the adopted estimator to suppress aliasing. In fact, extending the monitored frequency range beyond $\mathscr{B}$ would not affect the detectability of the active subbands unlike the uniform sampling case where f_{US} grows proportional to B. Figure 3.3 shows $E\left[X_{e,TRS}(t_r, f)\right]$ for $f \in [1,2]\,\text{GHz}$ where $SNR = -1\,\text{dB}$, e.g. the sampling is preceded by a filter limiting the noise bandwidth.

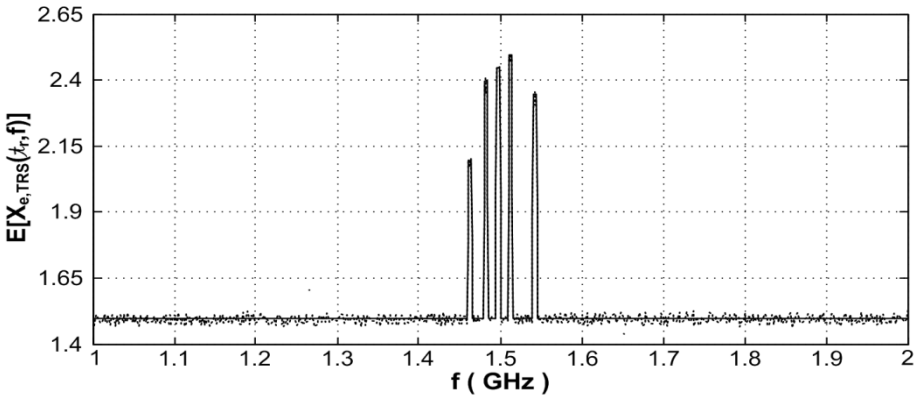

Figure 3.3: $E\left[X_{e,TRS}(t_r, f)\right]$ for $f \in [1,2]$ GHz, $SNR = -1\,\text{dB}$ and $\alpha = 65\,\text{MHz}$. From equations (solid line) and simulations (dotted line).

Increasing the sampling rate is one of the means available to restrain (to an extent) the $C_{TRS}(f)$ estimation inaccuracies from a single realisation of the incoming signal, i.e. $\Lambda_{TRS}(t_r, f)$. Figure 3.4 exhibits $\sigma^2_{e,TRS}(f_C)$ for a varying average sampling rate where $f_C = 1.4975$ GHz is the central frequency of the middle active subband in Figure 3.1. It can be seen from the figure that the variance declines but does not vanish as α increases; it

settles to a nearly constant level. This is due to the fact that a substantial part of $\sigma^2_{e,TRS}(f)$ is unaffected by the average sampling rate. Estimate averaging is utilised later in the thesis to ensure that the estimation and detection procedures meets the sought performance.

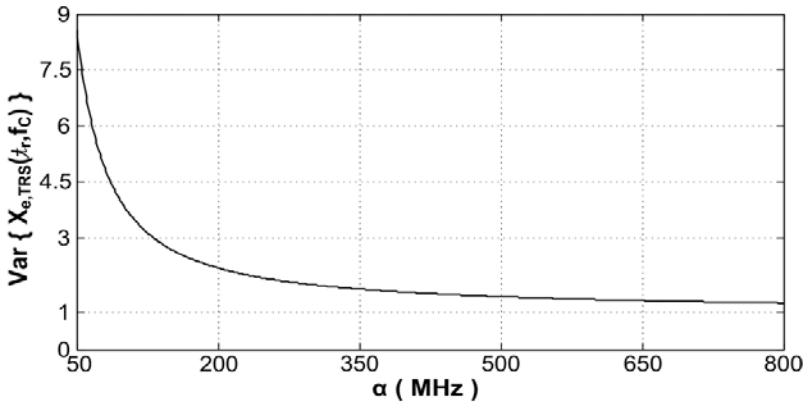

Figure 3.4: Variance of the TRS estimator at $f_C = 1.4975\,\text{GHz}$ for a varying average sampling rate.

3.4 Random Sampling on Grid (RSG)

Despite the capability of the total random sampling scheme to alleviate the spectrum aliasing limitations even for arbitrarily low average sampling rates, theoretically any two or more of its sample points can be arbitrarily close. This imposes infinitely high instantaneous sampling frequencies, i.e. TRS requests infinitely fast data acquisition device(s). Early work on randomised sampling, which was limited to power spectral density estimation, used sampling schemes that suffered from a similar defect, e.g. additive random sampling with Poisson distribution [90-94, 104, 113].

Random sampling on grid described in §2.3.3 provides safeguards by retaining a minimum distance between any two points in the sampling sequence (see Figure 2.5). The possible sample positions are limited to an underlying uniformly distributed time locations. The density of the uniform grid, which encompasses N_g grid points, is set by the rate f_g. Each of the grid points can be selected only once with equal probability. Hence RSG, unlike a number of randomised sampling schemes such as TRS, offers solutions that are well suited for practical implementation in hardware. The periodogram-type estimator for the RSG scheme is defined by:

$$X_{e,RSG}(t_r, f) = \frac{(N_g - 1)T_0}{N(N-1)\mu_d} \left| \sum_{n=1}^{N} y(t_n) w(t_n) e^{-j2\pi f t_n} \right|^2 \tag{3.27}$$

where

$$\mu_d = \sum_{n=1}^{N_g} w^2(nT_g) \tag{3.28}$$

noting that the N_g nominated uniformly distributed time instants are placed within the time analysis window $\mathcal{T}_r = [t_r, t_r + T_0]$. In the next subsection, we show that the estimator in (3.27) is a suitable tool for DASP provided an appropriately chosen grid density. The detailed derivations of the RSG equations are presented in Appendix B.

3.4.1 Estimator's Expected Value and Accuracy for RSG

By introducing a random variable c_n which takes a value of "1" if the *n-th* grid point is considered and "0" otherwise, it can be shown that:

$$E\left[X_{e,RSG}(t_r, f) \middle| x(t) \right] = \frac{(N_g - N)T_0}{(N-1)N_g\mu_d} \sum_{n=1}^{N_g} x^2(nT_g)w^2(nT_g) + \frac{(N_g - 1)T_0P_N}{(N-1)N_g} + \frac{\left|X_W^d(t_r, f)\right|^2}{f_g\mu_d} \tag{3.29}$$

such that

$$X_W^d(t_r, f) = \sum_{n=1}^{N_g} x(nT_g)w(nT_g)e^{-j2\pi fnT_g} \tag{3.30}$$

is the discrete-time Fourier transform of the processed signal. Thus:

$$C_{RSG}(f) = E\left[X_{e,RSG}(t_r, f) \right] = \frac{(N_g - N)T_0P_S + (N_g - 1)T_0P_N}{(N-1)N_g} + \frac{T_0E\left[\left|X_W^d(t_r, f)\right|^2 \right]}{N_g\mu_d} \tag{3.31}$$

where $P_S = E\left[x^2(nT_g) \right]$ and P_N are the signal and AWGN powers respectively. It can be noticed that $C_{RSG}(f)$ comprises a constant frequency independent component, i.e. the first term in (3.31), in addition to a frequency representation of the signal. Ultimately, the adequacy of $X_{e,RSG}(t_r, f)$ for unveiling the activity of the monitored spectral subbands relies on the second term of (3.31). The latter is the expected value of a scaled conventional uniform sampling periodogram [49]. It can be shown that $E\left[\left|X_W^d(t_r, f)\right|^2 \right] = \Phi_X^d(f) * \left|W(f)\right|^2$ where $\Phi_X^d(f)$ is the PSD of the Discrete-time (DT) signal and is given by:

$$\Phi_X^d(f) = f_g \sum_{k=-\infty}^{+\infty} \Phi_X(f - kf_g) . \tag{3.32}$$

The $\Phi_X(f)$ is the PSD of the incoming continuous-time multiband signal $x(t)$. Provided that f_g is chosen appropriately, $X_{e,RSG}(\not{t}_r, f)$ which is an unbiased estimator of $C_{RSG}(f)$ poses as a legitimate tool for revealing the active spectral components in the received signal regardless of the used average sampling rate. The grid frequency is selected such that only one copy of the windowed PSD of the continuous-time signal appears within the monitored frequency range $\mathcal{B}$ according to (3.32), i.e. $\Phi_X(f)\Phi_X(f-kf_g)=0$ if $k\neq 0$ where $k\in\mathbb{Z}$. If the received signal is down-converted to baseband, the grid sampling frequency f_g should comply with Nyquist criterion, i.e. $f_g \geq 2B$ (B is the bandwidth of the overseen spectrum range). Nonetheless, the underlying grid density can be set employing the bandpass sampling technique [31].

It is noted that the estimator in (3.27) does not demand knowledge of the signal's PSD. The underlying grid rate f_g is dictated by the width and the position of the examined frequency range which is presumed to be foreknown.

From (3.31) and (3.32), it can be seen that the use of RSG limits the range of surveyed frequencies based on f_g. For TRS, we do not have such a constraint due to the scheme's aliasing-suppression property for all frequencies. RSG exhibits similar potential, but rather confined to the predefined monitored spectral subbands for a commensurate f_g value.

We recall that the variance is a crucial factor that gives an insight into the accuracy of the $C_{RSG}(f)$ estimation. Calculating the variance equips the user with the means to evaluate the estimator's accuracy and guarantee its performance by taking the necessary measures. We have:

$$\sigma^2_{e,RSG}(f)=\operatorname{var}\left\{X_{e,RSG}(\not{t}_r,f)\right\}=\left[\frac{(N_g-1)}{(N-1)\mu}\right]^2\operatorname{var}\left\{\left|X_{RG}(f)\right|^2\right\} \tag{3.33}$$

where $\left|X_{RG}(f)\right|^2=R^2_{RG}(f)+I^2_{RG}(f)$, $R_{RG}(f)=\sum_{n=1}^{N}y(t_n)w(t_n)\cos\left(2\pi ft_n-\theta_{RSG}(f)\right)$ and $I_{RG}(f)=\sum_{n=1}^{N}y(t_n)w(t_n)\sin\left(2\pi ft_n-\theta_{RSG}(f)\right)$. For large N and $N_g >> N$, $R_{RG}(f)$ and $I_{RG}(f)$ can be approximated by a normal distribution according to the CLT. Moderate values of N are typically considered to be sufficient in practical cases [52, 103]. Consequently, the variance of $X_{e,RSG}(\not{t}_r,f)$ reduces to:

$$\sigma^2_{e,RSG}(f) = \mathrm{var}\left\{X_{e,RSG}(\mathscr{t}_r, f)\right\} = 2\left[\frac{(N_g - 1)T_0}{(N-1)N\mu_d}\right]^2 \left[\sigma^4_{R_{RG}}(f) + \sigma^4_{I_{RG}}(f)\right] \quad (3.34)$$

utilising the unnormalised chi-squared distribution characteristics where:

$$\sigma^2_{R_{RG}}(f) = E\left[R^2_{RG}(f)\right] = \frac{NE^d_{WC}(f)}{N_g}\left[\frac{(N_g - N)P_S}{(N_g - 1)} + P_N\right] + \frac{N(N-1)}{N_g(N_g-1)}\lambda^d_R(f) \quad (3.35)$$

$$\sigma^2_{I_{RG}}(f) = E\left[I^2_{RG}(f)\right] = \frac{NE^d_{WS}(f)}{N_g}\left[\frac{(N_g - N)P_S}{(N_g - 1)} + P_N\right] + \frac{N(N-1)}{N_g(N_g-1)}\lambda^d_I(f) \quad (3.36)$$

$$E^d_{WC}(f) = \sum\nolimits_{n=1}^{N_g} w^2(nT_g)\cos^2\left(2\pi fnT_g - \theta_{RSG}(f)\right) \quad (3.37)$$

$$\lambda^d_R(f) = \sum_{n=1}^{N_g}\sum_{m=1}^{N_g} R_X(nT_g - mT_g)w(nT_g)w(mT_g)\cos\left(2\pi fnT_g - \theta_{RSG}(f)\right) \times\cos\left(2\pi fmT_g - \theta_{RSG}(f)\right) \quad (3.38)$$

$$E^d_{WS}(f) = \sum\nolimits_{n=1}^{N_g} w^2(nT_g)\sin^2\left(2\pi fnT_g - \theta_{RSG}(f)\right) \quad (3.39)$$

and

$$\lambda^d_I(f) = \sum_{n=1}^{N_g}\sum_{m=1}^{N_g} R_X(nT_g - mT_g)w(nT_g)w(mT_g)\sin\left(2\pi fnT_g - \theta_{RSG}(f)\right) \times\sin\left(2\pi fmT_g - \theta_{RSG}(f)\right) \quad (3.40)$$

such that $R_X(nT_g - mT_g)$ represents the DT autocorrelation function of the processed signal. The phase-shift $\theta_{RSG}(f)$ is introduced into (3.34)-(3.40) such that the zero mean $R_{RG}(f)$ and $I_{RG}(f)$ are independent $\forall f$, i.e. $E\left[R_{RG}(f)I_{RG}(f)\right] = 0$. Then,

$$\theta_{RSG}(f) = 0.5\mathrm{arccot}\left(\left\{E\left[\tilde{R}^2_{RG}(f)\right] - E\left[\tilde{I}^2_{RG}(f)\right]\right\} \Big/ 2\zeta_{RSG}(f)\right) \quad (3.41)$$

where $E\left[\tilde{R}^2_{RG}(f)\right]$ and $E\left[\tilde{I}^2_{RG}(f)\right]$ are identical to (3.35) and (3.36) respectively such that $\theta_{RSG}(f)$ is omitted from (3.37)-(3.40) as $\tilde{R}_{RG}(f) = \sum\nolimits_{n=1}^{N} y(t_n)w(t_n)\cos\left(2\pi ft_n\right)$ and $\tilde{I}_{RG}(f) = \sum\nolimits_{n=1}^{N} y(t_n)w(t_n)\sin\left(2\pi ft_n\right)$. Whereas,

$$\zeta_{RSG}(f) = \frac{N\sum\limits_{n=1}^{N_g} w^2(nT_g)\cos(2\pi fnT_g)\sin(2\pi fnT_g)}{N_g}\left[\frac{(N_g - N)P_S}{(N_g - 1)} + P_N\right] + \frac{N(N-1)\lambda^d_{RI}(f)}{N_g(N_g-1)} \quad (3.42)$$

and

$$\lambda_{RI}^{d}(f)=\sum_{n=1}^{N_g}\sum_{m=1}^{N_g}R_X(nT_g-mT_g)w(nT_g)w(mT_g)\cos\left(2\pi fnT_g\right)\sin\left(2\pi fmT_g\right). \tag{3.43}$$

By scrutinising (3.34)-(3.36), it can be seen that a higher average sampling rate leads to minimising the variance of the estimator. Moreover, increasing the grid rate f_g results in deterioration in the estimator's accuracy. These two observations are illustrated in the following numerical example where we demonstrate the suitability of $X_{e,RSG}(t_r,f)$ for a low sampling rate spectrum sensing procedure and verify the accuracy of the derived expressions via simulations. For instance, we establish that the normality assumption for a finite N does not have a noticeable impact on the accuracy of the conducted analysis.

3.4.2 RSG Simulations

Here we study the same multiband system described in §3.3.2 where the PSD of the received test signal is depicted in Figure 3.1. A Hanning window of width $T_0=8\mu$s is utilised and the SNR is -1 dB. The signal is down-converted to baseband prior to sampling, i.e. baseband processing. As a result, the processed bandwidth is $f\in[-100,100]$ MHz where the active spectral subbands of the analogue signal now reside in $f\in\pm[10,15]\cup\pm[30,35]\cup\pm[45,50]\cup\pm[60,65]\cup\pm[90,95]$ MHz. An average sampling rate of $\alpha=60$ MHz is selected which is significantly lower than $f_{US}\geq 200$ MHz. A grid sampling frequency of $f_g=250$ MHz is applied; it is satisfactory according to (3.32) as $\Phi_X(f)\Phi_X(f-kf_g)=0$ if $k\neq 0$ (k is an integer). Figure 3.5 exhibits $C_{RSG}(f)$ in (3.31) and $\sigma^2_{e,RSG}(f)$ defined in (3.34)-(3.43) versus the estimator's experimental/statistical mean and mean squared error respectively. The latter two are obtained from 10000 independent experiments.

As seen in Figure 3.5, $C_{RSG}(f)$ is an adequate spectral representation for the detection pursuit. If uniform sampling was deployed at a similar rate, aliasing would have resulted in the unfolding of the active subbands replicas into the monitored bandwidth. This would make a correct detection decision unfeasible. RSG suppressed aliasing in its classical sense within the overseen frequency range and allowed exposing the activity of the system subbands. This demonstrates the potential of this sampling scheme to eliminate the spectrum aliasing constraints within a finite spectral region mandated by the grid density.

Besides, it can be recognised from Figures 3.5a and 3.6b that the analytical and experimental results coincide which ascertains the accuracy of the developed formulas.

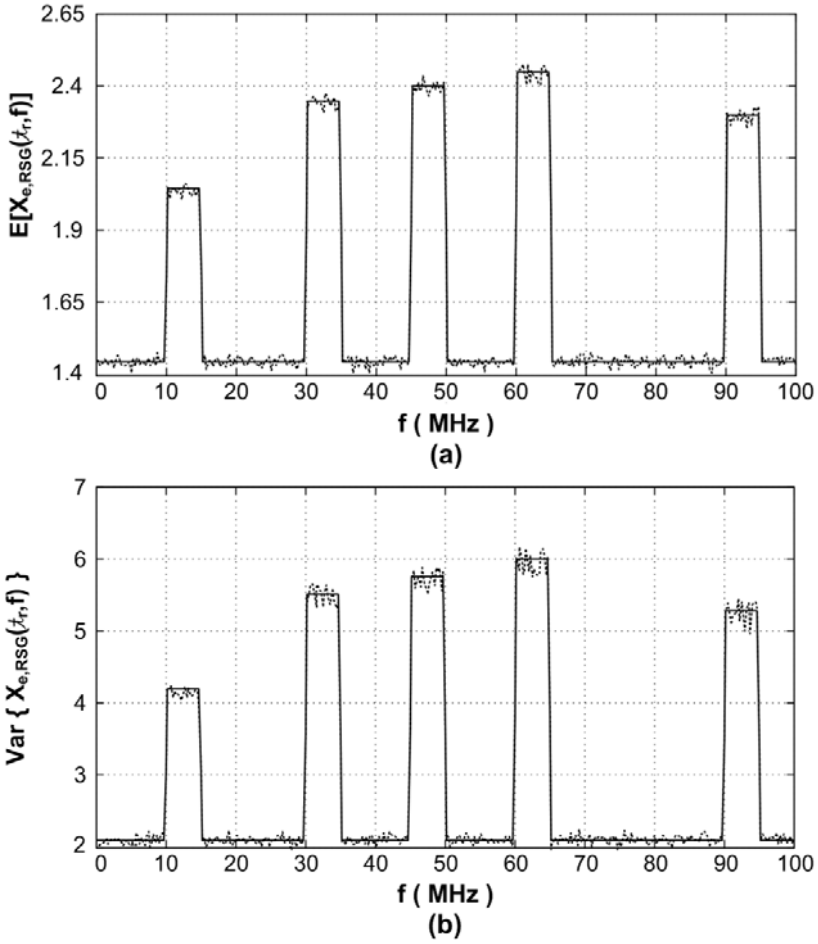

Figure 3.5: The mean and the variance of the RSG estimator from equations (solid lines) and simulations (dotted lines). (a) $C_{RSG}(f)$ from equation (3.31) and the experimental mean. (b) $\sigma^2_{RSG}(f)$ from equations (3.34)-(3.43) and MSE from simulations.

To show the effect of α and f_g on the estimator's accuracy, $\sigma^2_{e,RSG}(f_C)$ is depicted in Figure 3.6 for various sampling frequencies and permissible grid densities. The frequency point $f_C = 47.5\,\text{MHz}$ is the central frequency of the active subband located in the $[45,50]\,\text{MHz}$ range. For the RSG scheme, f_g (typically $f_g >> \alpha$) should preserve the usefulness of $C_{RSG}(f)$ for the handled detection problem, i.e. avoids aliasing within $\mathcal{B}$. It can be noticed from Figure 3.6 that increasing α minimises $\sigma^2_{e,RSG}(f)$, whilst increasing f_g results in a small growth in the estimator's variance. Nevertheless, the rate at which the variance declines as α surges decays remarkably after the sampling rate exceeds a certain

value, the reduction in $\sigma^2_{e,RSG}(f)$ becomes insignificant. This again justifies the necessity of averaging a number of the periodogram-type estimates in order to control the estimation quality. Although the targeted spectrums of each of $X_{e,RSG}(\mathcal{t}_r, f)$ and $X_{e,TRS}(\mathcal{t}_r, f)$ are different, RSG generally offers a better quality of estimation within the examined bandwidth since RSG tends to TRS as f_g approaches infinity.

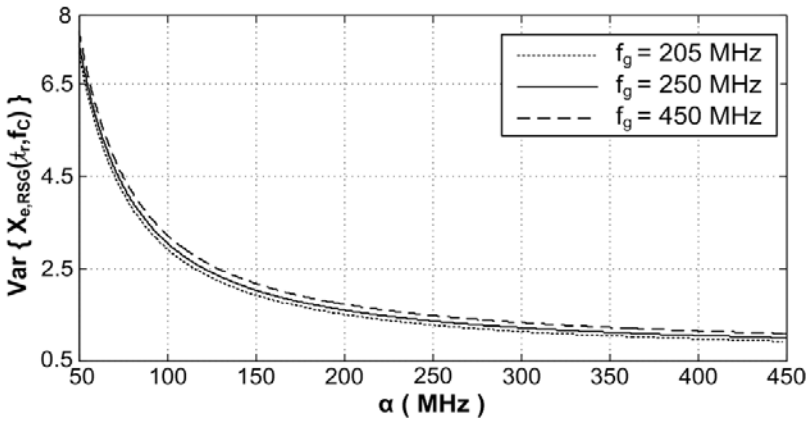

Figure 3.6: Variance of $X_{e,RSG}(\mathcal{t}_r, f_C)$ for various average sampling rates and grid densities, $f_C = 47.5\,\text{MHz}$.

3.5 Stratified-Jittered Sampling

The studied stratified sampling entails dividing the time analysis window into a number of non-overlapping partitions/strata, i.e. $\mathcal{S}_1, \mathcal{S}_2, \ldots, \mathcal{S}_N$ as in [98]. One sampling instant is selected per partition and its probability density function is: $p_n(t) = 1/|\mathcal{S}_n|$ if $t \in \mathcal{S}_n$ and zero elsewhere such that $|\mathcal{S}_n|$ is the width of the stratum $\mathcal{S}_n$. The purpose of deploying stratified sampling is to suppress spectrum aliasing where no previous knowledge of the signal spectral support is presumed. Accordingly, Stratified Sampling with Equal Partitions (SSEP) is a practical stratification technique that is applied here (see §2.3.3). However, the presented analysis in this chapter and the associated formulas (their detailed derivations are included in Appendix C) can be straightforwardly extended to stratification where the sizes of the strata are unequal. Unlike total random sampling and other randomised sampling schemes, SSEP guarantees a minimum distance between any two of its sample points as discussed in §3.5.3. It can also lower the data acquisition speed compared to the RSG scheme.

We utilise the periodogram-type tool given by:

$$X_{e,SSEP}(\mathscr{t}_r, f) = \frac{1}{\mu\alpha^2}\left|\sum_{n=1}^{N} y(t_n)w(t_n)e^{-j2\pi f t_n}\right|^2 \tag{3.44}$$

to estimate a detectable frequency representation of the received signal from a finite set of noisy signal samples, i.e. $\{y(t_n)\}_{n=1}^{N}$, collected within $\mathscr{T}_r$. Whereas, μ is the energy of the windowing function defined in (3.9) and $\alpha = N/T_0$ is the average sampling rate. Below, we show that the smeared-aliasing introduced by stratified sampling, distinct from the TRS and RSG cases, is not constant across the monitored frequency range $\mathscr{B}$.

3.5.1 Estimator's Expected Value and Accuracy for SSEP

In order to scrutinise the alias-free suppression capability of stratified sampling, the estimator's expected value is examined. It is shown to be (see Appendix C):

$$C_{SSEP}(f) = E\left[X_{e,SSEP}(\mathscr{t}_r, f)\right] = \frac{(P_S + P_N)}{\alpha} + \frac{1}{\mu}\Phi_X(f) * |W(f)|^2 - \frac{\chi(f)}{\mu} \tag{3.45}$$

recalling that $W(f) = \int_{\mathscr{T}_r} w(t)e^{-j2\pi ft}dt$, $P_S = E\left[x^2(t)\right]$, P_N is the AWGN variance and $\Phi_X(f)$ is the PSD of the incoming multiband signal $x(t)$. Whereas,

$$\chi(f) = \sum_{n=1}^{N} \Phi_X(f) * |V_n(f)|^2 \tag{3.46}$$

such that

$$V_n(f) = \int_{\mathscr{S}_n} w(t)e^{-j2\pi ft}dt\,. \tag{3.47}$$

It follows from (3.45) that $C_{SSEP}(f)$ consists of a detectable feature given by the windowed signal's PSD, i.e. $\Phi_X(f) * |W(f)|^2/\mu$, plus two components that represent the smeared-aliasing phenomenon owed to the deployment of nonuniform sampling (excluding the AWGN contribution, i.e. P_N/α). The frequency-independent component $(P_S + P_N)/\alpha$ merely serves as amplitude offset at all frequencies, whilst $\chi(f)/\mu$ minimises the latter's effect in the vicinity of the signal's spectral component(s), i.e. attenuates smeared-aliasing at such frequencies. To illustrate this property of stratified sampling, consider a rectangular $w(t)$ which produces $V_n(f)e^{j2\pi f\tau_n} = \text{sinc}(f/\alpha)/\alpha$ and $\mu = T_0$ such that τ_n is the time

instant denoting the centre of the n-th stratum. Thus $\chi(f)/\mu = \Phi_X(f) * \left|\text{sinc}(f/\alpha)\right|^2 / \alpha$ and:

$$C_{SSEP}(f) = \frac{P_S + P_N - \Phi_X(f) * \left|\text{sinc}(f/\alpha)\right|^2}{\alpha} + \frac{1}{\mu}\Phi_X(f) * \left|W(f)\right|^2 . \qquad (3.48)$$

If we assume that α is considerably larger than the width of the individual system subband, the main-lobe of $\left|\text{sinc}(f/\alpha)\right|^2$ will be notably wider than B_C. The convolution outcome of $\Phi_X(f) * \left|\text{sinc}(f/\alpha)\right|^2$ yields a proportion of the area underneath the PSD of the active subbands. This is distinct from the effect of $\left|W(f)\right|^2 = \left|T_0 \text{sinc}(T_0 f)\right|^2$ in (3.48) which serves the purpose of smoothing $\Phi_X(f)$, noting that $T_0 > 1/B_C$ as discussed in the §5.1.3. Hence $C_{SSEP}(f)$ in (3.48) shows that the contribution of $\chi(f)/\mu$ depends on the location of the active subbands and their power levels as well as on $\alpha = N/T_0$. If the active channels are within a close proximity of each other, the outcome of the convolution $\Phi_X(f) * \left|\text{sinc}(f/\alpha)\right|^2$ in $\chi(f)/\mu$ would represent more of the area underneath $\Phi_X(f)$, i.e. P_S, as opposed to when they are spread across the frequency range of interest. Larger α would have a similar impact as $\left|\text{sinc}(f/\alpha)\right|^2$ main-lobe becomes wider, i.e. the convolution incorporates more of the signal's power. Accordingly, the smeared-aliasing level for SSEP varies across the assessed bandwidth such that $P_S/\alpha \geq \chi(f)/\mu$. This aspect of stratified sampling along with the effect of the active subbands location on $\chi(f)/\mu$ is demonstrated in the numerical examples in the next subsection. Therefore, $X_{e,SSEP}(t_r, f)$ is an unbiased estimator of $C_{SSEP}(f)$ which is a detectable frequency representation of the incoming signal. It is a suitable tool for a spectrum sensing routine where the sampling rates are substantially low.

In order to assess the accuracy of the $C_{SSEP}(f)$ estimation using $X_{e,SSEP}(t_r, f)$ in (3.44), we calculate the estimator's variance $\sigma^2_{e,SSEP}(f) = \text{var}\left\{X_{e,SSEP}(t_r, f)\right\}$. The t_r is discarded for the simplicity of the notation whenever needed. Similar to the TRS and RSG, first we start with:

$$X_{e,SSEP}(t_r, f) = \frac{1}{\mu}\left|X_{SS}(f)\right|^2 = \frac{1}{\mu}\left[R^2_{SS}(f) + I^2_{SS}(f)\right] \qquad (3.49)$$

where $X_{SS}(f) = T_0 \sum_{n=1}^{N} y(t_n) w(t_n) e^{-j2\pi f t_n} \big/ N$. Whilst the phase-shifted real and imaginary parts of $X_{SS}(f)$ are given by:

$$R_{SS}(f) = T_0 \sum_{n=1}^{N} y(t_n) w(t_n) \cos\left(2\pi f t_n - \theta_{SS}(f)\right) \big/ N \tag{3.50}$$

$$I_{SS}(f) = T_0 \sum_{n=1}^{N} y(t_n) w(t_n) \sin\left(2\pi f t_n - \theta_{SS}(f)\right) \big/ N \tag{3.51}$$

If the zero mean $R_{SS}(f)$ and $I_{SS}(f)$ are of normal distribution, the estimator in (3.44) has unnormalised chi-squared distribution with two degrees of freedom $\forall f$ provided that $R_{SS}(f)$ and $I_{SS}(f)$ are uncorrelated [103]. Below, it is illustrated that the normality condition holds and $\sigma^2_{e,SSEP}(f)$ is derived where $\theta_{SSEP}(f)$ is selected such that $E\left[R_{SS}(f) I_{SS}(f)\right] = 0$.

Each of $R_{SS}(f)$ and $I_{SS}(f)$ are the sum of N independent random variables which are not identically distributed, i.e. the classical central limit theorem does not apply. Instead, we prove that the Lyapunov condition [103, p.338] is satisfied. For this purpose, we assume that $x(t)$ is not only wide sense stationary but also $E\left[\left|x(t)\right|^{\nu}\right]$ is a constant for some $\nu = \nu_0 > 2$. Let $X_{SS}(f) e^{j\theta(f)} = \sum_{n=1}^{N} F_n(f)$ where $F_n(f) = T_0\, y(t_n) w(t_n) e^{-j2\pi f (t_n - \theta(f))} \big/ N$. Now, we show that the Lyapunov condition given by:

$$\lim_{N\to\infty} \mathscr{K}_N = \lim_{N\to\infty} \frac{\sum_{n=1}^{N} E\left[\left|F_n(f) - E\left[F_n(f)\right]\right|^{\nu}\right]}{\left(\sum_{n=1}^{N} \mathrm{var}\left\{F_n(f)\right\}\right)^{0.5\nu}} = 0 \tag{3.52}$$

for some $\nu > 2$ is fulfilled, i.e. $\mathrm{Re}\left\{X_{SS}(f) e^{j\theta(f)}\right\} \big/ \sigma_1 = R_{SS}(f) \big/ \sigma_1$ and $\mathrm{Im}\left\{X_{SS}(f) e^{j\theta(f)}\right\} \big/ \sigma_2 = I_{SS}(f) \big/ \sigma_2$ are jointly asymptotically normal. Each of σ_1^2 and σ_2^2 are the asymptotic variances of $R_{SS}(f)$ and $I_{SS}(f)$ respectively. It can be easily seen that $E\left[F_n\right] = 0$. Following the aforementioned assumption on $x(t)$, we have: $E\left[\left|F_n\right|^2\right] = \alpha^{-2} \kappa_2$ and $E\left[\left|F_n\right|^{\nu_0}\right] = \alpha^{-\nu_0} \kappa_{\nu_0}$ where κ_2 and κ_{ν_0} are constants; the signal and AWGN are independent. Subsequently, $\lim_{N\to\infty} \mathscr{K}_N = \lim_{N\to\infty} \frac{\text{const.}}{N^{0.5\nu_0 - 1}} = 0$ proving (3.52), i.e. $R_{SS}(f)/\sigma_1$ and

$I_{SS}(f)/\sigma_2$ are jointly asymptotically normal. It has been observed that $R_{SS}(f)$ and $I_{SS}(f)$ are approximately normal even for moderate values of N. This is exploited here where $\sigma^2_{R_{SS}}(f) = \text{var}\{R_{SS}(f)\}$, $\sigma^2_{I_{SS}}(f) = \text{var}\{I_{SS}(f)\}$ are calculated for a finite number of collected samples.

As a result, provided that $\theta_{SS}(f)$ values guarantee $E[R_{SS}(f)I_{SS}(f)] = 0$, we have:

$$\sigma^2_e(f) = \text{var}\{X_{e,SSEP}(\mathcal{X}_r, f)\} = 2\left[\sigma^4_{R_{SS}}(f) + \sigma^4_{I_{SS}}(f)\right]/\mu^2 \tag{3.53}$$

according to chi-squared distribution [103] where:

$$\sigma^2_{R_{SS}}(f) = \frac{(P_S + P_N)E_{WC}(f)}{\alpha} - \chi_R(f) + \lambda_R(f) \tag{3.54}$$

$$\sigma^2_{I_{SS}}(f) = \frac{(P_S + P_N)E_{WS}(f)}{\alpha} - \chi_I(f) + \lambda_I(f). \tag{3.55}$$

Each of $E_{WC}(f)$, $E_{WS}(f)$, $\lambda_R(f)$ and $\lambda_I(f)$ are defined by (3.19), (3.22), (3.20) and (3.23) respectively such that:

$$\theta_{SS}(f) = 0.5\text{arccot}\left(0.5\left\{E\left[\tilde{R}^2_{SS}(f)\right] - E\left[\tilde{I}^2_{SS}(f)\right]\right\}/\zeta_{SS}(f)\right) \tag{3.56}$$

replaces $\theta_{TRS}(f)$. Whilst,

$$\chi_R(f) = \sum_{n=1}^{N}\int_{\mathcal{S}_n}\int_{\mathcal{S}_n} R_X(t_1 - t_2)w(t_1)w(t_2)\cos\left(2\pi f t_1 - \theta_{SS}(f)\right)\cos\left(2\pi f t_2 - \theta_{SS}(f)\right)dt_1 dt_2 \tag{3.57}$$

$$\chi_I(f) = \sum_{n=1}^{N}\int_{\mathcal{S}_n}\int_{\mathcal{S}_n} R_X(t_1 - t_2)w(t_1)w(t_2)\sin\left(2\pi f t_1 - \theta_{SS}(f)\right)\sin\left(2\pi f t_2 - \theta_{SS}(f)\right)dt_1 dt_2. \tag{3.58}$$

Each of $E\left[\tilde{R}^2_{SS}(f)\right]$ and $E\left[\tilde{I}^2_{SS}(f)\right]$ are identical to (3.54) and (3.55) respectively such that $\theta_{SS}(f)$ is omitted from their corresponding terms since

$\tilde{R}_{SS}(f) = \sum_{n=1}^{N} y(t_n)w(t_n)\cos\left(2\pi f t_n\right)/\alpha$ and $\tilde{I}_{SS}(f) = \sum_{n=1}^{N} y(t_n)w(t_n)\sin\left(2\pi f t_n\right)/\alpha$. Whereas,

$$\zeta_{SS}(f) = \left(P_S + P_N\right)\int_{\mathcal{T}_r} w^2(t)\cos(2\pi f t)\sin(2\pi f t)dt\Big/\alpha - \chi_{RI}(f) + \lambda_{RI}(f) \tag{3.59}$$

$$\chi_{RI}(f) = \sum_{n=1}^{N}\int_{\mathcal{S}_n}\int_{\mathcal{S}_n} R_X(t_1 - t_2)w(t_1)w(t_2)\cos(2\pi f t_1)\sin(2\pi f t_2)dt_1 dt_2 \tag{3.60}$$

and $\lambda_{RI}(f)$ is defined in (3.26).

3.5.2 Numerical Examples on SSEP

We revisit the system studied in the TRS and RSG cases; it operates over the frequency range $\mathcal{B} = [1.45, 1.55]$ GHz. The SSEP average sampling rate is chosen to be $\alpha = 40$ MHz, which is well below the minimum valid admissible bandpass uniform sampling counterpart, i.e. 222 MHz. A Blackman window of width $T_0 = 8\,\mu$s is used and the signal-to-noise ratio is -1 dB. In Figure 3.7, the derived analytical mean in (3.45) and variance in (3.53)-(3.60) are compared to the experimental/simulations mean and MSE respectively. The latter two are procured from 10000 independent experiments. The PSD of the test signal is exhibited in Figure 3.1 for $f > 0$.

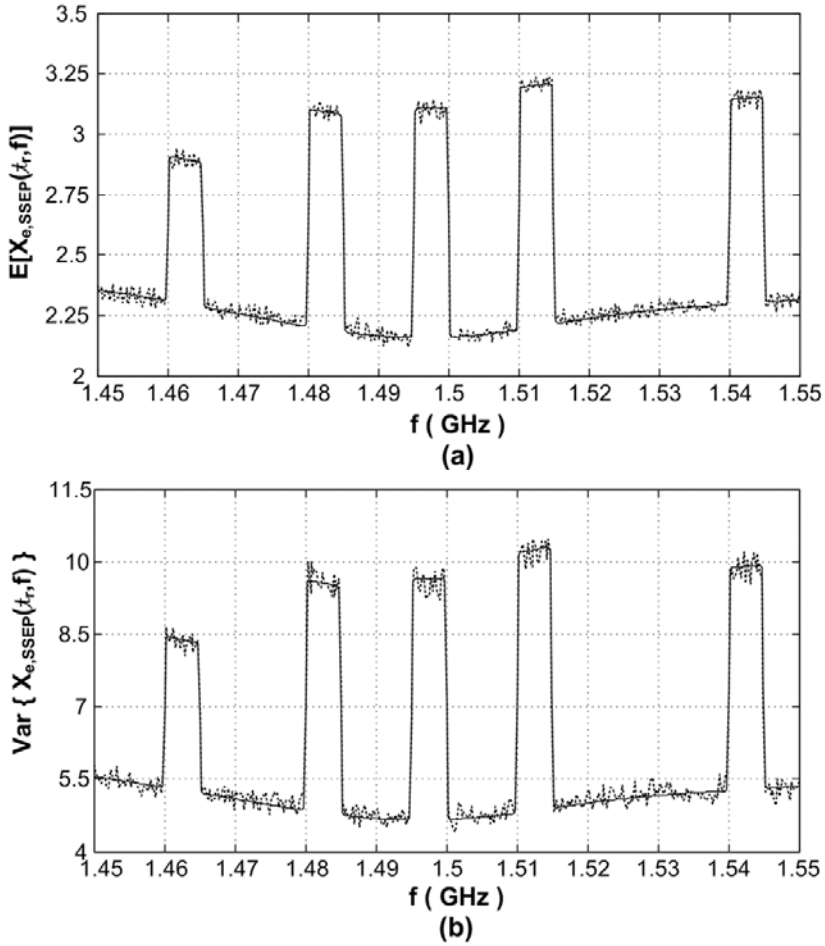

Figure 3.7: $X_{e,SSEP}(t_r, f)$ analytical mean from equation (3.45) and variance from equations (3.53)-(3.60) versus the experimental ones. (a) $C_{SSEP}(f)$ from equation (solid line) and experimental mean (dotted line). (b) $\sigma^2_{e,SSEP}(f)$ from equation (solid line) and mean squared error (dotted line).

The simulation results in Figure 3.7 confirms the accuracy of the provided mean and variance formulas of $X_{e,SSEP}(\not{t}_r, f)$. It is clear from Figure 3.7a that $C_{SSEP}(f)$ is a detectable frequency representation of the incoming signal and hence $X_{e,SSEP}(\not{t}_r, f)$ is a suitable tool for detection. To manifest the effect of $\chi(f)/\mu$ in (3.45), i.e. the varying smeared-aliasing level, Figure 3.8 shows $C_{SSEP}(f)$ for four different distributions of the engaged subbands and the $(P_S + P_N)/\alpha$ term in (3.45). Figure 3.9 exhibits the smeared-aliasing decay factor $\chi(f)/\mu$ for the four plots in Figure 3.8. The PSD of the present signal in each of these distributions is depicted in Table 3.1.

Table 3.1: PSD of the active subbands in Figures 3.8 and 3.9, frequency is in GHz.

$\Phi_X(f)$	Figure 3.8a	Figure 3.8b	Figure 3.8c	Figure 3.8d
0.6	$f \in \pm[1.475,1480]$	$f \in \pm[1.505,1.51]$	$f \in \pm[1.475,1.48]$	$f \in \pm[1.5,1.505]$
0.85	$f \in \pm[1.515,1.52]$	$f \in \pm[1.515,1.52]$	$f \in \pm[1.465,1.47]$	$f \in \pm[1.54,1.545]$
0.9	$f \in \pm[1.455,1.46]$	$f \in \pm[1.525,1.53]$	$f \in \pm[1.45,1.455]$	$f \in \pm[1.455,1.46]$
0.95	$f \in \pm[1.495,1.5]$	$f \in \pm[1.495,1.5]$	$f \in \pm[1.545,1.55]$	$f \in \pm[1.49,1.495]$
1	$f \in \pm[1.535,1.54]$	$f \in \pm[1.535,1.54]$	$f \in \pm[1.535,1.54]$	$f \in \pm[1.51,1.515]$
0	elsewhere	elsewhere	elsewhere	elsewhere

Figures 3.8 and 3.9 demonstrate that the position of the active subbands mandates the contribution of $\chi(f)/\mu$ to $C_{SSEP}(f)$. The observations are summarised by:

- Figure 3.8a: the influence of the smeared-aliasing reduction factor spreads across $\mathcal{B}$ where the active subbands are sparsely placed.
- Figure 3.8b: $\chi(f)/\mu$ values peak near/at the frequencies of the occupied channels and vanish near the lowest frequencies in the examined bandwidth where the smeared-aliasing settles to a constant level, i.e. P_S/α.
- Figure 3.8c: the $\chi(f)/\mu$ has its maximum values near the active channels which reside at the edges of $\mathcal{B}$. Whereas, $\chi(f)/\mu$ effect diminishes as we move towards the centre of the monitored bandwidth where the smeared-aliasing level approaches P_S/α.

o Figure 3.8d: the smeared-aliasing reduction factor contribution is focused near the middle of $\mathcal{B}$ where three out of the five active subbands are present. Its values stabilise as we approach the edges of the overseen bandwidth.

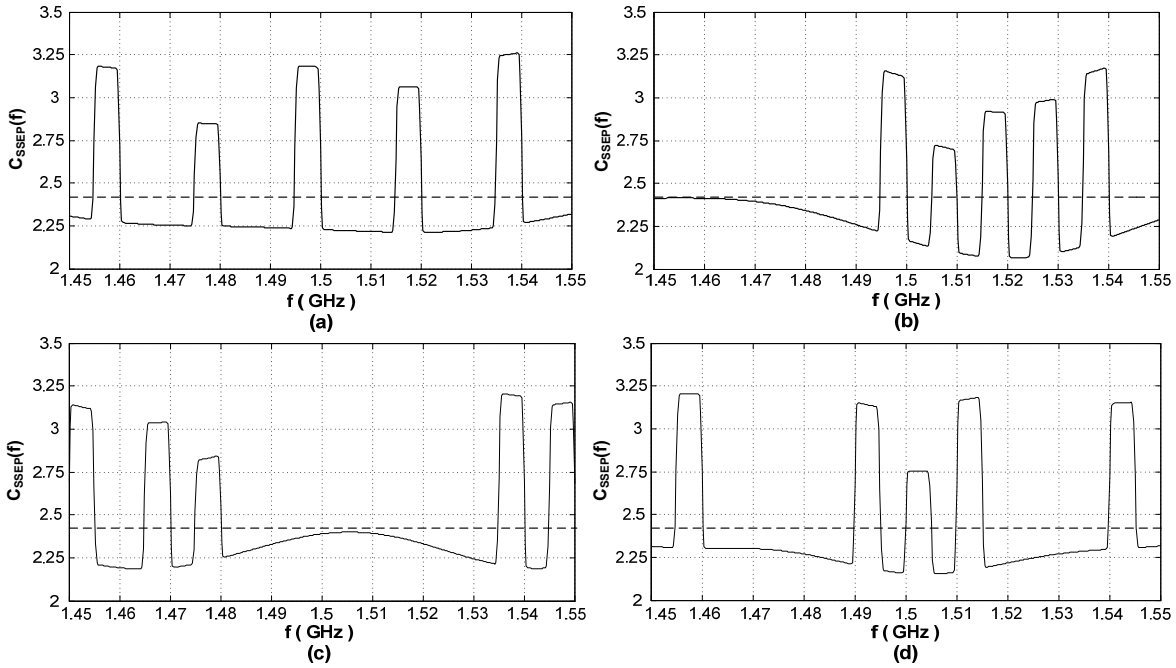

Figure 3.8: $C_{SSEP}(f)$ (solid lines) for various distributions of the active subbands and $(P_S + P_S)/\alpha$ (dashed lines). Channels locations and power levels are depicted in Table 3.1.

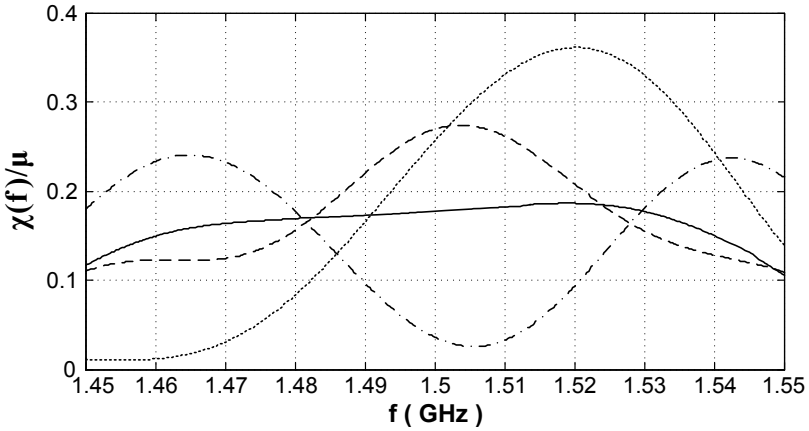

Figure 3.9: Smeared-aliasing decay factor $\chi(f)/\mu$ for various distributions of the active subbands shown in Table 3.1. For $C_{SSEP}(f)$ in Figure 3.8a (solid line), in Figure 3.8b (dotted line), Figure 3.8c (dashdot line) and in Figure 3.8d (dashed line).

To further understand the parameters that influence the magnitude of the smeared-aliasing reduction factor and its relation to the power of the present signal, let's consider a rectangular windowing function where $\chi(f)/\mu = \Phi_X(f) * \left|\text{sinc}(f/\alpha)\right|^2 / \alpha$. Figure 3.10

exhibits the PSD of a test signal along with the $|\text{sinc}(f/\alpha)|^2$ for various average sampling rates (only positive frequencies are shown). The signal's active components are clustered at the centre of the monitored frequency range $\mathcal{B} = [f_{in}, f_{in} + B]$. We recall that the rectangular window was assumed for simplicity and the conclusions withdrawn from the simulations apply to any windowing function.

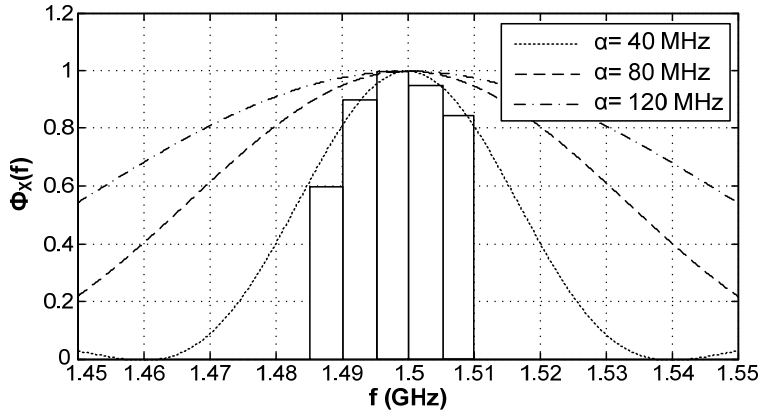

Figure 3.10: PSD of a continuous-time multiband signal (solid line) and $|\text{sinc}((f-f_0)/\alpha)|^2$ for various average sampling rates where $f_0 = 1.5\,\text{GHz}$.

It can be noticed from Figure 3.10 that the outcome of the convolution $\Phi_X(f) * |\text{sinc}(f/\alpha)|^2$ incorporates part of the total power of the present signal especially in the vicinity of the active signal spectral components. This is more visible when the active subbands are close to each other or when $|\text{sinc}(f/\alpha)|^2$ main-lobe is wide. For example, consider the central frequency $f_C = 1.4975\,\text{GHz}$ of the active channel residing in $[1.495, 1.5]\,\text{GHz}$. As α increases, the convolution outcome becomes a better approximation of the area underneath the signal's PSD for $f > 0$. Assuming $f_{in} >> B$, the $\chi(f)/\mu$ factor becomes a better approximation of $0.5P_S/\alpha$. Figure 3.11a shows $\chi(f_C)/\mu$ and $0.5P_S/\alpha$ for the signal in Figure 3.10 where the average sampling rate varies. Figure 3.11b depicts their relative error $|\chi(f_C)/\mu - 0.5P_S/\alpha| / [0.5P_S/\alpha]$. It is clear from the figure that $\chi(f_C)/\mu$ declines and approaches $0.5P_S/\alpha$ as the average sampling rate increases where their differences becomes insignificant as the relative error reduces to under 2%.

The varying smeared-aliasing phenomenon that accompanies stratified sampling can have implications on spectrum sensing that utilises SARS, this is addressed in Chapter 5.

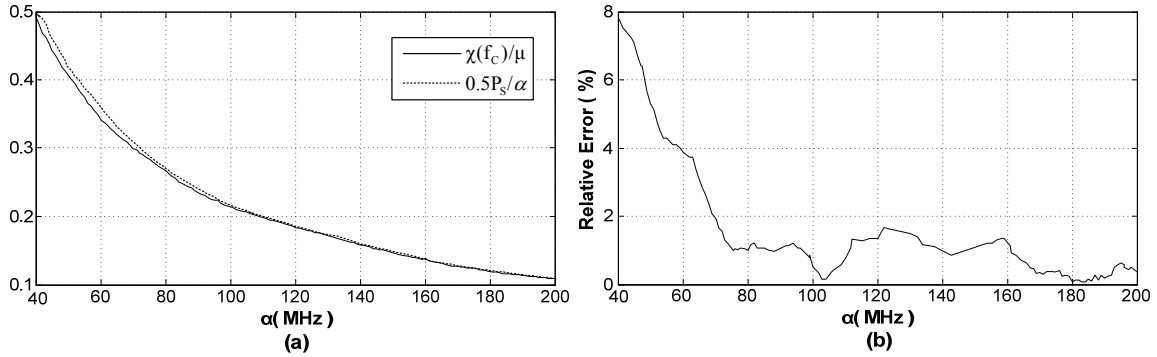

Figure 3.11: (a) $\chi(f_C)/\mu$ and $0.5P_S/\alpha$ where $f_C = 1.4975$ GHz is the central frequency of the middle active channel in Figure 3.10. (b) Relative error $\left|\chi(f_C)/\mu - 0.5P_S/\alpha\right| / \left[0.5P_S/\alpha\right]$.

3.5.3 Stratified Sampling with Two ADCs Versus Other Schemes

Similar to the random sampling on grid scheme, stratified sampling with equal partitions maintains a minimum distant between its samples ensuring a finite data collection rate. It can be implemented in practice by deploying two interleaved Analogue to Digital Converters (ADCs). ADC1 captures the samples $y(t_1), y(t_3), y(t_5), \ldots$ lying in the partitions $\mathcal{S}_1, \mathcal{S}_3, \mathcal{S}_5, \ldots$ and ADC2 takes the samples $y(t_2), y(t_4), y(t_6), \ldots$ belonging to the rest of the strata, i.e. $\mathcal{S}_2, \mathcal{S}_4, \mathcal{S}_6, \ldots$. As a result, the minimum distance between any two SSEP samples captured by the same acquisition device is $d_{\min} = 1/\alpha$ (see Figure 3.12). Subsequently, the maximum imposed instantaneous sampling rate (sampling speed of the each ADC) is α where $0.5\alpha \le \beta_n \le \alpha$. The instantaneous sampling frequency is: $\beta_n = 1/(t_n - t_{n-1})$ which change for each two pairs of sampling instants. The maximum β_n of randomised sampling schemes such as total random sampling and Additive Random Sampling (ARS) with Poisson distribution can be infinitely high, i.e. they demand infinitely fast ADC(s). Thus SSEP can remarkably reduce the required acquisition device(s) sampling speed(s). Its rates are also notably lower than the minimum admissible uniform sampling ones whose $\beta_n = f_{US} \ge 2B$.

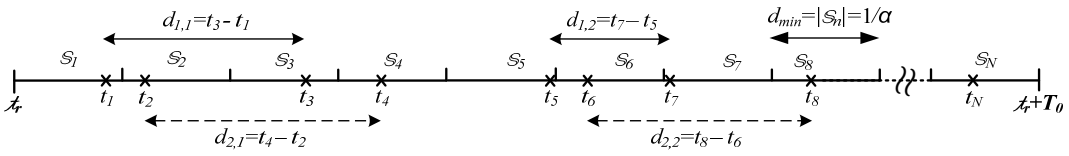

Figure 3.12: An SSEP sequence with two ADCs (crosses are the sample positions). Samples collected by ADC1 are $d_{1,1}, d_{1,2}, \ldots$ seconds apart and the ones by ADC2 are $d_{2,1}, d_{2,2}, \ldots$ seconds apart.

In order to illustrate the benefits of SSEP, Table 3.2 depicts the sampling rates of uniform sampling, TRS, RSG, ARS and SSEP using two interleaved ADCs. We assume that the monitored bandwidth is of width $B = 100\,\text{MHz}$. The uniform sampling rate is bounded by $f_{US} \geq 200\,\text{MHz}$ (200 MHz is utilised for the RSG underlying grid density). Whilst, an $\alpha = 60\,\text{MHz}$ is selected for the randomised schemes. Two ADCs are employed and the shown rates are per one ADC.

Table 3.2: Sampling rates in MHz for a number of sampling schemes per one ADC.

Sampling scheme	Average sampling rate	Maximum β_n
Uniform Sampling	100	100
TRS	30	Infinity
RSG	30	100
ARS	30	Infinity
SSEP	30	60

It can be seen from Table 3.2 that stratified sampling can offer more savings in terms of the acquisition device speed compared to the random sampling on grid scheme. The latter's need for an underlying uniform grid with certain density dictates its maximum instantaneous sampling frequency. However, SSEP varying smeared-aliasing level can impose a limit on the minimum usable average randomised sampling rate when conducting spectrum sensing as shown later in the thesis. Generally, Table 3.2 demonstrates the benefits gained from randomised sampling in terms of the sampling rates compared to the classical uniform sampling. More than two ADCs can be deployed for SSEP to further relax the demanded sampling rates.

As the shapes of each of the $C_{TRS}(f)$, $C_{RSG}(f)$ and $C_{SSEP}(f)$ are distinct, comparing the variances/accuracies of each of the total random sampling, random sampling on grid and stratified sampling estimators in a fair manner is implausible. Nonetheless, the requirements of each of the aforementioned schemes to reliability perform spectrum sensing are compared in the spectrum sensing chapter.

3.6 Spectrum Dynamic Range (SDR)

The spectrum dynamic range is defined as the ratio between the highest magnitude spectrum point belonging to the processed signal and the lowest magnitude spectrum value within the range of observed frequencies $\mathcal{B} = [f_{min}, f_{min} + B]$. With uniform sampling, the SDR is typically high and considered to be infinity for noiseless environments. A decline in the SDR is usually attributed to the presence of noise or the spectral leakage originating from the finite time analysis window. On the other hand, the spectrum of the studied randomised sampling schemes comprises a smeared-aliasing component active at all frequencies albeit the presence or absence of noise. Thus with randomised sampling the dynamic range is always finite. As the examined signals are of multiband nature, the SDR is determined for each of the active system subbands according to:

$$SDR_k = \frac{C(f_k)}{\min\limits_{f \in \mathcal{B}} [C(f)]} \tag{3.61}$$

for $k = 1, 2, \ldots, M$ where $C(f) = E[X_e(f)]$ is the targeted frequency representation for the generic estimator in (3.5), f_k is the frequency of the highest spectral peak in the examined k-th subband and M is the number of simultaneously active channels. Alternatively, one spectrum dynamic range can be defined for the entire monitored frequency range, i.e.

$$SDR = \max_{f \in \mathcal{B}} [C(f)] \Big/ \min_{f \in \mathcal{B}} [C(f)] \tag{3.62}$$

or $SDR = \max\limits_{k=1,2,\ldots,M} (SDR_k)$. It is noted that $C(f)$ incorporates the contributions of the present noise and the smeared-aliasing phenomenon, for instance see (3.11), (3.31) and (3.45).

Let $D(f) = \Phi_X(f) * |W(f)|^2 / \mu$ and $D_k = D(f_k)$, we can write: $P_{S,k} \le 2B_C D_k$ is the power in the k-th active subband of width B_C (double sided power spectral density is assumed). Utilising (3.11) for the TRS scheme, we have:

$$SDR_{k,TRS} = 1 + \frac{(N-1)\alpha D_k}{N[P_S + P_N]} \tag{3.63}$$

where P_S and P_N are the total power of the present multiband signal and the power of the AWGN respectively. Adopting a conservative approach, (3.63) emerges as:

$$SDR_{k,TRS} \approx 1 + \frac{(N-1)\alpha}{N 2\phi_k B_C \left(1 + SNR^{-1}\right)} \tag{3.64}$$

where $SNR = P_S / P_N$ is the signal-to-noise ratio and $\phi_k = P_S / P_{S,k}$ is the ratio of the power in the scrutinised subband to that of the present multiband signal. It can be noticed from (3.64) that as the average sampling rate increases diminishing the smeared-aliasing contribution, the spectrum dynamic range improves. Similarly for the RSG, we have:

$$SDR_{k,RSG} \approx 1 + \frac{0.5\alpha(N-1)N_g / B_C\phi_k}{N(N_g - N) + N(N_g - 1)SNR^{-1}} \tag{3.65}$$

and for SSEP:

$$SDR_{k,SSEP} \approx \frac{\left[(1 - 0.5\varpi_1) + SNR^{-1}\right] + 0.5\alpha / B_C\phi_k}{(1 - 0.5\varpi_0) + SNR^{-1}} \ . \tag{3.66}$$

Each of the $0 \le \varpi_0 \le 1$ and $0 \le \varpi_1 \le 1$ represent the contribution of the smeared-aliasing reduction factor $\chi(f)/\mu$ at the frequency point where $\min_{f \in \mathcal{B}}\left(C(f)\right)$ is recorded and f_k in (3.61) respectively. We recall from §3.5.2 that $\chi(f)/\mu$ is related to the total power of the present signal such that: $\chi(f)/\mu = 0.5\varpi(f)P_S/\alpha$ where $0 \le \varpi(f) \le 1$ assuming $f_{in} >> B$.

Formulas (3.64)-(3.66) clearly demonstrate that SDR for randomised sampling estimators is largely influenced by the nature/characteristics of the sampling scheme. It also shows that the smeared-aliasing phenomenon plays a cardinal role in setting the spectrum dynamic range of the processed signal. Table 3.3 depicts the SDR of selected active subbands from Figures 3.2, 3.5 and 3.8 along with the SDR in (3.62). The central frequency f_C of the considered subband in Table 3.3 is identical to the f_k frequency point in (3.61). The table clearly exhibits the close match between the results provided by (3.64)-(3.66) and those measured from the figures. In practice, an estimate of $C(f)$ using $X_e(t_r, f)$ would include an estimation error which can alter the spectrum dynamic range. In the above analysis, a zero estimation error was presumed, e.g. averaging an infinite number of estimates from uncorrelated signal windows.

Table 3.3: SDR of Figures 3.2, 3.5 and 3.8, f_C is the subband's central frequency. SDR_k from (3.64)-(3.66) and the measured SDR_k as well as SDR from the figures.

Figure	Sampling Scheme	α (MHz)	T_0 (μs)	f_C (GHz)	SNR (dB)	SDR_k (dB)	Measured SDR_k (dB)	Measured SDR (dB)
3.2a	TRS	65	10	1.4625	-1 dB	1.464	1.465	2.224
3.2a	TRS	65	10	1.5125	-1 dB	2.222	2.224	2.224
3.2a	TRS	65	10	1.5425	-1 dB	1.9538	1.9554	2.224
3.5a	RSG	60	10	0.0125	-1 dB	1.5092	1.5067	2.2820
3.5a	RSG	60	10	0.0625	-1 dB	2.281	2.2820	2.2820
3.5a	RSG	60	8	0.925	-1 dB	1.9116	2.0072	2.2820
3.7a	SSEP	40	8	1.4625	-1 dB	1.158	1.2793	1.7271
3.7a	SSEP	40	8	1.4825	-1 dB	1.5482	1.5622	1.7271
3.7a	SSEP	40	8	1.4975	-1 dB	1.5318	1.5840	1.7271

As commonly known, high spectrum dynamic range eases the requirement on the spectral analysis device and forms a safety margin for any inaccuracies that might be incurred. From (3.64)-(3.66), the spectrum dynamic range of randomised sampling can be set by choosing the appropriate α. Assuming that T_0 is fixed, the spectrum dynamic range depends on the number of samples per signal analysis window, i.e. N. For a dynamic range greater than or equal to ρ, i.e. $C(f_k) \geq \rho \min_{f \in \mathcal{B}} \left(C(f) \right)$ where $\rho > 1$, the number of samples needed for the TRS scheme with regard to the k-th active subband can be easily shown to be:

$$N_{TRS} \geq 2B_C \phi_k T_0 \left(\rho - 1 \right) \left[1 + SNR^{-1} \right] + 1 \tag{3.67}$$

, for RSG:

$$N_{RSG} \geq \frac{(\rho - 1)\left[N_g T_0 + (N_g - 1) T_0 SNR^{-1} \right] + 0.5 N_g / B_C \phi_k}{0.5 N_g / B_C \phi_k + (\rho - 1) T_0} \tag{3.68}$$

and for SSEP:

$$N_{SSEP} \geq 2B_C \phi_k T_0 \left\{ \rho \left[(1 - 0.5\varpi_0) P_S + P_N \right] - \left[(1 - 0.5\varpi_1) P_S + P_N \right] \right\}. \tag{3.69}$$

Although the adopted estimators allow detecting the active transmissions albeit the sampling rates, each of (3.67)-(3.69) gives the user an indication of the needed average sampling rate if the spectrum dynamic range is an issue. They are not necessary conditions for performing reliable spectrum sensing.

3.7 Summary and Final Remarks

Randomised sampling in conjunction with appropriate processing algorithms facilitates signal processing that is not restricted by the aliasing phenomenon. The nonuniform sampling rate is not limited by the processed bandwidth, antithetical to the uniform sampling case. Three randomised sampling schemes, namely total random sampling, random sampling on grid and stratified/jittered sampling, were investigated. Periodogram-type estimators, each tailored to the corresponding sampling scheme, were analysed. The provided analytical expressions (derived in Appendices A, B and C) capture the ability of these estimators to suppress the aliasing phenomenon within a wide range of monitored frequencies exposing the present spectral components of the incoming signal. They are unbiased estimators of detectable frequency representations (incorporate the signal's power spectral density) of the concurrently active spectral subbands despite the used low sampling rates (sub-Nyquist and possibly sub-Landau). The accuracy of the estimation process is assessed by quantifying the estimators' variances, which indicated that further measures (such as estimate averaging) are needed to combat the high uncertainty levels accompanying the periodogram-type estimators. The results of the conducted simulations concur with those obtained from the derived formulas demonstrating the analysis precision. The properties of each of the considered randomised sampling schemes and their spectral analysis are summarised in the table on the next page. With regards to the spectrum dynamic range of the targeted frequency representations, the developed guidelines guarantee that the smeared-aliasing component is constrained, i.e. the SDR conforms to a requested predefined level(s). In general, the spectrum dynamic range for randomised sampling is finite and lower than that obtained with uniform sampling.

As noticed from the schemes summary, the nature and the shape of the obtained spectrum are profoundly affected by the type of the randomised sampling scheme and its properties. Whilst the TRS simplicity is its mean feature, its suitability for implementation in hardware is rather limited as it requires infinitely fast data acquisition device(s). On the other hand, the random sampling on grid scheme ensures that a minimum distance is preserved between any two sample points. It is also well-suited for FFT-like algorithm, e.g. the zero filling in [5, p.67], to efficiently implement the estimator. However, RSG demands a dense underlying uniform grid imposing an acquisition device capable of matching the

grid rate. Alternatively, stratified sampling with equal partitions can reduce the demands on the ADC(s) speed(s) by deploying two (or more) interleaved acquisition devices. It equates the maximum instantaneous sampling rate to the average sampling one which is remarkably low. This offers substantial savings in terms of the ADC(s) speed(s) compared to RSG. Nevertheless, the spectrum of the stratified sampling scheme has a varying smeared-aliasing level that can have implications on the scheme's ability to perform reliable detection at arbitrarily low sampling rates. A closed form formula of the smeared-aliasing variations is provided.

Task	Spectrum Properties and the Sampling Scheme Features
Spectral Analysis of TRS using: $X_{e,TRS}(\not{t}_r, f)$ in (3.8)	Suppresses aliasing equally across all frequencies facilitating the detection of the signal's spectral components within arbitrarily wide frequency ranges. The introduced smeared-aliasing is constant and is a white-noise-like component present at all frequencies. The TRS instantaneous sampling frequency can be infinitely high as any two or more of the sampling points can be arbitrarily close.
Spectral Analysis of RSG using: $X_{e,RSG}(\not{t}_r, f)$ in (3.27)	The aliasing suppression is confined to the monitored frequency range provided an adequately chosen underlying grid density. This limits the possible overseen frequency range(s). The grid density is dependent on the width and location of the surveyed bandwidth. The smeared-aliasing level is constant within the monitored frequency range(s). The RSG maximum instantaneous sampling rate is equal to that of the grid rate.
Spectral Analysis of SSEP using: $X_{e,SSEP}(\not{t}_r, f)$ in (3.44)	The ability of SSEP to suppress-aliasing across all frequencies enables it to perform reliable detection in wide frequency ranges. The smeared-aliasing level varies across the overseen bandwidth depending on the positions and power levels of the concurrently active spectral subbands. The smeared-aliasing level settles to a constant level far away from the signal's spectral components. SSEP with two ADCs (can be more) guarantee that the maximum required instantaneous sampling frequency is less than or equal to the average sampling one.

3.7 Summary and Final Remarks

Whilst the studied sampling schemes present themselves as legitimate means to conduct spectrum sensing using significantly low sampling rates, the parameters of their spectrum estimators should be selected appropriately in order to meet a sought system performance, e.g. the probability of correct detection. This evokes choosing the width of the signal analysis window, the average sampling rate and the number of estimate averages. The latter tactic aims at confirming that the spectrum estimation process is completed with certain level of confidence. The selection of such parameters amid specified detection requirements is treated in Chapter 5.

Chapter 4

SARS Properties for Cyclostationary Signals

The Spectral Analysis of Randomised Sampling (SARS) has been conducted heretofore under the assumption that the incoming transmissions are Wide Sense Stationary (WSS). This has served the purpose of gaining insight into the behaviour and characteristics of the periodogram tool for the examined Total Random Sampling (TRS), Random Sampling on Grid (RSG) and Stratified Sampling with Equal Partitions (SSEP) schemes. However, a wide range of digitally modulated signals are of a cyclostationary nature. Here, we revisit the periodogram-type estimators studied in Chapter 3 and investigate the impact of processing cyclostationary communication signals on their performance.

4.1 The Adopted Estimators and Cyclostationarity

The autocorrelation function and power spectral density of the incoming transmissions modelled in the next section are time-varying, e.g. see (4.6), unlike those of the previously considered WSS signals. Circumventing the cyclostationarity of such processes (e.g. via phase randomisation) is a widely adopted practice in the communications literature whenever the process cyclic frequency is not of interest, e.g. [13, 15, 17, 49-51, 114]. In [119], Gardner exposed the defects of such practices in an attempt to correct any incurred errors, especially when the signal includes several (more than one) periodic components whose periods are not integer multiples of each other, such as the symbol and carrier periods. To improve the estimation accuracy we will be averaging a number of spectrum estimates calculated from various signal windows (see §5.1.2), hence it is vital to evaluate the response of the employed spectral analysis tools as the time analysis window

$\mathcal{T}_r = [\lambda_r, \lambda_r + T_0]$ changes. In this chapter, the effect of the signal's nonstationarity is acknowledged and its repercussions on the spectral analysis of randomised sampling are explored. The two main observations are:

- The adopted estimators continue to be suitable tools for the spectrum sensing pursuit. A spectral fragment within each transmission subband, referred to as the "*guarded region*", is identified where the estimated spectrum includes detectable features that are independent of time.
- A phenomenon exhibited by abrupt increases in the estimators' standard deviations at selected frequency points for some modulation schemes is unveiled.

The detailed derivations of the presented expressions in the following sections are provided in Appendix D.

Upon utilising the periodogram-type estimators in the spectrum sensing procedure, a finite number of spectral points are calculated per monitored spectral subband to determine its status (we aspire to use one frequency point per channel, see §5.1.2). The estimator's behaviour at those sensed frequency points, denoted by $\{f_k\}$, is of particular interest. Establishing the appropriate positions of $\{f_k\}$ given the cyclostationary nature of the processed signals and quantifying the estimators' accuracy at these locations is crucial.

4.2 Incoming Signal

Let $x_{T,m}(t)$ be the continuous-time signal transmitted over the m-th system active spectral subband by a communication source that deploys a linear digital modulation scheme. It can be expressed by: $x_{T,m}(t) = x_{i,m}(t) + x_{q,m}(t)$ where

$$x_{i,m}(t) = i_m(t)\cos(2\pi f_{C,m}t) \tag{4.1}$$

and

$$x_{q,m}(t) = q_m(t)\cos(2\pi f_{C,m}t + 0.5\pi)\,. \tag{4.2}$$

The in-phase $i_m(t)$ and quadrature $q_m(t)$ components are baseband signals where $i_m(t) = \sum_{n=-\infty}^{+\infty} a_{n,m} p_{i,m}(t + nT_{S,m})$, $q_m(t) = \sum_{n=-\infty}^{+\infty} b_{n,m} p_{q,m}(t + nT_{S,m})$, $f_{C,m}$ is the carrier frequency of the m-th subband and $f_{S,m} = 1/T_{S,m}$ is the baud rate. The coefficients $\{a_{n,m}\}_{n\in\mathbb{Z}}$

and $\{b_{n,m}\}_{n\in\mathbb{Z}}$ are zero mean Independent Identically Distributed (IID) random variables with variances of $\sigma_{a,m}^2$ and $\sigma_{b,m}^2$ respectively, they represent the transmitted symbols. The baseband shaping filter(s) in the in-phase and quadrature branches are $p_{i,m}(t)$ and $p_{q,m}(t)$. The transmission can be modelled as:

$$x_m(t) = \sum_{n=-\infty}^{+\infty} a_{n,m} s_{i,m}(t,n) + \sum_{n=-\infty}^{+\infty} b_{n,m} s_{q,m}(t,n) \tag{4.3}$$

where

$$s_{i,m}(t,n) = \left[p_{i,m}(t + nT_{S,m}) \cos(2\pi f_{C,m} t) \right] * h_m(t) \tag{4.4}$$

and

$$s_{q,m}(t,n) = \left[p_{q,m}(t + nT_{S,m}) \cos(2\pi f_{C,m} t + 0.5\pi) \right] * h_m(t). \tag{4.5}$$

The $h_m(t)$ in (4.4) and (4.5) represents the impulse response of the propagation channel over the m-th subband combined with any other attenuation or boosting operation of the power level of the incoming transmission.

It is in the interest of the forthcoming analysis to find certain first and second order moments of the processed signal. It can be easily checked that $E[x_m(t)] = 0$. Since $a_{n,m}$ and $b_{n,m}$ are independent, it is clear that $E[x_{i,m}(t_1) x_{q,m}(t_2)] = 0$. The autocorrelation function of the signal in (4.3) is:

$$R_{X,m}(t, t+\tau) = \sigma_{a,m}^2 \sum_{n=-\infty}^{+\infty} s_{i,m}(t,n) s_{i,m}(t+\tau,n) + \sigma_{b,m}^2 \sum_{n=-\infty}^{+\infty} s_{q,m}(t,n) s_{q,m}(t+\tau,n) \tag{4.6}$$

whilst

$$R_X(t, t+\tau) = \sum_{m=1}^{M} R_{X,m}(t, t+\tau) \tag{4.7}$$

is for the M independent concurrently active subbands. It can be noticed that (4.6) and (4.7) are time-varying, such stochastic processes are commonly regarded as Wide Sense Cyclostationary (WSCS) including the cases when the symbol period is not an integer multiple of the carrier period [51].

4.3 Targeted Frequency Representations

To assess the adequacy of $X_{e,TRS}(\mathcal{t}_r, f)$ in (3.8), $X_{e,RSG}(\mathcal{t}_r, f)$ in (3.27) and $X_{e,SSEP}(\mathcal{t}_r, f)$ in (3.44) for the detection task, their expected values are re-evaluated for the transmissions in (4.3). Similar to (3.11) for the total random sampling scheme, (3.31) for random sampling on grid and (3.45) for stratified sampling with equal partitions, it can be seen that:

$$C_{TRS}(\mathcal{t}_r, f) = E\left[X_{e,TRS}(\mathcal{t}_r, f)\right] = \frac{N\left[P_S(\mathcal{t}_r) + P_N\right]}{(N-1)\alpha} + \frac{1}{\mu} E\left[\left|X_W(\mathcal{t}_r, f)\right|^2\right] \tag{4.8}$$

$$C_{RSG}(\mathcal{t}_r, f) = E\left[X_{e,RSG}(\mathcal{t}_r, f)\right] = \frac{(N_g - N)P_S^d(\mathcal{t}_r) + (N_g - 1)P_N}{(N-1)f_g} + \frac{E\left[\left|X_W^d(\mathcal{t}_r, f)\right|^2\right]}{\mu_d f_g} \tag{4.9}$$

$$C_{SSEP}(\mathcal{t}_r, f) = E\left[X_{e,SSEP}(\mathcal{t}_r, f)\right] = \frac{P_S(\mathcal{t}_r) + P_N}{\alpha} + \frac{E\left[\left|X_W(\mathcal{t}_r, f)\right|^2\right]}{\mu} - \frac{\chi(\mathcal{t}_r, f)}{\mu} \tag{4.10}$$

where N is the number of collected signal samples that are contaminated with AWGN of variance P_N, $\mu = \int_{\mathcal{T}_r} w^2(t)dt$, $w(t)$ is the windowing function, the signal's weighted power is:

$$P_S(\mathcal{t}_r) = \frac{1}{\mu} \int_{\mathcal{T}_r} E\left[x^2(t)\right] w^2(t)dt \tag{4.11}$$

and $X_W(\mathcal{t}_r, f) = \int_{\mathcal{T}_r} x(t)w(t)e^{-j2\pi ft}dt$. The $f_g = 1/T_g$ is the underlying grid rate for the RSG scheme, $\mu_d = \sum_{n=1}^{N_g} w^2(nT_g)$, $X_W^d(\mathcal{t}_r, f) = \sum_{n=1}^{N_g} x(nT_g)w(nT_g)e^{-j2\pi fnT_g}$, N_g is the number of the grid points in $\mathcal{T}_r$, and

$$P_S^d(\mathcal{t}_r) = \frac{1}{\mu_d} \sum_{n=1}^{N_g} E\left[x^2(nT_g)\right] w^2(nT_g). \tag{4.12}$$

The grid rate should be high enough in order to guarantee the usefulness of $C_{RSG}(\mathcal{t}_r, f)$ as discussed in §3.4, i.e. $X_W(\mathcal{t}_r, f)X_W(\mathcal{t}_r, f - nf_g) = 0$ for $n \neq 0$ and $n \in \mathbb{Z}$ which implies $\left|X_W^d(\mathcal{t}_r, f)\right|^2 = f_g^2 \sum_{n\in\mathbb{Z}} \left|X_W(\mathcal{t}_r, f - nf_g)\right|^2$. Whereas, $\chi(\mathcal{t}_r, f) = \sum_{n=1}^{N} E\left[\left|X_{S_n}(\mathcal{t}_r, f)\right|^2\right]$ is the smeared-aliasing reduction factor, $X_{S_n}(\mathcal{t}_r, f) = \int_{\mathcal{S}_n} x(t)w(t)e^{-j2\pi ft}dt$ and $\mathcal{S}_n$ is the n-th stratum of the SSEP scheme.

From (4.8)-(4.10), the estimators' expected values consist of frequency independent components and the expected value of the classical continuous-time periodogram, i.e. $E\left[\left|X_W(\not{t}_r,f)\right|^2\right]\Big/\mu$ as well as the $E\left[\left|X_{\mathrm{S}_n}(\not{t}_r,f)\right|^2\right]\Big/\mu$ in the SSEP case. Whilst the frequency independent components represent the smeared-aliasing phenomenon (except for the noise contribution), they do not overshadow the distinct feature(s) of $E\left[\left|X_W(\not{t}_r,f)\right|^2\right]$ related to the active transmissions. Here, we demonstrate that $E\left[\left|X_W(\not{t}_r,f)\right|^2\right]$ facilitates detecting the M simultaneously active subbands and is independent of $\not{t}_r$ at certain frequencies.

Define: $H_m(f)=\int_{-\infty}^{+\infty}h_m(t)e^{-j2\pi ft}dt$, $P_{i,m}(f)=\int_{-\infty}^{+\infty}p_{i,m}(t)e^{-j2\pi ft}dt$ and $P_{q,m}(f)=\int_{-\infty}^{+\infty}p_{q,m}(t)e^{-j2\pi ft}dt$. To simplify the notation, let: $\hat{P}_{i,m}(f)=H_m(f+f_{C,m})P_{i,m}(f)$, $\breve{P}_{i,m}(f)=H_m(f-f_{C,m})P_{i,m}(f)$, $\hat{P}_{q,m}(f)=H_m(f+f_{C,m})P_{q,m}(f)$ and $\breve{P}_{q,m}(f)=H_m(f-f_{C,m})P_{q,m}(f)$. In Appendix D.1, it is shown that:

$$E\left[\left|X_W(\not{t}_r,f)\right|^2\right]=0.25\sum_{m=1}^{M}\sigma_{a,m}^2 f_{S,m}F_{i,m}(\not{t}_r,f)+\sigma_{b,m}^2 f_{S,m}F_{q,m}(\not{t}_r,f) \tag{4.13}$$

where

$$\begin{aligned}F_{i,m}(\not{t}_r,f)=\sum_{n=-\infty}^{+\infty}\Big[&\hat{P}_{i,m}(f-f_{C,m})\hat{P}_{i,m}^{*}(f-f_{C,m}-nf_{S,m})\\&+\breve{P}_{i,m}(f+f_{C,m})\breve{P}_{i,m}^{*}(f+f_{C,m}-nf_{S,m})\Big]*\Big[W(f)W^{*}(f-nf_{S,m})\Big]\end{aligned} \tag{4.14}$$

and

$$\begin{aligned}F_{q,m}(\not{t}_r,f)=\sum_{n=-\infty}^{+\infty}\Big[&\hat{P}_{q,m}(f-f_{C,m})\hat{P}_{q,m}^{*}(f-f_{C,m}-nf_{S,m})\\&+\breve{P}_{q,m}(f+f_{C,m})\breve{P}_{q,m}^{*}(f+f_{C,m}-nf_{S,m})\Big]*\Big[W(f)W^{*}(f-nf_{S,m})\Big]\end{aligned} \tag{4.15}$$

assuming $f_{C,m}>>B_C$ (B_C is the width of an individual monitored spectral subband). Whereas, $W(f)=\int_{\mathcal{T}_r}w(t)e^{-j2\pi ft}dt$, $*$ denotes the convolution operation and X^{*} insinuates the conjugate of a complex variable X.

The baud rate is normally related to the bandwidth $B_{W,m}$ of the baseband shaping filter(s) $p_{i,m}(t)$ and $p_{q,m}(t)$. It is limited by [50]:

$$0.5B_{W,m}<f_{S,m}\le B_{W,m} \tag{4.16}$$

where $B_{W,m} \le B_C$. This implies: $P_{i,m}(f)P_{i,m}(f-nf_{S,m})=0$ and $P_{q,m}(f)P_{q,m}(f-nf_{S,m})=0$ if $n \notin \{-1,0,1\}$. Consequently, (4.13) reduces to:

$$E\left[\left|X_W(\mathcal{t}_r,f)\right|^2\right] = 0.25\sum_{m=1}^{M}\sigma_{a,m}^2 f_{S,m}\left\{\left[\left|\widehat{P}_{i,m}(f-f_{C,m})\right|^2+\left|\breve{P}_{i,m}(f+f_{C,m})\right|^2\right]*\left|W(f)\right|^2+\varepsilon_{i,m}(\mathcal{t}_r,f)\right\}$$
$$+\sigma_{b,m}^2 f_{S,m}\left\{\left[\left|\widehat{P}_{q,m}(f-f_{C,m})\right|^2+\left|\breve{P}_{q,m}(f+f_{C,m})\right|^2\right]*\left|W(f)\right|^2+\varepsilon_{q,m}(\mathcal{t}_r,f)\right\} \quad (4.17)$$

such that $\varepsilon_{i,m}(\mathcal{t}_r,f)$ and $\varepsilon_{q,m}(\mathcal{t}_r,f)$ are the summands in (4.14) and (4.15) respectively when $n=\pm 1$. Evidently, $E\left[\left|X_W(\mathcal{t}_r,f)\right|^2\right]$ embodies a detectable feature depicted by the windowed squared magnitude of the Fourier transform of the transmission filter(s) shaped by the propagation channel response. According to (4.14) and (4.15), $\varepsilon_{i,m}(\mathcal{t}_r,f)$ and $\varepsilon_{q,m}(\mathcal{t}_r,f)$ are of zero values at the centre of the active system subband provided that (4.16) is satisfied. This affirms that $E\left[\left|X_W(\mathcal{t}_r,f)\right|^2\right]$ at the central part of the transmission band, referred to hereafter as the *guarded region*, is independent of $\mathcal{t}_r$ and poses as the distinguishable component in each of $C_{TRS}(\mathcal{t}_r,f)$, $C_{RSG}(\mathcal{t}_r,f)$ and $C_{SSEP}(\mathcal{t}_r,f)$. The latter includes the smeared-aliasing reduction factor, i.e. $\chi(\mathcal{t}_r,f)/\mu = \sum_{n=1}^{N} E\left[\left|X_{S_n}(\mathcal{t}_r,f)\right|^2\right]\Big/\mu$, which is shown in Appendix D to be independent of $\mathcal{t}_r$ at select frequency points similar to $E\left[\left|X_W(\mathcal{t}_r,f)\right|^2\right]$. It is noted that the expected value of the continuous-time periodogram represents the signal's windowed power spectral density, i.e. $\Phi_X(f)*\left|W(f)\right|^2\big/\mu$, for wide sense stationary signals and is independent of the position of the time analysis window $\mathcal{T}_r$.

Therefore, the adopted estimators are admissible tools to unveil the presence of the active transmissions within the overseen frequency range(s) where the examined frequency points $\{f_k\}$ are placed at/near the centre of the monitored subbands, i.e. within the identified *guarded regions*. Accordingly, averaging a number of spectrum estimates from various $\mathcal{T}_r$'s to enhance the estimation accuracy does not influence the detectability of the spectral components of the present multiband signal since $E\left[\left|X_W(\mathcal{t}_r,f_k)\right|^2\right]$ is independent of $\mathcal{t}_r$.

4.4 Estimation Accuracy

The variance expressions of the total random sampling estimator in §3.3.1, random sampling on grid estimator in §3.4.1 and stratified sampling with equal partitions estimator in §3.5.1 are restated in Appendix D.2, taking into account the cyclostationarity of the signal. We also develop simplified approximations of: $\sigma^2_{e,TRS}(\mathcal{t}_r, f_k) = \mathrm{var}\left\{X_{e,TRS}(\mathcal{t}_r, f_k)\right\}$, $\sigma^2_{e,RSG}(\mathcal{t}_r, f_k) = \mathrm{var}\left\{X_{e,RSG}(\mathcal{t}_r, f_k)\right\}$ and $\sigma^2_{e,SSEP}(\mathcal{t}_r, f_k) = \mathrm{var}\left\{X_{e,SSEP}(\mathcal{t}_r, f_k)\right\}$ prior to utilising them in the next chapter to formulate a reliable spectrum sensing routine. Below, the impact of the signal's cyclostationarity on the estimators' accuracies is outlined where the detailed calculations are presented in Appendix D.3 for each of the studied sampling schemes. Numerical examples are given in §4.5 to demonstrate the effect of the transmission type on the estimators' variances.

4.4.1 Total Random Sampling Estimator

We start by defining:

$$\lambda_R(\mathcal{t}_r, f) = \int_{\mathcal{T}_r}\int_{\mathcal{T}_r} R_X(t_1,t_2)w(t_1)w(t_2)\cos\left(2\pi f t_1 - \theta(\mathcal{t}_r, f)\right)\cos\left(2\pi f t_2 - \theta(\mathcal{t}_r, f)\right)dt_1 dt_2 \qquad (4.18)$$

and

$$\lambda_I(\mathcal{t}_r, f) = \int_{\mathcal{T}_r}\int_{\mathcal{T}_r} R_X(t_1,t_2)w(t_1)w(t_2)\sin\left(2\pi f t_1 - \theta(\mathcal{t}_r, f)\right)\sin\left(2\pi f t_2 - \theta(\mathcal{t}_r, f)\right)dt_1 dt_2 \qquad (4.19)$$

such that $R_X(t_1,t_2) = E\left[x(t_1)x(t_2)\right]$ is the signal's autocorrelation function in (4.7) and $\theta(\mathcal{t}_r, f)$ is the phase-shift either for TRS as in (3.24) or for SSEP as in (3.56). It is noted that:

$$\lambda_R(\mathcal{t}_r, f) + \lambda_I(\mathcal{t}_r, f) = \mu D(\mathcal{t}_r, f) \qquad (4.20)$$

where

$$D(\mathcal{t}_r, f) = E\left[\left|X_W(\mathcal{t}_r, f)\right|^2\right] \Big/ \mu\,. \qquad (4.21)$$

Thus we can write:

$$\lambda_R^2(\mathcal{t}_r, f) + \lambda_I^2(\mathcal{t}_r, f) = \eta_D(\mathcal{t}_r, f)\mu^2 D^2(\mathcal{t}_r, f) \qquad (4.22)$$

where

$$0.5 \le \eta_D(\mathcal{t}_r, f) \le 1 \qquad (4.23)$$

since $0.5\mu^2 D^2(\lambda_r, f) \le \lambda_R^2(\lambda_r, f) + \lambda_I^2(\lambda_r, f) \le \mu^2 D^2(\lambda_r, f)$. As a result:

$$\sigma^2_{e,TRS}(\lambda_r, f_k) \approx \frac{N^2}{(N-1)^2}\left\{\frac{\left[P_S(\lambda_r)+P_N\right]^2}{\alpha^2} + \frac{2(N-1)\left[P_S(\lambda_r)+P_N\right]D(\lambda_r, f_k)}{N\alpha} + 2\eta_D(\lambda_r, f_k)\left[\frac{N-1}{N}D(\lambda_r, f_k)\right]^2\right\} \tag{4.24}$$

and $\eta_D(\lambda_r, f)$ is mandated by:

$$\Gamma(\lambda_r, f) = \lambda_R(\lambda_r, f) - \lambda_I(\lambda_r, f) \tag{4.25}$$

according to (4.22) and (4.23). For instance, if $\lambda_R(\lambda_r, f_k) \approx \lambda_I(\lambda_r, f_k)$, the factor $\eta_D(\lambda_r, f_k) \approx 0.5$. If $\lambda_R(\lambda_r, f_k) \approx 0$, i.e. $\lambda_I(\lambda_r, f_k) \approx D(\lambda_r, f_k)/\mu$, then $\eta_D(\lambda_r, f_k) \approx 1$. Deciding the value of $\eta(\lambda_r, f_k)$, referred to in the sequel as the variance deterioration factor, is of paramount importance since it forms a substantial part of the estimator's variance. Here, we illustrate that $\eta_D(\lambda_r, f_k)$ in (4.24) is affected by the nature of the incoming transmissions.

First, we have: $\lambda_R(\lambda_r, f) = \psi_1(\lambda_r, f) + \psi_2(\lambda_r, f)$ and $\lambda_I(\lambda_r, f) = \psi_1(\lambda_r, f) - \psi_2(\lambda_r, f)$, i.e.

$$\Gamma(\lambda_r, f) = 2\psi_2(\lambda_r, f) \tag{4.26}$$

where

$$\psi_1(\lambda_r, f) = 0.5\sum_{m=1}^{M}\int_{\mathcal{T}_r}\int_{\mathcal{T}_r} R_{X,m}(t_1, t_2)w(t_1)w(t_2)\cos\left(2\pi f(t_1 - t_2)\right)dt_1 dt_2 \tag{4.27}$$

and

$$\psi_2(\lambda_r, f) = 0.25\sum_{m=1}^{M} e^{j2\theta(\lambda_r, f)}G_m(\lambda_r, f) + e^{-j2\theta(\lambda_r, f)}G_m^*(\lambda_r, f) \tag{4.28}$$

for the M simultaneously active subbands. Hence $\psi_2(\lambda_r, f)$ sets the values of $\eta_D(\lambda_r, f)$ owing to (4.25) and (4.26), for example $\eta(\lambda_r, f_k) \approx 0.5$ if $\psi_2(\lambda_r, f_k) \approx 0$. To exhibit the impact of the signal's cyclostationarity on (4.24), we assume that the Fourier transform of the $w(t)$ reduces to a Dirac delta $\delta(f)$, i.e. very long time analysis window. Subsequently,

$$\begin{aligned} G_m(\lambda_r, f) = {} & 0.125 f_{S,m}\left[H_m(f)\right]^2\left\{\sigma^2_{a,m}\left[P_{i,m}(f - f_{C,m})\right]^2 - \sigma^2_{b,m}\left[P_{q,m}(f - f_{C,m})\right]^2\right\}\sum_{n=-\infty}^{+\infty}\delta(f - f_{C,m} - 0.5nf_{S,m}) \\ & + 0.125 f_{S,m}\left[H_m(f)\right]^2\left\{\sigma^2_{a,m}\left[P_{i,m}(f + f_{C,m})\right]^2 - \sigma^2_{b,m}\left[P_{q,m}(f + f_{C,m})\right]^2\right\}\sum_{n=-\infty}^{+\infty}\delta(f + f_{C,m} - 0.5nf_{S,m}). \end{aligned} \tag{4.29}$$

Formula (4.29) shows that $\psi_2(\lambda_r, f)$ in (4.26) can have nonzero values concentrated at frequencies equal to shifted multiples of half of the symbol rate, i.e. $\pm f_{C,m} - 0.5nf_{S,m}$ $(n \in \mathbb{Z})$, and belong to the transmission band provided that $\sigma_{a,m}^2 P_{i,m}(f) \neq \sigma_{b,m}^2 P_{q,m}(f)$. For a range of modulations schemes, e.g. QAM and QPSK, this condition is not satisfied where typically $\sigma_{a,m}^2 = \sigma_{b,m}^2$ and the shaping filters in the in-phase and quadrature branches are presumed to be identical, i.e. $\left[P_{i,m}(f)\right]^2 - \left[P_{q,m}(f)\right]^2 = 0$. Clearly, in this case $\psi_2(\lambda_r, f) \approx 0$ and $\eta_D(\lambda_r, f) \approx 0.5$ within the m-th active subband. Any mismatch between these two branches, i.e. $\sigma_{a,m}^2 P_{i,m}(f) - \sigma_{b,m}^2 P_{q,m}(f) \neq 0$, can lead to discrepancies between $\lambda_R(\lambda_r, f)$ and $\lambda_I(\lambda_r, f)$, which result in surges in the variance values at selected frequency points according to (4.22), (4.23) and (4.29). Such a mismatch can be due to implementation imperfections at the transmitter end. For a BPSK signal, formula (4.29) becomes:

$$\begin{aligned} G_m(\lambda_r, f) = 0.125 f_{S,m} \sigma_{a,m}^2 \left[H_m(f)\right]^2 \sum_{n=-\infty}^{+\infty} & \left[P_{i,m}(f - f_{C,m})\right]^2 \delta(f - f_{C,m} - 0.5nf_{S,m}) \\ & + \left[P_{i,m}(f + f_{C,m})\right]^2 \delta(f + f_{C,m} - 0.5nf_{S,m}). \end{aligned} \tag{4.30}$$

It indicates that $\psi_2(\lambda_r, f)$ and consequently $\eta_D(\lambda_r, f)$ acquire their maximum values, i.e. $\eta_D(\lambda_r, f) \approx 1$, at/near the frequency points $f_n = \pm f_{C,m} - 0.5nf_{S,m}$ and $n \in \mathbb{Z}$ such that $f_n \in \pm\left[f_{C,m} - 0.5B_{W,m}, f_{C,m} + 0.5B_{W,m}\right]$ for the m-th active channel. This produces a notable deterioration in the estimator's accuracy according to (4.24).

Therefore, the performance of the periodogram-type estimator can be significantly affected by the signal's cyclostationarity and any processing task that relies on the spectral analysis, e.g. spectrum sensing, should consider the possible presence of such phenomenon. It can be noticed from (4.29) that such a severe decline in the estimation accuracy can take place at the central part of the system channels, i.e. within the predefined *guarded region*. This can undermine the reliability of the detection technique and necessitates taking counter measures, especially if the spectrum at the sensed frequency points $\{f_k\}$ is subject to the aforementioned additional inaccuracies. With regards to handling wide sense stationary signals as in Chapter 3, the sharp accuracy decay phenomenon is not observed and it is shown in Appendix D.3.4 that $\eta_D(\lambda_r, f) \approx 0.5$ is commensurate (see also the numerical examples in §3.3.2, §3.4.2 and §3.5.2).

4.4.2 Random Sampling on Grid Estimator

The variance of the RSG estimator is closely approximated in Appendix D.2 by:

$$\sigma^2_{e,RSG}(\mathcal{t}_r, f_k) \approx \left[\frac{N_g - N}{(N-1)f_g}\right]^2 \left[P_S^d(\mathcal{t}_r) + \frac{(N_g - 1)}{(N_g - N)} P_N\right]^2 + \frac{2(N_g - N)}{(N-1)f_g}\left[P_S^d(\mathcal{t}_r) + \frac{(N_g - 1)P_N}{(N_g - N)}\right] D^d(\mathcal{t}_r, f_k) + 2\eta_D^d(\mathcal{t}_r, f_k)\left[D^d(\mathcal{t}_r, f_k)\right]^2 \tag{4.31}$$

where

$$D^d(\mathcal{t}_r, f) = \frac{1}{\mu_d f_g} E\left[\left|X_W^d(\mathcal{t}_r, f)\right|^2\right] \tag{4.32}$$

and

$$0.5 \le \eta_D^d(\mathcal{t}_r, f) \le 1. \tag{4.33}$$

The latter parameter stems from: $\lambda_R^d(\mathcal{t}_r, f) + \lambda_I^d(\mathcal{t}_r, f) = \mu_d f_g D^d(\mathcal{t}_r, f)$ and

$$\left\{\lambda_R^d(\mathcal{t}_r, f)\right\}^2 + \left\{\lambda_I^d(\mathcal{t}_r, f)\right\}^2 = \eta_D^d(\mathcal{t}_r, f)\left\{\mu_d f_g D^d(\mathcal{t}_r, f)\right\}^2 \tag{4.34}$$

whilst

$$\lambda_R^d(\mathcal{t}_r, f) = \sum_{n=1}^{N_g}\sum_{m=1}^{N_g} R_X(nT_g, mT_g) w(nT_g) w(mT_g) \cos\left(2\pi f n T_g - \theta_{RSG}(\mathcal{t}_r, f)\right) \cos\left(2\pi f m T_g - \theta_{RSG}(\mathcal{t}_r, f)\right) \tag{4.35}$$

$$\lambda_I^d(\mathcal{t}_r, f) = \sum_{n=1}^{N_g}\sum_{m=1}^{N_g} R_X(nT_g, mT_g) w(nT_g) w(mT_g) \sin\left(2\pi f n T_g - \theta_{RSG}(\mathcal{t}_r, f)\right) \sin\left(2\pi f m T_g - \theta_{RSG}(\mathcal{t}_r, f)\right). \tag{4.36}$$

If $\lambda_R^d(\mathcal{t}_r, f_k) \approx 0$, i.e. $\lambda_I^d(\mathcal{t}_r, f_k) \approx \mu_d f_g D^d(\mathcal{t}_r, f_k)$, thus $\eta_D^d(\mathcal{t}_r, f_k) \approx 1$. Alternatively, if $\lambda_R^d(\mathcal{t}_r, f_k) \approx \lambda_I^d(\mathcal{t}_r, f_k)$, then $\eta_D^d(\mathcal{t}_r, f_k) \approx 0.5$. Hence the value of $\eta_D(\mathcal{t}_r, f)$ is dictated by:

$$\Gamma^d(\mathcal{t}_r, f) = \lambda_R^d(\mathcal{t}_r, f) - \lambda_I^d(\mathcal{t}_r, f) = 2\psi_2^d(\mathcal{t}_r, f) \tag{4.37}$$

where

$$\psi_2^d(\mathcal{t}_r, f) = 0.25\sum\nolimits_{m=1}^{M}\left\{e^{j2\theta_{RSG}(\mathcal{t}_r, f)} G_m^d(\mathcal{t}_r, f) + e^{-j2\theta_{RSG}(\mathcal{t}_r, f)}\left[G_m^d(\mathcal{t}_r, f)\right]^*\right\} \tag{4.38}$$

and it is shown in Appendix D.3 that:

$$G_m^d(\mathcal{t}_r, f) = \frac{f_{S,m} f_g^2}{8}\sum_{n=-\infty}^{+\infty}\left[H_m(f - nf_g)\right]^2 \left\{\sigma_{a,m}^2\left[P_{i,m}(f - f_{C,m} - nf_g)\right]^2 - \sigma_{b,m}^2\left[P_{q,m}(f - f_{C,m} - nf_g)\right]^2\right\} \sum_{l=-\infty}^{+\infty}\delta(f - f_{C,m} - 0.5lf_{S,m} - nf_g) + \left[H_m(f - nf_g)\right]^2 \times \left\{\sigma_{a,m}^2\left[P_{i,m}(f + f_{C,m} - nf_g)\right]^2 - \sigma_{b,m}^2\left[P_{q,m}(f + f_{C,m} - nf_g)\right]^2\right\} \sum_{l=-\infty}^{+\infty}\delta(f + f_{C,m} - 0.5lf_{S,m} - nf_g) \tag{4.39}$$

assuming an infinitely long signal analysis window for simplicity. For the BPSK modulation scheme, (4.39) reduces to:

$$G_m^d(\mathcal{t}_r,f)=\frac{f_{S,m}f_g^2\sigma_{a,m}^2}{8}\sum_{n=-\infty}^{+\infty}\left[H_m(f-nf_g)\right]^2\left\{\left[P_{i,m}(f-f_{C,m}-nf_g)\right]^2\sum_{l=-\infty}^{+\infty}\delta(f-f_{C,k}-0.5lf_{S,k}-nf_g)\right.$$
$$\left.+\left[P_{i,m}(f+f_{C,m}-nf_g)\right]^2\sum_{l=-\infty}^{+\infty}\delta(f+f_{C,m}-0.5lf_{S,m}-nf_g)\right\}. \tag{4.40}$$

It can be seen from (4.31), (4.33), (4.34) and (4.39) that the random sampling on grid estimator, similar to the TRS one, can be subject to abrupt increases in its variance values at selected frequency points due to the cyclostationarity of the signal. For instance, if the incoming transmission over the m-th channel is of a BPSK type, the estimated spectrum suffers from additional estimation errors at $f=f_{C,k}$ due to the fact that $\sigma_{e,RSG}^2(\mathcal{t}_r,f_k)$ value surges at such frequencies since $\eta_D^d(\mathcal{t}_r,f_{C,k})\approx 1$ given (4.31), (4.34), (4.38) and (4.40).

4.4.3 Stratified Sampling with Equal Partitions Estimator

The smeared-aliasing reduction factor:

$$A(\mathcal{t}_r,f)=\frac{1}{\mu}\chi(\mathcal{t}_r,f)=\frac{1}{\mu}\sum_{n=1}^{N}E\left[\left|\int_{\mathcal{S}_n}x(t)w(t)e^{-j2\pi ft}dt\right|^2\right] \tag{4.41}$$

consists of:

$$\chi_R(\mathcal{t}_r,f)=\sum_{n=1}^{N}\int_{\mathcal{S}_n}\int_{\mathcal{S}_n}R_X(t_1,t_2)w(t_1)w(t_2)\cos\left(2\pi ft_1-\theta_{SS}(\mathcal{t}_r,f)\right)\cos\left(2\pi ft_2-\theta_{SS}(\mathcal{t}_r,f)\right)dt_1dt_2 \tag{4.42}$$

$$\chi_I(\mathcal{t}_r,f)=\sum_{n=1}^{N}\int_{\mathcal{S}_n}\int_{\mathcal{S}_n}R_X(t_1,t_2)w(t_1)w(t_2)\sin\left(2\pi ft_1-\theta_{SS}(\mathcal{t}_r,f)\right)\sin\left(2\pi ft_2-\theta_{SS}(\mathcal{t}_r,f)\right)dt_1dt_2\ . \tag{4.43}$$

Then,

$$\chi_R(\mathcal{t}_r,f)+\chi_I(\mathcal{t}_r,f)=\mu A(\mathcal{t}_r,f) \tag{4.44}$$

and

$$\chi_R^2(\mathcal{t}_r,f)+\chi_I^2(\mathcal{t}_r,f)=\eta_A(\mathcal{t}_r,f)\mu^2A^2(\mathcal{t}_r,f) \tag{4.45}$$

where

$$0.5\le\eta_A(\mathcal{t}_r,f)\le 1 \tag{4.46}$$

is controlled by $\Gamma_A(\mathcal{t}_r,f)=\chi_R(\mathcal{t}_r,f)-\chi_I(\mathcal{t}_r,f)$. On the other hand,

$$\chi_R(\lambda_r,f)\lambda_R(\lambda_r,f)+\chi_I(\lambda_r,f)\lambda_I(\lambda_r,f)=\eta_{DA}(\lambda_r,f)\mu^2 D(\lambda_r,f)A(\lambda_r,f) \tag{4.47}$$

and hence

$$0.5\le\eta_{DA}(\lambda_r,f)\le 1 \tag{4.48}$$

where $D(\lambda_r,f)$ is defined in (4.21). As a result, we attain:

$$\begin{aligned}\sigma^2_{e,SSEP}(\lambda_r,f_k)=&\frac{\left[P_S(\lambda_r)+P_N\right]^2}{\alpha^2}+2\eta_A(\lambda_r,f_k)A^2(\lambda_r,f_k)+2\eta_D(\lambda_r,f_k)D^2(\lambda_r,f_k)\\&-\frac{2\left[P_S(\lambda_r)+P_N\right]}{\alpha}A(\lambda_r,f_k)+\frac{2\left[P_S(\lambda_r)+P_N\right]}{\alpha}D(\lambda_r,f_k)-4\eta_{DA}(\lambda_r,f_k)D(\lambda_r,f_k)A(\lambda_r,f_k).\end{aligned} \tag{4.49}$$

The behaviour of $\eta_D(\lambda_r,f)$ in (4.49) is identical to that for the TRS estimator in (4.24). The value of $\eta_A(\lambda_r,f)$ in (4.49) is set by $\Gamma_A(\lambda_r,f)$; $\eta_A(\lambda_r,f_k)$ can reach its maximum values at selected frequency points for certain modulation schemes (see Appendix D.3.3). If either $\chi_R(\lambda_r,f_k)\approx\chi_I(\lambda_r,f_k)\approx 0.5\mu A(\lambda_r,f_k)$ or $\lambda_R(\lambda_r,f_k)\approx\lambda_I(\lambda_r,f_k)\approx 0.5\mu A(\lambda_r,f_k)$, we have: $\eta_{DA}(\lambda_r,f_k)\approx 0.5$. On the contrary, if $\lambda_R(\lambda_r,f_k)\approx 0$, i.e. $\lambda_I(\lambda_r,f_k)\approx\mu D(\lambda_r,f_k)$, then $\eta_{DA}(\lambda_r,f_k)\approx 1$; $\chi_R(\lambda_r,f_k)\approx 0$ or $\chi_I(\lambda_r,f_k)\approx 0$ would have an identical effect.

4.4.4 Remarks on the Accuracy Deterioration Parameters

Selecting the values of $\eta_D(\lambda_r,f)$, $\eta_D^d(\lambda_r,f)$, $\eta_A(\lambda_r,f)$ and $\eta_{DA}(\lambda_r,f)$ can seem to be a burdensome task that requires an exact knowledge of the processed signal. However, we recall that the aim behind the conducted spectral analysis is to perform spectrum sensing and the developed variance expressions in (4.24), (4.31) and (4.49) are utilised in the next chapter to formulate a reliable detection procedure. If no exact knowledge of the signal and its characteristics are available, the user has to resort to conservative measures, e.g. $\eta_D(\lambda_r,f_k)=\eta_D^d(\lambda_r,f)=\eta_A(\lambda_r,f_k)=\eta_{DA}(\lambda_r,f_k)=1$, to avoid any unforeseen inaccuracies. If more information about the signal becomes available (e.g. the modulation scheme, $\sigma^2_{a,m}P_{i,m}(f)-\sigma^2_{b,m}P_{q,m}(f)$ and the symbol rate) the user can make a more informed choice of $\eta_D(\lambda_r,f)$, $\eta_D^d(\lambda_r,f)$, $\eta_A(\lambda_r,f)$ and $\eta_{DA}(\lambda_r,f)$.

It is noted that the preceding estimation accuracy analysis for WSCS signals presumed an infinitely long signal time window to simplify the calculations. In practice, the analysis time window is finite and any differences between $\lambda_R(\lambda_r,f)$ and $\lambda_I(\lambda_r,f)$, $\lambda_R^d(\lambda_r,f)$ and $\lambda_I^d(\lambda_r,f)$, or $\chi_R(\lambda_r,f)$ and $\chi_I(\lambda_r,f)$ do not only occur at the identified frequencies in

§4.4.1, §4.4.2 and §4.4.3, but also in their vicinities depending on T_0. This implies that the remarkable surges in the estimators' variances for sources whose $\sigma_{a,m}^2 P_{i,m}(f) \neq \sigma_{b,m}^2 P_{q,m}(f)$ can appear in the neighbourhood of $f_n = \pm f_{C,m} - 0.5nf_{S,m}$ ($n \in \mathbb{Z}$ and f_n points belong to the spectral support of the transmission band). Numerical examples are given below to depict this fact (see Figure 4.3). To avoid such cases, the user can employ long signal analysis windows. They lead to longer wait times before an estimation result is obtained and the time needed to detect the active spectral components is significantly increased. This degrades the benefits of the spectrum sensing approach, especially for continuous real-time sensing where a number of estimates from various signal windows are averaged before a detection decision is made.

4.5 Numerical Examples

Consider a system operating over 10 non-overlapping spectral subbands residing inside $\mathcal{B} = [1.45,1.55]$ GHz, i.e. $f_{\min} = 1.45$ GHz, the width of each channel is $B_C = 10$ MHz and the total monitored bandwidth is $B = 100$ MHz. A Blackman window of width $T_0 = 10\mu s$ and an average sampling rate of $\alpha = 90$ MHz are used. The SNR is -1.5 dB and two concurrently active transmissions with equal power levels are present. The variances of the TRS, RSG and SSEP estimators are tested for various modulation schemes; the symbol rate of the active subband with the central frequency $f_{C,3} = 1.475$ GHz is $f_{S,3} = 6$ MSym/s and the one centred at $f_{C,7} = 1.515$ GHz has a baud rate of $f_{S,7} = 9$ MSym/s. All the displayed Mean Squared Errors (MSEs) are attained from 50000 independent experiments.

In Figure 4.1, the variance $\sigma_{e,TRS}^2(t_r, f)$ defined in (4.24) for the entire overseen range of frequencies is compared against the MSE. The corresponding $\eta_D(t_r, f)$ is calculated from (4.22), i.e. $\eta_D(t_r, f) = \left[\lambda_R^2(t_r, f) + \lambda_I^2(t_r, f)\right] / \left[\mu^2 D^2(t_r, f)\right]$. The two transmissions in Figure 4.1a are BPSK modulated signals and those in Figure 4.1b are 16QAM whose $\sigma_{a,m}^2 P_{i,m}(f) = \sigma_{b,m}^2 P_{q,m}(f)$. From the former figure, it can be seen that the estimator's variance grows noticeably at/near the predicted frequency points in (4.30), i.e. $f_{n_3} = f_{C,3} - 0.5nf_{S,3}$ and $f_{n_7} = f_{C,7} - 0.5nf_{S,7}$ such that $n = \{-1,0,1\}$ where an $\eta_D(t_r, f_{n_1}) \approx 1$ is recorded. In Figure 4.1b, the estimator retains its consistency within the active subbands where $\eta_D(t_r, f) \approx 0.5$. The close match between the analytical and simulation results in

both plots in Figure 4.1 confirms the accuracy of the approximation in (4.24). Figure 4.2a exhibits $\lambda_R(\mathcal{t}_r, f)$ and $\lambda_I(\mathcal{t}_r, f)$ for the BPSK signals in Figure 4.1a. It shows that $\Gamma(\mathcal{t}_r, f)$ in (4.25) peaks at $\{f_{n_3}\}$ and $\{f_{n_7}\}$ causing the considerable decay in the estimation accuracy. Whereas, $\Gamma(\mathcal{t}_r, f) \approx 0$ for the 16QAM transmission in Figure 4.2b.

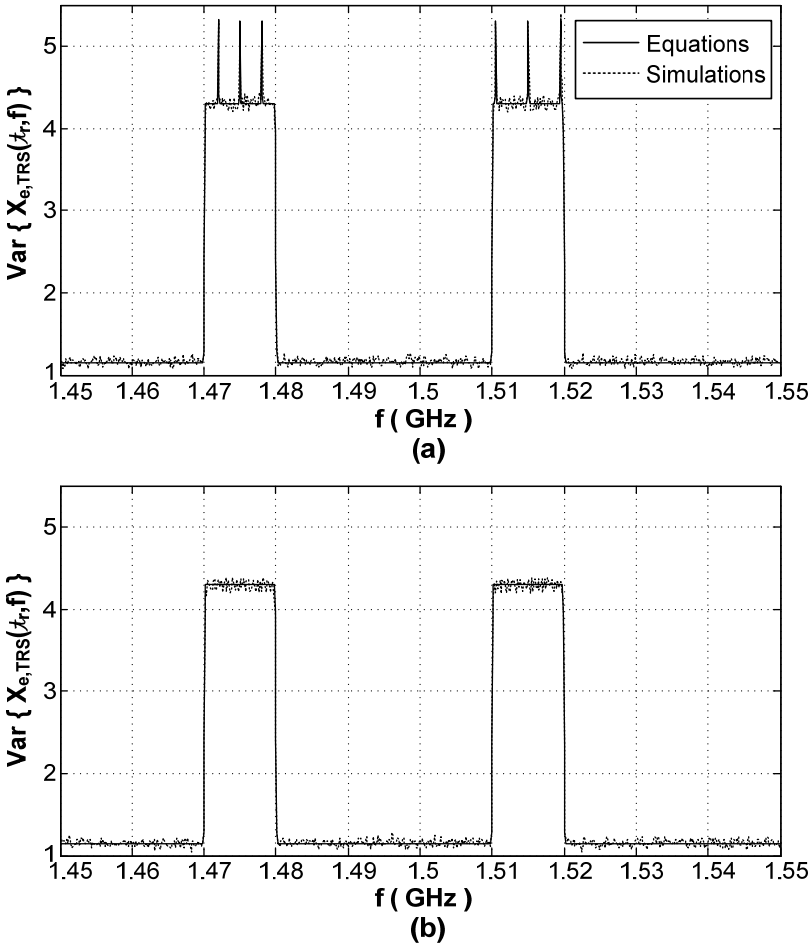

Figure 4.1: The variance of the TRS estimator from equation (4.24) and simulations. (a) For BPSK transmissions. (b) For 16QAM transmissions.

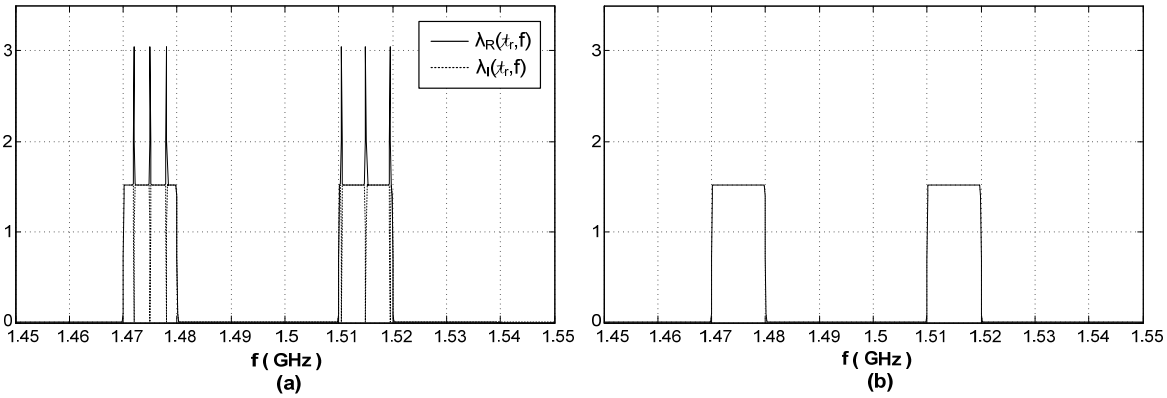

Figure 4.2: $\lambda_R(\mathcal{t}_r, f)$ and $\lambda_I(\mathcal{t}_r, f)$ for the examples in Figure 4.1. (a) For BPSK modulations. (b) For 16QAM modulations.

To demonstrate the effect of the width of the time analysis window on the frequency region(s) that are affected by the cyclostationarity of the signal, Figure 4.3 depicts the variance of the TRS estimator for the BPSK transmissions in Figure 4.1a and various T_0 values. We zoom around the occupied subband centred at $f_{C,3} = 1.475\,\text{GHz}$. It can be noted from Figure 4.3 that the sharp decline in the estimator's accuracy spreads to the vicinity of the identified frequencies $\{f_{n_3}\}$. This becomes more visible for shorter $\mathcal{T}_r = [t_r, t_r + T_0]$. Nonetheless, the deterioration reaches its highest levels at $\{f_{n_3}\}$ and diminishes as we move away from these frequencies.

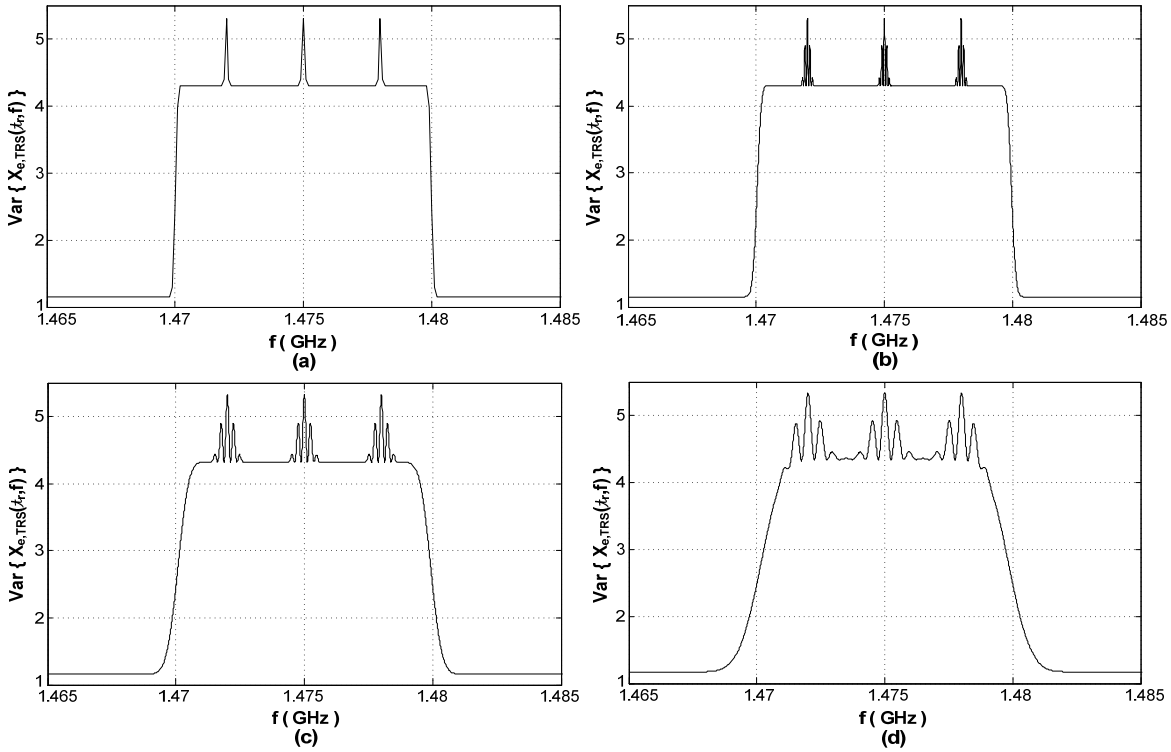

Figure 4.3: $\sigma^2_{e,TRS}(t_r, f)$ in (4.24) for the BPSK transmissions in Figure 4.1a using various T_0 values; zoomed around $f = 1.475\,\text{GHz}$. (a) $T_0 = 10\mu s$. (b) $T_0 = 5\mu s$. (c) $T_0 = 2\mu s$. (d) $T_0 = 1\mu s$.

In Figures 4.4 and 4.5, the transmission with the carrier frequency $f_{C,3} = 1.475\,\text{GHz}$ is of a BPSK nature whilst the subband whose central frequency is $f_{C,7} = 1.515\,\text{GHz}$ is occupied by a QPSK signal. The variance of the RSG estimator $\sigma^2_{e,RSG}(t_r, f)$ in (4.31) is displayed in Figure 4.4 along with the MSE, the grid rate is $f_g = 240\,\text{MHz}$. It can be observed that

$\sigma^2_{e,RSG}(\not{t}_r, f)$ notably increases at/near $f_{n_3} = f_{C,3} - 0.5nf_{S,3}$ where $n = \{-1,0,1\}$ only for the BPSK transmission unlike the QPSK one as anticipated. Similar observations are made for the SSEP case in the numerical example in Figure 4.5 despite the additional complications due to the smeared-aliasing reduction factor featured by $\eta_A(\not{t}_r, f)$ and $\eta_{DA}(\not{t}_r, f)$ in (4.49).

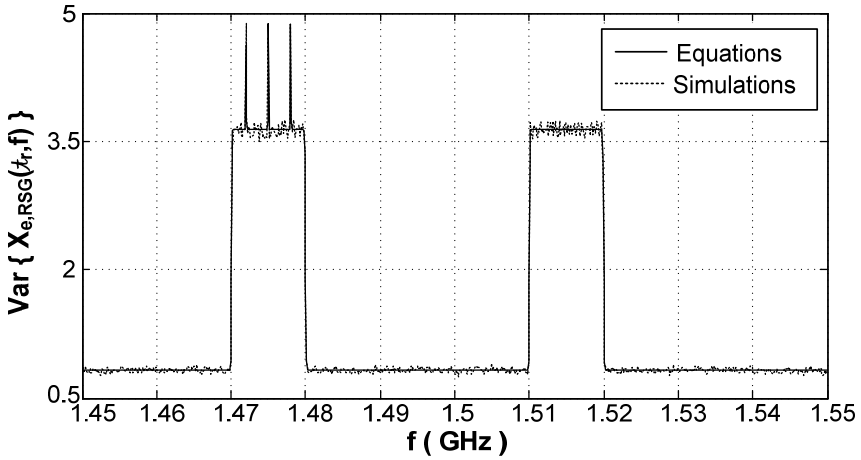

Figure 4.4: RSG estimator's variance from equation (4.31) and simulations where transmission with the central frequencies $f_{C,3} = 1.475$ GHz and $f_{C,7} = 1.515$ GHz are BPSK and QPSK respectively.

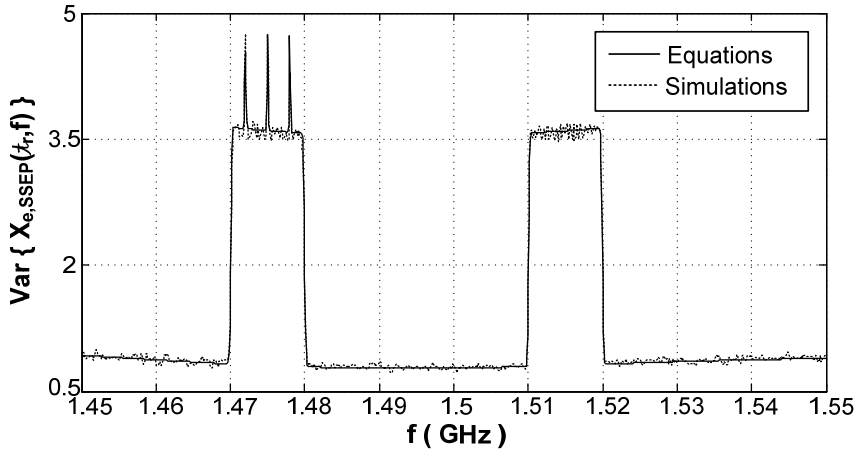

Figure 4.5: SSEP estimator's variance from equation (4.49) and simulations where the subbands with the central frequencies $f_{C,3} = 1.475$ GHz and $f_{C,7} = 1.515$ GHz are occupied by BPSK and QPSK transmissions respectively.

4.6 Chapter Summary and Discussion

Processing cyclostationary signals alters the behaviour and the statistical characteristics of the adopted periodogram tool, an influence we explored in this chapter. By placing the

examined frequency points $\{f_k\}$ at the central parts of the monitored subbands (i.e. in the revealed *guarded regions*) the TRS, RSG and SSEP estimators continue to be legitimate tools to unveil the presence of active spectral components in the surveyed range of frequencies. However, for certain modulation schemes such as BPSK, the estimation accuracy notably declines due to the variance abruptly surging at predefined frequencies that belong to the transmission band. These frequencies are prescribed by the transmission carrier frequency (which is one of the affected spectral points) and the symbol rate. If the latter two parameters are *a priori* known, the regions where the additional estimation performance decay occurs can be avoided. It was illustrated that increasing the width of the signal analysis window confines the accuracy deterioration to very narrow frequency regions. Although such a precaution facilitates averting the possible repercussions of processing cyclostationary signals on the quality of the spectrum estimation, it leads to a longer processing time. For other modulation schemes, e.g. QAM with matched in-phase and quadrature processing chains, the estimation accuracy is similar to that of the wide sense stationary signals where the sharp increases in the variance levels are not experienced.

In the studied communication systems, no previous knowledge of either the symbol rate or the modulation scheme is assumed, i.e. predicting the locations of any estimation accuracy decline is not feasible. Furthermore, short signal analysis windows are highly desired since they lead to fast efficient spectrum sensing that can conform to stringent sensing time requirements of real-time processing. Thus placing $\{f_k\}$ at the central parts of the overseen subbands and adopting a conservative approach towards the accuracy of the spectrum estimation is a reasonable approach to undertake.

Chapter 5

Multiband Spectrum Sensing in Wideband Communication Systems

Spectrum sensing involves scanning predefined part(s) of the radio spectrum in search of meaningful activity such as an ongoing transmission or the occurrence of an event. Standard communications laboratory test equipment, e.g. spectrum analysers, can perform similar functionality. They conventionally sweep the spectrum using a narrowband tuneable bandpass filter(s) and determine the energy within each of the scanned spectral bands. The spectral support of the present signal is displayed based on whether the attained energy in a given frequency band exceeds a certain noise floor. Such instruments are usually bulky and expensive; consequently their solutions are inadequate for the investigated wireless communication systems whose resources (e.g. cost, weight, size and power) are limited.

Spectrum sensing has a wide diversity of application areas including astronomy [76, 77], interception [120], seismology [121], communication systems [15, 122] and many others. Notably, the conceptualised Cognitive Radio (CR) technology has recently revived and intensified the research into effective sensing techniques [10, 14-20, 123]. The majority of these methods, which deploy digital signal processing, are uniform sampling based, see Table 5.1. The remarkably high sampling rates imposed by classical DSP (especially for wideband applications) obstruct the wide spread of such promising technologies and restrict their applicability.

In this chapter, we propose a Multiband Spectrum Sensing (MSS) approach that utilises randomised sampling and its spectral analysis to accomplish the sensing task using

considerably low sampling rates. Since the spectrum sensing procedure does not necessitate signal reconstructing, it is shown that the sampling rates can be arbitrarily low for some randomised sampling schemes. Most importantly, general guidelines are provided to ensure that the developed MSS satisfies certain detection probabilities set by the user. These recommendations exhibit the trade-off between the required sampling rate and the length of the signal observation window (sensing time) in a given scenario. Additionally, a number of miscellaneous system considerations are addressed.

5.1 System Model

5.1.1 Wideband Spectrum Sensing and Detection Probabilities

We recall from §1.2 that the studied systems operate over L non-overlapping contiguous spectral subbands/channels occupying the frequency range $\mathcal{B} = [f_{\min}, f_{\min} + B]$. Each of the channels is of width B_C and $B = LB_C$ is the total processed bandwidth. The incoming multiband signal consists of an unknown M number of concurrently active transmissions and is given by:

$$x(t) = \sum_{m=1}^{M} x_m(t) = \sum_{m=1}^{M} x_{T,m}(t) * h_m(t) \tag{5.1}$$

where $*$ denotes the convolution operation. The maximum expected number of simultaneously active subbands at any time is $L_A \geq M$. Whereas, $x_m(t)$ and $h_m(t)$ are the incoming signal given in (4.3)-(4.5) corresponding to the m-th subband and the impulse response of its propagation channel respectively; the latter is assumed to be deterministic. The collected samples of the received signal $y(t)$ are contaminated with Additive White Gaussian Noise (AWGN) with variance P_N, i.e. $y(t_n) = x(t_n) + n(t_n)$. The objective is to devise a method that is capable of scanning the overseen frequency range $\mathcal{B}$ and reliably identifying the active subbands. It should operate at rates significantly lower than those requested by uniform-sampling-based approaches where $f_{US} \geq 2B$ [31]; $2B$ is referred to as Nyquist rate thereafter.

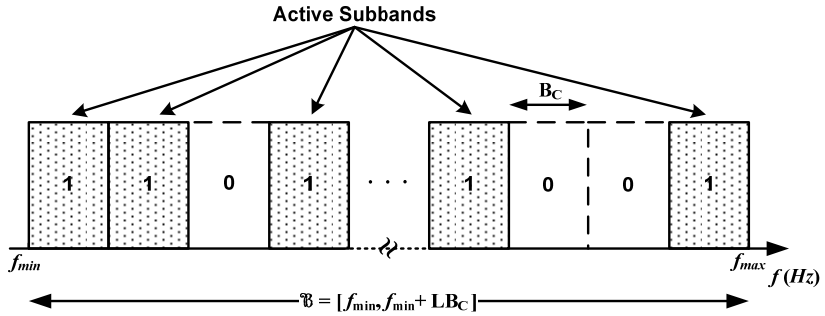

Figure 5.1: Illustration of the occupancy of the system subbands ("0" indicates that no transmission is present over the subband and "1" signifies the presence of an activity).

Evidently, the spectrum sensing problem boils down to choosing between the hypothesis ("0"), i.e. $\mathcal{H}_{0,k}$ which represents the absence of any activity within the k-th subband, and the alternative hypothesis ("1"), i.e. $\mathcal{H}_{1,k}$ which infers the presence of a transmission. An example where some of the subbands are occupied is exhibited in Figure 5.1. The performance of a spectrum sensing technique is commonly measured by the Receiver Operating Characteristics (ROC) that captures the relation between the probability of false alarm $P_{f,k} = \Pr\left\{\mathcal{H}_{1,k} \middle| \mathcal{H}_{0,k}\right\}$ and the probability of detection $P_{d,k} = \Pr\left\{\mathcal{H}_{1,k} \middle| \mathcal{H}_{1,k}\right\}$ in the k-th system subband [10, 15, 17-20, 124]. These probabilities are typically interrelated via the detection threshold γ_k whose value trades $P_{d,k}$ for $1 - P_{f,k}$ and vice versa. Accordingly, the reliability and robustness of the proposed spectrum sensing approach is reflected by its ability to fulfil a set of sought detection probabilities, i.e. $P_{d,k}$ and $P_{f,k}$ for one or more of the monitored system channels. Here, guidelines are derived to guarantee meeting such demands.

5.1.2 Proposed Sensing Approach

Unlike methods that employ spectral analysis to estimate the subband(s) energy, e.g. the classical energy detector (see §5.2), the introduced sensing procedure comprises three steps:

1) Randomly sampling the incoming signal at substantially low rates

2) Estimating the magnitude of the signal spectrum at selected frequency point(s)

3) Comparing the magnitude(s) with pre-calculated threshold(s)

Having a spectrograph that is relatively smooth would permit assessing fewer frequency points per system subband to determine its status. We seek to inspect one frequency point per channel, i.e. L spectral points are calculated. Consequently, the spectrum sensing problem can be described by the conventional binary hypothesis testing:

$$\begin{aligned} \mathcal{H}_{0,k}: &\quad \hat{X}_e(f_k) < \gamma_k \\ \mathcal{H}_{1,k}: &\quad \hat{X}_e(f_k) \geq \gamma_k \qquad ,k = 1,2,\ldots,L \end{aligned} \tag{5.2}$$

where $\hat{X}_e(f)$ is the estimated magnitude spectrum and γ_k is the threshold. The frequency points $\{f_k\}_{k=1}^{L}$ are placed at the centre of the system subbands as discussed in Chapter 4.

The standard deviations of the used periodogram-type estimators, i.e. $X_{e,TRS}(\mathcal{t}_r, f)$ in (3.8), $X_{e,RSG}(\mathcal{t}_r, f)$ in (3.27) and $X_{e,SSEP}(\mathcal{t}_r, f)$ in (3.44), were shown in Chapters 3 and 4 to be of the same order as their expected values. To control such uncertainties, we average a K number of estimates in (5.2). They are calculated from K signal windows each of width T_0, i.e. $\mathcal{T}_r = [\mathcal{t}_r, \mathcal{t}_r + T_0]$ for $r = 1,2,\ldots,K$, such that:

$$\hat{X}_e(f) = \frac{1}{K}\sum_{r=1}^{K} X_e(\mathcal{t}_r, f). \tag{5.3}$$

This entails shifting $\mathcal{T}_r$ and repositioning of the windowing function $w(t)$. Each of:

$$\hat{X}_{e,TRS}(f) = \frac{1}{K}\sum_{r=1}^{K} X_{e,TRS}(\mathcal{t}_r, f) \tag{5.4}$$

for Total Random Sampling (TRS),

$$\hat{X}_{e,RSG}(f) = \frac{1}{K}\sum_{r=1}^{K} X_{e,RSG}(\mathcal{t}_r, f) \tag{5.5}$$

for Random Sampling on Grid (RSG) and

$$\hat{X}_{e,SSEP}(f) = \frac{1}{K}\sum_{r=1}^{K} X_{e,SSEP}(\mathcal{t}_r, f) \tag{5.6}$$

for Stratified Sampling with Equal Partitions (SSEP) replace the generic estimator $\hat{X}_e(f)$ in (5.2). Here, non-overlapping uncorrelated signal windows are considered.

In this chapter, we show that (5.4)-(5.6) deliver reliable spectrum sensing that meets preset detection probabilities provided the suitable selection of the following: the width of the time analysis window T_0, the average sampling rate $\alpha = N/T_0$ and the number of estimate averages K. The latter two parameters are the available means to curb any perturbations or anomalies in the estimation process, i.e. guarantee a certain level of accuracy. Any recommendations on the values of α and K should take into account severe system conditions to safeguard the response of the MSS method, e.g. the maximum spectrum occupancy and the highest harmful effect of the smeared-aliasing phenomenon. This approach is adopted in this research to develop the pursued guidelines and obtain the analytical expressions of the threshold values in (5.2).

5.1.3 Signal Analysis Window

Achieving the minimum sensing time is a highly desirable feature for any spectrum sensing technique, particularly if sensing is a continuous real-time operation that has to fulfil specific time constraints, e.g. the CR IEEE 802.22 highlights such a requirement. Hence we aim to utilise a short time analysis window $\mathcal{T}_r$ where the sensing time is KT_0 according to (5.4)-(5.6). Furthermore, since the processed signals are of stationary or cyclostationary nature, attaining low resolution spectrographs via a short time analysis window $\mathcal{T}_r$ facilitates minimising the number of needed frequency points per system subband to establish any activity within, i.e. save on computations noting that one frequency point per channel is examined in (5.2). Using the theorem of minimum number of zero-crossings of bandlimited signals as discussed in [45, p. 170] and exploiting the frequency-time duality characteristic [44] enables us to deploy the number of zero-crossings per channel as a criterion to describe the resolution of the spectrum. A zero-crossing is perceived as a notable fluctuation in the magnitude spectrum and having two crossings per active channel is a reasonable assumption. As a result, an indicative practical guideline on the width of the time window is given by:

$$T_0 \geq \frac{1}{B_C}. \tag{5.7}$$

However, T_0 should be long enough such that the windowing effect does not overshadow the estimators' detectable feature(s) in (4.8)-(4.10), e.g. $\left|\widehat{P}_{i,m}(f - f_{C,m})\right|^2 * |W(f)|^2$ and

$\left|\breve{P}_{i,m}(f+f_{C,m})\right|^2 * \left|W(f)\right|^2$. Its value should not also introduce high levels of spectral leakage that can limit the performance of the multiband spectrum sensing routine. For instance, if we consider a rectangular window, we have: $\left|W(f)\right|^2 = \left|T_0 \text{sinc}(T_0 f)\right|^2$. Its first zero crossing is at $1/T_0$ after which $\left|W(f)\right|^2$ decays rapidly. The T_0 specified in (5.7) ensures that the leakage is kept to the minimum where the bandwidth of a transmission occupying an active subband is $B_{W,m} \leq B_C$. Windowing functions other than the rectangular one, e.g. Blackman which have significantly lower side-lobes, can be employed to further limit the spectral leakage. For more details on the characteristics of various windowing functions, the reader is referred to the comprehensive reviews in [109, 110].

Therefore, the chosen T_0 should strike a balance between spectrum smoothness and usefulness of each of $C_{TRS}(t_r, f) = E\left[X_{e,TRS}(t_r, f)\right]$ in (4.8), $C_{RSG}(t_r, f) = E\left[X_{e,RSG}(t_r, f)\right]$ in (4.9) and $C_{SSEP}(t_r, f) = E\left[X_{e,SSEP}(t_r, f)\right]$ in (4.10). Experimental results showed that exceeding (5.7) a number of times suffices in practice. In the sequel T_0 is presumed to be fixed, i.e. predefined by the user.

5.2 Spectrum Sensing Methods

In Table 5.1, we list a number of popular spectrum sensing techniques; review papers such as [10, 14-20] compare these methods stating their advantages and disadvantages. We divided them into two categories: parametric and nonparametric. The parametric ones rely on previous knowledge of the incoming signal and its characteristics. For instance, matched filtering (coherent detector) demands the exact signal shape whilst the cyclostationary detector (feature detector) requests *a priori* knowledge of the modulation scheme and its baud rate. On the other hand, nonparametric techniques are not specific to a particular type of signals and thus branded as generic. They are deemed to be more appropriate for the pursued multiband spectrum sensing where limited information about the incoming signal is presumed.

Some spectrum sensing methods are intrinsically geared to deal with one frequency subband at a time as depicted in Table 5.1, i.e. narrowband spectrum sensing. To apply these methods to the multiband scenario, the incoming multiband signal should be filtered using a bank of fine-tuned narrowband bandpass filters to separate the concurrently active

transmissions into their corresponding spectral subbands. Alternatively, wideband spectrum sensing approaches permit the simultaneous sensing of the system channels; they usually involve estimating the spectrum of the received signal [10, 12, 14-19]. A major implementation challenge lies in the prohibitively high sampling rates required by conventional spectral analysis tools; they are uniform sampling based and have to operate at or above the Nyquist rate. Whereas, we usher in a new wideband spectrum sensing approach that overcomes the sampling rate limitation by resorting to the randomised sampling and processing methodology.

Table 5.1: Spectrum sensing approaches.

	Approach	Minimum Sampling rate	Multiband	Computational Complexity**
Nonparametric	Energy detector	Nyquist	✓	Low
	Multitaper spectrum estimation	Nyquist	✓	High
	Wavelet-based detection	Nyquist	✓	Moderate
	Compressive-sensing based	Sub-Nyquist	✓	High
	Introduced Technique	Sub-Nyquist	✓	Low
Parametric	Matched-filtering detection	Nyquist	✗	Low
	Cyclostationary Detector	Nyquist	✗	Moderate
	Covariance-based detector	Nyquist	✗	Moderate

Recently, there has been an immense interest in the emerging Compressive Sensing or Sampling (CS) trend due to its ability to mitigate the bandwidth constraints of uniform sampling [125, 126]. It promotes the use of sub-Nyquist sampling rates exploiting the sparsity of the processed signal when expressed in a certain basis, e.g. Fourier and wavelets. Spectrum sensing methods that rely on CS principle are emerging, e.g. [23, 24, 127, 128], where the handled radio signals are known to be sparse in the frequency

** The computational complexity in Table 5.1 is an indicative measure where the energy detector is used as a benchmark to decide whether a sensing method is of high or low complexity. Energy detector involves taking the FFT of the signal and averaging. A technique which entails computationally demanding operations, e.g. solving some optimisation problem, is considered high complexity.

domain. It is noted that the CS leverages come at a considerable computational cost that accompanies the optimisations it entails. The computational complexity is one of the crucial factors that need to be taken into account upon comparing various sensing techniques as noticed in Table 5.1. In this context, the introduced MSS approach has a remarkably low computational load compared to the compressive-sensing-based ones. A concrete scientifically comprehensive comparison between CS-based spectrum sensing and our approach is outside the scope of this thesis (see §6.2).

The Energy Detector (ED) in Table §5.1 resembles the introduced MSS technique; both involve similar operations. Hence we briefly discuss the ED and in §5.3.3 the reliability recommendations for a detector closely related to the classical ED are provided; they guarantee that the detector delivers the specified probabilities of detection and false alarm.

Energy Detector

The energy detector, otherwise known as radiometer [124], is one of the simplest means to decide between $\mathcal{H}_{0,k}$ (i.e. the k-th subband is inactive) and $\mathcal{H}_{1,k}$ (i.e. the k-th subband is active) [10, 14-18]. The received signal is transformed to the frequency domain, say via Fast Fourier Transform (FFT), and the energy within each monitored subband is measured by adding the squares of the FFT bins that belong to the subband in question. We have:

$$\begin{aligned} \mathcal{H}_{0,k}: &\quad Y_k(f_i) = V_k(f_i) \\ \mathcal{H}_{1,k}: &\quad Y_k(f_i) = H_k(f_i)X_{T,k}(f_i) + V_k(f_i) \qquad ,k = 1,2,\ldots,L \end{aligned} \tag{5.8}$$

where $Y_k(f_i)$ represents the spectrum of the received signal, $V_k(f_i)$ is the AWGN, $H_k(f_i)$ signifies the propagation channel gain, $X_{T,k}(f_i)$ is the incoming signal and the frequency points $\{f_i\}_{i=1}^{I}$ belong to k-th subband. The decision is taken upon assessing $T_k = \sum_{i=1}^{I} |Y_k(f_i)|^2$ where :

$$\begin{aligned} \mathcal{H}_{0,k}: &\quad T_k < \gamma_k \\ \mathcal{H}_{1,k}: &\quad T_k \geq \gamma_k \qquad ,k = 1,2,\ldots,L \end{aligned} \tag{5.9}$$

where γ_k is the decision threshold. Typically, a number of $Y_k(f_i)$ are calculated from several signal windows and then averaged to enhance the accuracy of the energy measurements [10-12, 114]. Averaging a *"sufficient number"* of those estimates to achieve

a certain level of precision is a widely adopted premise, e.g. [10, 114, 115, 117, 118]. It can lead to collecting unnecessarily excess amounts of data.

Whilst the ED requests a large number of frequency points per subband to measure the energy within, our approach only demands calculating one spectral point per channel. It is noted that placing an equal I number of FFT-bins per system subband can impose some restrictions on the locations of the surveyed channels, especially if the processed signal is not down-converted to baseband. Nonetheless, generally the computational complexity of the ED and the introduced method are comparable. In §5.3.3, the uniform sampling energy detector is modified where one frequency point per subband is examined in (5.9). Although the ED is commonly viewed as a simple and easily implementable technique [10, 14-20], it and the proposed randomised-sampling-based approach have disadvantages. Both methods do not differentiate between the transmitted signal, noise or any Narrowband Interference (NBI).

The threshold values in (5.9) dictate the probabilities of false alarm $P_{f,k}(\gamma_k) = \Pr\left\{\mathscr{H}_{1,k} \middle| \mathscr{H}_{0,k}\right\}$ and those of detection $P_{d,k}(\gamma_k) = \Pr\left\{\mathscr{H}_{1,k} \middle| \mathscr{H}_{1,k}\right\}$ in the k-th subband. To restrain the maximum $P_{f,k}(\gamma_k)$, the ED demands previous knowledge of the AWGN variance. It can be estimated when the overseen spectral subbands are passive [10, 14-20, 116]. To ensure satisfying a minimum $P_{d,k}(\gamma_k)$, the energy detector requests prior knowledge of the power of the signal occupying each of the system subbands or their Power Spectral Densities (PSDs). They can be learnt *a priori* when the subbands are active [17, 114, 116, 129].

5.3 Reliable Multiband Spectrum Sensing

The objective in this section is to derive prescriptive recommendations on how to choose the average sampling rate $\alpha = N/T_0$ and the number of estimate averages K (i.e. the sensing time KT_0) for the introduced MSS approach using (5.4)-(5.6) such that we achieve:

$$P_{f,k}(\gamma_k) \leq \Delta_k \tag{5.10}$$

and

$$P_{d,k}(\gamma_k) \geq \ell_k \tag{5.11}$$

for the k-th system subband. Each of Δ_k and ℓ_k refer to the maximum allowed $P_{f,k}(\gamma_k)$ and the minimum sought $P_{d,k}(\gamma_k)$ respectively in the targeted channel. Acquiring (5.10) and (5.11) also involves determining the adequate threshold values for the detection criterion in (5.2). Distinctive ROC plots, i.e. $P_{d,k}(\gamma_k)$ versus $P_{f,k}(\gamma_k)$ for a γ_k sweep, are attained for every combined α and K values since the latter two dictate the statistical characteristics of the employed estimator in consonance with (4.8)-(4.10), (4.24), (4.31) and (4.49). Owed to nonuniform sampling, the estimated spectrum suffers from smeared-aliasing artefact which is present at all frequencies for both hypothesises $\mathcal{H}_{0,k}$ and $\mathcal{H}_{1,k}$. It embodies a form of the signal and noise powers of all the active subbands as indicated by (4.8)-(4.10). The lack of an activity in subband k does not imply that noise is the only contributor to the estimated spectrum within the channel's frequency range unlike the uniform sampling adversaries, e.g. energy detector in (5.8).

On the other hand, the detection requirements of the system's L subbands can be compactly represented by:

$$\mathbf{P_f}(\boldsymbol{\gamma}) = \left[P_{f,1}(\gamma_1), P_{f,2}(\gamma_2), \ldots, P_{f,L}(\gamma_L)\right]^T \preceq \boldsymbol{\Delta} \tag{5.12}$$

$$\mathbf{P_d}(\boldsymbol{\gamma}) = \left[P_{d,1}(\gamma_1), P_{d,2}(\gamma_2), \ldots, P_{d,L}(\gamma_L)\right]^T \succeq \mathbf{l} \tag{5.13}$$

for

$$\boldsymbol{\gamma} = \left[\gamma_1, \gamma_2, \ldots, \gamma_L\right]^T \tag{5.14}$$

where $\boldsymbol{\Delta} = \left[\Delta_1, \Delta_2, \ldots, \Delta_L\right]^T$ and $\mathbf{l} = \left[\ell_1, \ell_2, \ldots, \ell_L\right]^T$. Each of $\preceq$ and $\succeq$ refers to an element by element comparison of the vectors, e.g. $\mathbf{P_f}(\boldsymbol{\gamma}) \preceq \boldsymbol{\Delta}$ implies that $P_{f,1}(\gamma_1) \le \Delta_1$, $P_{f,2}(\gamma_2) \le \Delta_2$, etc. Clearly, detecting a weak or high performance subband would necessitate more estimate averages and higher sampling rates compared to another channel with stronger power level or lower detection specifications. It entails further restraining of the estimator's inaccuracies. If the user aims to fulfil the detection probabilities of more than one channel, he/she should survey the demands of the subbands in question and select the highest recommended α and K values.

5.3.1 Reliability Guidelines

The pursued guidelines should consider the onerous system conditions, e.g. L_A active channels and the highest possible harmful effect of smeared-aliasing. If the number of the concurrently active subbands at a given time is $M < L_A$, the guidelines become conservative. The smeared-aliasing issue is mostly relevant to the stratified sampling case where the varying smeared-aliasing level can obscure the detection routine if it is not taken into account. It is noted that an active subband with a higher power level would introduce a bigger error to the estimation process compared to a weaker channel. Such inaccuracies are observed within the frequency range allocated to the active subband as well as across $\mathcal{B}$ due to the smeared-aliasing phenomenon. Consequently, we should cater for the L_A strongest concurrently active subbands to guarantee the response of the spectrum sensing technique; this group of channels is denoted by $\mathbb{L}_A$. We assume that the total signal power is approximately equal in both $\mathcal{H}_{0,k}$ and $\mathcal{H}_{1,k}$ to simplify the formulas; however in [130, 131] we consider the scenario where the power can vary between the two hypothesises.

According to one-sided Chebychev's inequality (also known by Cantelli's inequality), $\Pr\{X \geq E[X] + e\sigma_X\} \leq 1/(1+e^2)$ and $\Pr\{X > E[X] - e\sigma_X\} \geq 1 - 1/(1+e^2)$ where X is a random variable with a standard deviation σ_X and $e \geq 0$ [132]. From (5.10) given Chebychev's inequality, the threshold levels for $\mathcal{H}_{0,k}$ (i.e. when the k-th subband is idle) are down-limited by $\gamma_k \geq \gamma_{\min,k}$ where

$$\gamma_{\min,k} = m_{0,k} + e_{0,k}\sigma_{0,k} \tag{5.15}$$

$m_{0,k} = E\left[\hat{X}_e(f_k)\right]$, $\sigma_{0,k} = \sqrt{\text{var}\left\{\hat{X}_e(f_k)\right\}}$, $e_{0,k} = \sqrt{-1 + 1/\Delta_k}$ and $e_{0,k} \geq 0$. Whereas, $\hat{X}_e(f)$ is the estimated spectrum in (5.2). Noting (5.11), we have $\gamma_k \leq \gamma_{\max,k}$ for $\mathcal{H}_{1,k}$ (i.e. when the targeted channel is engaged) such that:

$$\gamma_{\max,k} = m_{1,k} - e_{1,k}\sigma_{1,k} \tag{5.16}$$

$m_{1,k} = E\left[\hat{X}_e(f_k)\right]$, $\sigma_{1,k} = \sqrt{\text{var}\left\{\hat{X}_e(f_k)\right\}}$, $e_{1,k} = \sqrt{-1 + 1/(1-\ell_k)}$ and $e_{1,k} \geq 0$. This leads to:

$$\gamma_{\min,k} \leq \gamma_k \leq \gamma_{\max,k} \tag{5.17}$$

and by substituting (5.15) and (5.16) into (5.17), we obtain:

$$m_{1,k} - m_{0,k} \geq c_{0,k}\sigma_{0,k} + c_{1,k}\sigma_{1,k} \tag{5.18}$$

which prescribes the reliability condition of the proposed MSS procedure for the k-th subband.

Although Chebychev's inequality provides the upper and lower limits of the probability of a random variable exceeding certain values, it does not indicate how conservative these bounds are, e.g. the actual attainable probabilities can arbitrarily surpass the minimum specified one. As illustrated in the simulations in §5.4, Chebychev's inequality can lead to over-conservative measures in terms of sampling rate and estimate averaging. Assuming that the estimated spectrum $\hat{X}_e(f)$ has certain distribution is shown to produce guidelines with a reasonable level of conservativeness. Nevertheless, (5.15)-(5.18) applies to any distribution of $\hat{X}_e(f)$ and the adopted one is a special case.

We recall from Chapter 3 that the estimators $X_{e,TRS}(\mathcal{t}_r, f)$ in (3.8), $X_{e,RSG}(\mathcal{t}_r, f)$ in (3.27) and $X_{e,SSEP}(\mathcal{t}_r, f)$ in (3.44) are approximately of a chi-squared distribution with two degrees of freedom. Subsequently, $\hat{X}_{e,TRS}(f)$ in (5.4), $\hat{X}_{e,RSG}(f)$ in (5.5) and $\hat{X}_{e,SSEP}(f)$ in (5.6) are similarily of chi-squared distribution but with $2K$ degrees of freedom. The Cumulative Distribution Function (CDF) of a random variable with chi-squared distribution with Z degrees of freedom can be closely approximated by a normal CDF for a moderately large Z [103]. Hence the CDF of $\hat{X}_e(f_k)$ can be assumed to be approximately equal to that of a normal distribution with the same mean and variance. Such approximation has insignificant repercussions on the dependability of the introduced sensing approach as demonstrated in the numerical examples in the next section. Thereupon, the probability of false alarm and that of detection are:

$$P_{f,k}(\gamma_k) = \Pr\left(\hat{X}_e(f_k) \geq \gamma_k \middle| H_{0,k}\right) = Q\left(\frac{\gamma_k - m_{0,k}}{\sigma_{0,k}}\right) \tag{5.19}$$

and

$$P_{d,k}(\gamma_k) = \Pr\left(\hat{X}_e(f_k) \geq \gamma_k \middle| H_{1,k}\right) = Q\left(\frac{\gamma_k - m_{1,k}}{\sigma_{1,k}}\right) \tag{5.20}$$

respectively where

$$Q(x)=\frac{1}{\sqrt{2\pi}}\int_{x}^{+\infty}e^{-\tau^2/2}d\tau \tag{5.21}$$

is the tail probability of a zero mean unit-variance normal random variable and is a monotonically nonincreasing function. Since $P_{f,k}(\gamma_k)\le\Delta_k$, the threshold levels for $\mathcal{H}_{0,k}$ are defined by:

$$\gamma_k\ge\gamma_{\min,k}=m_{0,k}+Q^{-1}(\Delta_k)\sigma_{0,k} \tag{5.22}$$

and likewise:

$$\gamma_k\le\gamma_{\max,k}=m_{1,k}+Q^{-1}(\ell_k)\sigma_{1,k} \tag{5.23}$$

for $\mathcal{H}_{1,k}$ given $P_{d,k}(\gamma_k)\ge\ell_k$. Therefore,

$$m_{1,k}-m_{0,k}\ge Q^{-1}(\Delta_k)\sigma_{0,k}-Q^{-1}(\ell_k)\sigma_{1,k} \tag{5.24}$$

is the equivalent of the dependability condition in (5.18) for a normally distributed $\hat{X}_e(f)$. Below, we utilise (5.24) to derive a combined lower limit on the required average sampling rate and number of estimate averages for each of the TRS, RSG and SSEP schemes. It can be noticed that initially $E\left[\hat{X}_e(f_k)\right]$ and $\text{var}\left\{\hat{X}_e(f_k)\right\}$ should be determined for each of the studied schemes.

5.3.1.1 Total Random Sampling

Following (4.8) and (5.4), it can be easily checked that:

$$\hat{C}_{TRS}(f_k)=E\left[\hat{X}_{e,TRS}(f_k)\right]=\frac{N}{(N-1)\alpha}\left[P_{SA}+P_N\right]+\frac{1}{\mu}E\left[\left|X_W(\mathcal{t}_r,f_k)\right|^2\right] \tag{5.25}$$

noting that $E\left[\left|X_W(\mathcal{t}_r,f_k)\right|^2\right]$ is independent of $\mathcal{t}_r$ when the f_k point is in the *guarded region* recognised in §4.3. The average weighted total signal power in the observation window $T_{obs}=KT_0$ is:

$$P_{SA}=\frac{1}{K}\sum_{r=1}^{K}P_S(\mathcal{t}_r) \tag{5.26}$$

where $P_S(\mathcal{t}_r)=\int_{\mathcal{T}_r}E\left[x^2(t)\right]w^2(t)dt/\mu$ in (4.11). Since the K estimates in (5.4) are calculated from non-overlapping uncorrelated signal windows, the variance of the TRS estimator, i.e. $\hat{\sigma}^2_{e,TRS}(f_k)=\text{var}\left\{\hat{X}_{e,TRS}(f_k)\right\}$, is given by:

$$\hat{\sigma}^2_{e,TRS}(f_k) = \frac{1}{K^2}\sum_{r=1}^{K}\sigma^2_{e,TRS}(\mathcal{t}_r, f_k)\,. \tag{5.27}$$

To compute $\hat{\sigma}^2_{e,TRS}(f)$ we use the simplified variance expression in (4.24). Deciding the value of $0.5 \le \eta_D(\mathcal{t}_r, f) \le 1$ defined in (4.23) is of paramount importance as it stipulates a substantial part of the variance and reflects the effect of processing cyclostationary signals on the estimator's performance. If no previous knowledge of the transmission modulation scheme and/or its symbol rate is available, a conservative approach is to take into account the worst case scenario, i.e. $\eta_D(\mathcal{t}_r, f_k) = 1$. However, any prior information about the incoming signal can be used to set $\eta_D(\mathcal{t}_r, f_k)$ and/or possibly choose the position of the frequency points $\{f_k\}_{k=1}^{L}$ in an attempt to avoid any undesired frequencies where the accuracy of the estimation process deteriorates noticeably with the aid of (4.26)-(4.29). Let $\hat{\eta}_{D,k}$ be the average $\eta_D(\mathcal{t}_r, f_k)$ value across the K signal windows. Substituting the individual $\sigma^2_{e,TRS}(\mathcal{t}_r, f_k)$ into (5.27), we arrive at:

$$\hat{\sigma}^2_{e,TRS}(f_k) \approx \frac{N^2}{(N-1)^2 K}\left\{\frac{P'_{SA} + 2P_{SA}P_N + P_N^2}{\alpha^2} + \frac{2(N-1)(P_{SA}+P_N)D_k}{N\alpha} + 2\hat{\eta}_{D,k}\left(\frac{N-1}{N}D_k\right)^2\right\} \tag{5.28}$$

where $D_k = D(\mathcal{t}_r, f_k) = E\left[\left|X_W(\mathcal{t}_r, f_k)\right|^2\right]\Big/\mu$ and

$$P'_{SA} = \frac{1}{K}\sum_{r=1}^{K}P_S^2(\mathcal{t}_r)\,. \tag{5.29}$$

Thus in summary:

$$\hat{C}_{TRS}(f_k) = \begin{cases} m_{0,k} = \dfrac{N}{(N-1)\alpha}(P_{SA}+P_N) & \text{for} \quad \mathcal{H}_{0,k} \\ m_{1,k} = \dfrac{N}{(N-1)\alpha}(P_{SA}+P_N) + D_k & \text{for} \quad \mathcal{H}_{1,k} \end{cases} \tag{5.30}$$

$$\hat{\sigma}^2_{e,TRS}(f_k) \approx \begin{cases} \sigma^2_{0,k} = \dfrac{N^2}{(N-1)^2 K}\left(\dfrac{P'_{SA} + 2P_{SA}P_N + P_N^2}{\alpha^2}\right) & \text{for} \quad \mathcal{H}_{0,k} \\ \sigma^2_{1,k} = \dfrac{N^2}{(N-1)^2 K}\left\{\dfrac{P'_{SA} + 2P_{SA}P_N + P_N^2}{\alpha^2} + \dfrac{2(N-1)(P_{SA}+P_N)D_k}{N\alpha} + 2\hat{\eta}_{D,k}\left(\dfrac{N-1}{N}D_k\right)^2\right\}. & \text{for} \quad \mathcal{H}_{1,k} \end{cases} \tag{5.31}$$

According to Parseval's theorem: $\int_{\mathcal{T}_r} E\left[x^2(t)\right] w^2(t)dt = \int_{-\infty}^{+\infty} E\left[\left|X_W(\mathcal{t}_r, f)\right|^2\right] df$, then we can write: $P_{SA} \le \sum_{n\in\mathbb{L}_A} 2B_C D_n$ which approximates the area underneath the integral for a reasonably long analysis window $\mathcal{T}_r$. Adopting a conservative approach and substituting (5.30) as well as (5.31) into (5.24), we obtain:

$$K = K_{TRS} \ge \left\{ \frac{2NB_C}{(N-1)\alpha} Q^{-1}\left(\Delta_k\right) \phi_k \left(1 + SNR^{-1}\right) - \frac{2NB_C}{(N-1)\alpha} Q^{-1}\left(\ell_k\right) \sqrt{\phi_k^2 \left(1 + SNR^{-1}\right)^2 + \frac{\phi_k \alpha (N-1)\left(1 + SNR^{-1}\right)}{NB_C} + \frac{\hat{\eta}_{D,k}\alpha^2}{2}\left(\frac{N-1}{NB_C}\right)^2} \right\}^2 \quad (5.32)$$

where $SNR = P_{SA} / P_N$ is the signal-to-noise ratio and

$$\phi_k = \sum_{n\in\mathbb{L}_A} D_n \big/ D_k \quad (5.33)$$

is the ratio of the sum of $E\left[\left|X_W(\mathcal{t}_r, f_n)\right|^2\right]/\mu$, $n \in \mathbb{L}_A$, to that of the targeted subband, i.e. D_k. Alternatively, it can be represented by:

$$\phi_k = P_{SA} \big/ P_{SA,k} \quad (5.34)$$

such that $P_{SA,k}$ is the average power of the transmission over the k-th subband and P_{SA} is the total average power of the present multiband signal.

Formula (5.32) gives a conservative lower bound on the number of windows that need to be averaged as a function of the spectrum occupancy, average sampling rate, signal-to-noise ratio and the sought system performance. This recommendation can be used to decide on the required average sampling rate for a number of estimate averages possibly imposed by practical constraints (e.g. latency) in a continuous processing environment. It is a clear indication of the trade-off between the requested sampling rate and the number of estimate averages, i.e. sensing time, in relation to achieving certain probabilities of detection and false alarm. Formula (5.32) affirms that the sensing task can be reliably accomplished with arbitrarily low sampling rates at the expense of infinitely long signal observation window. Parameter ϕ_k can be learnt/estimated *a priori* when the transmissions are known to be present [17, 114, 116, 129], this is further discussed in §5.3.2. It is noted that $\phi_k = L_A$ if the incoming transmissions are of equal power levels. In the next two subsections, we develop the equivalent of (5.32) for the RSG and SSEP schemes.

5.3.1.2 Random Sampling on Grid

Utilising (4.9), it can be shown that:

$$\hat{C}_{RSG}(f_k) = E\left[\hat{X}_{e,RSG}(f_k)\right] = \begin{cases} m_{0,k} = \dfrac{(N_g - N)T_0 P_{SA}^d + T_0(N_g - 1)P_N}{N_g(N-1)} & \text{for} \quad \mathcal{H}_{0,k} \\ m_{1,k} = \dfrac{(N_g - N)T_0 P_{SA}^d + (N_g - 1)T_0 P_N}{(N-1)N_g} + D_k^d & \text{for} \quad \mathcal{H}_{1,k} \end{cases} \tag{5.35}$$

where $D_k^d = D^d(\mathcal{t}_r, f_k)$, $D^d(\mathcal{t}_r, f) = E\left[\left|X_W^d(\mathcal{t}_r, f)\right|^2\right] \Big/ \mu_d f_g$,

$$P_{SA}^d(\mathcal{t}_r) = \frac{1}{K}\sum\nolimits_{r=1}^{K} P_S^d(\mathcal{t}_r) \tag{5.36}$$

and $P_S^d(\mathcal{t}_r) = \sum_{n=1}^{N_g} E[x^2(nT_g)]w^2(nT_g)/\mu_d$. We note that $D^d(\mathcal{t}_r, f_k)$ is independent of $\mathcal{t}_r$ since f_k is placed at the centre of the system subband. The underlying uniform grid rate f_g is chosen such that $X_W(f)X_W(f - nf_g) = 0$ for $n \neq 0$, $n \in \mathbb{Z}$. By using (4.31), $\hat{\sigma}_{e,RSG}^2(f_k) = \text{var}\left\{\hat{X}_{e,RSG}(f_k)\right\}$ reduces to:

$$\hat{\sigma}_{e,RSG}^2(f_k) = \begin{cases} \sigma_{0,k}^2 = \dfrac{(N_g - N)^2}{f_g^2(N-1)^2 K}\left[P_{SA}'^d + \dfrac{2(N_g - 1)}{(N_g - N)}P_{SA}^d P_N + \dfrac{(N_g - 1)^2}{(N_g - N)^2}P_N^2\right] & \text{for} \quad \mathcal{H}_{0,k} \\ \sigma_{1,k}^2 = \dfrac{(N_g - N)^2}{f_g^2(N-1)^2 K}\left[P_{SA}'^d + \dfrac{2(N_g - 1)}{(N_g - N)}P_{SA}^d P_N + \dfrac{(N_g - 1)^2}{(N_g - N)^2}P_N^2\right] & \\ \quad + \dfrac{2(N_g - N)}{f_g(N-1)K}\left[P_{SA}^d + \dfrac{(N_g - 1)}{(N_g - N)}P_N\right]D_k^d + \dfrac{2\hat{\eta}_{D,k}^d\left[D_k^d\right]^2}{K} & \text{for} \quad \mathcal{H}_{1,k} \end{cases} \tag{5.37}$$

where

$$P_{SA}'^d = \frac{1}{K}\sum_{r=1}^{K}\left[P_{SA}^d(\mathcal{t}_r)\right]^2 \tag{5.38}$$

and $\hat{\eta}_{D,k}^d$ is the average $\eta_D^d(\mathcal{t}_r, f_k)$ in the K signal segments; $\eta_D^d(\mathcal{t}_r, f_k)$ is defined in (4.33). The value of $\hat{\eta}_{D,k}^d$ is mandated by the type of the incoming transmission, e.g. if the signal is BPSK modulated then $\hat{\eta}_{D,k}^d = 1$ is suitable (see §4.4.2). However, if the processed signal is Wide Sense Stationary (WSS) then $\hat{\eta}_{D,k}^d = 0.5$. Substituting (5.35) and (5.37) into the reliability condition in (5.24), we obtain:

$$K = K_{RSG} \geq \left\{ \tilde{K}_{RSG} Q^{-1}(\Delta_k) - Q^{-1}(\ell_k) \sqrt{\tilde{K}_{RSG}^2 + 2\tilde{K}_{RSG} + 2\hat{\eta}_{D,k}^d} \right\}^2 \tag{5.39}$$

where

$$\tilde{K}_{RSG} = \frac{2B_C \phi_k N(N_g - N)}{N_g (N-1)\alpha} \left[1 + \frac{(N_g - 1)SNR^{-1}}{(N_g - N)} \right]. \tag{5.40}$$

Formula (5.39) exhibits the cost of using a low sampling rate in terms of sensing time KT_0; the sampling frequency can be arbitrarily low. The parameter ϕ_k is defined in (5.33) since D_k and D_k^d are identical for a suitably selected f_g.

5.3.1.3 Stratified Sampling with Equal Partitions

The estimated spectrum for stratified sampling includes the smeared-aliasing reduction factor $A(\lambda_r, f) = \chi(\lambda_r, f)/\mu$ given in (4.41); $A(\lambda_r, f)$ appears in the estimator's expected value in (4.10) and its variance in (4.49). Let $A_{0,k} = \chi(\lambda_r, f_k)/\mu$ and $A_{1,k} = \chi(\lambda_r, f_k)/\mu$ in $\mathcal{H}_{0,k}$ and $\mathcal{H}_{1,k}$ respectively; f_k is placed at the centre of the subband. It was illustrated in §3.5 that $A(\lambda_r, f)$ is related to the total power of the present multiband signal such that: $A(\lambda_r, f) = \varpi(\lambda_r, f) P_S(\lambda_r)/\alpha$ where $0 \leq \varpi(\lambda_r, f) \leq 1$. Hence we can write: $A_{0,k} = \varpi_{0,k} P_{SA}/\alpha$ in $\mathcal{H}_{0,k}$ and $A_{1,k} = \varpi_{1,k} P_{SA}/\alpha$ in $\mathcal{H}_{1,k}$ where $0 \leq \varpi_{0,k} \leq 1$ and $0 \leq \varpi_{1,k} \leq 1$ for the K averaged $X_{e,SSEP}(\lambda_r, f)$ in (5.6). From (4.10) and (4.49), the characteristics of $\hat{X}_{e,SSEP}(f)$ can be summarised by:

$$\hat{C}_{SSEP}(f_k) = E\left[\hat{X}_{e,SSEP}(f_k) \right] = \begin{cases} m_{0,k} = \dfrac{P_{SA}\left[1 - \varpi_{0,k}\right] + P_N}{\alpha} & \text{for } \mathcal{H}_{0,k} \\ m_{1,k} = \dfrac{P_{SA}\left[1 - \varpi_{1,k}\right] + P_N}{\alpha} + D_k & \text{for } \mathcal{H}_{1,k} \end{cases} \tag{5.41}$$

$$\hat{\sigma}^2_{e,SSEP}(f_k) = \begin{cases} \sigma^2_{0,k} = \dfrac{1}{K}\left\{ \dfrac{P'_{SA} + 2P_{SA}P_N + P_N^2}{\alpha^2} + \dfrac{2\hat{\eta}_{A,k}\varpi_{0,k}^2 P'_{SA}}{\alpha^2} - \dfrac{2\varpi_{0,k}\left(P'_{SA} + P_{SA}P_N\right)}{\alpha^2} \right\} & \text{for } \mathcal{H}_{0,k} \\ \sigma^2_{1,k} = \dfrac{1}{K}\left\{ \dfrac{P'_{SA} + 2P_{SA}P_N + P_N^2}{\alpha^2} + \dfrac{2\hat{\eta}_{A,k}\varpi_{1,k}^2 P'_{SA}}{\alpha^2} + 2\hat{\eta}_{D,k} D_k^2 \right. & \\ \qquad \left. - \dfrac{2\varpi_{1,k}\left(P'_{SA} + P_{SA}P_N\right)}{\alpha^2} + \dfrac{2\left(P_{SA} + P_N\right)}{\alpha} D_k - \dfrac{4\hat{\eta}_{DA,k}\varpi_{1,k} P_{SA} D_k}{\alpha} \right\} & \text{for } \mathcal{H}_{1,k} \end{cases} \tag{5.42}$$

where $\hat{\sigma}^2_{e,SSEP}(f) = \mathrm{var}\left\{\hat{X}_{e,SSEP}(f)\right\}$. Parameters $\hat{\eta}_{D,k}$, $\hat{\eta}_{A,k}$ and $\hat{\eta}_{DA,k}$ are the chosen values of $\eta_{D,k}(\measuredangle_r, f_k)$ in (4.23), $\eta_{A,k}(\measuredangle_r, f_k)$ in (4.46) and $\eta_{DA}(\measuredangle_r, f_k)$ in (4.48) respectively for $\hat{X}_{e,SSEP}(f)$. They depict the impact of processing a cyclostationary signal on the accuracy of the spectrum estimation. For instance, if the incoming transmission is a QPSK modulated signal with balanced in-phase and quadrature branches, then $\hat{\eta}_{D,k} = \hat{\eta}_{A,k} = 0.5$ (see §4.4.3 for a more detailed discussion). Nonetheless, if the modulation scheme and the symbol rate of the transmitted signal are not known, $\hat{\eta}_{D,k} = \hat{\eta}_{A,k} = 1$ to circumvent any unexpected decay in the detector's performance.

It is noted that the contribution of $A(\measuredangle_r, f)$ to the estimated spectrum is dictated by the position as well as the power level of the concurrently active subbands. As a result, the reliability condition in (5.24) should incorporate the highest harmful effect of the varying smeared-aliasing factor on the sensing routine. This evokes considering the following: 1) the maximum possible $\gamma_{\min,k} = m_{0,k} + Q^{-1}(\Delta_k)\sigma_{0,k}$ in (5.22) , i.e. the maximum $m_{0,k}$ where $\varpi_{0,k} = 0$ to ensure that $P_{f,k}(\gamma_k) \le \Delta_k$ and 2) the minimum $\gamma_{\max,k} = m_{1,k} + Q^{-1}(\ell_k)\sigma_{1,k}$ in (5.23) , i.e. minimum $m_{1,k}$ where $\varpi_{1,k} = 0.5$ to protect $P_{d,k}(\gamma_k) \ge \ell_k$ assuming $f_k >> B$. Subsequently, (5.24) emerges as:

$$\sqrt{K}\left[D_k - 0.5P_{SA}/\alpha\right] \ge \sqrt{\frac{P'_{SA} + 2P_{SA}P_N + P_N^2}{\alpha^2}}Q^{-1}(\Delta_k)$$
$$-Q^{-1}(\ell_k)\sqrt{\left\{\frac{P'_{SA} + 2P_{SA}P_N + P_N^2}{\alpha^2} + \frac{\hat{\eta}_{A,k}P'_{SA}}{2\alpha^2} + 2\hat{\eta}_{D,k}D_k^2 - \frac{\left(P'_{SA} + P_{SA}P_N\right)}{\alpha^2} + \frac{2\left(P_{SA} + P_N\right)D_k}{\alpha} - \frac{2\hat{\eta}_{DA,k}P_{SA}D_k}{\alpha}\right\}}. \quad (5.43)$$

In practice, the probability of detection is usually $\ell_k \ge 0.5$ yielding $Q^{-1}(\ell_k) \le 0$ whereas the probability of false alarm is $\Delta_k \le 0.5$ producing $Q^{-1}(\Delta_k) \ge 0$. Thus $D_k - 0.5P_{SA}/\alpha$ in (5.43) should be positive to attain a lower limit on K since $\sigma_{1,k} > \sigma_{0,k} \ge 0$. The stratified-sampling-based MSS method is dependable if and only if:

$$D_k - \frac{0.5P_{SA}}{\alpha} > 0\,. \quad (5.44)$$

This imposes a lower limit on the minimum valid average sampling rate and is caused by the varying smeared-aliasing aspect of stratified sampling. The permissible stratified

sampling rates are typically well below the minimum uniform sampling ones required to monitor the frequency range $\mathcal{B} = [f_{\min}, f_{\min} + B]$ where $\alpha << 2B$. Provided that (5.44) is satisfied, (5.43) reduces to:

$$K = K_{SSEP} \geq \left\{ \frac{2B_C\phi_k\left(1+SNR^{-1}\right)Q^{-1}\left(\Delta_k\right) - Q^{-1}\left(\ell_k\right)\tilde{K}_{SSEP}}{\alpha - B_C\phi_k} \right\}^2 \tag{5.45}$$

where

$$\begin{aligned} \tilde{K}^2_{SSEP} = {} & 4B_C^2\phi_k^2\left(1+SNR^{-1}\right)^2 + 2B_C^2\phi_k^2\hat{\eta}_{A,k} - 4B_C^2\phi_k^2\left(1+SNR^{-1}\right) \\ & + 4B_C\phi_k\alpha\left(1+SNR^{-1}\right) - 4B_C\alpha\phi_k\hat{\eta}_{DA,k} + 2\alpha^2\hat{\eta}_{D,k} \end{aligned} \tag{5.46}$$

and ϕ_k is defined in (5.33) or (5.34). If we presume that the transmission is a QAM signal modelled by (4.3) and whose $\sigma^2_{a,m}P_{i,m}(f) - \sigma^2_{b,m}P_{q,m}(f) = 0$, (5.45) simplifies to:

$$K_{SSEP} \geq \left\{ \frac{2B_C\phi_k\left(1+SNR^{-1}\right)Q^{-1}\left(\Delta_k\right) - Q^{-1}\left(\ell_k\right)\left[2B_C\phi_k\left(0.5+SNR^{-1}\right)+\alpha\right]}{\alpha - B_C\phi_k} \right\} \tag{5.47}$$

which is also the case for wide sense stationary signals.

Formula (5.45) states the number of windows that need to be averaged to achieve $P_{f,k}(\gamma_k) \leq \Delta_k$ and $P_{d,k}(\gamma_k) \geq \ell_k$. It exhibits the potential of the introduced MSS technique to accomplish the sensing task with significantly low stratified sampling rates at the expense of longer signal observation windows KT_0. Unlike TRS and RSG where α can be arbitrarily low, stratified sampling imposes a low limit on the operational average sampling rates according to (5.44).

The guidelines for TRS, RSG and SSEP employ (5.24) assuming normally distributed $\hat{X}_{e,TRS}(f)$, $\hat{X}_{e,RSG}(f)$ and $\hat{X}_{e,SSEP}(f)$. Generalising those results using the reliability condition that is based on Chebychev's inequality in (5.18) can be easily realised by replacing $Q^{-1}(\Delta_k)$ with $c_{0,k}$ and $Q^{-1}(\ell_k)$ with $-c_{1,k}$ in each of (5.32), (5.39) and (5.45), e.g. in [133, 134].

5.3.2 Threshold Levels and a Discussion on the Required Parameters

Although the recommendations in (5.32), (5.39) and (5.45) guarantee delivering predefined probabilities of detection and false alarm, they do not advise on the threshold levels in the hypothesis testing described in (5.2). By conforming to those guidelines, the detector's receiver operating characteristics curve includes a region where $P_{f,k}(\gamma_k) \le \Delta_k$ and $P_{d,k}(\gamma_k) \ge \ell_k$. To operate in latter domain, the used threshold levels should comply with:

$$m_{0,k} + Q^{-1}(\Delta_k)\sigma_{0,k} \le \gamma_k \le m_{1,k} + Q^{-1}(\ell_k)\sigma_{1,k} \tag{5.48}$$

where $\gamma_{\min,k} = m_{0,k} + Q^{-1}(\Delta_k)\sigma_{0,k}$ and $\gamma_{\max,k} = m_{1,k} + Q^{-1}(\ell_k)\sigma_{1,k}$. The $m_{0,k}$, $m_{1,k}$, $\sigma_{0,k}$ and $\sigma_{1,k}$ in (5.48) are presented in (5.30) and (5.31) for TRS, in (5.35) and (5.37) for RSG and in (5.41) and (5.42) for SSEP.

To demonstrate the prior knowledge needed to calculate the detection decision thresholds, assume that the incoming multiband signal is WSS. Consequently, it can be checked that for the total random sampling scheme the values of $\gamma_{\min,k}$ and $\gamma_{\max,k}$ are:

$$\gamma_{\min,k}^{TRS} = \frac{N(P_S + P_N)}{(N-1)\alpha}\left[1 + \frac{Q^{-1}(\Delta_k)}{\sqrt{K_{TRS}}}\right] \quad ; \quad \gamma_{\max,k}^{TRS} = \left[\frac{N(P_S + P_N)}{(N-1)\alpha} + D_k\right]\left[1 + \frac{Q^{-1}(\ell_k)}{\sqrt{K_{TRS}}}\right] \tag{5.49}$$

, for random sampling on grid:

$$\gamma_{\min,k}^{RSG} = \left[1 + \frac{Q^{-1}(\Delta_k)}{\sqrt{K_{RSG}}}\right]\left[\frac{(N_g - N)P_S^d + (N_g - 1)P_N}{f_g(N-1)}\right];$$

$$\gamma_{\max,k}^{RSG} = \left[\frac{(N_g - N)P_S^d + (N-1)P_N}{(N-1)f_g} + D_k^d\right]\left[1 + \frac{Q^{-1}(\ell_k)}{\sqrt{K_{RSG}}}\right] \tag{5.50}$$

and for stratified sampling with equal partitions:

$$\gamma_{\min,k}^{SSEP} = \frac{(P_S + P_N)}{\alpha}\left[1 + \frac{Q^{-1}(\Delta_k)}{\sqrt{K_{SSEP}}}\right] \; ; \; \gamma_{\max,k}^{SSEP} = \left[D_k + \frac{0.5P_S + P_N}{\alpha}\right]\left[1 + \frac{Q^{-1}(\ell_k)}{\sqrt{K_{SSEP}}}\right] \tag{5.51}$$

where $P_S = P_{SA} = E\left[x^2(t)\right]$ and $P_S^d = P_{SA}^d = E\left[x^2(nT_g)\right]$ are the total power of the present multiband signal.

Inspecting (5.49) and (5.51), it can be noticed that calculating $\gamma_{\min,k}^{TRS}$ and $\gamma_{\min,k}^{SSEP}$, which ensure that $P_{f,k}(\gamma_k) \le \Delta_k$, requires knowledge of the combined signal plus noise power $P_S + P_N$. The latter depends on the number of simultaneously active subbands and their power levels, i.e. $P_S + P_N$ can dynamically vary from one sensing operation to another. Determining $\gamma_{\min,k}^{RSG}$ demands similar information to that of the TRS and SSEP cases since $(N_g - N)/(N_g - 1) \approx 1$ for $N_g >> N$ which is a mild assumption for a typical scenario. On the other hand, establishing $\gamma_{\max,k}^{TRS}$, $\gamma_{\max,k}^{RSG}$ and $\gamma_{\max,k}^{SSEP}$ requests prior awareness of $D_k = E\left[\left|X_W(\lambda_r, f_k)\right|^2\right]/\mu$ and D_k^d to safeguard $P_{d,k}(\gamma_k) \ge \ell_k$. Those magnitude spectrum points are the peaks of the signal's power spectral density for WSS processes. Furthermore, $\gamma_{\max,k}^{SSEP}$ imposes knowing the total signal power P_S and the noise power P_N.

Thresholding regimes of some widely used spectrum sensing methods, e.g. energy detector [10, 14-20, 116], demand previous knowledge of the noise power to stop the probabilities of false alarm exceeding certain levels. Additionally, they require the power levels of the individual transmissions or their PSDs to make sure that the probabilities of detection are maintained above particular values. Estimating the noise power (which varies over time) can be a challenging endeavour due to the necessity of separating the signal from noise [17, 135]. Whereas, the introduced MSS approach only demands estimating the combined $P_S + P_N$ power without the need to separate them to deliver $P_{f,k}(\gamma_k) \le \Delta_k$. The $P_S + P_N$ can be obtained from the captured noisy samples as proposed later in §5.5. A primitive cheap analogue sensor can be otherwise employed at the receiver to continuously measure the total present energy/power of the noisy incoming multiband signal. With regards to $P_{d,k}(\gamma_k) \ge \ell_k$, both the ED and our approach request similar knowledge about the spectrum of the continuous-time signal. Parameter D_k or D_k^d can be estimated *a priori* when the subbands are active as in [17, 114, 116, 129]. Such information can be used to set ϕ_k in (5.33) to determine α and K_{TRS}, K_{RSG} or K_{SSEP}. Therefore, the previous knowledge required by the proposed randomised-sampling-based MSS technique is comparable (can be argued to be more reasonable) to that requested by other popular methods. Evidently, establishing $\gamma_{\min,k}^{TRS}$, $\gamma_{\min,k}^{RSG}$ and $\gamma_{\min,k}^{SSEP}$ demands less information about the incoming signal

compared to $\gamma_{\max,k}^{TRS}$, $\gamma_{\max,k}^{RSG}$ and $\gamma_{\max,k}^{SSEP}$; this is also the case for the classical ED. It is noted that the above discussion and deductions apply to cyclostationary signals.

At this juncture, it is practical to decide the values of α and K_{TRS}, K_{RSG} or K_{SSEP} offline according to (5.32), (5.39) and (5.45) to enforce $P_{f,k}(\gamma_k) \leq \Delta_k$ and $P_{d,k}(\gamma_k) \geq \ell_k$ for the expected system conditions. Whereas, γ_k in (5.48) is calculated for every detection operation in (5.2) since $\gamma_{\min,k}$ and $\gamma_{\max,k}$ are directly related to the currently active subbands rather than the maximum spectrum occupancy utilised to attain (5.32), (5.39) and (5.45).

5.3.3 Randomised Versus Uniform Sampling

Instead of measuring the energy in each of the overseen subbands as in (5.8)-(5.9) for the energy detector, we can employ uniform sampling periodograms to detect the active transmissions via assessing the estimated spectral peaks using (5.2). This usually imposes less estimate averages compared to the randomised sampling schemes where the estimated spectrum suffers from the wideband smeared-aliasing component. If the random sampling on grid scheme admits all the underlying uniform grid samples, i.e. $N = N_g$, the sensing approach becomes uniform-sampling-based. It can be seen from (5.39) that the number of estimate averages for a uniform-sampling-based multiband detection that utilises (5.2) and (5.3) is given by:

$$K = K_{US} \geq \left\{ \frac{2B_C \phi_k SNR^{-1} Q^{-1}(\Delta_k)}{f_{US}} - Q^{-1}(\ell_k) \sqrt{\frac{4B_C^2 \phi_k^2 SNR^{-2}}{f_{US}^2} + \frac{4B_C \phi_k SNR^{-1}}{f_{US}} + 2\hat{\eta}_{D,k}^{d}} \right\}^2 \qquad (5.52)$$

where $f_{US} \geq 2B$ is the uniform sampling rate. The f_{US} is proportional to the width of the monitored bandwidth $\mathcal{B}$ to avoid spectrum aliasing. Whereas, the randomised sampling average sampling rates are independent of B and can be remarkably low. Comparing the efficiency of uniform and randomised sampling approaches based only on the average sampling rates can be regarded as partial. The detection decision in both cases relies on calculating a form of discrete time Fourier transform from a finite set of the signal samples, e.g. DFT or an optimised version whenever applicable. Therefore, the number of processed samples is a critical factor in deciding the MSS efficiency.

The corresponding total numbers of processed samples for TRS, RSG, SSEP and uniform sampling spectrum sensing approaches are:

$$N_{TRS} \geq T_0 \alpha K_{TRS} \tag{5.53}$$

$$N_{RSG} \geq T_0 \alpha K_{RSG} \tag{5.54}$$

$$N_{SSEP} \geq T_0 \alpha K_{SSEP} \tag{5.55}$$

and

$$N_{US} \geq T_0 f_{US} K_{US} \tag{5.56}$$

respectively, where T_0 is the width of an individual signal analysis window. Generally, in low spectrum occupancy environments, i.e. $L_A / L << 1$, randomised sampling provides tangible savings not only on the average sampling rates but also on the overall numbers of processed samples. Extending the monitored bandwidth assuming a constant SNR (e.g. the sampling is preceded by a filter to limit the noise bandwidth/power), a fixed maximum number of simultaneously active subbands L_A and same detection requirements does not impose any additional cost on the number of collected samples for randomised-sampling-based multiband spectrum sensing as indicated in (5.53)-(5.55). On the contrary, in such cases the number of requested uniformly distributed samples grows at a rate equivalent to f_{US} where $f_{US} \geq 2B$. This shows that as the spectrum occupancy decreases, the benefits of exploiting nonuniform sampling in terms of the amount of the processed data becomes more visible. Low spectrum utilisation is faced in various applications for example CR networks and some wireless sensor networks applications as discussed in §1.1.

5.4 Numerical Examples on the Reliability Recommendations

Consider a communication system operating over the frequency range $[1.35,1.45]$GHz which is divided into $L = 20$ contiguous disjointed spectral subbands, 5 MHz each (i.e. $B = LB_C = 100$ MHz and $B_C = 5$ MHz). The sensed frequency points in (5.2) are labelled $f_1, f_2, \ldots, f_L$, i.e. one per monitored subband. The maximum expected number of concurrently active channels at any time is two, i.e. $L_A = 2$, $B_A = 10$ MHz and $L_A / L = 0.1$. A Blackman window of width 1.25 μs and an average sampling rate of $\alpha = 56$ MHz are used, the SNR is –0.25 dB. Whereas, the minimum valid bandpass uniform sampling rate

that would avoid spectrum aliasing within the overseen frequency range $\mathcal{B} = [f_{\min}, f_{\min} + B]$, $f_{\min} = 1.35\,\text{GHz}$, is $f_{US} = 224\,\text{MHz}$. The grid rate f_g of the random sampling on grid scheme is equal to the uniform sampling one where $f_g = f_{US} = 224\,\text{MHz}$. We assume that the transmissions are of equal power levels (e.g. uniform power transmission strategies are adopted at the source due to lack of knowledge of the propagation channel [116]). They are subsequently shaped by the frequency response of the propagation channel corresponding to each of the monitored subbands in $\mathcal{B}$, it is displayed in Figure 5.2 for $\{f_k\}_{k=1}^{L}$ (e.g. estimated in advance at the sensing device). In this section, we demonstrate the introduced randomised-sampling-based MSS approach with the aid of numerical examples. The plots in Figures 5.3, 5.4, 5.5 and 5.8 are obtained from 25000 independent simulations.

Our objective is to achieve: $P_{f,12}(\gamma_{12}) \le 0.08$ (i.e. $\Delta_{12} = 0.08$) and $P_{d,12}(\gamma_{12}) \ge 0.965$ (i.e. $\ell_{12} = 0.965$) for the subband centred at f_{12}. It is referred to from now on as the targeted subband and is expected to be occupied by a BPSK modulated signal. Thus $\hat{\eta}_{D,12} = \hat{\eta}^{d}_{D,12} = \hat{\eta}_{A,12} = \hat{\eta}_{DA,12} = 1$ to revoke any deterioration in the accuracy of the employed periodogram-type estimators due to the type of the incoming cyclostationary signal. According to (5.32), (5.39) and (5.45), we need to average the following number of estimates: $K = K_{TRS} \ge 24$ for total random sampling (i.e. $K_{TRS,\min} = 24$) in $\hat{X}_{e,TRS}(f)$, $K = K_{RSG} \ge 21$ for random sampling on grid (i.e. $K_{RSG,\min} = 21$) in $\hat{X}_{e,RSG}(f)$ and $K = K_{SSEP} \ge 30$ for stratified sampling with equal partitions (i.e. $K_{SSEP,\min} = 30$) in $\hat{X}_{e,SSEP}(f)$. Figures 5.3a, 5.4a and 5.5a exhibit the ROC plots of the targeted subband for the TRS, RSG and SSEP estimators respectively for L_A active subbands using various numbers of estimate averages and sweeping across a range of possible threshold values; the asterisks indicates the minimum sought $P_{d,12}(\gamma_{12})$ and maximum permitted $P_{f,12}(\gamma_{12})$. Figures 5.3b, 5.4b and 5.5b display $P_{d,12}(\gamma_{12})$ and $P_{f,12}(\gamma_{12})$ for the threshold values determined by (5.48) utilising (5.30), (5.31), (5.35), (5.37), (5.41) and (5.42). The $P_{SA} + P_N$ power parameter in (5.48) is presumed to be supplied accurately by a separate block, e.g. an analogue power/energy sensor at the receiver.

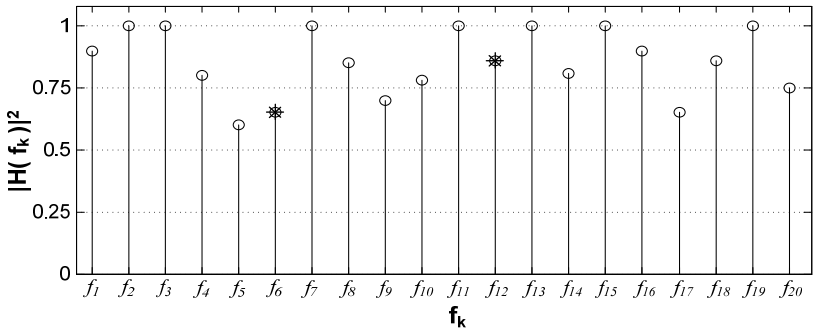

Figure 5.2: Propagation channel squared magnitude frequency response $\left|H(f_k)\right|^2$.

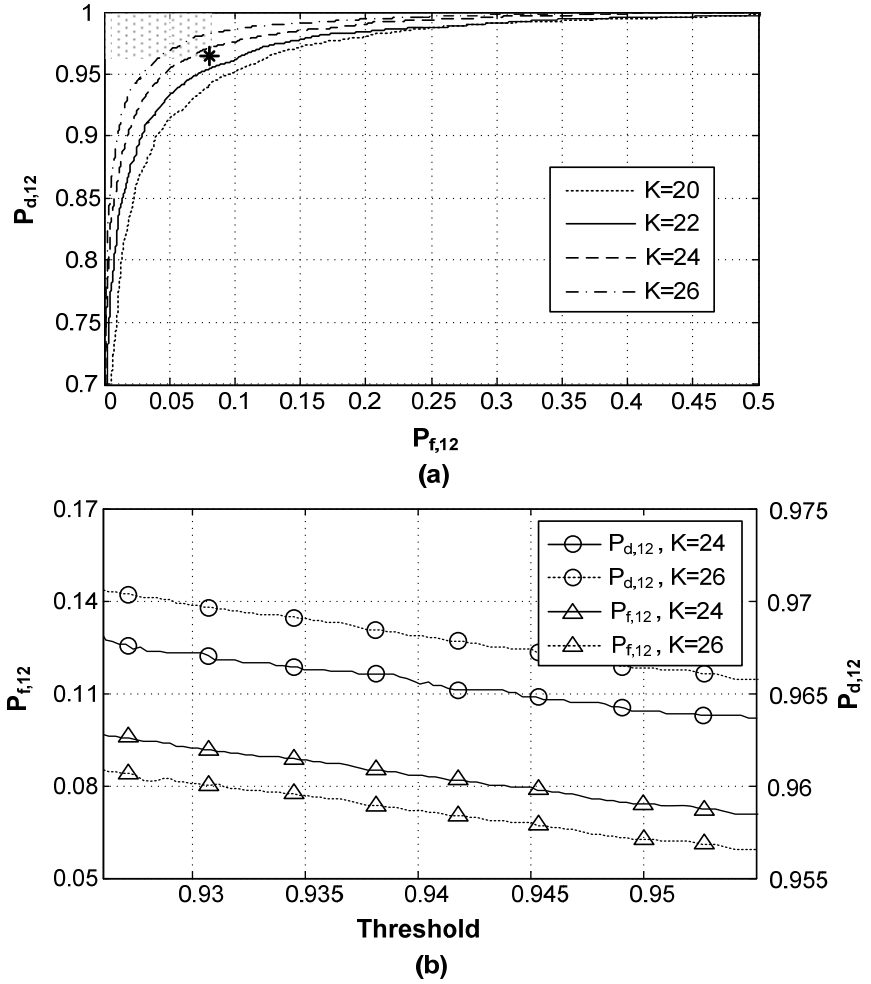

Figure 5.3: Detection probabilities of the targeted subband with central frequency f_{12} using TRS estimator for various numbers of averaged estimates in $\hat{X}_{e,TRS}(f_{12})$ and L_A active subbands. (a) ROC for a threshold sweep, asterisk is (Δ_{12}, ℓ_{12}). (b) $P_{f,12}(\gamma_{12})$ and $P_{d,12}(\gamma_{12})$ for $\gamma_{\min,12} \le \gamma_{12} \le \gamma_{\max,12}$ obtained from (5.48), (5.30) and (5.31).

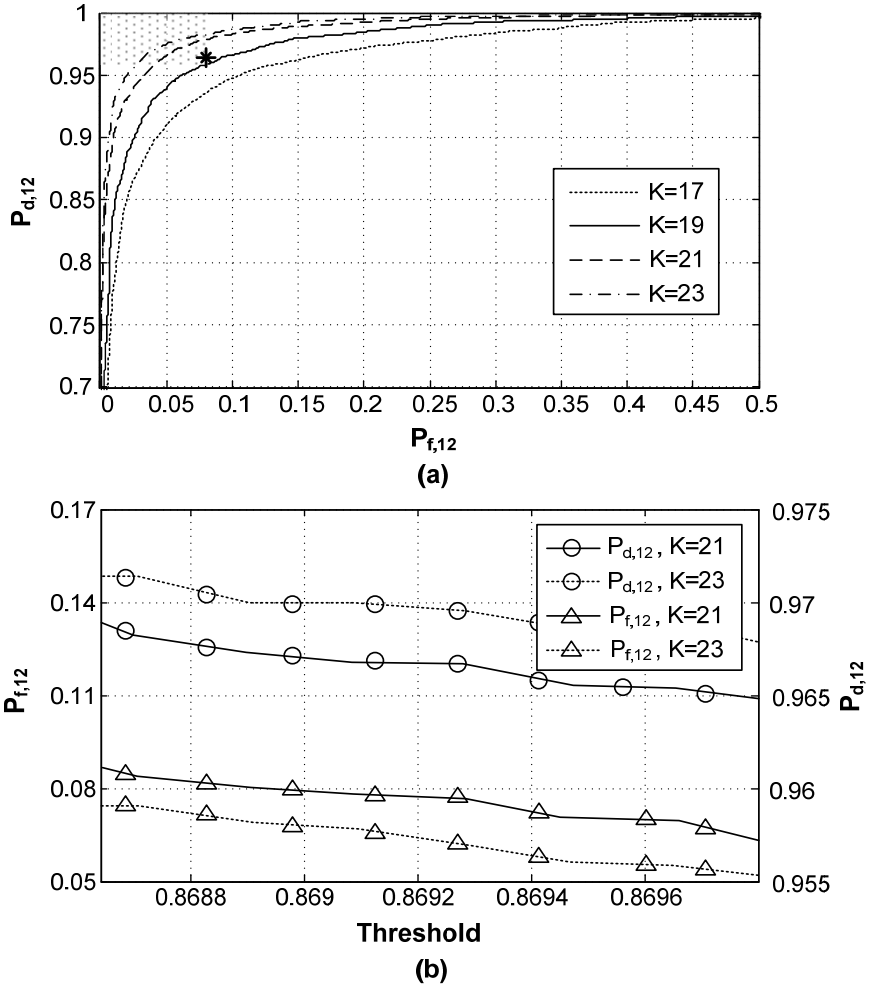

Figure 5.4: Detection probabilities of the targeted subband using RSG for various K values and L_A active channels. (a) ROC for a threshold sweep, asterisk is (Δ_{12}, ℓ_{12}). (b) $P_{f,12}(\gamma_{12})$ and $P_{d,12}(\gamma_{12})$ for $\gamma_{\min,12} \le \gamma_{12} \le \gamma_{\max,12}$ obtained from (5.48), (5.35) and (5.37).

It is evident from Figures 5.3, 5.4 and 5.5 that the pursued probabilities of the targeted subband were acquired by following the derived recommendations in (5.32), (5.39) and (5.45), i.e. when $K \ge K_{\min,TRS}$ for TRS, $K \ge K_{\min,RSG}$ for RSG and $K \ge K_{\min,SSEP}$ for TRS. The probabilities for $K_{\min,TRS}$, $K_{\min,RSG}$ and $K_{\min,SSEP}$ match to a great extent the minimum specified ones. This confirms the reasonable conservativeness of the provided guidelines and that the assumptions undertaken in the conducted analysis (including the normality one) did not have a noticeable effect on the accuracy of the obtained results. Figure 5.5 is distinct in this respect where $K_{\min,SSEP}$ is slightly more conservative compared to the TRS and RSG cases. It is due to the additional introduced precautions, i.e. $\varpi_{0,k} = 0$ and $\varpi_{1,k} = 0.5$, to accommodate the SSEP varying smeared-aliasing level feature. Figures 5.3b,

5.4b and 5.5b show that the requested probability of detection and false alarm are delivered by the thresholding regime in (5.48); this vindicates its effectiveness. If the reliability condition in (5.18) which is based on Chebychev's inequality was adopted in the above simulations, the recommended number of estimate averages would have significantly exceeded each of $K_{\min,TRS}$, $K_{\min,RSG}$ and $K_{\min,SSEP}$, e.g. $K \geq 185$ for the total random sampling case. This depicts the fact that Chebychev's inequality can be over-conservative compared to the embraced normality distribution premise.

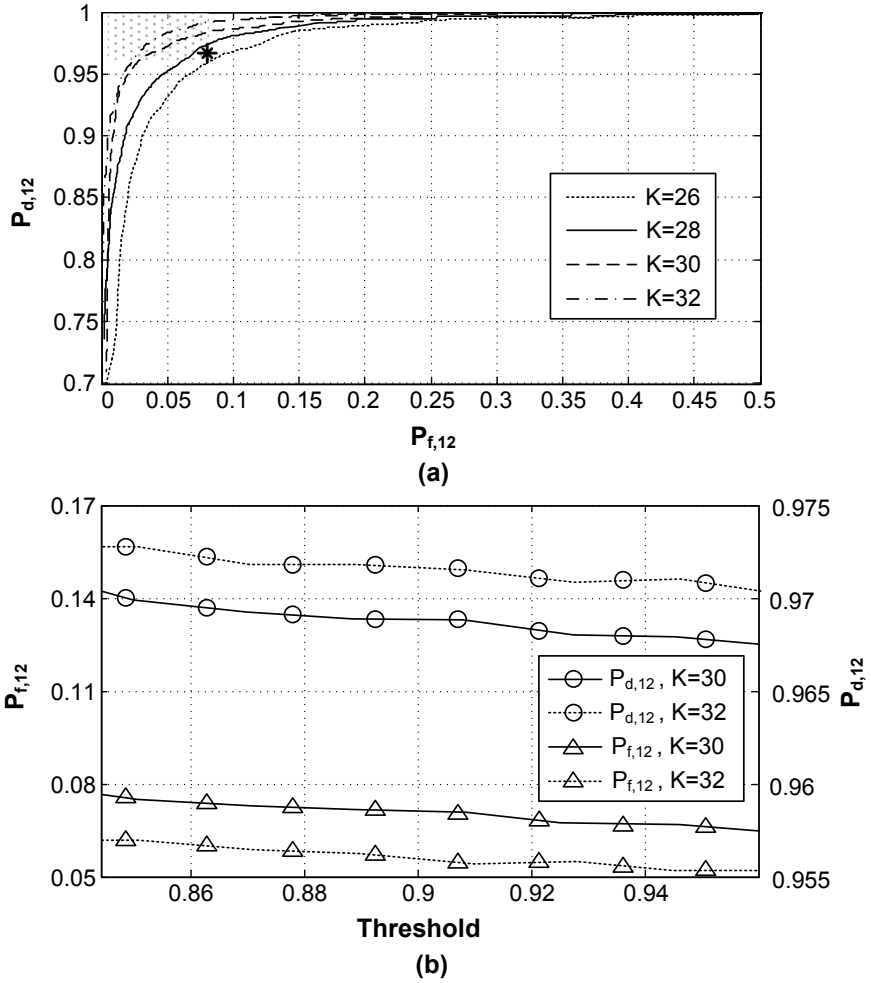

Figure 5.5: Detection probabilities of the targeted subband using SSEP for L_A active channels. (a) ROC for a threshold sweep, asterisk is (Δ_{12}, ℓ_{12}). (b) $P_{f,12}(\gamma_{12})$ and $P_{d,12}(\gamma_{12})$ for $\gamma_{\min,12} \leq \gamma_{12} \leq \gamma_{\max,12}$ obtained from (5.48), (5.41) and (5.42).

Unrecognising the effects of processing cyclostationary signals on the accuracy of the estimation and detection routines, i.e. $\hat{\eta}_{D,12} = \hat{\eta}^{d}_{D,12} = \hat{\eta}_{A,12} = \hat{\eta}_{DA,12} = 0.5$, leads to: $K \geq 20$, $K \geq 17$ and $K \geq 25$ for TRS, RSG and SSEP estimators respectively. This would have

undermined the dependability of the spectrum sensing algorithm where the sought ROC probabilities would not have been satisfied according to Figures 5.3, 5.4 and 5.5. Furthermore, if the smeared-aliasing decay factor of SSEP was not considered, i.e. $\varpi_{1,k} = 0$ in (5.41), (5.42) and (5.45), the minimum required K would have been 24, i.e. below the number of estimate averages demanded to reach $P_{f,12}(\gamma_{12}) \leq \Delta_{12}$ and $P_{d,12}(\gamma_{12}) \geq \ell_{12}$ for the targeted subband. This exhibits the need to take the necessary measures to adapt the sensing method to the varying smeared-aliasing aspect of stratified sampling.

Consequently, the desired system performance is achieved with an average sampling rate as low as 56 MHz, i.e. the randomised-sampling-based MSS offers a 75% saving on the sampling rate compared to uniform-sampling-based techniques. To gain a deeper insight into the benefits of our sensing approach, Table 5.2 displays the requirement of various sampling schemes in terms of achieving the predefined probabilities of detection and false alarm – formula (5.52) is used for the uniform sampling case. The table lists the maximum instantaneous sampling frequencies of each of the examined schemes, i.e. the maximum requested acquisition device(s) speed(s). Two interleaved Analogue to Digital Converters (ADCs) are employed and the shown rates are per one ADC.

Table 5.2: Detection requirements for various sampling schemes per one ADC. The targeted subband has: $P_{f,12}(\gamma_{12}) \leq 0.08$ and $P_{d,12}(\gamma_{12}) \geq 0.965$.

Sampling scheme	Average Sampling rate (MHz)	Maximum β_n (MHz)	Sensing Time (μs)
Uniform Sampling	112	112	10
TRS	28	Infinity	27.5
RSG	28	112	23.75
SSEP	28	56	32.5

The following observations are made from Table 5.2:

- **Uniform sampling:** imposes sampling rates that exceed twice the total width of the monitored bandwidth despite having the shortest sensing time.
- **Total random sampling:** the samples of a TRS sequence can be arbitrarily close requesting infinitely fast acquisition device(s) albeit offering more than 75% saving on the average sampling rate and more than 25% reduction on the total number of processed samples compared to uniform sampling.

- **Random sampling on grid:** provides more than 35% savings on the total number of processed samples compared to uniform sampling. The necessity of having a fast underlying uniform grid imposes an RSG instantaneous sampling rate equal to that of the uniform sampling.
- **Stratified sampling with equal partitions:** reduces the demanded acquisition device(s) speed(s) by 50% and the number of processed samples by 10% compared to uniform sampling.

Therefore, RSG provides tangible savings on the total number of processed samples and demands acquisition devices with capabilities similar to those utilised with uniform sampling. On the other hand, SSEP remarkably relaxes the speed requirements of the ADCs and reduces the number of collected data samples compared to uniform sampling at the expense of longer processing time. These conclusions demonstrate the trade-offs of each of the studied sampling schemes and are mainly relevant to the considered numerical example. Each scenario should be assessed individually with the aid of the developed analytical expressions in (5.32), (5.39), (5.45), (5.52) and (5.53)-(5.56).

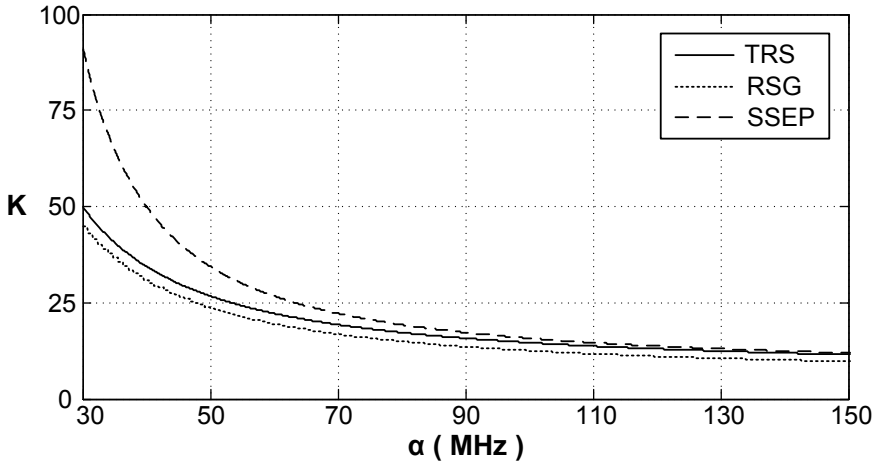

Figure 5.6: Required number of estimate averages to fulfil the detection probabilities of the targeted subband for each of TRS, RSG and SSEP estimators using various average sampling rates.

Figure 5.6 exhibits the number of estimate averages needed to meet the detection requirements of the targeted subband centred at f_{12} for TRS, RSG and SSEP versus a varying average sampling rate. The admissible rates for the stratified sampling case are approximately $\alpha \geq 11\text{MHz}$ according to (5.44). It is clear from the figure that RSG demands the least number of estimate averages whilst SSEP requests the most number of

averages. The discrepancies between the three schemes diminish as α increases. It is also noticed that the number of estimate averages declines as α increases revealing the cost of low average sampling rates in terms of longer sensing times. TRS can demand lower numbers of estimate averages compared to SSEP despite the fact that stratified sampling is proven in [98] to always deliver more accurate FT estimation than TRS. Nevertheless, SSEP with two ADCs provides substantial benefits in terms of the implementation feasibility as depicted in Table 5.2.

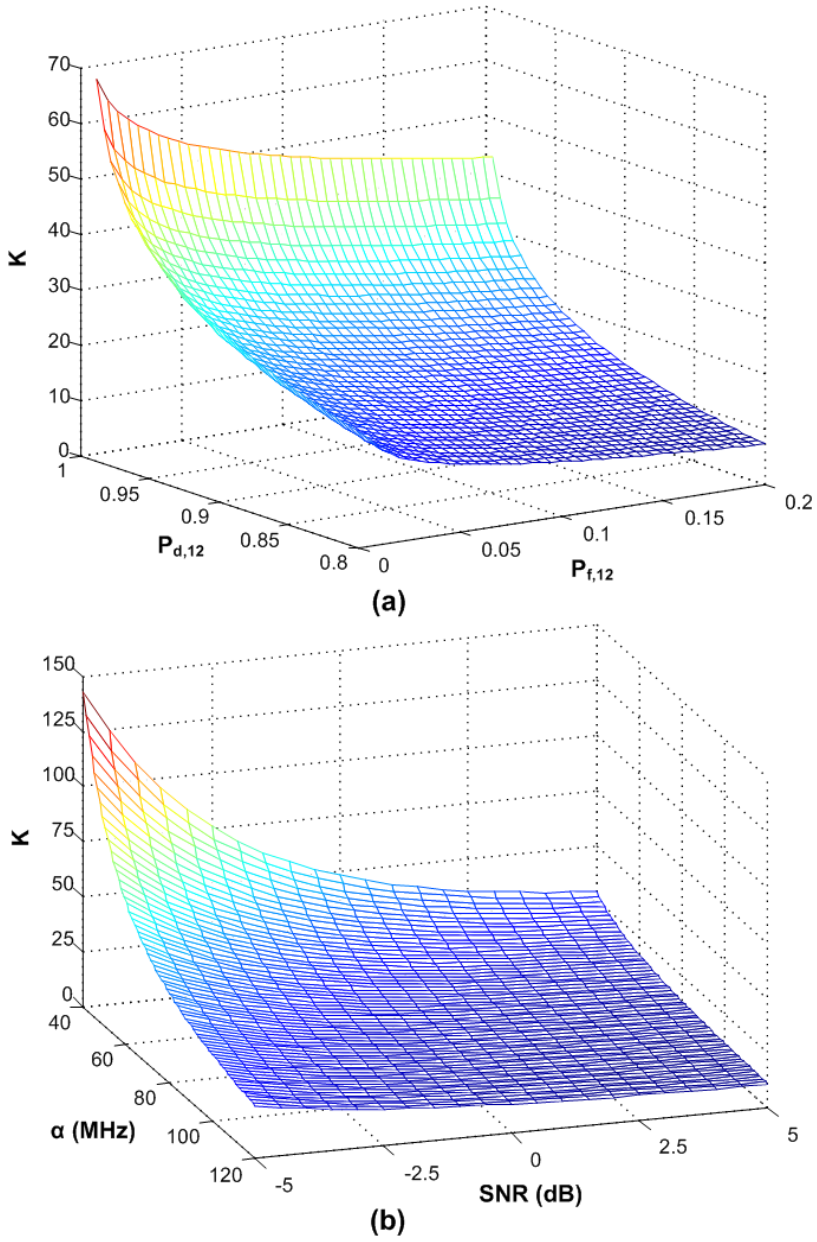

Figure 5.7: The number of estimate averages given by (5.45) for the targeted subband centred at f_{12} using SSEP. (a) For $\alpha = 56$ MHz and varying probabilities of detection and false alarm, (b) For $P_{f,12} \le \Delta_{12}$ and $P_{d,12} \ge \ell_{12}$ whilst α and SNR vary.

In practice, it is desired to have probabilities of detection close to one (e.g. to avoid any interference with the primary user in a cognitive radio network) and probabilities of false alarm close to zero (e.g. to maximize the opportunistic access to underutilised spectrum in CRs). Figure 5.7a shows the number of SSEP estimate averages for various maximum probabilities of false alarm and minimum probabilities of detection, i.e. varying Δ_{12} and ℓ_{12} values. It is noted that the normal distribution approximation is prone to inaccuracies at the tail probabilities, i.e. extreme $P_{f,k}(\gamma_k)$ and $P_{d,k}(\gamma_k)$ values. However, the latter probabilities lead to a considerable increase in the number of the summands (i.e. K) in $\hat{X}_{e,TRS}(f)$ in (5.4), $\hat{X}_{e,RSG}(f)$ in (5.5) and $\hat{X}_{e,SSEP}(f)$ in (5.6), e.g. see Figure 5.7a. This compensates for the aforementioned inaccuracies and strengthens the normality assumption. It was observed from simulations that the extreme $P_{f,k}(\gamma_k)$ and $P_{d,k}(\gamma_k)$ values do not hinder the conservative nature of the provided dependability guidelines. Figure 5.7b exhibits the requested number of estimate averages in $\hat{X}_{e,SSEP}(f)$ for the targeted subband where the average sampling rate and the signal-to-noise ratio vary. This exposes the effect of various system conditions on the requirements of the spectrum sensing procedure.

Let us assume that the system subband centred at f_6 whose $P_{f,6}(\gamma_6) \le 0.05$ and $P_{d,6}(\gamma_6) \ge 0.97$ is considered. It is expected to receive 16QAM modulated transmissions, i.e. $\hat{\eta}_{D,6} = 0.5$ is suitable. Figure 5.8 displays the ROC plots of the subband along with both sides of the reliability inequality (5.24) for the total random sampling scheme; the same number of estimate averages in Figure 5.3 is applied. It can be seen from the figure that the sought probabilities of the channel in question are not achieved where the (5.24) condition is not satisfied. This is due to the fact that the system subband with the central frequency f_6 imposes $\overline{K} \ge \overline{K}_{TRS,\min} = 28$ given its ROC probabilities, power level and the transmission modulation scheme. This demonstrates the compromise involved when a priority subband is specified by the user. To avert such cases, the user should survey the requisites of all the monitored channels and choose the highest combined K and α values to meet all the pursued $P_{f,k}(\gamma_k)$ and $P_{d,k}(\gamma_k)$ in the $\mathbf{P_f}(\boldsymbol{\gamma})$ and $\mathbf{P_d}(\boldsymbol{\gamma})$ vectors in (5.12) and (5.13) respectively. Equivalent analogy applies to RSG and SSEP.

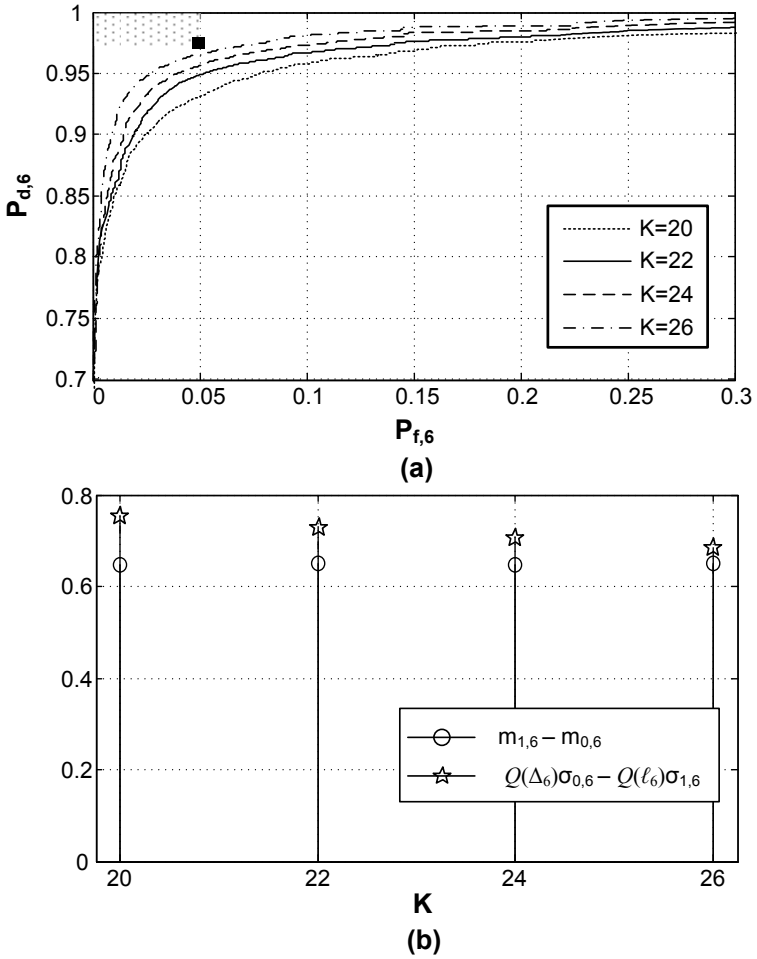

Figure 5.8: Detection probabilities of the subband centred at f_6 using TRS estimator for various numbers of estimate averages and L_A active subbands. (a) ROC for a threshold sweep, square is (Δ_6, ℓ_6). (b) Both sides of the reliability condition (5.24).

To illustrate the relationship between the spectrum occupancy, i.e. B_A / B where $B_A = L_A B_C$, and the total number of collected samples, consider the scenario where all the received transmissions are of equal power levels and have: $P_f(\gamma) \le 0.08$ and $P_d(\gamma) \ge 0.965$. Figure 5.9 exhibits the minimum required number of processed samples given by (5.53)-(5.56) for Uniform Sampling (US), TRS, RSG and SSEP for various spectrum occupancies; $SNR = -0.25$ dB which is assumed to be constant and $\alpha = 56$ MHz. It is noted from the figure that as the spectrum occupancy decreases, i.e. either by fewer subbands being simultaneously active or extending the overseen bandwidth, the gains of the randomised-sampling-based approach become more evident in terms of the total number of processed samples.

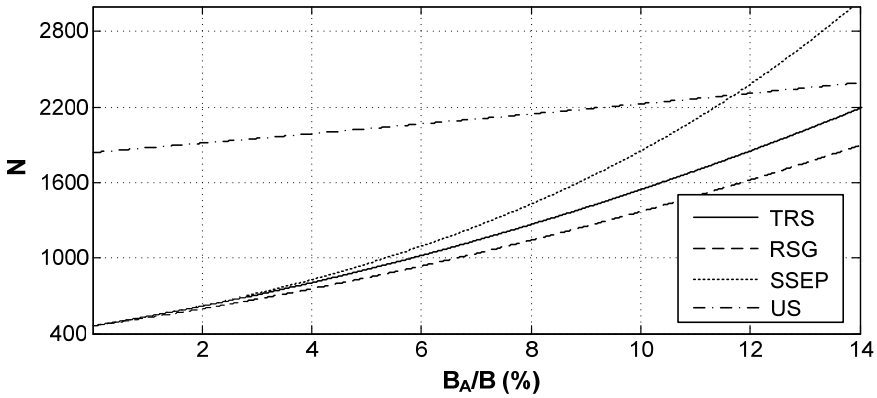

Figure 5.9: Total number of processed samples of each of TRS, RSG, SSEP and uniform sampling techniques for a varying spectrum occupancy, $\alpha = 65$ MHz, $SNR = -0.25$ dB and the ROC probabilities of the subband centred at f_{12}.

In summary, the preceding simulation testify the accuracy and reasonable level of conservativeness of the derived reliability recommendations in §5.3.1. The user is equipped with the necessary tools to assess the possible advantages of the introduced multiband spectrum sensing approach.

5.5 Applicability of the Introduced MSS Approach

The performance of the MSS techniques has been so far evaluated in a statistical sense, i.e. in terms of the realised probabilities of detection and false alarm. Here, we demonstrate the behaviour of the introduced sensing algorithm in a given detection operation, i.e. it is applied to a received waveform where the estimated spectrum $\hat{X}_e(f_k)$ in (5.3) and the result of the hypothesis testing in (5.2) are visualised. In practice, the simultaneously active transmissions can either stay static during the entire duration of the sensing operation, i.e. for $T_{obs} = KT_0$ seconds, or dynamically change. In the latter case, one or more of the monitored spectral subbands become active or inactive in the course of the detection process. The dynamic scenario is rarely investigated in the vast majority of the spectrum sensing studies, e.g. [10, 15, 17-20], where the subbands' statuses are presumed to remain static over a certain sensing time. In this section, we explore with the aid of simulations the response of our MSS routine to the situation where the overseen channels come on and off air whilst being surveyed.

Deciding whether the subband in question is active or not using (5.2) involves calculating the hypothesis testing threshold γ_k. We recall that the threshold values are bounded by:

$\gamma_{\min,k} \le \gamma_k \le \gamma_{\max,k}$ to satisfy $P_{f,k}(\gamma_k) \le \Delta_k$ and $P_{d,k}(\gamma_k) \ge \ell_k$. The lower threshold $\gamma_{\min,k}$, which restrains the probabilities of false alarm, is the same for all the system subbands. It only requires knowledge of the combined total power of the present multiband signal plus noise (i.e. $P_{SN} = P_{SA} + P_N$) according to (5.48) utilising (5.30), (5.31), (5.35), (5.37), (5.41) and (5.42) for the corresponding sampling scheme. It is noted that for stratified sampling $\varpi_{0,k} = 0$ and for random sampling on grid $(N_g - N)/(N_g - 1) \approx 1$ where typically $N_g >> N$. Relying on $\gamma_{\min,k}$ to set the decision threshold in (5.2) is a practical approach to adopt since $\gamma_{\min,k}$ is the same for all the channels and demands less prior information about the incoming signal compared to $\gamma_{\max,k}$. Similar thresholding strategy is commonly used in the literature mainly for the energy detector where $\gamma_{\min,k}$ is only a function of the noise power [10, 15, 17, 18]. In lieu of assuming that the P_{SN} is known as in §5.4 (e.g. supplied by an analogue sensor), here we obtain $P_{SA} + P_N$ from the captured nonuniformly distributed noisy signal samples via:

$$\tilde{P}_S(\mathcal{t}_r) = \frac{1}{T_0}\sum_{n=1}^{N} y^2(\tilde{t}_n) d_n \qquad , r = 1,2,\ldots,K \,. \quad (5.57)$$

The $\{\tilde{t}_n\}_{n=1}^{N}$ is the set of the N selected irregular sampling instants per time analysis window $\mathcal{T}_r = [\mathcal{t}_r, \mathcal{t}_r + T_0]$ arranged in an ascending order whilst d_n is the distance between two consecutive $\tilde{t}_n$ samples, i.e. $d_n = \tilde{t}_n - \tilde{t}_{n-1}$. Approximation (5.57) belongs to the subject of integration approximation over a finite interval. An estimate of P_{SN} is then attained from the K non-overlapping signal segments employing:

$$\hat{P}_{SN} = \frac{1}{K}\sum_{r=1}^{r} \tilde{P}_S(\mathcal{t}_r) \,. \quad (5.58)$$

The averaging is expected to eliminate/suppress the additional component in (5.57), i.e. $\sum_{n=1}^{N} x(\tilde{t}_n) n(\tilde{t}_n) d_n$ since $E[x(\tilde{t}_n) n(\tilde{t}_n)] = 0$. The capability of this thresholding method is demonstrated in the simulations below.

Now consider the multiband communication system described in §5.4 where $\mathcal{B} = [1.35,1.45]$ GHz, $L = 20$, $B_C = 5$ MHz and $B = 100$ MHz. The subbands' spectral peaks

are exhibited in Figure 5.2. An average sampling rate of $\alpha = 60\,\text{MHz}$ is chosen whereas $T_0 = 1.25\mu\text{s}$ and $SNR = -0.25\,\text{dB}$. In the following two examples, the static and the dynamic scenarios are examined separately, each with its own maximum number of concurrently active subbands, i.e. L_A. One frequency point is assessed per subband, it is placed at the centre of the channel, i.e. $\{f_k\}_{k=1}^{L}$ are the sensed spectral points.

5.5.1 Example 1: Static Situation

In this example, $L_A = 2$ and the two channels centred at f_6 and f_{12} are targeted; they are both occupied by a QAM type transmissions and have equal sensing requirements given by: $P_{f,k}(\gamma_k) \le 0.01$ and $P_{d,k}(\gamma_k) \ge 0.99$. According to (5.32), (5.39) and (5.45), we need to average: $K = K_{TRS} \ge 42$ estimates in $\hat{X}_{e,TRS}(f)$, $K = K_{RSG} \ge 36$ estimates in $\hat{X}_{e,RSG}(f)$ ($f_g = 244\,\text{MHz}$) and $K = K_{SSEP} \ge 55$ estimates in $\hat{X}_{e,SSEP}(f)$. In the simulations below, the combined signal plus noise power P_{SN} is estimated by (5.57) and (5.58) to determine the decision threshold $\gamma_{\min,k}$ in each detection operation.

Figure 5.10 shows the outcome of $\hat{X}_{e,TRS}(f)$, $\hat{X}_{e,RSG}(f)$ and $\hat{X}_{e,SSEP}(f)$ when the two channels centred at f_6 and f_{12} are simultaneously active. The transmissions remain statically active for $T > K_{SSEP}T_0 > K_{TRS}T_0 > K_{RSG}T_0$. Two independent detection experiments are depicted for each of the total random sampling, random sampling on grid and stratified sampling with equal partitions schemes where $K_{TRS} = 42$, $K_{RSG} = 36$ and $K_{SSEP} = 55$. The threshold levels obtained from the captured samples are displayed by the horizontal dashed line in each of the plots, whereas the asterisks indicate the active subbands.

It is clear from Figure 5.10 that the introduced MSS approach allows distinguishing the two active subbands with a significantly low average sampling rate. It is noticed that only the spectral points of the active subbands are above the calculated threshold level in all the presented experiments. This verifies the effectiveness of the proposed thresholding technique where the required signal plus noise power is procured from the collected samples. It was observed from further extensive experimental results that the distribution of the active subbands within the examined bandwidth does not affect the dependability of the spectrum sensing. To establish the rate at which the active channels are detected,

Monte-Carlo simulations have to be performed similar to the numerical examples on the reliability recommendations in §5.4.

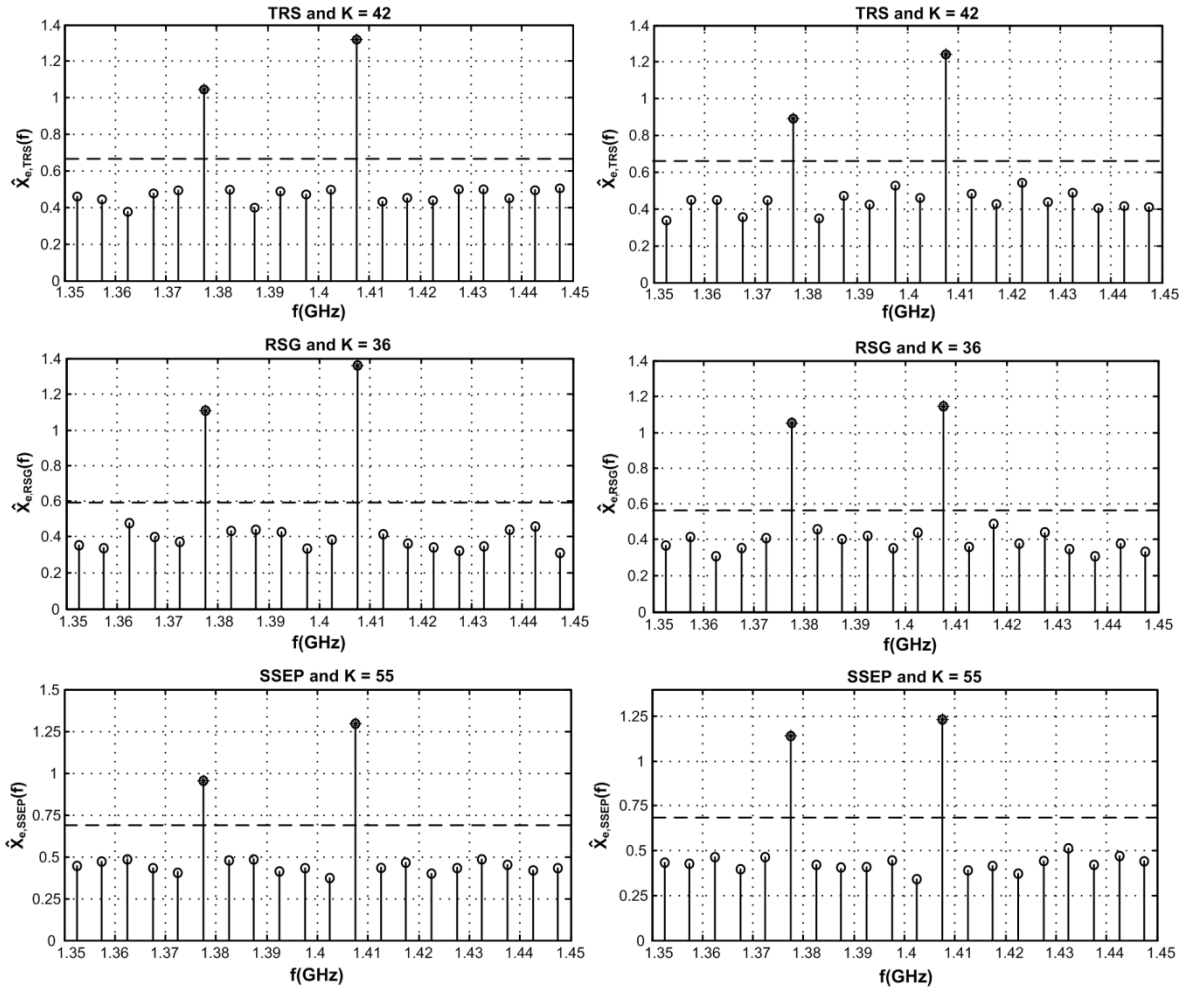

Figure 5.10: $\hat{X}_e(f_k)$ in (5.3) for the TRS, RSG and SSEP schemes, one frequency point per subband is calculated and two experiments are shown per sampling scheme. Decision threshold level (dashed line) using the proposed thresholding technique and (5.58), active subbands (asterisk).

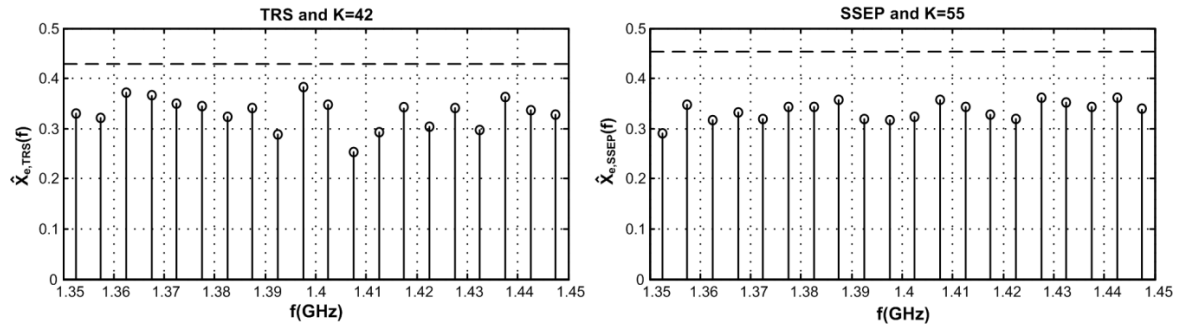

Figure 5.11: $\hat{X}_e(f_k)$ for TRS and SSEP when all the system subbands are inactive, decision threshold level (dashed line) using (5.58).

An interesting case is to assess the detection decision in case none of the channels are active. Figure 5.11 shows the detection results of two test experiments using $\hat{X}_{e,TRS}(f)$, and $\hat{X}_{e,SSEP}(f)$ when all the monitored subbands are ideal/silent (the system designer assumed 10 % spectrum utilisation). It is noted from Figure 5.11 that the MSS algorithm and the adopted thresholding regime is immune against such situations.

5.5.2 Example 2: Dynamic Situation

Four of the system subbands, i.e. the ones centred at f_2, f_6, f_{12} and f_{18}, are continuously monitored in this example over a long period of time employing $\hat{X}_{e,TRS}(f)$. The status of these channels dynamically change, i.e. their transmissions switch on and off whilst being surveyed. The maximum number of concurrently active subbands at any time is $L_A = 3$. The channels centred at f_2, f_6 and f_{12} have: $P_{f,k}(\gamma_k) \le 0.04$ and $P_{d,k}(\gamma_k) \ge 0.98$. In order to meet their detection requirements, $K \ge K_{\min} = 56$ estimates should be averaged in $\hat{X}_{e,TRS}(f) = \sum_{r=1}^{K} X_{e,TRS}(t_r, f)/K$. In Figures 5.12 and 5.13, we utilise $K = K_{\min}$. These figures display the status of the four scrutinised subbands ("1" is active and "0" is inactive) along with the detector's decision at certain time instants marked by crosses. We perform sensing every $T_p = K_{\min} T_0/8$ seconds, i.e. the detector's decision is checked at $t = nT_p$ ($n \in \mathbb{Z}$) time instants to establish if the subband in question is active (i.e. the cross is marked by "1") or passive (i.e. the cross is marked by "0"). This is distinct from the preceding Example 1 where the subbands were static and a decision was taken after the requested K spectrum estimates were averaged, i.e. the imposed sensing time KT_0 was accommodated. In Figure 5.12, the decision threshold $\gamma_k = \gamma_{\min,k}$ of the hypothesis testing in (5.2) is calculated using $\hat{P}_{SN}$ in (5.58) whereas in Figure 5.13 we presume that the exact $P_{SA} + P_N$ value is available at each of the marked time instants (e.g. provided by an analogue energy/power sensor).

It can be seen from Figures 5.12 and 5.13 that the detector requires some minimum elapse time before it can realise a change in the channels' activity and accordingly make a correct decision. During this period the detector's judgement is erroneous and unreliable. The aforementioned elapse time is less than or equal to the recommended $K_{\min} T_0$ sensing time

whether $P_{SA}+P_N$ is previously known or estimated. With regards to the particular case when a transmission goes offline:

- Utilising $\hat{P}_{SN}$ (Figure 5.12): only the decisions related to subband which went from being active to inactive are affected. After a certain period, i.e. $\tau \le K_{\min}T_0$ seconds, the change in the subband's activity is captured and reported by the detector.
- Accurate knowledge of $P_{SA}+P_N$ (Figure 5.13): the detector's judgement on the status of channels other than the one that witnessed the change is influenced. For example, the subband centred at f_{18} is decided to be active for a short period (although it is not) following the time instant when channel f_{16} went off the air.

Hence the thresholding regime that uses the estimated power from the collected samples is less affected by the sudden disappearance of a transmission. This is attributed to the fact that once a subband becomes idle, the total signal power drops whilst some of the averaged estimates in $\hat{X}_{e,TRS}(f)$ still embody data from the time when the channel was active. Consequently, the exact $P_{SA}+P_N$ can set the threshold level low leading to inactive channels being reported active. On the other hand, when a transmission swiftly appears, we observe that only the verdicts on the status of emerged channel are swayed either if $\hat{P}_{SN}$ is employed (Figure 5.12) or the accurate knowledge of $P_{SA}+P_N$ is assumed (Figure 5.13). However, it is noted that detector reacts faster to the appearance of a new transmission when $P_{SA}+P_N$ is estimated from the signal samples compared to being accurately known. This is referred to the sudden increase in the power level of the present multiband signal which is not fully featured in the estimated spectrum until after averaging a number of the estimates whose data encompass the contribution of the new active subband.

Therefore, estimating the required combined signal plus noise power, i.e. $P_{SA}+P_N$, from the captured noisy signal samples is an effective strategy to calculate the hypothesis testing decision threshold γ_k. Overall, the applicability and robustness of the introduced multiband spectrum sensing approach was illustrated in this section. The deductions are based not only on the shown two examples but also on a on a large number of simulated scenarios for each of the TRS, RSG and SSEP schemes.

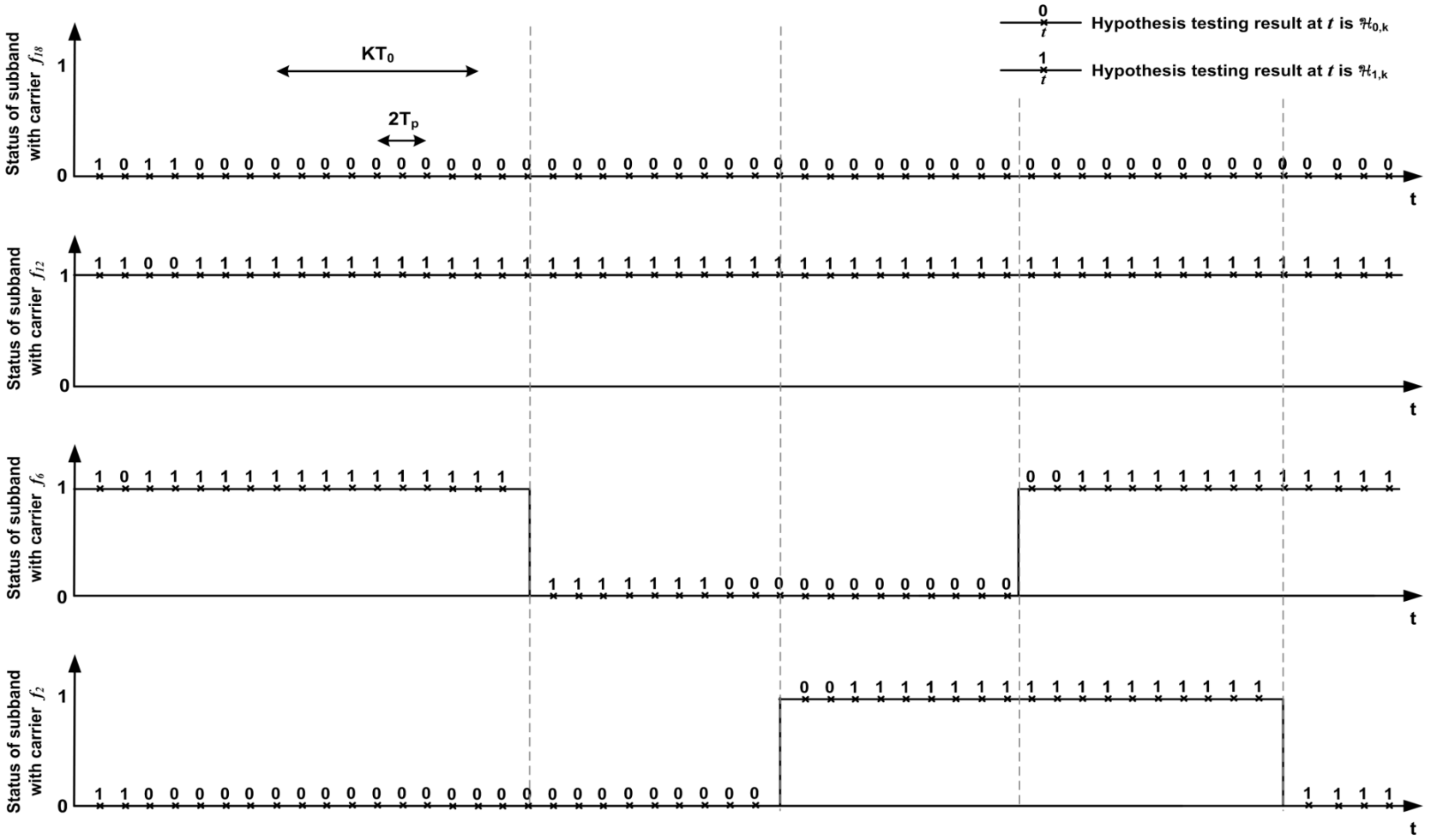

Figure 5.12: The status of the four examined subbands and the detection decision in (5.2) based on the outcome of $\hat{X}_{e,TRS}(f_k)$ and $\gamma_{\min,k}$, $P_S + P_N$ is estimated from the collected samples via (5.58). The time instants at which the spectrum is sensed (crosses), they are T_p seconds apart. Decision "1" indicated that an activity has been detected and "0" signifies the estimated spectrum is below the calculated threshold.

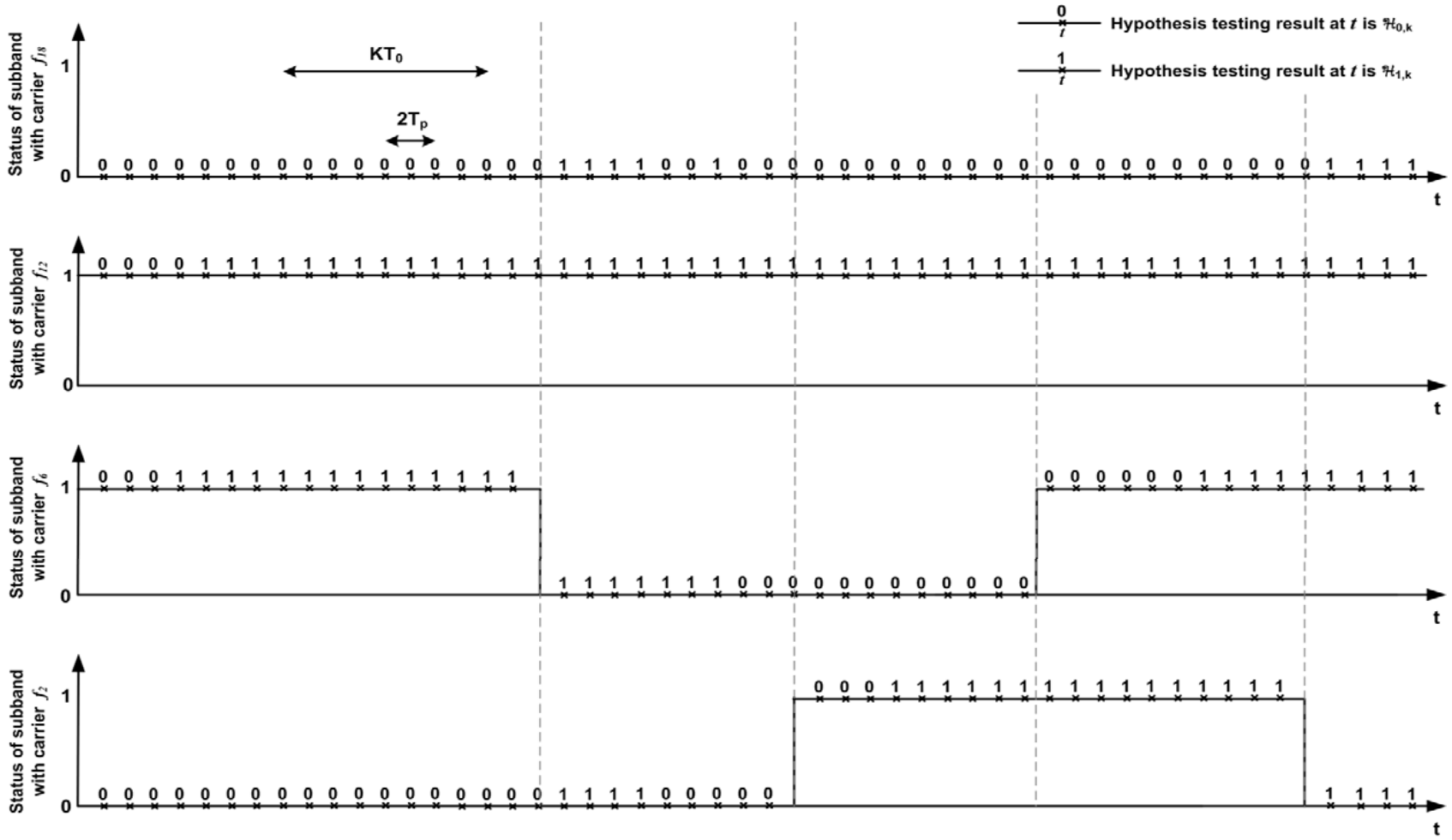

Figure 5.13: The status of the four examined subbands and the detection decision in (5.2) based on the outcome of $\hat{X}_{e,TRS}(f_k)$ and $\gamma_{\min,k}$, the parameter $P_S + P_N$ is assumed to be *a priori* known. The time instants at which the spectrum is sensed (crosses), they are T_p seconds apart. Decision "1" indicated that an activity has been detected and "0" signifies the estimated spectrum is below the calculated threshold.

5.6 Chapter Summary and Conclusions

A wideband randomised-sampling-based spectrum sensing approach was introduced in this chapter where simplicity and low computational complexity are among its key merits. It averages a number of periodogram-type estimators to reliably accomplish the sensing task using remarkably low average sampling rates compared to uniform-sampling-based techniques. Whilst the total random sampling and random sampling on grid rates can be arbitrarily low, there is a lower limit on the permissible stratified sampling rates depending on the power of the targeted spectral subband. Guidelines on the required average sampling rate α and the number of estimate averages K were developed amid sought probabilities of detection and false alarm for each of the TRS, RSG and SSEP schemes. They predetermine the amount of data and the sensing time that the MSS routine demands to deliver the specified detection performance. Those recommendations eliminate (or at least significantly reduce) the need for lengthy time-consuming Monte-Carlo simulations typically employed to check and refine the response of a particular detection method. They also equip the user with the necessary means to assess the possible advantages or disadvantages of the sensing technique and its requirements. The guidelines show that using lower sampling rates comes at the expense of longer signal observation window, i.e. sensing time. It is a trade-off that the user can evaluate by substituting the design parameters into the derived fairly compact and simple equations. Another factor that sheds light on the efficiency of randomised-sampling-based MSS is the total number of collected samples per detection operation. It is affected by the spectrum occupancy, i.e. the maximum expected number of concurrently active subbands at any time. In general, as the spectrum occupancy increases, the furnished savings in terms of the total number of processed samples diminish; this is regardless of the substantial reductions on the used averaged sampling rates.

The effect of processing cyclostationary signals on the performance of the adopted spectral analysis tools is embedded in the provided guidelines; it is represented by the design parameters $\hat{\eta}_{D,k}$, $\hat{\eta}^{d}_{D,k}$, $\hat{\eta}_{A,k}$ and $\hat{\eta}_{DA,k}$ for each of the examined randomised sampling schemes. This enables the user to countermeasure for any possible decline in the spectrum estimation accuracy due to nature of the received signal. If no information is available on the modulation schemes and the symbol rates of the incoming transmissions, more

spectrum estimates should be averaged, i.e. $\hat{\eta}_{D,k} = \hat{\eta}_{D,k}^{d} = \hat{\eta}_{A,k} = \hat{\eta}_{DA,k} = 1$, to guarantee that the sought probabilities of detection and false alarm are achieved. For instance, BPSK modulated signals cause notable deteriorations in the estimation accuracy as concluded in Chapter 4.

The introduced multiband spectrum sensing procedure demands some prior knowledge of the sensed environment. We divide these prerequisites into two groups: 1) the ones required to establish a lower bound on α and K for given detection probabilities and 2) parameters requested to determine the thresholds for the hypothesis testing in (5.2). The attained reliability recommendations in (5.32), (5.39) and (5.45) take into account onerous system conditions, e.g. maximum spectrum occupancy. Accordingly, a practical approach is to calculate the required α and K offline; if the user becomes aware of any changes in the system environment, he/she can refine or recalculate the α and K values. In Group 1 the design parameter that can be viewed as a limiting factor for the applicability of our MSS technique is the ratios of the power levels of the transmissions in the monitored subbands or the ratios of the peaks of their continuous-time spectrum, i.e. ϕ_k in (5.33) or (5.34). Various detection techniques in the literature demand such knowledge, e.g. the widely used energy detector. Those spectral peaks are assumed to be learnt/estimated in practice during the calibration stage of the system, e.g. when the overseen subbands are known to be definitely active [17, 114, 116, 129]. Hence knowing ϕ_k is not an extravagant request. With regards to Group 2, the detector imposes knowledge of the present combined signal plus noise power $P_{SA} + P_N$ which is mandated by the number of concurrently active channels at the time the sensing is performed. Estimating $P_{SA} + P_N$ from the collected noisy signal samples was demonstrated to be an effective strategy to determine the decision threshold. Alternatively, a primitive cheap analogue sensor can be employed at the receiver to keep track of the present energy/power. This can be viewed as an advantage over the popular ED. The latter demands knowing the noise power which changes over time, i.e. noise should be separated from the signal. Consequently, the design parameters requested by the introduced multiband spectrum sensing approach are reasonable and can be obtained in practice.

It is noted that correlated or overlapping signal windows scenario can be easily incorporated into our approach whenever the effect of correlation or overlapping on the

variance reduction following averaging is known, e.g. Welch periodograms [49, 108]. Moreover, the multiband joint detection reported in [116] to optimise the threshold vector $\boldsymbol{\gamma}$ in (5.14) for cognitive radio is applicable to the devised MSS technique. Cooperating among a number of sensing devices to collect spatial diversity, combat the shadow-fading effects and alleviate hidden terminal problems, e.g. [17, 18, 116, 129], may be implemented at a network level higher than the studied physical level.

Chapter 6

Conclusions and Future Work

The results presented in this thesis demonstrate the promising potential of nonuniform randomised sampling and its applicability to selected problems in wideband communication systems, namely spectrum sensing. This sampling paradigm goes against the common wisdom in data acquisition; conventionally uniform sampling is employed and is viewed as the natural option for many practitioners in the digital signal processing fraternity. However, uniform sampling DSP is adversely limited by the aliasing phenomenon. It imposes stringent requirements on the data acquisition model(s) whenever the handled task involves processing wide frequency ranges. Alternatively, the adopted digitisation and processing methodology, i.e. randomised sampling and processing, is shown throughout this research to provide more efficient processing algorithms. We focused on exploiting the aliasing suppression capabilities of randomised sampling to ease the onerous sampling rate demands of multiband spectrum sensing performed over wide bandwidths. Numerical examples and simulations verified the conducted analysis and drawn conclusions. Unveiling the spectral support of the present multiband signal clearly facilitates further processing, e.g. signal reconstruction.

The contributions of this research serve the purpose of better understanding the practice and limitations of randomised sampling in communication systems. Whilst the introduced solutions targeted spectrum sensing and were formulated within a generic multichannel communication system setup, it is strongly believed that they offer a framework for further generalisations and encourage/prompt researchers in the field to consider problems that could not be previously tackled due to the uniform sampling rate constraint. Consequently, much remains to be investigated. Below, we summarise the key contributions of this work and outline future research directions.

6.1 Summary

The expanding trend of an increased reliance on wireless communication services (with higher rates and thereby wider bandwidth requirements in most cases) is the catalyst for the continuously emerging communication paradigms and developing applications, e.g. Cognitive Radio (CR) and Wireless Sensor Networks (WSNs) discussed in Chapter 1. They call for digital signal processing that is capable of dealing with considerably wide bandwidths with emphasis on scenarios where the processed narrowband signals reside at *a priori* unknown locations within a wide range of overseen frequencies. Since the uniform sampling rates imposed by classical DSP in such cases exceed at least twice the total monitored bandwidth, they pose a major technical challenge. The motivation behind embracing the randomised sampling and processing methodology was its ability to mitigate the spectrum aliasing limitation. This allows the use of significantly low sampling rates compared to the uniform sampling counterpart. The tackled Multiband Spectrum Sensing (MSS) problem, which entails overseeing the activity of a number of predefined non-overlapping spectral subbands, was then described in Chapter 1. Accordingly, the need for spectral analysis tools that permits detection rather than exact spectrum estimation was acknowledged.

At this juncture, it was necessary to give a concise review of the sampling theory with Chapter 2 focusing on topics related to the theme of this research. For instance, the aliasing phenomenon of uniform sampling was identified and uniform bandpass and multiband sampling techniques were outlined. The limited applicability of the latter methods to the MSS problem was highlighted; they inherently depend on previous knowledge of the signal's spectral support, which is not available in the studied systems. Nonuniform randomised sampling was then suggested as an alternative sampling approach whose utilisation in conjunction with suitable processing algorithms is commonly known as Digital Alias-free Signal Processing (DASP). The various criteria for defining the alias-free characteristic were recognised noting their relevance to the spectral analysis of the signal rather than reconstruction. Subsequently, the DASP notion adopted in this thesis was stated, i.e. sampling and processing that facilitates detecting the present spectral components of the incoming signal without being limited by the processed bandwidth. This is attributed to the fact that for a finite number of captured samples the spectrum aliasing

phenomenon is never completely eliminated. Instead it is suppressed by a finite amount where a wideband component is introduced to the spectrum of the sampled signal and is referred to as smeared-aliasing.

The spectral analysis of three randomised sampling schemes, i.e. Total Random Sampling (TRS), Random Sampling on Grid (RSG) and Stratified Sampling with Equal Partitions (SSEP), using periodogram-type estimators was studied in Chapter 3 for wide sense stationary signals. It was shown that these periodograms are unbiased estimators of detectable frequency representations of the received multiband signals. They permit the unveiling of the active spectral components albeit the used sampling rates, i.e. they are adequate tools for the pursued DASP-based multiband spectrum sensing. Undertaking several measures to appropriate the periodogram-type estimators to the considered problem, i.e. spectrum sensing and not PSD estimation, was discussed. They included employing windowing functions to minimise spectral leakage due to the finite time analysis windows and averaging a number of estimates calculated from various signal windows. The latter aims at enhancing the estimation accuracy since periodograms standard deviations are known to be of the same order as their expected values. The analytical expressions of the mean and variance of the TRS, RSG and SSEP spectrum estimators were developed for a finite number of processed samples. This led to quantifying the level of smeared-aliasing for each of the examined schemes. For example, the smeared-aliasing level of SSEP varies across the monitored frequency range depending on the position of the signal's strong spectral components, whilst that of TRS and RSG remains constant within the surveyed bandwidth.

An important observation from the above analysis was that the characteristics of the sampling scheme have a profound impact on the shape and nature of the obtained spectrum. Accordingly, it was necessary to assess each of the schemes independently to establish its own merits. Whilst the smeared-aliasing components (their levels are inversely proportional to the used average sampling rate) do not hamper the detectability of the active monitored subbands, they cause deterioration in the dynamic range of the estimated spectrum. Formulas were derived in the last part of Chapter 3 to measure the Spectrum Dynamic Range (SDR) for each of the TRS, RSG and SSEP schemes. Additionally, guidelines on the required number of samples were provided to ensure that the SDR exceeds certain value, e.g. mandated by the user.

Although the stationarity assumption simplified the analysis in Chapter 3 and enabled concentrating on the characteristics of the adopted estimators, it was noted that a wide range of digitally modulated communication signals are cyclostationary stochastic processes. As a result, the behaviour of the periodogram-type estimators was re-evaluated in Chapter 4 for linearly modulated communication signals. It was shown that the total random sampling, random sampling on grid and stratified sampling with equal partitions estimators continue to be suitable tools for the spectrum sensing task. A spectrum region within each of the active transmission bands, i.e. named the *guarded region*, was identified. The estimated spectrum in the *guarded regions* embodies detectable frequency representation of the present transmissions and is independent of the position of the time analysis window. Nonetheless, it was illustrated that the estimation accuracy of the periodogram-type estimators can notably decline at/near selected frequencies within the active spectral subband for certain modulation schemes. The transmission's modulation type, baud rate and carrier frequency dictate these frequency points. Since no prior knowledge of the modulation scheme or its parameters is presumed, conservative measures can be taken to avert the potential additional high inaccuracy levels of the periodogram-type estimators for cyclostationary signals. The detailed calculations of the cyclostationarity effects were included in Appendix D.

A novel multiband spectrum sensing approach was introduced in Chapter 5 using the spectral analysis results in Chapters 3 and 4. Its operational average sampling rates can be arbitrarily low for the total random sampling and random sampling on grid schemes. Whereas for stratified sampling, a lower bound on the permissible rates was specified, it is still well below the minimum uniform sampling counterpart. Such a limitation is due to the scheme's varying smeared-aliasing level. The ability of stratified/jittered sampling to reduce smeared-aliasing in the vicinity of the signal's strong spectral components is viewed in the literature as an advantage, e.g. in [3, 5]. Besides, stratified sampling is proposed in [98] as a scheme that offers more accurate Fourier transform estimation of deterministic signals with higher rates of convergence compared to TRS. Here, it was shown that stratified sampling suffers from its smeared-aliasing reduction feature in the context of spectrum sensing and does not necessarily lead to a more efficient sensing technique compared to total random sampling. Generally, the substantially low sampling rates of the introduced MSS approach compared to uniform-sampling-based techniques

effectively ease the stringent sampling rate requirements of wideband spectrum sensing. It enables a more efficient use of the sensing device(s) resources, e.g. power, and avoids the possible need for a high cost dedicated premium DSP.

Ensuring the reliably of the spectrum sensing, i.e. it delivers predefined probabilities of detection and false alarm for one or more of the overseen spectral subbands, was one of the key targets and contributions of our approach. This entails performing spectrum estimation with a certain level of confidence where the needed resources are *a priori* known. The uncertainties in the estimation process, which originate from the randomness of the sampling process and that of the sampled signal in addition to the present noise, were captured in Chapter 3 and 4 by the variance metric for each of the TRS, RSG and SSEP schemes. Averaging a K number of the estimates calculated from non-overlapping signal windows, each of width T_0, was admitted as an additional means alongside the average sampling rate to improve the estimators' performance. Specifying the required sampling rate and the sensing time KT_0 are of paramount importance to the efficiency of the MSS procedure in lieu of assuming that the desired estimation accuracy is available from "*sufficient estimate averaging*" as in the majority of multiband spectrum sensing studies, e.g. [10, 21, 23, 24, 114, 115, 117, 118, 127, 128, 136].

In fact, papers on randomised sampling dating from the 1960's, e.g. Silverman and Shapiro [90], revealed that the signal's power spectral density can be estimated from *an infinitely long sampling sequence* captured at arbitrarily low sampling rates. Quantifying the relationship between the operational randomised sampling rate and the length of the signal observation window, which is finite in practice (unlike [90] and many papers that followed), is a problem that was resolved here in the context of the spectrum sensing. In Chapter 5, prescriptive recommendations were provided for each of TRS, RSG and SSEP to guarantee that the multiband spectrum sensing approach meets preset probabilities of detection and those of false alarm for one or more of the monitored subbands. Such guidelines depict the trade-off between the sampling rate and the length of the signal observation window (sensing time). They equip the user with the necessary means to predict the prerequisites and efficiency of the sensing technique. Those guidelines clearly show the amount of data required before the sought level of detection accuracy is achieved. This circumvents the downfall of processing unnecessarily excessive amounts of data and

the need for checking the method's performance via lengthy time-consuming Monte-Carlo simulations.

The analytical expressions for the threshold levels needed in the detection operation were developed in Chapter 5 and the prior knowledge demanded by our MSS approach was discussed. It was concluded that the latter is comparable to the previous information requested by other widely used existing methods. A technique to estimate the threshold levels from a set of collected samples was proposed and its effectiveness was demonstrated. The response of the introduced MSS approach to static and dynamic (i.e. subbands coming on and off air) system conditions was checked by simulations in Chapter 5. They depicted the ability of the detection procedure to detect the active channels utilising the set of collected noisy signal samples and highlighted the scope for future improvements (see §6.2). It was noted that the dynamic situations are the weak point of virtually all algorithms that deal with spectrum sensing. Typically, there is an indirect assumption that the situation, i.e. the simultaneously active subbands, stays static over a certain detection time. In our case, this time period is the sensing time KT_0.

Although each of TRS, RSG and SSEP facilitates detecting the active spectral subbands within the monitored bandwidth at remarkably low average sampling rates, their requirements in terms of implementation in hardware notably vary. Whilst the simple mathematical description of total random sampling is one of its main merits, the interest in its applicability in practice is rather limited since any two of its samples can be arbitrarily close. On the contrary, a minimum distance is maintained between any two points in any random sampling on grid sampling sequence. This distance is equal to the underlying uniform grid period that can still be high to reserve the usefulness of the estimator for the MSS task. This imposes fast ADC(s) that can match the demanded underlying grid rate despite the RSG potential to offer significant savings on the total number of processed samples. Stratified sampling with equal partitions with two ADCs (or more) equates the maximum instantaneous sampling rate to the average sampling rate providing a substantial saving in terms of the ADC(s) speed in addition to the average sampling rate. There have been several studies on implementing randomised samplers similar to the ones examined in this research, e.g. [1, 137-140]. They give good indications of the applicability of the devised technique in practice. Randomised sampling and nonuniform sampling have been lately gaining more prominence in the DSP community due to the increasing interest in

compressive sensing that employs irregular sampling in several studies, e.g. implementation examples are reported in [141-144].

6.2 Suggestions for Future Work and Outlook

Since this research sets a framework for applying randomised sampling and its processing to wideband spectrum sensing, there is plenty of scope for future research - some of which can be an extension of the results contained in this thesis. Below, we give an overview of the future work related to the subject and contributions of this research.

Applicability, Parameters Estimation and Dynamic Conditions

Applying the introduced multiband spectrum sensing approach to a particular application environment to demonstrate its efficiency is of an interest, e.g. CR in the TV channels spectral bands in IEEE 802.22 as in [116, 145]. In such environments, some knowledge of the system parameters is available, e.g. the permitted sensing time, propagation channel conditions and the power level of the transmitted signals, etc. This helps with calibrating and tailoring the sensing method to the needs of the monitored environment. Evaluating the performance of our MSS approach for modulation schemes other than the linearly modulated ones can identify schemes that might suit or challenge the detection procedure. This will strengthen the obtained results and extend their scope.

Creating a dependable methodology for estimating the parameters required by the devised sensing technique necessitates further investigation. For instance, the inaccuracies in estimating the present combined signal plus noise power, either obtained from the collected noisy samples or an analogue sensor that continuously records the present energy/power, can be added to the total uncertainties of the spectrum estimation routine. Consequently, conservative measures can be taken, e.g. more estimate averages, to ensure the reliability of the multiband spectrum sensing.

Deeper analysis of the effects of dynamic system situations (i.e. when transmissions come on and off the air, possibly during a sensing operation) on the detection performance would give a better insight into the robustness and tolerance of the introduced MSS approach to such conditions. This can lead to adaptively changing the number of estimate averages based on the level of measured signal plus noise power in a given sensing operation. Any

sudden drop in the measured power would indicate that fewer channels are concurrently active and hence the number of needed estimate averages can be reduced.

Signal Reconstruction

Signal reconstruction from nonuniform sampling data is a mature domain with more results than we can list here. In fact, this was a key factor in our decision to focus on the spectrum sensing task where few results (barely any) on randomised-sampling-based MSS were available in the open literature at the time this research commenced.

Generally, the necessary condition for perfect signal reconstruction is operating at sampling rates higher than twice the joint bandwidth of the concurrently active spectral subbands, i.e. above Landau rate. For some communication systems, e.g. cognitive radio and some WSN applications, the spectrum occupancy is typically low. Capitalising on this premise, signal reconstruction, which is preceded by determining the signal's spectral support, can yet be achieved while the sampling rates are considerably lower than those requested by uniform sampling. We anticipate using existing numerically stable reconstruction algorithms that are geared to deal with communication signals, e.g. reconstruction based on exponential basis functions in [146] or band splitting with recursive least squares in [4] and many others. It is also believed that the unfolding results on compressive sensing can provide effective reconstruction techniques for the nonuniformly sampled data. Most importantly, any adopted method should be able to handle the moving signal analysis window efficiently.

The possibility of accomplishing the reconstruction task accurately would allow interpolating the signal on a uniform grid. This enables departing from the nonuniform sampling environment and moving to the familiar uniform sampling one where a plethora of further processing algorithms are available.

Alternative Randomised Sampling Schemes

Analysing the Additive Random Sampling (ARS) scheme and its behaviour is yet to be considered. Its practical aspect in terms of implementation in hardware has been promoted by various researchers in the field, e.g. [5, 147]. Although results on power spectral density estimation using certain types of ARS have been published, e.g. [113], employing such

results for spectrum sensing requires further research. Additionally, randomised sampling schemes, which present themselves as straightforward extensions of those studied in this work, can be assessed. They include: stratified sampling on grid [148], the modified stratified sampling in [148] and antithetical sampling in [101].

Compressive Sensing and Other Spectrum Sensing Techniques

Some multiband spectrum sensing techniques, e.g. [23, 24, 127, 128], utilise the compressive sensing methodology to operate at sub-Nyquist sampling rates exploiting the spectrum sparsity of the processed signals. Such methods assume that the signal's empirical correlation matrix obtained from the collected samples estimate very accurately the signal's actual correlation matrix. If there are errors in the estimation of the aforementioned matrix, there is no technique known to the author (apart from time-consuming Monte-Carlo simulations) that would provide an indication on how reliable the whole approach is. The frequency-domain functions $C_{TRS}(\not{t}_r, f)$, $C_{RSG}(\not{t}_r, f)$ and $C_{SSEP}(\not{t}_r, f)$ that our estimators aim to approximate are very smooth. If they are known exactly, one can easily determine the level of the smeared-aliasing plus noise across all subbands and anything that is above the latter level would signify an active transmission. However, one of the goals of this research is to avoid extremely long averaging processes and instead estimate $C_{TRS}(\not{t}_r, f)$, $C_{RSG}(\not{t}_r, f)$ and $C_{SSEP}(\not{t}_r, f)$ from a finite and well-defined amount of data. The algorithms controlling the resultant uncertainties are then put in place in order to provide a mechanism for guaranteeing the performance of the overall system in terms of probabilities of detection and false alarm. Consequently, our main contributions could not be immediately compared to CS-based methods. In order to deliver a scientifically meaningful comparison, a considerable amount of mathematical analysis, e.g. spectrum estimation accuracy, combined with a variety of simulations would have to be made. They should take into account the various sampling schemes and various optimisation algorithms used in CS. This would contribute to an interesting discussion on whether periodograms or compressive sensing is the better tool for detecting the activity of the monitored channels.

Investigating the possibility of deriving reliability recommendations for the spectrum sensing techniques discussed in §5.2 is of an interest, e.g. the required quantity of data to

achieve certain probabilities of detection and false alarm. Only then the requirements of the introduced MSS procedure can be compared to those of the other methods.

Cyclic-spectral Estimator

An extension to the proposed approach in this thesis is to explore the possibility of employing a cyclic-spectral estimator to exploit the cyclostationarity of the processed signals as in [16, 51, 120, 149]. Estimating the spectral correlation function from nonuniformly sampled data can lead to a randomised-sampling-based feature detector, which is immune against the adverse effects of stationary noise and interference. Since the feature detector senses one subband at a time, i.e. a narrowband spectrum sensing technique, it can be used to refine preliminary results attained from coarse sensing performed by the introduced multiband spectrum sensing approach.

Appendix A

Spectral Analysis of Total Random Sampling

Here we derive the estimator's expected value $E\left[X_{e,TRS}(\mathcal{t}_r,f)\right]$ and its variance $\mathrm{var}\left\{X_{e,TRS}(\mathcal{t}_r,f)\right\}$ noting that the TRS sampling instants $\{t_n\}_{n=1}^{N}$ are IID random variables. Their PDF is defined by: $p_n(t)=1/T_0$ for $t\in\mathcal{T}_r$ and zero elsewhere.

A.1 Estimator's Expected Value for TRS

We start with,

$$C_{TRS}(f)=E\left[X_{e,TRS}(\mathcal{t}_r,f)\right]=\frac{T_0^2}{N(N-1)\mu}E\left[\left|\sum_{n=1}^{N}y(t_n)w(t_n)e^{-j2\pi ft_n}\right|^2\right]. \tag{A.1}$$

The estimator can be expressed by:

$$X_{e,TRS}(\mathcal{t}_r,f)=\frac{T_0^2}{N(N-1)\mu}\left\{\sum_{n=1}^{N}y^2(t_n)w^2(t_n)+\sum_{n=1}^{N}\sum_{\substack{m=1\\m\neq n}}^{N}y(t_n)w(t_n)y(t_m)w(t_m)e^{-j2\pi f(t_n-t_m)}\right\}. \tag{A.2}$$

Given that the components in the double summation in (A.2) are IID random variables:

$$\begin{aligned}E\left[X_{e,TRS}(\mathcal{t}_r,f)\middle|x(t)\right]=\frac{T_0^2}{N(N-1)\mu}\Big\{&NE\left[y^2(t_n)w^2(t_n)\middle|x(t)\right]\\&+N(N-1)E\left[y(t_n)w(t_n)e^{-j2\pi ft_n}\middle|x(t)\right]E\left[y(t_n)w(t_n)e^{j2\pi ft_n}\middle|x(t)\right]\Big\}.\end{aligned} \tag{A.3}$$

Since the signal and the zero mean AWGN of variance P_N are independent where $y(t_n)=x(t_n)+n(t_n)$, we obtain:

$$E\left[X_{e,TRS}(\not{t}_r,f)\middle|x(t)\right]=\frac{T_0^2}{N(N-1)\mu}\left\{E\left[x^2(t_n)w^2(t_n)\middle|x(t)\right]+\frac{\mu P_N}{\alpha}\right\}+\frac{N(N-1)}{T_0^2}\left\{E\left[x(t_n)w(t_n)e^{-j2\pi ft_n}\middle|x(t)\right]E\left[x(t_n)w(t_n)e^{j2\pi ft_n}\middle|x(t)\right]\right\}. \quad (A.4)$$

Noting that $E\left[x(t_n)w(t_n)\right]=\int_{-\infty}^{+\infty}x(t)w(t)\not{p}_n(t)dt$, (A.4) reduces to:

$$E\left[X_{e,TRS}(\not{t}_r,f)\middle|x(t)\right]=\frac{N}{(N-1)\mu\alpha}\left[\int_{\mathcal{T}_r}x^2(t)w^2(t)dt+\mu P_N\right]+\frac{1}{\mu}\left|X_W(\not{t}_r,f)\right|^2 \quad (A.5)$$

where $X_W(f)=\int_{\mathcal{T}_r}x(t)w(t)dt$. The processed WSS signal has a second moment, i.e. power, $P_S=E\left[x^2(t)\right]$ whilst the expected value of a windowed continuous-time periodogram is :

$$\frac{1}{\mu}E\left[\left|\int_{\mathcal{T}_r}x(t)w(t)e^{-j2\pi ft}dt\right|^2\right]=\frac{1}{\mu}\Phi_X(f)*\left|W(f)\right|^2 \quad (A.6)$$

where $\Phi_X(f)$ is the PSD of $x(t)$ and $W(f)=\int_{\mathcal{T}_r}w(t)e^{-j2\pi ft}dt$. Subsequently, (A.5) emerges as: $C_{TRS}(f)=N\left[P_S+P_N\right]/\left[(N-1)\alpha\right]+\Phi_X(f)*\left|W(f)\right|^2/\mu$ proving (3.11).

A.2 Estimator's Variance for TRS

The variance of $X_{e,TRS}(\not{t}_r,f)$ is given by:

$$\sigma^2_{e,TRS}(f)=\left[\frac{N}{(N-1)\mu}\right]^2\text{var}\left\{\left|X_{WS}(f)\right|^2\right\} \quad (A.7)$$

where $\left|X_{WS}(f)\right|^2=\left|T_0\sum_{n=1}^{N}y(t_n)w(t_n)e^{-j2\pi ft_n}/N\right|^2=\tilde{R}^2_{WS}(f)+\tilde{I}^2_{WS}(f)$,

$$\tilde{R}_{WS}(f)=T_0\sum_{n=1}^{N}y(t_n)w(t_n)\cos(2\pi ft_n)/N \quad (A.8)$$

and

$$\tilde{I}_{WS}(f)=T_0\sum_{n=1}^{N}y(t_n)w(t_n)\sin(2\pi ft_n)/N\,. \quad (A.9)$$

The parameter $\not{t}_r$ is discarded to simplify the notations. Each of $\tilde{R}_{WS}(f)$ and $\tilde{I}_{WS}(f)$ are the sum of N independent identically distributed random variables. They are assumed to be of a normal distribution according to the central limit theorem, e.g. $N\geq 30$ is

satisfactory in [15, 52, 114]. As a result, $\left|X_{WS}(\not{t}_r,f)\right|^2$ have approximately a chi-squared distribution with two degrees of freedom if $\zeta_{TRS}(f)=E\left[\tilde{R}_{WS}(f)\tilde{I}_{WS}(f)\right]=0$ where

$$\begin{aligned}\tilde{R}_{WS}(f)\tilde{I}_{WS}(f)=&\frac{T_0^{\,2}}{N^2}\sum_{n=1}^{N}y^2(t_n)w^2(t_n)\cos(2\pi ft_n)\sin(2\pi ft_n)\\&+\frac{T_0^{\,2}}{N^2}\sum_{n=1}^{N}\sum_{\substack{m=1\\m\neq n}}^{N}y(t_n)w(t_n)y(t_m)w(t_m)\cos(2\pi ft_n)\sin(2\pi ft_m)\end{aligned}. \tag{A.10}$$

Similar to (A.2)-(A.4), we obtained:

$$E\left[\tilde{R}_{WS}(f)\tilde{I}_{WS}(f)\middle|x(t)\right]=\frac{\int_{\mathcal{T}_r}\left[x^2(t)+P_N\right]w^2(t)\cos(2\pi ft)\sin(2\pi ft)dt}{\alpha}+\frac{(N-1)\tilde{R}_W(f)\tilde{I}_W(f)}{N} \tag{A.11}$$

where $\tilde{R}_W(f)=\int_{\mathcal{T}_r}x(t)w(t)\cos(2\pi ft)dt$ and $\tilde{I}_W(f)=\int_{\mathcal{T}_r}x(t)w(t)\sin(2\pi ft)dt$. This leads to (3.25): $\zeta_{TRS}(f)=\left(P_S+P_N\right)\int_{\mathcal{T}_r}w^2(t)\cos(2\pi ft)\sin(2\pi ft)dt\Big/\alpha+(N-1)\lambda_{RI}(f)/N$, i.e. $\tilde{R}_{WS}(f)$ and $\tilde{I}_{WS}(f)$ are not independent $\forall f$. These two random variables are approximately of normal distribution and hence being uncorrelated is a sufficient condition for being independent [103]. They can be replaced with uncorrelated ones without altering $X_{e,TRS}(\not{t}_r,f)$ since $\left|X_{WS}(f)e^{j\theta_{TRS}(f)}\right|^2=\left|X_{WS}(f)\right|^2$. Thus $\left|X_{WS}(f)\right|^2=\tilde{R}_{WS}^2(f)+\tilde{I}_{WS}^2(f)$ where $R_{WS}(f)=T_0\sum_{n=1}^{N}y(t_n)w(t_n)\cos\left(2\pi ft_n-\theta_{TRS}(f)\right)/N$ and $I_{WS}(f)=T_0\sum_{n=1}^{N}y(t_n)w(t_n)\sin\left(2\pi ft_n-\theta_{TRS}(f)\right)/N$. The purpose of the phase-shift $\theta_{TRS}(f)$ is to affirm that $E\left[R_{WS}(f)I_{WS}(f)\right]=0$ for every f. We can write:

$$R_{WS}(f)=\cos\left(\theta_{TRS}(f)\right)\tilde{R}_{WS}(f)+\sin\left(\theta_{TRS}(f)\right)\tilde{I}_{WS}(f) \tag{A.12}$$

$$I_{WS}(f)=-\sin\left(\theta_{TRS}(f)\right)\tilde{R}_{WS}(f)+\cos\left(\theta_{TRS}(f)\right)\tilde{I}_{WS}(f) \tag{A.13}$$

which produces:

$$0.5\sin\left(2\theta_{TRS}(f)\right)\left\{E\left[\tilde{I}_{WS}^2(f)\right]-E\left[\tilde{R}_{WS}^2(f)\right]\right\}+\cos\left(2\theta_{TRS}(f)\right)\zeta_{TRS}(f)=0. \tag{A.14}$$

By rearranging (B.14), we attain $\theta_{TRS}(f) = 0.5\text{arccot}\left(\left\{E\left[\tilde{R}_{WS}^2(f)\right] - E\left[\tilde{I}_{WS}^2(f)\right]\right\} \Big/ 2\zeta_{TRS}(f)\right)$ defined in (3.24). Similar to (A.2)-(A.5), (A.10) and (A.11) each of $E\left[\tilde{R}_{WS}^2(f)\right]$ and $E\left[\tilde{I}_{WS}^2(f)\right]$ can be determined. For example:

$$\begin{aligned} E\left[\tilde{R}_{WS}^2(f)\right] = \frac{T_0^{\,2}}{N} E\left[y^2(t_n) w^2(t_n) \cos^2(2\pi f t_n)\right] \\ + \frac{T_0^{\,2}(N-1)}{N} E\left[y(t_n) w(t_n) \cos(2\pi f t_n)\right] E\left[y(t_n) w(t_n) \cos(2\pi f t_n)\right] \end{aligned} \tag{A.15}$$

which leads to:

$$E\left[\tilde{R}_{WS}^2(f) \middle| x(t)\right] = \frac{T_0}{N} \int_{\mathcal{T}_r} \left[x^2(t) + P_N\right] \cos^2(2\pi f t) dt + \frac{(N-1)}{N} \left[\int_{\mathcal{T}_r} x(t) w(t) \cos(2\pi f t) dt\right]^2 \tag{A.16}$$

and then:

$$E\left[\tilde{R}_{WS}^2(f)\right] = \frac{\left(P_S + P_N\right) \tilde{E}_{WC}(f)}{\alpha} + \frac{\left(N-1\right)}{N} \tilde{\lambda}_R(f). \tag{A.17}$$

Analogously,

$$E\left[\tilde{I}_{WS}^2(f)\right] = \frac{\left(P_S + P_N\right) \tilde{E}_{WS}(f)}{\alpha} + \frac{\left(N-1\right)}{N} \tilde{\lambda}_S(f) \tag{A.18}$$

where $\tilde{\lambda}_R(f) = \int_{\mathcal{T}_r} \int_{\mathcal{T}_r} R_X(t_1 - t_2) w(t_1) w(t_2) \cos(2\pi f t_1) \cos(2\pi f t_2) dt_1 dt_2$, $R_X(t_1 - t_2) = E\left[x(t_1) x(t_2)\right]$

$\tilde{\lambda}_I(f) = \int_{\mathcal{T}_r} \int_{\mathcal{T}_r} R_X(t_1 - t_2) w(t_1) w(t_2) \sin(2\pi f t_1) \sin(2\pi f t_2) dt_1 dt_2$, $\tilde{E}_{WC}(f) = \int_{\mathcal{T}_r} w^2(t) \cos^2(2\pi f t) dt$ and $\tilde{E}_{WS}(f) = \int_{\mathcal{T}_r} w^2(t) \sin^2(2\pi f t) dt$. Having satisfied the necessary conditions for ensuring that $X_{e,TRS}(\mathcal{T}_r, f)$ is approximately of an unnormalised chi-squared distribution, we reach (3.17): $\sigma_{e,TRS}^2(f) = 2N^2 \left[\sigma_{R_{WS}}^4(f) + \sigma_{I_{WS}}^4(f)\right] \Big/ \left[(N-1)\mu\right]^2$.

Noting that $R_{WS}(f)$ and $I_{WS}(f)$ are zero mean, the formulas for $\sigma_{R_{WS}}^2(f) = E\left[R_{WS}^2(f)\right]$ and $\sigma_{I_{WS}}^2(f) = E\left[I_{WS}^2(f)\right]$ are identical to (A.17) and (A.18) respectively such that the phase-shift $\theta_{TRS}(f)$ is introduced to $\tilde{E}_{WC}(f)$, $\tilde{\lambda}_R(f)$, $\tilde{E}_{WS}(f)$ and $\tilde{\lambda}_I(f)$ as depicted in (3.19), (3.20), (3.22) and (3.23).

Appendix B

Spectral Analysis of Random Sampling on Grid

The mean and variance of the random sampling on grid spectrum estimator $X_{e,RSG}(\mathcal{t}_r, f)$ are calculated in this appendix. Recall that each of the underlying grid point can be selected only once with an equal probability for the studied RSG without replacement. We introduce a random variable c_n which is equal to "1" if the n-th grid point is considered in $X_{e,RSG}(\mathcal{t}_r, f)$ and "0" otherwise. It can been seen that: $\Pr\{c_n = 1\} = N/N_g$ whilst $\Pr\{c_n = 0\} = (N_g - N)/N_g$. Consequently, we have:

$$E[c_n] = N/N_g \tag{B.1}$$

whereas

$$E[c_n c_m] = \begin{cases} N/N_g & \text{for} \quad n = m \\ \dfrac{N}{N_g}\left(\dfrac{N-1}{N_g-1}\right) & \text{for} \quad n \neq m \end{cases} \tag{B.2}$$

and $\text{var}\{c_n\} = N\left[1 - N/N_g\right]/N_g$. The starting initial time instant $\mathcal{t}_r$ of the analysis window $\mathcal{T}_r = [\mathcal{t}_r, \mathcal{t}_r + T_0]$ is discarded from the equations below to simplify the notation whenever needed.

B.1 Estimator's Expected Value for RSG

By splitting the summation in $X_{e,RSG}(\mathcal{t}_r, f)$, we have:

$$X_{e,RSG}(\not{t}_r,f)=\frac{(N_g-1)T_0}{N(N-1)\mu_d}\left\{\sum_{n=1}^{N_g}c_n^2y^2(nT_g)w^2(nT_g)+\sum_{n=1}^{N_g}\sum_{\substack{m=1\\m\neq n}}^{N_g}c_nc_my(nT_g)w(nT_g)y(mT_g)w(mT_g)e^{-j2\pi fT_g(n-m)}\right\} \tag{B.3}$$

where the sample instants in (B.3) encompass all the underlying grid points and are no longer random. However, the randomness of the sampling scheme is depicted by the set of random variables $\{c_n\}_{n=1}^{N_g}$. Using (B.1) and (B.2), the estimator's conditional expectation is given by:

$$E\left[X_{e,RSG}(\not{t}_r,f)\middle|x(t)\right]=\frac{(N_g-1)T_0}{N(N-1)\mu_d}\left\{\frac{N}{N_g}\sum_{n=1}^{N_g}\left[x^2(nT_g)+P_N\right]w^2(nT_g)+\frac{N}{N_g}\left(\frac{N-1}{N_g-1}\right)\sum_{n=1}^{N_g}\sum_{\substack{m=1\\m\neq n}}^{N_g}x(nT_g)w(nT_g)x(mT_g)w(mT_g)e^{-j2\pi fT_g(n-m)}\right\} \tag{B.4}$$

as the zero mean AWGN and the signal are independent. Manipulating (B.4) to form the signal's discrete-time Fourier transform $X_W^d(\not{t}_r,f)=\sum_{n=1}^{N_g}x(nT_g)w(nT_g)e^{-j2\pi fnT_g}$, we reach:

$$E\left[X_{e,RSG}(\not{t}_r,f)\middle|x(t)\right]=\frac{(N_g-N)T_0}{(N-1)N_g\mu_d}\sum_{n=1}^{N_g}x^2(nT_g)w^2(nT_g)+\frac{(N_g-1)T_0P_N}{(N-1)N_g}+\frac{T_0\left|X_W^d(\not{t}_r,f)\right|^2}{N_g\mu_d} \tag{B.5}$$

and the $C_{RSG}(f)=E\left[X_{e,RSG}(\not{t}_r,f)\right]$ in (3.31) is subsequently attained.

B.2 Estimator's Variance for RSG

The estimator under scrutiny can be expressed by:

$$X_{e,RSG}(\not{t}_r,f)=\frac{(N_g-1)T_0}{N(N-1)\mu_d}\left[R_{RG}^2(f)+I_{RG}^2(f)\right] \tag{B.6}$$

where $R_{RG}(f)=\sum_{n=1}^{N}y(t_n)w(t_n)\cos\left(2\pi ft_n-\theta_{RSG}(f)\right)$,

$I_{RG}(f)=\sum_{n=1}^{N}y(t_n)w(t_n)\sin\left(2\pi ft_n-\theta_{RSG}(f)\right)$ and $\theta_{RSG}(f)$ is selected such that the latter two are uncorrelated, i.e. $E\left[R_{RG}(f)I_{RG}(f)\right]=0$ (they are zero mean). Similar to the TRS, the $X_{e,RSG}(\not{t}_r,f)$ variance is obtained by utilising chi-squared distribution characteristics making use of the central limit theorem. For $N_g>>N$, $R_{RG}(f)$ and $I_{RG}(f)$ are assumed to

be normally distributed according to the CLT for sufficiently large N, typically moderate values of N suffice in practice. Thus we attain the variance formula in (3.34) where $\sigma^2_{e,RSG}(f) = 2\left[(N_g-1)T_0\right]^2\left[\sigma^4_{R_{RG}}(f)+\sigma^4_{I_{RG}}(f)\right]\Big/\left[(N-1)N\mu_d\right]^2$. Here we show how to determine each of $\sigma^2_{R_{RG}}(f) = E\left[R^2_{RG}(f)\right]$, $\sigma^2_{I_{RG}}(f) = E\left[I^2_{RG}(f)\right]$ and the introduced phase-shift $\theta_{RSG}(f)$.

By splitting the summation analogous to (B.3) and (B.4), we can write:

$$\begin{aligned} E\left[R^2_{RG}(f)\middle|x(t)\right] &= E\left[c_k^2\right]\sum_{n=1}^{N_g}\left[x^2(nT_g)+P_N\right]w^2(nT_g)\cos^2\left(2\pi fnT_g-\theta_{RSG}(f)\right) \\ &\quad + E\left[c_kc_l\right]\left\{\left[\sum_{n=1}^{N_g}x(nT_g)w(nT_g)\cos\left(2\pi fnT_g-\theta_{RSG}(f)\right)\right]^2\right. \\ &\quad \left. -\sum_{n=1}^{N_g}x^2(nT_g)w^2(nT_g)\cos^2\left(2\pi fnT_g-\theta_{RSG}(f)\right)\right\} \end{aligned} \tag{B.7}$$

such that $k \neq l$. Using (B.1) and (B.2), we reach:

$$\begin{aligned} E\left[R^2_{RG}(f)\middle|x(t)\right] &= \left[\frac{N}{N_g}-\frac{N}{N_g}\left(\frac{N-1}{N_g-1}\right)\right]\sum_{n=1}^{N_g}x^2(nT_g)w^2(nT_g)\cos^2\left(2\pi fnT_g-\theta_{RSG}(f)\right) \\ &\quad + \frac{NP_N}{N_g}\sum_{n=1}^{N_g}w^2(nT_g)\cos^2\left(2\pi fnT_g-\theta_{RSG}(f)\right) \\ &\quad + \frac{N}{N_g}\left(\frac{N-1}{N_g-1}\right)\left[\sum_{n=1}^{N_g}x(nT_g)w(nT_g)\cos\left(2\pi fnT_g-\theta_{RSG}(f)\right)\right]^2. \end{aligned} \tag{B.8}$$

Since $R_X\left((m-n)T_g\right) = E\left[x(nT_g)x(mT_g)\right]$ is the discrete-time autocorrelation function of the WSS processed signal, (B.8) emerges as:

$$\begin{aligned} E\left[R^2_{RG}(f)\right] &= \frac{N}{N_g}\left[\frac{(N_g-N)}{(N_g-1)}P_S+P_N\right]\sum_{n=1}^{N_g}w^2(nT_g)\cos^2\left(2\pi fnT_g-\theta_{RSG}(f)\right) \\ &\quad + \frac{N}{N_g}\left(\frac{N-1}{N_g-1}\right)E\left[\sum_{n=1}^{N_g}x(nT_g)w(nT_g)\cos\left(2\pi fnT_g-\theta_{RSG}(f)\right)\right]^2 \end{aligned} \tag{B.9}$$

proving (3.35), (3.37) and (3.38). Likewise, the $\sigma^2_{I_{RG}}(f) = E\left[I^2_{RG}(f)\right]$ formula in (3.36) and its components can be found. Noting that:

$$\tilde{R}_{RG}(f) = R_{RG}(f)\cos\left(\theta_{RSG}(f)\right) + I_{RG}(f)\sin\left(\theta_{RSG}(f)\right) \tag{B.10}$$

as $\tilde{R}_{RG}(f)=\sum_{n=1}^{N}y(t_n)w(t_n)\cos(2\pi ft_n)$ and $\tilde{I}_{RG}(f)=\sum_{n=1}^{N}y(t_n)w(t_n)\sin(2\pi ft_n)$ whilst

$$\tilde{I}_{RG}(f)=I_{RG}(f)\cos(\theta_{RSG}(f))-R_{RG}(f)\sin(\theta_{RSG}(f)). \tag{B.11}$$

It can be easily seen that by stipulating $E[R_{RG}(f)I_{RG}(f)]=0$ we obtain $\theta_{RSG}(f)$ in (3.41). It is a function of $E[\tilde{R}_{RG}^2(f)]$, $E[\tilde{I}_{RG}^2(f)]$ and $\zeta_{RSG}(f)$. The former two are identical to $E[R_{RG}^2(f)]$ and $E[I_{RG}^2(f)]$ respectively following the elimination of $\theta_{RSG}(f)$. Whilst $\zeta_{RSG}(f)=E[\tilde{R}_{RG}(f)\tilde{I}_{RG}(f)]$ can be derived as follows:

$$\begin{aligned}E\left[\tilde{R}_{RG}(f)\tilde{I}_{RG}(f)\middle|x(t)\right]&=\sum_{n=1}^{N_g}E[c_n^2]\left[x^2(nT_g)+P_N\right]w^2(nT_g)\cos(2\pi fnT_g)\sin(2\pi fnT_g)\\&+\sum_{n=1}^{N_g}\sum_{\substack{m=1\\m\neq n}}^{N_g}E[c_nc_m]x(nT_g)w(nT_g)x(mT_g)w(mT_g)\cos(2\pi fnT_g)\sin(2\pi fmT_g)\end{aligned} \tag{B.12}$$

which reduces to:

$$\begin{aligned}&E\left[\tilde{R}_{RG}(f)\tilde{I}_{RG}(f)\middle|x(t)\right]\\&=\frac{N}{N_g}\left(\frac{N_g-N}{N_g-1}\right)\sum_{n=1}^{N_g}\left[x^2(nT_g)+\frac{N_g-1}{N_g-N}P_N\right]w^2(nT_g)\cos(2\pi fnT_g)\sin(2\pi fnT_g)\\&+\frac{N}{N_g}\left(\frac{N-1}{N_g-1}\right)\sum_{n=1}^{N_g}\sum_{m=1}^{N_g}x(nT_g)w(nT_g)x(mT_g)w(mT_g)\cos(2\pi fnT_g)\sin(2\pi fmT_g).\end{aligned} \tag{B.13}$$

in a similar manner to (B.7) and (B.8). By taking the expectation of (B.13) with respect to the processed signal, we reach (3.42).

Appendix C

Spectral Analysis of Stratified Sampling

We derive the formulas for the mean and the variance of the periodogram-type estimator that deploys stratified sampling with equal partitions. The sample points $\{t_n\}_{n=1}^{N}$ of the SSEP are independent random variables whose PDFs are defined by: $p_n(t) = 1/|\mathcal{S}_n|$ if $t \in \mathcal{S}_n$ and zero elsewhere where $|\mathcal{S}_n|$ is the width of the subinterval $\mathcal{S}_n$.

C.1 Estimator's Expected Value for SSEP

We can write:

$$E\left[X_{e,SSEP}(\mathcal{F}_r, f) \middle| x(t) \right] = \frac{1}{\mu\alpha^2} \left\{ \sum_{n=1}^{N} E\left[\left\{ x^2(t_n) + n^2(t_n) \right\} w^2(t_n) \middle| x(t) \right] + \sum_{n=1}^{N} \sum_{\substack{m=1 \\ m \neq n}}^{N} E\left[x(t_n) x(t_m) w(t_n) w(t_m) e^{-j2\pi f t_n} e^{j2\pi f t_m} \middle| x(t) \right] \right\} \tag{C.1}$$

which leads to

$$E\left[X_{e,SSEP}(\mathcal{F}_r, f) \middle| x(t) \right] = \frac{1}{\mu\alpha} \left\{ \sum_{n=1}^{N} \int_{\mathcal{S}_n} \left[x^2(t) + P_N \right] w^2(t) dt - \alpha \sum_{n=1}^{N} \left| \int_{\mathcal{S}_n} x(t) w(t) e^{-j2\pi f t} dt \right|^2 + \alpha \sum_{n=1}^{N} \int_{\mathcal{S}_n} x(t_1) w(t_1) e^{-j2\pi f t_1} dt_1 \sum_{m=1}^{N} \int_{\mathcal{S}_m} x(t_2) w(t_2) e^{j2\pi f t_2} dt_2 \right\} \tag{C.2}$$

noting that $|\mathcal{S}_n| = 1/\alpha$ for stratified sampling with equal partitions. It follows that:

$$E\left[X_{e,SSEP}(\mathcal{F}_r, f) \middle| x(t) \right] = \frac{\int_{\mathcal{F}_r} x^2(t) w^2(t) dt + \mu P_N}{\mu\alpha} + \frac{\left| X_W(f) \right|^2}{\mu} - \frac{1}{\mu} \sum_{n=1}^{N} \left| \int_{\mathcal{S}_n} x(t) w(t) e^{-j2\pi f t} dt \right|^2 . \tag{C.3}$$

It can be noticed that the second term in (C.3) and the summands in the third one represent a windowed classical continuous-time periodograms [103]. Subsequently, the estimator expected value reduces to: $C_{SSEP}(f)=\left(P_S+P_N\right)/\alpha+\Phi_X(f)*\left|W(f)\right|^2/\mu-\chi(f)/\mu$ in (3.45) where $\chi(f)=\sum_{n=1}^{N}\Phi_X(f)*\left|V_n(f)\right|^2$, $V_n(f)=\int_{\mathbb{S}_n}w(t)e^{-j2\pi ft}dt$ and $\Phi_X(f)$ is the power spectral density of the incoming analogue signal.

C.2 Estimator's Variance for SSEP

According to (3.49)-(3.51):

$$\sigma^2_{e,SSEP}(f)=\frac{1}{\mu^2}\operatorname{var}\left\{R^2_{SS}(f)+I^2_{SS}(f)\right\} \tag{C.4}$$

recalling that $R_{SS}(f)=\sum_{n=1}^{N}y(t_n)w(t_n)\cos\left(2\pi ft_n-\theta_{SS}(f)\right)/\alpha$ and $I_{SS}(f)=\sum_{n=1}^{N}y(t_n)w(t_n)\sin\left(2\pi ft_n-\theta_{SS}(f)\right)/\alpha$ are asymptotically normally distributed. The phase shift $\theta_{SS}(f)$ defined in (3.56) is selected such that $E\left[R_{SS}(f)I_{SS}(f)\right]=0$ in order to ensure that $X_{e,SSEP}(\not{t}_r,f)$ is approximately of a chi-squared distribution $\forall f$. Consequently, the variance of $X_{e,SSEP}(\not{t}_r,f)$ is given in (3.53)-(3.55). For example, consider $\sigma^2_{I_{SS}}(f)=E\left[I^2_{SS}(f)\right]$ in (3.55). Similar to (C.1) and (C.2), we have:

$$\begin{aligned}E\left[I^2_{SS}(f)\middle|x(t)\right]=\frac{1}{\alpha^2}\Bigg\{&\sum_{n=1}^{N}E\left[\left\{x^2(t_n)+n^2(t_n)\right\}w^2(t_n)\sin^2\left(2\pi ft_n-\theta_{SS}(f)\right)\middle|x(t)\right]\\&+\sum_{n=1}^{N}\sum_{\substack{m=1\\m\neq n}}^{N}E\left[x(t_n)w(t_n)\sin\left(2\pi ft_n-\theta_{SS}(f)\right)\middle|x(t)\right]E\left[x(t_m)w(t_m)\sin\left(2\pi ft_m-\theta_{SS}(f)\right)\middle|x(t)\right]\Bigg\}\end{aligned} \tag{C.5}$$

which results in:

$$\begin{aligned}E\left[I^2_{SS}(f)\middle|x(t)\right]=\frac{1}{\alpha^2}\Bigg\{&\sum_{n=1}^{N}\left|\mathbb{S}_n\right|\int_{\mathbb{S}_n}\left[x^2(t)+P_N\right]w^2(t)\sin^2\left(2\pi ft-\theta_{SS}(f)\right)dt\\&+\sum_{n=1}^{N}\sum_{\substack{m=1\\m\neq n}}^{N}\left|\mathbb{S}_n\right|^2\int_{\mathbb{S}_n}x(t_1)w(t_1)\sin\left(2\pi ft_1-\theta_{SS}(f)\right)dt_1\int_{\mathbb{S}_m}x(t_2)w(t_2)\sin\left(2\pi ft_2-\theta_{SS}(f)\right)dt_2\Bigg\}.\end{aligned} \tag{C.6}$$

Then,

$$E\left[I_{SS}^2(f)\middle|x(t)\right]=\frac{1}{\alpha}\int_{\mathcal{T}_r}\left[x^2(t)+P_N\right]w^2(t)\sin^2\left(2\pi ft-\theta_{SS}(f)\right)dt$$
$$+\left|\int_{\mathcal{T}_r}x(t)w(t)\sin\left(2\pi ft-\theta_{SS}(f)\right)dt\right|^2-\sum_{n=1}^{N}\left|\int_{\mathcal{S}_n}x(t)w(t)\sin\left(2\pi ft-\theta_{SS}(f)\right)dt\right|^2 \quad \text{(C.7)}$$

that yields:

$$E\left[I_{SS}^2(f)\right]=\left[P_S+P_N\right]\int_{\mathcal{T}_r}w^2(t)\sin^2\left(2\pi ft-\theta_{SS}(f)\right)dt\Big/\alpha+\lambda_I(f)-\chi_I(f) \quad \text{(C.8)}$$

where $\lambda_I(f)=\int_{\mathcal{T}_r}\int_{\mathcal{T}_r}R_X(t_1-t_2)w(t_1)w(t_2)\sin\left(2\pi ft_1-\theta_{SS}(f)\right)\sin\left(2\pi ft_2-\theta_{SS}(f)\right)dt_1dt_2$,

$\chi_I(f)=\sum_{n=1}^{N}\int_{\mathcal{S}_n}\int_{\mathcal{S}_n}R_X(t_1-t_2)w(t_1)w(t_2)\sin\left(2\pi ft_1-\theta_{SS}(f)\right)\sin\left(2\pi ft_2-\theta_{SS}(f)\right)dt_1dt_2$ and $R_X(\tau)$ is the autocorrelation function of the WSS processed signal. Similarly, each of $\sigma_{R_{SS}}^2(f)=E\left[R_{SS}^2(f)\right]$, $E\left[\tilde{R}_{SS}^2(f)\right]$, $E\left[\tilde{I}_{SS}^2(f)\right]$ and $\zeta_{SS}(f)=E\left[\tilde{R}_{SS}(f)\tilde{I}_{SS}(f)\right]$ can be calculated.

Appendix D

Cyclostationary Signals and Periodogram-type Estimators

In this appendix, we give the detailed derivations of $E\left[\left|X_W(t_r,f)\right|^2\right]$ for the signals in §4.3. The variance expressions for each of the TRS, RSG and SSEP estimators are restated and simplified approximations are developed. Additionally, the calculations for the parameters that affect the spectrum estimation quality for the class of examined cyclostationary signals are presented.

For the simplicity of the notation, the analysis in Sections D.1 and D.3 is conducted for a single active subband. The subscripts, which index the active channels, are accordingly discarded. Some useful identities that are frequently used in the following sections are listed at the end of the appendix.

We recall that the incoming signal is modelled by:

$$x(t)=\sum_{n=-\infty}^{+\infty}a_n s_i(t,n)+\sum_{n=-\infty}^{+\infty}b_n s_q(t,n) \tag{D.1}$$

, $s_i(t,n)=\left[p_i(t+nT_S)\cos(2\pi f_C t)\right]*h(t)$ and $s_q(t,n)=\left[p_q(t+nT_S)\cos(2\pi f_C t+0.5\pi)\right]*h(t)$. Whereas, f_C is the carrier frequency, $f_S=1/T_S$ is the baud rate and $h(t)$ denotes the impulse response of the propagation channel over the assessed spectral subband. The coefficients $\{a_n\}_{n\in\mathbb{Z}}$ and $\{b_n\}_{n\in\mathbb{Z}}$ represent the transmitted symbols. They are zero mean IID random variables with variances of σ_a^2 and σ_b^2 respectively. The autocorrelation function of $x(t)$ is given by:

$$R_X(t,t+\tau)=\sigma_a^2\sum_{n=-\infty}^{+\infty}s_i(t,n)s_i(t+\tau,n)+\sigma_b^2\sum_{n=-\infty}^{+\infty}s_q(t,n)s_q(t+\tau,n) \tag{D.2}$$

D.1 Estimators' Expected Values

We note that:

$$E\left[\left|X_W(\not{t}_r,f)\right|^2\right]=\int_{-\infty}^{+\infty}\int_{-\infty}^{+\infty}R_X(t,t+\tau)w(t)w(t+\tau)e^{-j2\pi f\tau}d\tau dt \tag{D.3}$$

can be written as: $E\left[\left|X_W(\not{t}_r,f)\right|^2\right]=\int_{-\infty}^{+\infty}w(t)\int_{-\infty}^{+\infty}R_X(t,t+\tau)w(t+\tau)e^{-j2\pi f\tau}d\tau dt$. The inner integral in the latter equation is the Fourier transform of the autocorrelation function with respect to τ. Then,

$$E\left[\left|X_W(\not{t}_r,f)\right|^2\right]=\int_{-\infty}^{+\infty}w(t)\left[\mathcal{F}\left\{R_X(t,t+\tau),\tau\right\}\right]*\left[W(f)e^{j2\pi ft}\right]dt \tag{D.4}$$

where $W(f)=\int_{\not{t}_r}^{\not{t}_r+T_0}w(t)e^{-j2\pi ft}dt$. Utilising (DD.1) and (DD.2):

$$\begin{aligned}\mathcal{F}\left\{R_X(t,t+\tau),\tau\right\}=&\,0.5\sigma_a^2H(f)e^{j2\pi ft}\sum_{n=-\infty}^{+\infty}s_i(t,n)\left[P_i(f-f_C)e^{j2\pi(f-f_C)nT_S}+P_i(f+f_C)e^{j2\pi(f+f_C)nT_S}\right]\\&-j0.5\sigma_b^2H(f)e^{j2\pi ft}\sum_{n=-\infty}^{+\infty}s_q(t,n)\left[P_q(f-f_C)e^{j2\pi(f-f_C)nT_S}-P_q(f+f_C)e^{j2\pi(f+f_C)nT_S}\right]\end{aligned} \tag{D.5}$$

where $H(f)=\int_{-\infty}^{+\infty}h(t)e^{-j2\pi ft}dt$, $P_i(f)=\int_{-\infty}^{+\infty}p_i(t)e^{-j2\pi ft}dt$ and $P_q(f)=\int_{-\infty}^{+\infty}p_q(t)e^{-j2\pi ft}dt$. The response of the propagation channel over the considered system subband is a bandpass signal occupying the range of frequency allocated to the subband in question. Assuming $f_C>>B_C$, we can write the following: $P_i(f-f_C-nf_S)H(f-2f_C-nf_S)=0$, $P_q(f+f_C-nf_S)H(f+2f_C-nf_S)=0$, $P_q(f-f_C+nf_S)H(f-2f_C-nf_S)=0$ and $P_q(f+f_C-nf_S)H(f+2f_C-nf_S)=0$ ($n\in\mathbb{Z}$). Thus by substituting (DD.5)-(DD.8) into (D.5), we obtain:

$$\mathcal{F}\left\{R_X(t,t+\tau),\tau\right\}=0.25{\sigma_a}^2f_S\xi_i(t,f)+0.25{\sigma_b}^2f_S\xi_q(t,f) \tag{D.6}$$

where

$$\begin{aligned}\xi_i(t,f)=&\,H(f)P_i(f-f_C)\sum_{n=-\infty}^{+\infty}H^*(f-nf_S)P_i^*(f-f_C-nf_S)e^{-j2\pi nf_St}\\&+H(f)P_i(f+f_C)\sum_{n=-\infty}^{+\infty}H^*(f-nf_S)P_i^*(f+f_C-nf_S)e^{-j2\pi nf_St}\end{aligned} \tag{D.7}$$

$$\begin{aligned}\xi_q(t,f) = H(f)P_q(f-f_C)\sum_{n=-\infty}^{+\infty} H^*(f-nf_S)P_q^*(f-f_C-nf_S)e^{-j2\pi nf_S t} \\ + H(f)P_q(f+f_C)\sum_{n=-\infty}^{+\infty} H^*(f-nf_S)P_q^*(f+f_C-nf_S)e^{-j2\pi nf_S t}.\end{aligned} \tag{D.8}$$

Subsequently, (D.4) can be expressed by:

$$\begin{aligned}E\left[\left|X_W(\mathcal{t}_r,f)\right|^2\right] = 0.25\sigma_a^2 f_S\int_{-\infty}^{+\infty} w(t)\xi_i(t,f) * \left[W(f)e^{j2\pi ft}\right]dt \\ + 0.25\sigma_b^2 f_S\int_{-\infty}^{+\infty} w(t)\xi_q(t,f) * \left[W(f)e^{j2\pi ft}\right]dt.\end{aligned} \tag{D.9}$$

Let:

$$F_i(\mathcal{t}_r,f) = \int_{-\infty}^{+\infty} w(t)\left[\xi_i(t,f)\right] * \left[W(f)e^{j2\pi ft}\right]dt \tag{D.10}$$

and

$$F_q(\mathcal{t}_r,f) = \int_{-\infty}^{+\infty} w(t)\left[\xi_q(t,f)\right] * \left[W(f)e^{j2\pi ft}\right]dt \tag{D.11}$$

, then

$$E\left[\left|X_W(\mathcal{t}_r,f)\right|^2\right] = 0.25\sigma_a^2 f_S F_i(\mathcal{t}_r,f) + 0.25\sigma_b^2 f_S F_q(\mathcal{t}_r,f). \tag{D.12}$$

Now we simplify the $F_i(\mathcal{t}_r,f)$ and $F_q(\mathcal{t}_r,f)$ terms in (D.12). First,

$$\begin{aligned}F_i(\mathcal{t}_r,f) = \left[H(f)P_i(f-f_C)\sum_{n=-\infty}^{+\infty} H^*(f-nf_S)P_i^*(f-f_C-nf_S)\right] * \left[W(f)\int_{-\infty}^{+\infty} w(t)e^{j2\pi(f-nf_S)t}dt\right] \\ + \left[H(f)P_i(f+f_C)\sum_{n=-\infty}^{+\infty} H^*(f-nf_S)P_i^*(f+f_C-nf_S)\right] * \left[W(f)\int_{-\infty}^{+\infty} w(t)e^{j2\pi(f-nf_S)t}dt\right]\end{aligned}$$

which yields:

$$\begin{aligned}F_i(\mathcal{t}_r,f) = \left[H(f)P_i(f-f_C)\sum_{n=-\infty}^{+\infty} H^*(f-nf_S)P_i^*(f-f_C-nf_S)\right] * \left[W(f)W^*(f-nf_S)\right] \\ + \left[H(f)P_i(f+f_C)\sum_{n=-\infty}^{+\infty} H^*(f-nf_S)P_i^*(f+f_C-nf_S)\right] * \left[W(f)W^*(f-nf_S)\right].\end{aligned} \tag{D.13}$$

Equivalently, we attain:

$$\begin{aligned}F_q(\mathcal{t}_r,f) = \left[H(f)P_q(f-f_C)\sum_{n=-\infty}^{+\infty} H^*(f-nf_S)P_q^*(f-f_C-nf_S)\right] * \left[W(f)W^*(f-nf_S)\right] \\ + \left[H(f)P_q(f+f_C)\sum_{n=-\infty}^{+\infty} H^*(f-nf_S)P_q^*(f+f_C-nf_S)\right] * \left[W(f)W^*(f-nf_S)\right].\end{aligned} \tag{D.14}$$

Since the symbol rate and the bandwidth of the shaping filters, i.e. B_W, are related by $0.5B_W < f_S \le B_W$, we have: $P_i(f)\sum_{n=-\infty}^{+\infty} P_i(f-nf_S)=0$ and $P_q(f)\sum_{n=-\infty}^{+\infty} P_q(f-nf_S)=0$ if $n \notin \{-1,0,1\}$. This results in:

$$E\left[\left|X_W(\mathcal{t}_r,f)\right|^2\right] = 0.25\sigma_a^2 f_S\left\{\left[\left|H(f)P_i(f-f_C)\right|^2+\left|H(f)P_i(f+f_C)\right|^2\right]*\left|W(f)\right|^2+\varepsilon_i(\mathcal{t}_r,f)\right\}$$
$$+0.25\sigma_b^2 f_S\left\{\left[\left|H(f)P_q(f-f_C)\right|^2+\left|H(f)P_q(f+f_C)\right|^2\right]*\left|W(f)\right|^2+\varepsilon_q(\mathcal{t}_r,f)\right\} \tag{D.15}$$

where

$$\varepsilon_i(\mathcal{t}_r,f)=\sum_{n=\pm 1}\left\{H(f)H^*(f-nf_S)\left[P_i(f-f_C)P_i^*(f-f_C-nf_S)\right.\right.$$
$$\left.\left.+P_i(f+f_C)P_i^*(f+f_C-nf_S)\right]\right\}*\left\{W(f)W^*(f-nf_S)\right\} \tag{D.16}$$

$$\varepsilon_q(\mathcal{t}_r,f)=\sum_{n=\pm 1}\left\{H(f)H^*(f-nf_S)\left[P_q(f-f_C)P_q^*(f-f_C-nf_S)\right.\right.$$
$$\left.\left.+P_q(f+f_C)P_q^*(f+f_C-nf_S)\right]\right\}*\left\{W(f)W^*(f-nf_S)\right\}. \tag{D.17}$$

For $f=f_k$ such that f_k is placed in the *guarded-region*, i.e. at/near the centre of the transmission band, $\varepsilon_i(\mathcal{t}_r,f)=\varepsilon_q(\mathcal{t}_r,f)=0$ and consequently:

$$E\left[\left|X_W(\mathcal{t}_r,f)\right|^2\right] = 0.25\sigma_a^2 f_S\left[\left|H(f)P_i(f-f_C)\right|^2+\left|H(f)P_i(f+f_C)\right|^2\right]*\left|W(f)\right|^2$$
$$+0.25\sigma_b^2 f_S\left[\left|H(f)P_q(f-f_C)\right|^2+\left|H(f)P_q(f+f_C)\right|^2\right]*\left|W(f)\right|^2. \tag{D.18}$$

If $\hat{P}_i(f)=H(f+f_C)P_i(f)$, $\breve{P}_i(f)=H(f-f_C)P_i(f)$, $\hat{P}_q(f)=H(f+f_C)P_q(f)$ and $\breve{P}_q(f)=H(f-f_C)P_q(f)$, each of (D.6), (D.13), (D.14) and (D.15) can be rewritten as:

$$\mathcal{F}\left\{R_X(t,t+\tau),\tau\right\} = 0.25{\sigma_a}^2 f_S e^{-j2\pi nf_S t}\sum_{n=-\infty}^{+\infty}\hat{P}_i(f-f_C)\hat{P}_i^*(f-f_C-nf_S)+\breve{P}_i(f+f_C)\breve{P}_i^*(f+f_C-nf_S)$$
$$+0.25{\sigma_b}^2 f_S e^{-j2\pi nf_S t}\sum_{n=-\infty}^{+\infty}\hat{P}_q(f-f_C)\hat{P}_q^*(f-f_C-nf_S)+\breve{P}_q(f+f_C)\breve{P}_q^*(f+f_C-nf_S) \tag{D.19}$$

$$F_i(\mathcal{t}_r,f)=\sum_{n=-\infty}^{+\infty}\left[\hat{P}_i(f-f_C)\hat{P}_i^*(f-f_C-nf_S)+\breve{P}_i(f+f_C)\breve{P}_i^*(f+f_C-nf_S)\right]*\left[W(f)W^*(f-nf_S)\right] \tag{D.20}$$

$$F_q(\mathscr{t}_r,f)=\sum_{n=-\infty}^{+\infty}\left[\widehat{P}_q(f-f_C)\widehat{P}_q^{*}(f-f_C-nf_S)+\breve{P}_q(f+f_C)\breve{P}_q^{*}(f+f_C-nf_S)\right]*\left[W(f)W^{*}(f-nf_S)\right] \tag{D.21}$$

and finally

$$\begin{aligned}E\left[\left|X_W(\mathscr{t}_r,f)\right|^2\right]=&\,0.25\sigma_a^2 f_S\left\{\left[\left|\widehat{P}_i(f-f_C)\right|^2+\left|\breve{P}_i(f+f_C)\right|^2\right]*\left|W(f)\right|^2+\varepsilon_i(\mathscr{t}_r,f)\right\}\\&+0.25\sigma_b^2 f_S\left\{\left[\left|\widehat{P}_q(f-f_C)\right|^2+\left|\breve{P}_q(f+f_C)\right|^2\right]*\left|W(f)\right|^2+\varepsilon_q(\mathscr{t}_r,f)\right\}.\end{aligned} \tag{D.22}$$

For the stratified sampling with equal partitions scheme, the estimator's expected value include the smeared-aliasing reduction factor: $\chi(\mathscr{t}_r,f)/\mu=\sum_{n=1}^{N}E\left[\left|X_{S_n}(\mathscr{t}_r,f)\right|^2\right]\Big/\mu$ such that $X_{S_n}(\mathscr{t}_r,f)=\int_{\mathbb{S}_n}x(t)w(t)e^{-j2\pi ft}dt$. This factor attenuates the smeared-aliasing level in the vicinity of the active spectral components, see §3.5. From the preceding derivations, it can be easily noticed that $E\left[\left|X_{S_n}(\mathscr{t}_r,f)\right|^2\right]$ is independent of $\mathscr{t}_r$ and represents a windowed form of the squared magnitude of the shaping filters near/at the centre of the active subband similar to (D.22). For instance, let $w_{S_n}(t)=w(t)w_n(t)$ such that $w_n(t)=1$ if $t\in\mathbb{S}_n$ and zero elsewhere. Then,

$$E\left[\left|X_{S_n}(\mathscr{t}_r,f)\right|^2\right]=\int_{-\infty}^{+\infty}\int_{-\infty}^{+\infty}R_X(t,t+\tau)w_{S_n}(t)w_{S_n}(t+\tau)e^{-j2\pi f\tau}d\tau dt \tag{D.23}$$

and steps identical to (D.4)-(D.21) can be followed where $W_{S_n}(f)=\int_{-\infty}^{+\infty}w_{S_n}(t)e^{-j2\pi ft}dt$ replaces $W(f)$.

D.2 Variances of TRS, RSG and SSEP

Analogous to (3.17)-(3.23), we have:

$$\sigma_{e,TRS}^2(\mathscr{t}_r,f)=\operatorname{var}\left\{X_{e,TRS}(\mathscr{t}_r,f)\right\}=2\left\{\frac{N}{(N-1)\mu}\right\}^2\left[\sigma_{R_{WS}}^4(\mathscr{t}_r,f)+\sigma_{I_{WS}}^4(\mathscr{t}_r,f)\right] \tag{D.24}$$

where

$$\sigma_{R_{WS}}^2(\mathscr{t}_r,f)=\frac{\tilde{E}_{WC}(\mathscr{t}_r,f)}{\alpha}+\frac{N-1}{N}\lambda_R(\mathscr{t}_r,f) \tag{D.25}$$

$$\sigma^2_{I_{WS}}(\mathscr{t}_r, f) = \frac{\tilde{E}_{WS}(\mathscr{t}_r, f)}{\alpha} + \frac{N-1}{N}\lambda_I(\mathscr{t}_r, f) \tag{D.26}$$

, $\lambda_R(\mathscr{t}_r, f) = \int_{\mathscr{T}_r}\int_{\mathscr{T}_r} R_X(t_1,t_2)w(t_1)w(t_2)\cos\left(2\pi f t_1 - \theta_{TRS}(\mathscr{t}_r, f)\right)\cos\left(2\pi f t_2 - \theta_{TRS}(\mathscr{t}_r, f)\right)dt_1 dt_2$,

$$\tilde{E}_{WC}(\mathscr{t}_r, f) = \int_{\mathscr{T}_r}\left\{E\left[x^2(t)\right] + P_N\right\}w^2(t)\cos^2\left(2\pi f t - \theta_{TRS}(\mathscr{t}_r, f)\right)dt \tag{D.27}$$

, $\lambda_I(\mathscr{t}_r, f) = \int_{\mathscr{T}_r}\int_{\mathscr{T}_r} R_X(t_1,t_2)w(t_1)w(t_2)\sin\left(2\pi f t_1 - \theta_{TRS}(\mathscr{t}_r, f)\right)\sin\left(2\pi f t_2 - \theta_{TRS}(\mathscr{t}_r, f)\right)dt_1 dt_2$,

and

$$\tilde{E}_{WS}(\mathscr{t}_r, f) = \int_{\mathscr{T}_r}\left\{E\left[x^2(t)\right] + P_N\right\}w^2(t)\sin^2\left(2\pi f t - \theta_{TRS}(\mathscr{t}_r, f)\right)dt\,. \tag{D.28}$$

The phase-shift $\theta_{TRS}(\mathscr{t}_r, f)$ is defined accordingly in (3.24) whilst $R_X(t_1,t_2)$ is the signal's autocorrelation function in (4.7).

Similarly, from (3.34)-(3.40) the variance of the RSG estimator is given by:

$$\sigma^2_{e,RSG}(\mathscr{t}_r, f) = 2\left\{\frac{(N_g-1)T_0}{N(N-1)\mu_d}\right\}^2\left[\sigma^4_{R_{RG}}(\mathscr{t}_r, f) + \sigma^4_{I_{RG}}(\mathscr{t}_r, f)\right] \tag{D.29}$$

where

$$\sigma^2_{R_{RG}}(\mathscr{t}_r, f) = \frac{N(N_g-N)}{N_g(N_g-1)}\tilde{E}^d_{WC}(\mathscr{t}_r, f) + \frac{N(N-1)}{N_g(N_g-1)}\lambda^d_R(\mathscr{t}_r, f) \tag{D.30}$$

$$\sigma^2_{I_{RG}}(\mathscr{t}_r, f) = \frac{N(N_g-N)}{N_g(N_g-1)}\tilde{E}^d_{WS}(\mathscr{t}_r, f) + \frac{N(N-1)}{N_g(N_g-1)}\lambda^d_I(\mathscr{t}_r, f) \tag{D.31}$$

$$\tilde{E}^d_{WC}(\mathscr{t}_r, f) = \sum_{n=1}^{N_g}\left\{E\left[x^2(t_n)\right] + \frac{(N_g-1)}{(N_g-N)}P_N\right\}w^2(t_n)\cos^2\left(2\pi f t_n - \theta_{RSG}(f)\right) \tag{D.32}$$

$$\tilde{E}^d_{WS}(\mathscr{t}_r, f) = \sum_{n=1}^{N_g}\left\{E\left[x^2(t_n)\right] + \frac{(N_g-1)}{(N_g-N)}P_N\right\}w^2(t_n)\sin^2\left(2\pi f t_n - \theta_{RSG}(\mathscr{t}_r, f)\right) \tag{D.33}$$

$\lambda^d_R(\mathscr{t}_r, f) = \sum_{n=1}^{N_g}\sum_{m=1}^{N_g} R_X(t_n,t_m)w(t_n)w(t_m)\cos\left(2\pi f t_n - \theta_{RSG}(\mathscr{t}_r, f)\right)\cos\left(2\pi f t_m - \theta_{RSG}(\mathscr{t}_r, f)\right)$ and

$\lambda^d_I(\mathscr{t}_r, f) = \sum_{n=1}^{N_g}\sum_{m=1}^{N_g} R_X(t_n,t_m)w(t_n)w(t_m)\sin\left(2\pi f t_n - \theta_{RSG}(\mathscr{t}_r, f)\right)\sin\left(2\pi f t_m - \theta_{RSG}(\mathscr{t}_r, f)\right)$.

The $R_X(nT_g, mT_g)$ is the discrete-time autocorrelation function and $\theta_{RSG}(\mathscr{t}_r, f)$ is duly defined in (3.41).

For the stratified sampling with equal partitions scheme, we have:

$$\sigma^2_{e,SSEP}(\mathcal{t}_r,f)=\frac{2}{\mu^2}\left[\sigma^4_{R_{SS}}(\mathcal{t}_r,f)+\sigma^4_{I_{SS}}(\mathcal{t}_r,f)\right] \tag{D.34}$$

where

$$\sigma^2_{R_{SS}}(\mathcal{t}_r,f)=\frac{\tilde{E}_{WC}(\mathcal{t}_r,f)}{\alpha}-\chi_R(\mathcal{t}_r,f)+\lambda_R(\mathcal{t}_r,f) \tag{D.35}$$

$$\sigma^2_{I_{SS}}(\mathcal{t}_r,f)=\frac{\tilde{E}_{WS}(\mathcal{t}_r,f)}{\alpha}-\chi_I(f)+\lambda_I(f) \tag{D.36}$$

, $\chi_R(\mathcal{t}_r,f)=\sum_{n=1}^{N}\int_{\mathcal{S}_n}\int_{\mathcal{S}_n}R_X(t_1,t_2)w(t_1)w(t_2)\cos\left(2\pi ft_1-\theta_{SS}(\mathcal{t}_r,f)\right)\cos\left(2\pi ft_2-\theta_{SS}(\mathcal{t}_r,f)\right)dt_1dt_2$

and $\chi_I(\mathcal{t}_r,f)=\sum_{n=1}^{N}\int_{\mathcal{S}_n}\int_{\mathcal{S}_n}R_X(t_1,t_2)w(t_1)w(t_2)\sin\left(2\pi ft_1-\theta_{SS}(\mathcal{t}_r,f)\right)\sin\left(2\pi ft_2-\theta_{SS}(\mathcal{t}_r,f)\right)dt_1dt_2$.

The phase-shift $\theta_{TRS}(\mathcal{t}_r,f)$ in $\lambda_R(\mathcal{t}_r,f)$, $\tilde{E}_{WC}(\mathcal{t}_r,f)$, $\lambda_I(\mathcal{t}_r,f)$ and $\tilde{E}_{WS}(\mathcal{t}_r,f)$ in (D.25)-(D.28) is replaced with $\theta_{SS}(\mathcal{t}_r,f)$ which can be attained from (3.56).

Now, we develop simplified approximations of the variances in (D.24), (D.29) and (D.34) at the sensed frequency points $\{f_k\}$. From (D.27), we can write:

$$\tilde{E}_{WC}(\mathcal{t}_r,f_k)=0.5\int_{\mathcal{T}_r}\left\{E\left[x^2(t)\right]+P_N\right\}w^2(t)\left[1+\cos\left(4\pi f_kt-2\theta_{TRS}(\mathcal{t}_r,f_k)\right)\right]dt. \tag{D.37}$$

The term that includes the sinusoid represents a widowed Cosine transform of the signal's second moment plus a constant at the frequency point $2f_k$, which is a high frequency outside the monitored frequency range. This is expected to be of a negligible value in comparison to $\int_{\mathcal{T}_r}\left\{E\left[x^2(t)\right]+P_N\right\}w^2(t)dt$ and similar argument applies to $\tilde{E}_{WS}(\mathcal{t}_r,f)$ in (D.28). Thus $\tilde{E}_{WC}(\mathcal{t}_r,f_k)\approx\tilde{E}_{WS}(\mathcal{t}_r,f_k)\approx 0.5\mu\left[P_S(\mathcal{t}_r)+P_N\right]$ in (D.25), (D.26), (D.35) and (D.36) where $P_S(\mathcal{t}_r)=\int_{\mathcal{T}_r}E\left[x^2(t)\right]w^2(t)dt\big/\mu$. Likewise, for the RSG scheme we have: $\tilde{E}^d_{WC}(\mathcal{t}_r,f_k)\approx\tilde{E}^d_{WS}(\mathcal{t}_r,f_k)\approx 0.5\mu_d\left[P^d_S(\mathcal{t}_r)+(N_g-1)P_N\big/(N_g-N)\right]$ and

$P^d_S(\mathcal{t}_r)=\sum_{n=1}^{N_g}E\left[x^2(nT_g)\right]w^2(nT_g)\big/\mu_d$

From (4.18) and (4.19) it can be noticed that $\lambda_R(\mathcal{t}_r,f)+\lambda_I(\mathcal{t}_r,f)=\mu D(\mathcal{t}_r,f)$ where $D(\mathcal{t}_r,f)=E\left[\left|X_W(\mathcal{t}_r,f)\right|^2\right]\big/\mu$, i.e.

$$0.5\mu^2 D^2(\mathscr{t}_r,f) \le \lambda_R^2(\mathscr{t}_r,f) + \lambda_I^2(\mathscr{t}_r,f) \le \mu^2 D^2(\mathscr{t}_r,f). \tag{D.38}$$

As a result, $\lambda_R^2(\mathscr{t}_r,f) + \lambda_I^2(\mathscr{t}_r,f) = \eta_D(\mathscr{t}_r,f)\mu^2 D^2(\mathscr{t}_r,f)$ and $0.5 \le \eta_D(\mathscr{t}_r,f_k) \le 1$. Whilst $\lambda_R^d(\mathscr{t}_r,f) + \lambda_I^d(\mathscr{t}_r,f) = \mu_d f_g D^d(\mathscr{t}_r,f)$ and $D^d(\mathscr{t}_r,f) = E\left[\left|X_W^d(\mathscr{t}_r,f)\right|^2\right] \Big/ \mu_d f_g$, we obtain:

$$0.5\left\{\mu_d f_g D^d(\mathscr{t}_r,f)\right\}^2 \le \left\{\lambda_R^d(\mathscr{t}_r,f)\right\}^2 + \left\{\lambda_I^d(\mathscr{t}_r,f)\right\}^2 \le \left\{\mu_d f_g D^d(\mathscr{t}_r,f)\right\}^2. \tag{D.39}$$

Hence $\left\{\lambda_R^d(\mathscr{t}_r,f)\right\}^2 + \left\{\lambda_I^d(\mathscr{t}_r,f)\right\}^2 = \eta_D^d(\mathscr{t}_r,f)\left\{\mu_d f_g D^d(\mathscr{t}_r,f)\right\}^2$ where $0.5 \le \eta_D^d(\mathscr{t}_r,f) \le 1$. Consequently, each of (D.24) and (D.29) reduces to:

$$\sigma_{e,TRS}^2(\mathscr{t}_r,f_k) \approx \frac{N^2}{(N-1)^2}\left\{\frac{\left[P_S(\mathscr{t}_r)+P_N\right]^2}{\alpha^2} + \frac{2(N-1)\left[P_S(\mathscr{t}_r)+P_N\right]D(\mathscr{t}_r,f_k)}{N\alpha} + 2\eta_D(\mathscr{t}_r,f_k)\left(\frac{N-1}{N}D(\mathscr{t}_r,f_k)\right)^2\right\}$$

and

$$\sigma_{e,RSG}^2(\mathscr{t}_r,f_k) \approx \left[\frac{N_g-N}{(N-1)f_g}\right]^2\left[P_S^d(\mathscr{t}_r) + \frac{(N_g-1)}{(N_g-N)}P_N\right]^2 + \frac{2(N_g-N)}{(N-1)f_g} \times \left[P_S^d(\mathscr{t}_r) + \frac{(N_g-1)P_N}{(N_g-N)}\right]D^d(\mathscr{t}_r,f_k) + 2\eta_D^d(\mathscr{t}_r,f_k)\left[D^d(\mathscr{t}_r,f_k)\right]^2.$$

For SEEP, we can write: $\chi_R(\mathscr{t}_r,f) + \chi_I(\mathscr{t}_r,f) = \mu A(\mathscr{t}_r,f)$ from (4.42) and (4.43) such that $A(\mathscr{t}_r,f) = \frac{1}{\mu}\sum_{n=1}^{N} E\left[\left|\int_{\mathscr{S}_n} x(t)w(t)e^{-j2\pi ft}dt\right|^2\right]$. It follows that:

$$0.5\mu^2 A^2(\mathscr{t}_r,f) \le \chi_R^2(\mathscr{t}_r,f) + \chi_I^2(\mathscr{t}_r,f) \le \mu^2 A^2(\mathscr{t}_r,f) \tag{D.40}$$

and subsequently $\chi_R^2(\mathscr{t}_r,f) + \chi_I^2(\mathscr{t}_r,f) = \eta_A(\mathscr{t}_r,f)A^2(\mathscr{t}_r,f)$ where $0.5 \le \eta_A(\mathscr{t}_r,f) \le 1$. Whereas, $\chi_R(\mathscr{t}_r,f)\lambda_R(\mathscr{t}_r,f) + \chi_I(\mathscr{t}_r,f)\lambda_I(\mathscr{t}_r,f) = \eta_{DA}(\mathscr{t}_r,f)D(\mathscr{t}_r,f)A(\mathscr{t}_r,f)$ such that $0.5 \le \eta_{DA}(\mathscr{t}_r,f_k) \le 1$. Utilising (D.34)-(D.36), we reach:

$$\sigma_{e,SSEP}^2(\mathscr{t}_r,f) = \frac{\left[P_S(\mathscr{t}_r)+P_N\right]^2}{\alpha^2} + 2\eta_A(\mathscr{t}_r,f)A^2(\mathscr{t}_r,f) + 2\eta_D(\mathscr{t}_r,f)D^2(\mathscr{t}_r,f) - \frac{2\left[P_S(\mathscr{t}_r)+P_N\right]}{\alpha}A(\mathscr{t}_r,f) + \frac{2\left[P_S(\mathscr{t}_r)+P_N\right]}{\alpha}D(\mathscr{t}_r,f) - 4\eta_{DA}D(\mathscr{t}_r,f)A(\mathscr{t}_r,f).$$

In the next section of this appendix, we examine the possible values each of $\eta_D(\mathcal{t}_r, f)$, $\eta_D^d(\mathcal{t}_r, f)$ and $\eta_A(\mathcal{t}_r, f)$ can take given the type of the incoming signal.

D.3 Accuracy Deterioration Factor

D.3.1 Total Random Sampling

Here we aim at revealing the differences between $\lambda_R(\mathcal{t}_r, f)$ in (4.18) and $\lambda_I(\mathcal{t}_r, f)$ in (4.19), i.e. quantifying $\Gamma(\mathcal{t}_r, f_k) = \lambda_R(\mathcal{t}_r, f_k) - \lambda_I(\mathcal{t}_r, f_k)$. Generic phase-shift $\theta(\mathcal{t}_r, f)$ is used, however the ones that were derived for each of the investigated randomized sampling schemes can be substituted. We start by writing: $\lambda_R(\mathcal{t}_r, f) = \psi_1(\mathcal{t}_r, f) + \psi_2(\mathcal{t}_r, f)$ and $\lambda_I(\mathcal{t}_r, f) = \psi_1(\mathcal{t}_r, f) - \psi_2(\mathcal{t}_r, f)$ such that:

$$\psi_1(\mathcal{t}_r, f) = 0.5\int_{\mathcal{T}_r}\int_{\mathcal{T}_r} R_X(t_1,t_2)w(t_1)w(t_2)\cos\left(2\pi f(t_1-t_2)\right)dt_1dt_2,$$

$$\psi_2(\mathcal{t}_r, f) = 0.25\int_{\mathcal{T}_r}\int_{\mathcal{T}_r} R_X(t_1,t_2)w(t_1)w(t_2)\left[e^{-j[2\pi f(t_1+t_2)-2\theta(\mathcal{t}_r,f)]} + e^{j[2\pi f(t_1+t_2)-2\theta(\mathcal{t}_r,f)]}\right]dt_1dt_2$$ and

$R_X(t_1,t_2)$ is given in (D.2). Consequently, $\Gamma(\mathcal{t}_r, f_k) = 2\psi_2(\mathcal{t}_r, f)$ and $\psi_2(\mathcal{t}_r, f)$ can be expressed by:

$$\psi_2(\mathcal{t}_r, f) = 0.25\left[e^{j2\theta(\mathcal{t}_r,f)}G(\mathcal{t}_r, f) + e^{-j2\theta(\mathcal{t}_r,f)}G^*(\mathcal{t}_r, f)\right] \tag{D.41}$$

and $G(\mathcal{t}_r, f) = \sigma_a^2 G_i(\mathcal{t}_r, f) + \sigma_b^2 G_q(\mathcal{t}_r, f)$ where

$$G_i(\mathcal{t}_r, f) = \sum_{n=-\infty}^{+\infty}\int_{\mathcal{T}_r}\int_{\mathcal{T}_r} s_i(t_1,n)s_i(t_2,n)w(t_1)w(t_2)e^{-j2\pi f(t_1+t_2)}dt_1dt_2 \tag{D.42}$$

$$G_q(\mathcal{t}_r, f) = \sum_{n=-\infty}^{+\infty}\int_{\mathcal{T}_r}\int_{\mathcal{T}_r} s_q(t_1,n)s_q(t_2,n)w(t_1)w(t_2)e^{-j2\pi f(t_1+t_2)}dt_1dt_2\,. \tag{D.43}$$

Employing (DD.3), we have:

$$G_i(\mathcal{t}_r, f) = 0.25\sum_{n=-\infty}^{+\infty}\left\{\left[H(f)P_i(f-f_C)e^{j2\pi(f-f_C)nT_S} + H(f)P_i(f+f_C)e^{j2\pi(f+f_C)nT_S}\right] * W(f)\right\}^2 \tag{D.44}$$

whereas (DD.4) yields:

$$G_q(\mathcal{t}_r, f) = -0.25\sum_{n=-\infty}^{+\infty}\left\{\left[H(f)P_q(f-f_C)e^{j2\pi(f-f_C)nT_S} - H(f)P_q(f+f_C)e^{j2\pi(f+f_C)nT_S}\right] * W(f)\right\}^2. \tag{D.45}$$

Assuming $W(f) \to \delta(f)$, i.e. very long signal observation window, (D.44) and (D.45) reduce to:

$$G_i(\not{t}_r, f) = 0.25\left[H(f)\right]^2 \left\{ \left[P_i(f - f_C)\right]^2 \sum_{n=-\infty}^{+\infty} e^{j4\pi(f-f_C)nT_S} + \left[P_i(f + f_C)\right]^2 \sum_{n=-\infty}^{+\infty} e^{j4\pi(f+f_C)nT_S} \right\}$$
$$= 0.125 f_S \left[H(f)\right]^2 \left\{ \left[P_i(f - f_C)\right]^2 \sum_{n=-\infty}^{+\infty} \delta(f - f_C - 0.5nf_S) + \left[P_i(f + f_C)\right]^2 \sum_{n=-\infty}^{+\infty} \delta(f + f_C - 0.5nf_S) \right\} \tag{D.46}$$

and

$$G_q(\not{t}_r, f) = -0.25\left[H(f)\right]^2 \left\{ \left[P_q(f - f_C)\right]^2 \sum_{n=-\infty}^{+\infty} e^{j4\pi(f-f_C)nT_S} + \left[P_q(f + f_C)\right]^2 \sum_{n=-\infty}^{+\infty} e^{j4\pi(f+f_C)nT_S} \right\}$$
$$= -0.125 f_S \left[H(f)\right]^2 \left\{ \left[P_q(f - f_C)\right]^2 \sum_{n=-\infty}^{+\infty} \delta(f - f_C - 0.5nf_S) + \left[P_q(f + f_C)\right]^2 \sum_{n=-\infty}^{+\infty} \delta(f + f_C - 0.5nf_S) \right\} \tag{D.47}$$

respectively. Thus:

$$G(\not{t}_r, f) = 0.125 f_S \left[H(f)\right]^2 \left\{ \sigma_a^2 \left[P_i(f - f_C)\right]^2 - \sigma_b^2 \left[P_q(f - f_C)\right]^2 \right\} \sum_{n=-\infty}^{+\infty} \delta(f - f_C - 0.5nf_S)$$
$$+ 0.125 f_S \left[H(f)\right]^2 \left\{ \sigma_a^2 \left[P_i(f + f_C)\right]^2 - \sigma_b^2 \left[P_q(f + f_C)\right]^2 \right\} \sum_{n=-\infty}^{+\infty} \delta(f + f_C - 0.5nf_S). \tag{D.48}$$

As a result $G(\not{t}_r, f) \approx 0$ and $\psi_2(\not{t}_r, f) \approx 0$ if $P_i(f - f_C) = P_q(f - f_C)$ and $\sigma_a^2 = \sigma_b^2$.

D.3.2 Random Sampling on Grid

Any differences between each of $\lambda_R^d(\not{t}_r, f)$ in (4.35) and $\lambda_I^d(\not{t}_r, f)$ in (4.36), i.e. $\Gamma^d(\not{t}_r, f) = \lambda_R^d(\not{t}_r, f) - \lambda_I^d(\not{t}_r, f) \neq 0$, can result in a significant decline in the performance of the RSG estimator. Below, we assess $\Gamma^d(\not{t}_r, f)$ in order to establish the values of $\eta_D^d(\not{t}_r, f)$ in (4.31).

We have: $\lambda_R^d(\not{t}_r, f) = \psi_1^d(\not{t}_r, f) + \psi_2^d(\not{t}_r, f)$ and $\lambda_I^d(\not{t}_r, f) = \psi_1^d(\not{t}_r, f) - \psi_2^d(\not{t}_r, f)$ where $\psi_1^d(\not{t}_r, f) = 0.5\sum_{n=1}^{N_g}\sum_{m=1}^{N_g} R_X(nT_g, mT_g) w(nT_g) w(mT_g) \cos\left(2\pi f(nT_g - mT_g)\right)$ and $\psi_2^d(\not{t}_r, f) = 0.5\sum_{n=1}^{N_g}\sum_{m=1}^{N_g} R_X(nT_g, mT_g) w(nT_g) w(mT_g) \cos\left(2\pi f(nT_g + mT_g) - 2\theta_{RSG}(\not{t}_r, f)\right)$.

Hence $\Gamma^d(\not{t}_r, f) = 2\psi_2^d(\not{t}_r, f)$ and $\psi_2^d(\not{t}_r, f)$ dictate the values of $0.1 \le \eta_D^d(\not{t}_r, f) \le 1$. Similar to (D.41) noting (D.2), $\psi_2^d(\not{t}_r, f)$ can be stated as:

$$\psi_2^d(\measuredangle_r, f) = 0.25\left\{e^{j2\theta_{RSG}(\measuredangle_r, f)} G^d(\measuredangle_r, f) + e^{-j2\theta_{RSG}(\measuredangle_r, f)}\left[G^d(\measuredangle_r, f)\right]^*\right\} \tag{D.49}$$

such that $G^d(\measuredangle_r, f) = \sigma_a^2 G_i^d(\measuredangle_r, f) + \sigma_b^2 G_q^d(\measuredangle_r, f)$,

$$G_i^d(\measuredangle_r, f) = \sum_{l=-\infty}^{+\infty}\sum_{n=1}^{N_g}\sum_{m=1}^{N_g} s_i(nT_g, l)s_i(mT_g, l)w(nT_g)w(mT_g)e^{-j2\pi f T_g(n+m)} \tag{D.50}$$

and

$$G_q^d(\measuredangle_r, f) = \sum_{l=-\infty}^{+\infty}\sum_{n=1}^{N_g}\sum_{m=1}^{N_g} s_q(nT_g, l)s_q(mT_g, l)w(nT_g)w(mT_g)e^{-j2\pi f T_g(n+m)} \ . \tag{D.51}$$

Utilising (DD.9) as well as (DD.10) and assuming a very long signal observation window, i.e. $W(f) \to \delta(f)$, we obtain:

$$\begin{aligned} G_i^d(\measuredangle_r, f) = \frac{f_S f_g^2}{8}\sum_{n=-\infty}^{+\infty}\left[H(f-nf_g)\right]^2 \Bigg\{&\left[P_i(f-f_C-nf_g)\right]^2 \sum_{l=-\infty}^{+\infty}\delta(f-f_C-nf_g-0.5lf_S) \\ &+\left[P_i(f+f_C-nf_g)\right]^2 \sum_{l=-\infty}^{+\infty}\delta(f+f_C-nf_g-0.5lf_S)\Bigg\} \end{aligned} \tag{D.52}$$

$$\begin{aligned} G_q^d(\measuredangle_r, f) = -\frac{f_S f_g^2}{8}\sum_{n=-\infty}^{+\infty}\left[H(f-nf_g)\right]^2 \Bigg\{&\left[P_q(f-f_C-nf_g)\right]^2 \sum_{l=-\infty}^{+\infty}\delta(f-f_C-nf_g-0.5lf_S) \\ &+\left[P_q(f+f_C-nf_g)\right]^2 \sum_{l=-\infty}^{+\infty}\delta(f+f_C-nf_g-0.5lf_S)\Bigg\}. \end{aligned} \tag{D.53}$$

where $P_i(f-f_C)P_i(f-f_C-nf_g) = 0$ and $P_q(f-f_C)P_q(f-f_C-nf_g) = 0$ if $n \neq 0$ (n is an integer). Thus:

$$\begin{aligned} &G^d(\measuredangle_r, f) = 0.125 f_S f_g^2 \sum_{n=-\infty}^{+\infty} \\ &\left[H(f-nf_g)\right]^2\left\{\sigma_a{}^2\left[P_i(f-f_C-nf_g)\right]^2 - \sigma_b{}^2\left[P_q(f-f_C-nf_g)\right]^2\right\}\sum_{l=-\infty}^{+\infty}\delta(f-f_C-0.5lf_S-nf_g) \\ &+\left[H(f-nf_g)\right]^2\left\{\sigma_a{}^2\left[P_i(f+f_C-nf_g)\right]^2 - \sigma_b{}^2\left[P_q(f+f_C-nf_g)\right]^2\right\}\sum_{l=-\infty}^{+\infty}\delta(f+f_C-0.5lf_S-nf_g) \end{aligned}$$

and for a BPSK signal:

$$\begin{aligned} G^d(\measuredangle_r, f) = \frac{f_S f_g^2 \sigma_a{}^2}{8}\sum_{n=-\infty}^{+\infty}\left[H(f-nf_g)\right]^2 \Bigg\{&\left[P_i(f-f_C-nf_g)\right]^2 \sum_{l=-\infty}^{+\infty}\delta\left(f-f_C-\frac{lf_S}{2}-nf_g\right) \\ &+\left[P_i(f+f_C-nf_g)\right]^2 \sum_{l=-\infty}^{+\infty}\delta\left(f+f_C-\frac{lf_S}{2}-nf_g\right)\Bigg\}. \end{aligned} \tag{D.54}$$

D.3.3 Stratified Sampling with Equal Partitions

The value of $\eta_A(\mathscr{t}_r, f)$ in (4.49) is set by: $\Gamma_A(\mathscr{t}_r, f) = \chi_R(\mathscr{t}_r, f) - \chi_I(\mathscr{t}_r, f)$ where $\chi_R(\mathscr{t}_r, f)$ is defined in (4.42) and $\chi_I(\mathscr{t}_r, f)$ in (4.43). As $\Gamma_A(\mathscr{t}_r, f)$ tends to zero, $\eta_A(\mathscr{t}_r, f)$ tends to its minimum values (i.e. $\eta_A(\mathscr{t}_r, f) \to 0.5$) and vice versa. In this subsection, we show that $\Gamma_A(\mathscr{t}_r, f)$ can reach its extreme values at selected frequency points for certain types of linearly modulated signals. Since quantifying $\Gamma_A(\mathscr{t}_r, f)$ is more complex than $\Gamma(\mathscr{t}_r, f)$ in (4.25) and $\Gamma^d(\mathscr{t}_r, f)$ in (4.37), some inquisitive assumptions are made below to demonstrate the $\eta_A(\mathscr{t}_r, f)$ behaviour for the class of studied cyclostationary signals.

Each of $\chi_R(\mathscr{t}_r, f)$ and $\chi_I(\mathscr{t}_r, f)$ can be expressed by: $\chi_R(\mathscr{t}_r, f) = \psi_1^A(\mathscr{t}_r, f) + \psi_2^A(\mathscr{t}_r, f)$ and $\chi_I(\mathscr{t}_r, f) = \psi_1^A(\mathscr{t}_r, f) - \psi_2^A(\mathscr{t}_r, f)$ respectively where:

$$\psi_1^A(\mathscr{t}_r, f) = \sum_{n=1}^{N} \int_{\mathbb{S}_n} \int_{\mathbb{S}_n} R_X(t_1, t_2) w(t_1) w(t_2) \cos\left(2\pi f (t_1 - t_2)\right) dt_1 dt_2 \tag{D.55}$$

and

$$\psi_2^A(\mathscr{t}_r, f) = 0.5 \sum_{n=1}^{N} e^{-j2\theta_{SS}(\mathscr{t}_r, f)} G_n^A(\mathscr{t}_r, f) + e^{j2\theta_{SS}(\mathscr{t}_r, f)} \left[G_n^A(\mathscr{t}_r, f)\right]^* \tag{D.56}$$

such that

$$G_n^A(\mathscr{t}_r, f) = \int_{\mathbb{S}_n} \int_{\mathbb{S}_n} R_X(t_1, t_2) w(t_1) w(t_2) e^{j2\pi f (t_1 + t_2)} dt_1 dt_2. \tag{D.57}$$

Hence,

$$\Gamma_A(\mathscr{t}_r, f) = 2\psi_2^A(\mathscr{t}_r, f) \tag{D.58}$$

and $\eta_A(\mathscr{t}_r, f)$ is directly controlled by $\psi_2^A(\mathscr{t}_r, f)$. To assess $\psi_2^A(\mathscr{t}_r, f)$, we assume that $|\mathbb{S}_n|$ tends to infinity and subsequently $T_0 \to \infty$, whilst the number of samples N is kept fixed to maintain the average sampling rate. Similar to (D.41)-(D.48), we have:

$$\begin{aligned} G_n^A(\mathscr{t}_r, f) = {} & \frac{f_S \left[H(f)\right]^2}{8} \left\{ \sigma_a^2 \left[P_i(f - f_C)\right]^2 - \sigma_b^2 \left[P_q(f - f_C)\right]^2 \right\} \sum_{n=-\infty}^{+\infty} \delta(f - f_C - 0.5 n f_S) \\ & + \frac{f_S \left[H(f)\right]^2}{8} \left\{ \sigma_a^2 \left[P_i(f + f_C)\right]^2 - \sigma_b^2 \left[P_q(f + f_C)\right]^2 \right\} \sum_{n=-\infty}^{+\infty} \delta(f + f_C - 0.5 n f_S). \end{aligned} \tag{D.59}$$

Formula (D.59) demonstrates that if $\left[\sigma_a P_i(f)\right]^2 \neq \left[\sigma_b P_q(f)\right]^2$ then $\eta_A(\not{t}_r, f)$ can reach its maximum value at $f = \pm f_C - 0.5nf_S$ ($n \in \mathbb{Z}$) such that f belongs to the frequency range of either $P_i(f - f_C)$ or $P_i(f + f_C)$.

D.3.4 Wide Sense Stationary Signals

We reveal by simple analysis that $\Gamma(\not{t}_r, f) = \lambda_R(\not{t}_r, f) - \lambda_I(\not{t}_r, f) \approx 0$ for wide sense stationary processes, i.e. choosing $\eta_D(\not{t}_r, f_k) \approx 0.5$ in (4.24) is appropriate. First, we have: $\Gamma(\not{t}_r, f_k) = 2\psi_2(\not{t}_r, f)$ where

$\psi_2(\not{t}_r, f) = 0.25\left[e^{j2\theta(\not{t}_r, f)} G(\not{t}_r, f) + e^{-j2\theta(\not{t}_r, f)} G^*(\not{t}_r, f)\right]$ in (D.41) such that:

$$G(\not{t}_r, f) = \int_{\mathcal{T}_r} \int_{\mathcal{T}_r} R_X(t_1 - t_2) w(t_1) w(t_2) e^{-j2\pi f(t_1 + t_2)} dt_1 dt_2 \tag{D.60}$$

and $R_X(t_1 - t_2) = E\left[x(t_1)x(t_2)\right]$ is the autocorrelation function of the WSS signal. Assuming an infinity long signal observation window for simplicity and letting $\tau = t_1 - t_2$, we can write:

$$G(\not{t}_r, f) = \int_{-\infty}^{+\infty} \left[\int_{-\infty}^{+\infty} R_X(\tau) e^{-j2\pi f \tau} d\tau \right] e^{-j4\pi f t_2} dt_2 \tag{D.61}$$

which produces:

$$G(\not{t}_r, f) = 0.5\Phi_X(f)\delta(f) \tag{D.62}$$

where $\Phi_X(f)$ is the signal's power spectral density. It follows from (D.62) that $G(\not{t}_r, f) \approx 0$ and $\Gamma(\not{t}_r, f) \approx 0$ for the processed real WSS multiband signal and hence $\eta_D(\not{t}_r, f_k) \approx 0.5$. Similar analysis applies to $\eta_D^d(\not{t}_r, f)$ for RSG and $\eta_A(\not{t}_r, f)$ for SSEP.

D.4 Useful Identities

We list a number of useful identities that are used in Sections D.1, D.2 and D.3 of this appendix. They are aimed at facilitating the analysis of cyclostationary signals.

$$\mathcal{F}\left\{s_i\left(t+\tau,n\right),\tau\right\} = 0.5e^{j2\pi ft}H(f)\left[P_i(f-f_C)e^{j2\pi(f-f_C)nT_S} + P_i(f+f_C)e^{j2\pi(f+f_C)nT_S}\right] \tag{DD.1}$$

$$\mathcal{F}\left\{s_q\left(t+\tau,n\right),\tau\right\} = -j0.5e^{j2\pi ft}H(f)\left[P_q(f-f_C)e^{j2\pi(f-f_C)nT_S} - P_q(f+f_C)e^{j2\pi(f+f_C)nT_S}\right] \tag{DD.2}$$

$$\mathcal{F}\left\{s_i(t,n),t\right\} = 0.5H(f)\left[P_i(f-f_C)e^{j2\pi(f-f_C)nT_S} + P_i(f+f_C)e^{j2\pi(f+f_C)nT_S}\right] \tag{DD.3}$$

$$\mathcal{F}\left\{s_q(t,n),t\right\} = -j0.5H(f)\left[P_q(f-f_C)e^{j2\pi(f-f_C)nT_S} - P_q(f+f_C)e^{j2\pi(f+f_C)nT_S}\right] \tag{DD.4}$$

$$\begin{aligned}\sum_{n=-\infty}^{+\infty} s_i(t,n)e^{j2\pi(f-f_C)nT_S} = 0.5f_S\sum_{n=-\infty}^{+\infty} P_i^*(f-f_C-nf_S)\Big[H^*(f-2f_C-nf_S)e^{-j2\pi(f-2f_C-nf_S)t}) \\ +H^*(f-nf_S)e^{-j2\pi(f-nf_S)t}\Big]\end{aligned} \tag{DD.5}$$

$$\begin{aligned}\sum_{n=-\infty}^{+\infty} s_q(t,n)e^{j2\pi(f-f_C)nT_S} = -\frac{jf_S}{2}\sum_{n=-\infty}^{+\infty} P_q^*(f-f_C-nf_S)\Big[H^*(f-2f_C-nf_S)e^{-j2\pi(f-2f_C-nf_S)t} \\ -H^*(f-nf_S)e^{-j2\pi(f-nf_S)t}\Big]\end{aligned} \tag{DD.6}$$

$$\begin{aligned}\sum_{n=-\infty}^{+\infty} s_i(t,n)e^{j2\pi(f+f_C)nT_S} = 0.5f_S\sum_{n=-\infty}^{+\infty} P_i^*(f+f_C-nf_S)\Big[H^*(f+nf_S)e^{-j2\pi(f-nf_S)t} \\ +H^*(f+2f_C-nf_S)e^{-j2\pi(f+2f_C-nf_S)t}\Big]\end{aligned} \tag{DD.7}$$

$$\begin{aligned}\sum_{n=-\infty}^{+\infty} s_q(t,n)e^{j2\pi(f+f_C)nT_S} = -\frac{jf_S}{2}\sum_{n=-\infty}^{+\infty} P_q^*(f+f_C-nf_S)\Big[H^*(f-nf_S)e^{-j2\pi(f-nf_S)t} \\ -H^*(f+2f_C-nf_S)e^{-j2\pi(f+2f_C-nf_S)t}\Big]\end{aligned} \tag{DD.8}$$

$$\begin{aligned}\sum_{n=1}^{N_g} s_i(nT_g,l)e^{-j2\pi flT_g} = 0.5f_g\sum_{n=-\infty}^{+\infty} H(f-nf_g)\Big[P_i(f-nf_g-f_C)e^{j2\pi(f-nf_g-f_C)lT_S} \\ +P_i(f-nf_g+f_C)e^{j2\pi(f-nf_g+f_C)lT_S}\Big]\end{aligned} \tag{DD.9}$$

$$\begin{aligned}\sum_{n=1}^{N_g} s_q(nT_g,l)e^{-j2\pi flT_g} = -j0.5f_g\sum_{n=-\infty}^{+\infty} H(f-nf_g)\Big[P_q(f-nf_g-f_C)e^{j2\pi(f-nf_g-f_C)lT_S} \\ -P_q(f-nf_g+f_C)e^{j2\pi(f-nf_g+f_C)lT_S}\Big]\end{aligned} \tag{DD.10}$$

References

[1] I. Bilinskis and M. Mikelsons, Randomised Signal Processing, London, Prentice Hall, 1992.

[2] R. J. Martin, Irregular Sampled Signals: Theories and Techniques for Analysis, PhD Thesis, University College London, 1998.

[3] J. J. Wojtiuk, Randomised Sampling for Radio Design, PhD Thesis, University of South Australia, 2000.

[4] N. Allay, Applications of Nonuniform Sampling Techniques in Digital Signal Processing and Communication Systems, PhD Thesis, University of Westminster, 2006.

[5] F. Papenfuβ, Digital Signal Processing of Nonuniform Sampled Signals, Dissertation at Universität Rostock, Publisher: Shaker Verlag, 2007.

[6] I. Bilinskis, Digital Alias-free Signal Processing, New York, John Wiley and Sons, 2007.

[7] D. D. Qu, Nonuniform Sampling Algorithms for DASP-based Instrumentation , PhD Thesis, University of Westminster, London, 2008.

[8] "Facilitating Opportunities For Flexible, Efficient, and Reliable Spectrum Use Employing Cognitive Radio Technologies", FCC Report and Order, FCC-05-57A1, March 2005.

[9] Federal Communications Commission- First Report, and Order and Further Notice of Proposed Rulemaking, "*Unlicensed Operation in TV Broadcast Bands*", FCC 06-156, Oct 2006.

[10] D. Cabric, S. M. Mishra, and R. W. Brodersen, "Implementation Issues in Spectrum Sensing for Cognitive Radios," *proceedings of Asilomar Conf. on Sig., Sys. and Comp.*, Nov. 2004, pp.772- 776.

[11] E. Hossain and V. K. Bhargava, Cognitive Wireless Communication Networks, New York, Springer Verlag, 2007.

[12] A. Sahai, N. Hoven, and R. Tandra, "Some Fundamental Limits on Cognitive Radio," *proceedings of Allerton Conference on Communication, Control, and Computing*, 2004, pp.1-11.

[13] S. Haykin, "Cognitive Radio: Brain Empowered Wireless Communications," *IEEE Journal of Selection Areas in Communications*, vol.23, pp.201-220, 2005.

[14] A. Ghasemi and E. S. Sousa, "Spectrum Sensing in Cognitive Radio Networks: Requirements, Challenges and Design Trade-offs," *IEEE Communications Magazine*, vol.46, pp.32-39, 2008.

[15] Z. Quan, S. Cui, H. V. Poor, and A. H. Sayed, "Collaborative Wideband Sensing for Cognitive Radios," *IEEE Signal Processing Magazine*, vol.25, pp.60-73, 2008.

[16] S. Haykin, D. J. Thomson, and J. H. Reed, "Spectrum Sensing for Cognitive Radio," *Proceedings of the IEEE*, vol.97, pp.849-877, 2009.

[17] T. Yucek and H. Arslan, "A Survey of Spectrum Sensing Algorithms for Cognitive Radio Applications," *IEEE Communications Surveys & Tutorials*, vol.11, pp.116-130, 2009.

[18] J. Ma, G. Y. Li, and B. H. Juang, "Signal Processing in Cognitive Radio," *Proceedings of the IEEE*, vol.97, pp.805-823, 2009.

[19] Y. Zeng, Y. C. Liang, A. T. Hoang, and R. Zhang, "A Review on Spectrum Sensing for Cognitive Radio: Challenges and Solutions," *EURASIP Journal on Advances in Signal Processing*, vol.2010, pp.2-2, 2010.

[20] B. Wang and K. J. R. Liu, "Advances in Cognitive Radio Networks: A Survey," *IEEE Journal of Selected Topics in Signal Processing*, vol.5, pp.5-23, 2011.

[21] Z. Tian and G. B. Giannakis, "A Wavelet Approach to Wideband Spectrum Sensing for Cognitive Radios," *proceedings of Int. Conf. on Cognitive Radio Oriented Wireless Networks and Communications*, Greece, June 2006, pp.1-5.

[22] D. Cabric, I. D. O'Donnell, M. S. W. Chen, and R. W. Brodersen, "Spectrum Sharing Radios," *IEEE Circuits and Systems Magazine*, vol.6, pp.30-45, 2006.

[23] Z. Tian and G. B. Giannakis, "Compressed Sensing for Wideband Cognitive Radios," *proceedings of IEEE Int. Conf. on Acoustics, Speech and Signal Processing (ICASSP '07)*, June 2006, pp.1357-1360.

[24] Y. L. Polo, Y. Wang, A. Pandharipande, and G. Leus, "Compressive Wide-band Spectrum Sensing," *proceedings of IEEE Int. Conf. on Acoustics, Speech and Signal Processing (ICASSP '09)*, Texas, 2009, pp.2337-2340.

[25] H. Urkowitz, "Energy Detection of Unknown Deterministic Signals," *Proceedings of the IEEE*, vol.55, pp.523-531, 1967.

[26] A. Wang and A. Chandrakasan, "Energy-efficient DSPs for Wireless Sensor Networks," *IEEE Signal Processing Magazine*, vol.19, pp.68-78, 2002.

[27] B. Lu, T. G. Habetler, R. G. Harley, J. A. Guitierrez, and D. B. Durocher, "Energy Evaluation Goes Wireless," *IEEE Wireless Communications Magazine*, pp.17-23, 2007.

[28] A. Millot, R. Feliachi, R. Weber, and C. Leger, "Wireless Water Quality Monitoring in the ISM Frequency Band: A Software and Cognitive Radio Approach," *proceedings of 18th European Signal Processing Conference*, Aalborg, Denmark, 2010, pp.875-879.

[29] E. Fasolo, M. Rossi, J. Widmer, and M. Zorzi, "In-network Aggregation Techniques for Wireless Sensor Networks: a Survey," *IEEE Wireless Communications*, vol.14, pp.70-87, 2007.

[30] A. A. Abbasi and M. Younis, "A Survey on Clustering Algorithms for Wireless Sensor Networks," *Computer Communications*, vol.30, pp.2826-2841, 2007.

[31] R. G. Vaughan, N. L. Scott, and D. R. White, "The Theory of Bandpass Sampling," *IEEE Trans. on Signal Processing*, vol.39, pp.1973-1984, 1991.

[32] H. J. Landau, "Necessary Density Conditions for Sampling and Interpolation of Certain Entire Functions," *Acta Math*, vol.117, pp.37-52, 1967.

[33] N. S. Shankar, C. Cordeiro, and K. Challapali, "Spectrum Agile Radios: Utilization and Sensing Architectures," *proceedings of IEEE Int. Symp. on New Frontiers in Dynamic Spectrum Access Networks*, California, USA, Dec 2005, pp.160-169.

[34] Y. Hur, J. Park, W. Woo, K. Lim, C. H. Lee, H. S. Kim, and J. Laskar, "A Wideband Analog Multi-resolution Spectrum Sensing (MRSS) Technique for Cognitive Radio (CR) Systems," *proceedings of IEEE Int. Symp. on Circuits and Systems (ISCAS '06)*, Greece, May 2006, pp.pp. 4090-4093.

[35] Y. Yuan, P. Bahl, R. Chandra, P. A. Chou, J. I. Ferrell, T. Moscibroda, S. Narlanka, and Y. Wu, "KNOWS: Cognitive Radio Networks Over White Spaces," *proceedings of IEEE Int. Symp. on New Frontiers in Dynamic Spectrum Access Networks*, Dublin, Ireland, April 2007, pp.416-427.

[36] Y. Eldar and T. Michaeli, "Beyond Bandlimited Sampling," *IEEE Signal Processing Magazine*, vol.26, pp.48-68, 2009.

[37] P. P. Vaidyanathan, "Generalizations of the Sampling Theorem: Seven Decades After Nyquist," *IEEE Trans. on Circuits and Systems I: Fundamental Theory and Applications*, vol.48, pp.1094-1109, 2002.

[38] J. Benedetto and P. J. S. G. Ferreira, Modern Sampling Theory: Mathematics and Applications, Birkhauser, 2001.

[39] M. Unser, "Sampling-50 Years After Shannon," *Proceedings of the IEEE*, vol.88, pp.569-587, 2000.

[40] J. R. Higgins, Sampling Theory in Fourier and Signal Analysis: Foundation, London, Oxford University Press, 1996.

[41] A. I. Zayed, Advanced in Shannon's Sampling Theory, Boca Rotan, CRC Press, 1993.

[42] R. J. Marks, Advanced Topics in Shannon Sampling and Interpolation Theory, New York, Springer-Verlag, 1993.

[43] R. J. Marks, Introduction to Shannon Sampling and Interpolation Theory, New York, Springer-Verlag, 1991.

[44] A. J. Jerri, "Shannon Sampling Theorem - Its Various Extensions and Applications : A Tutorial Review," *Proceedings of the IEEE*, vol.65, pp.1565-1596, 1977.

[45] F. Marvasti, Nonuniform Sampling Theory and Practice, New York, Kluwer Academic, 2001.

[46] A. Aldroubi and K. Gronhenig, "Nonuniform Sampling and Reconstruction in Shift Invariant Spaces," *SIAM Reviews*, vol.43, pp.585-620, 2001.

[47] F. Marvasti, A Unified Approach to Zero-crossing and Nonuniform Sampling, Illinois, Oak Park, 1987.

[48] P. Z. Peebles, JR., Probability, Random Variables and Random Signal Principles, New York, McGraw-Hill, 1993.

[49] M. H. Hayes, Statistical Digital Signal Processing and Modeling, John Wiley & Sons, 1996.

[50] S. Haykin, Communication Systems, NY, John Wiley & Sons, 2001.

[51] W. A. Gardner, Introduction to Random Processes with Applications to Signals and Systems, NY, MacMillan, 1985.

[52] A. Papoulis, Probability, Random Variables and Stochastic Processes , 3rd Edition, New York, McGraw-Hill, 1991.

[53] H. Nyquist, "Certain Topics in Telegraph Transmission Theory," *AIEE Transactions*, vol.47, pp.617-644, 1928.

[54] C. E. Shannon "Communications in the Presence of Noise," *Proceedings of the IRE*, vol.37, pp.10-21, 1949.

[55] E. Meijering, "A Chronology of Interpolation: From Ancient Astronomy to Modern Signal and Image Processing," *Proceedings of the IEEE*, vol.90, pp.319-342, 2002.

[56] R. Martin, "One-sided Sampling Series Gives Fast Reconstruction Algorithms," *IEEE Trans. on Signal Processing*, vol.47, pp.1770-1772, 1999.

[57] M. Maqusi, "Truncation Error Bounds for Sampling Expansions of Sequence Band-limited Signals," *IEEE Trans. on Acoustic, Speech and Signal Processing*, vol.ASSP-26, 1978.

[58] J. L. Brown, Jr., "Bounds for Truncation Error in Sampling Expansions of Band-limited Signals," *IEEE Trans. Inform. Theory*, vol. IT-15, pp.440-444, 1969.

[59] A. Papoulis, "Truncated Sampling Expansions," *IEEE Trans. on Automatic Control*, vol.AC-12, pp.604-605, 1967.

[60] K. Yao and J. B. Thomas, "On the Truncation Error Bounds for Sampling Representations of Band-Limited Signals," *IEEE Trans. on Aerospace and Electronic Systems*, vol.AES-2, pp.640-647, 1966.

[61] F. Haber, "Rapidly Converging sample weighting functions," *IEEE trans. on Comm. Sys.*, vol.12, pp.116-117, 1964.

[62] H. D. Helmes and J. B. Thomas, "Truncation Error of Sampling Theorem Expansions," *Proceedings of the IRE*, vol.50, pp. 179-184, 1962.

[63] B. I. Ahmad and A. Tarczynski, "Evaluation of Several Reconstruction Methods of Bandlimited Signals," *proceedings of IEEE Int. Conf on Signals, Circuits and Systems*, Tunisia, November 2008, pp.1-5.

[64] C. B. Feldman and W. R. Bennett, "Bandwidth and Transmission Performance," *Bell Systems Technology Journal*, vol.28, pp.490-595, 1949.

[65] A. Kohlenberg, "Exact Interpolation of Bandlimited Functions," *Journal of Applied Physics*, vol.24, pp.1432-1436, 1952.

[66] R. G. Lyons, Understanding Digital Signal Processing, Reading, Massachusetts, Addison Wesley Longman, 1997.

[67] Y.-R. Sun, Generalized Bandpass Sampling Receivers for Software Defined Radio, PhD Thesis, Royal Institute of Technology, Sweden, 2006.

[68] J. D. Gaskill, Linear systems, Fourier transforms, and Optics, New York, Wiley, 1978.

[69] J. L. Brown, "On Uniform Sampling of Amplitude Modulated Signals," *IEEE Transactions on Aerospace and Electronic Systems*, pp.633-635, 1983.

[70] M. M. Dodson and A. M. Silva, "An Algorithm for Optimal Regular Sampling," *Signal Processing*, vol.17, pp.169-174, 1989.

[71] R. Venkataramani and Y. Bresler, "Sampling Theorems for Uniform and Periodic Nonuniform MIMO Sampling of Multiband Signals," *IEEE Transactions on Signal Processing*, vol.51, pp.3152-3163, 2003.

[72] R. Venkataramani and Y. Bresler, "Perfect Reconstruction Formulas and Bounds on Aliasing Error in Sub-Nyquist Nonuniform sampling of Multiband Signals," *IEEE Trans. on Information Theory*, vol.46, pp.2173-2183, 2000.

[73] R. Venkataramani and Y. Bresler, "Optimal Sub-Nyquist Nonuniform Sampling and Reconstruction for Multiband Signals," *IEEE Trans. on Signal Processing*, vol.49, pp.2301-2313, 2001.

[74] M. Mishali and Y. C. Eldar, "Blind Multiband Signal Reconstruction: Compressed Sensing For Analog Signals," *IEEE Trans. on Signal Processing*, vol.57, pp.993-1009, 2009.

[75] J. D. Scargle, "Studies in Astronomical Time Series Analysis. III: Fourier Transforms, Autocorrelation Functions and Crosscorrelation Functions of Unevenly Spaced Data," *The Astronomical Journal*, vol.343, pp.874-887, 1989.

[76] J. D. Scargle, "Studies in Astronomical Time Series Analysis. II: Statistical Aspects of Spectral Analysis of Unevenly Spaced Data," *The Astronomical Journal*, vol.263, pp.835-853, 1982.

[77] N. R. Lomb, "Least-squares Frequency Analysis of Un-equally Spaced Data," *Astrophysics and Space Science*, vol.39, pp.447-462, 1967.

[78] J. Mateo and P. Laguna, "Analysis of Heart Rate Variability in the Presence of Extopic Beats Using the Heart Timing Signal," *IEEE Trans. on Biomedical Engineering*, vol.50, pp.334-343, 2003.

[79] P. Laguna, G. B. Moody, and R. G. Mark, "Power Spectral Density of Unevenly Spaced Data by Least-Square Analysis: Performance and Application to Heart Rate Signals," *IEEE Trans. on Biomedical Engineering*, vol.45, No. 6, pp.698-715, 1998.

[80] M. Sambridge, J. Braun, and H. McQueen, "Geophysical Parametrization and Interpolation of Irregular Data Using Natural Neighbours," *International Geophysical Journal*, vol.122, pp.837-857, 2007.

[81] R. Sturges, "On Interpolating Gappy Records for Time-Series Analysis," *Journal of Geophysical Research*, vol.88, pp.9736-9740, 1983.

[82] A. Tarczynski and V. Valimaki, "Modifying FIR and IIR Filters for Processing Signals with Lost Samples," *proceedings of IEEE Nordic Signal Processing Symposium*, Helsinki, Sept 1997, pp.359-362.

[83] P. J. S. G. Ferreira, "Interpolation in the Time and Frequency Domains," *IEEE Signal Processing Letters*, vol.3, pp.176-178, 1996.

[84] P. J. S. G. Ferreira, "Noniterative and Fast Iterative Methods for Interpolation and Extrapolation," *IEEE Trans. on Signal Processing*, vol.42, pp.3278-3282, 1994.

[85] V. A. Kazakov and S. D. Rodriquez, "Sampling-Reconstruction Procedure of Gaussian Processes with Jitter Characterised by the Beta Distribution," *IEEE Trans. on Instrumentation and Measurement*, vol.56, pp.1814-1824, 2007.

[86] T. M. Souders, D. R. Flach, C. Hagwood, and G. L. Yang, "The Effects of Timing Jitter in Sampling Systems," *IEEE Trans. on Instrumentation and Measurement*, vol.39, pp.80-85, 2002.

[87] F. J. Beutler and O. A. Z. Leneman, "Random Sampling of Random Processes: Stationary Point Processes," *Information and Control*, vol.9, pp.325-346, 1966.

[88] O. A. Z. Leneman, "Random Sampling of Random Processes: Impulse Processes," *Information and Control*, vol.9, pp.347-363, 1966.

[89] F. J. Beutler and O. A. Z. Leneman, "The Theory of Stationary-Point Processes," *Acta Math*, vol.116, pp.159-197, 1966.

[90] H. S. Shapiro and R. A. Silverman, "Alias-free Sampling of Random Noise," *SIAM Journal of Applied Mathematics*, vol.8, pp.225-236, 1960.

[91] F. Beutler, "Alias-free Randomly Timed Sampling of Stochastic Processes," *IEEE Trans. on Information Theory*, vol. IT-16, pp.147-152, 1970.

[92] E. Masry, "Random Sampling and Reconstruction of Spectra," *Information and Control* vol.19, pp.275-288, 1971.

[93] E. Masry, "Alias Free Sampling: An Alternative Conceptualization and Its Applications," *IEEE Trans. on Information Theory*, vol.24, pp.317-324, 1978.

[94] E. Masry, "Non-parametric Covariance Estimation from Irregular-spaced Data," *Advances in Applied Probability*, vol.15, pp.113-132, 1983.

[95] M. Greitans and R. Shavelis, "Signal-dependent Techniques for Non-stationary Signal Sampling and Reconstruction," *proceedings of 18th European Signal Processing Conference (EUSIPCO '09)*, Glasgow, Scotland, August 2009, pp.2613-2617.

[96] A. Tarczynski and N. Allay, "Spectral Analysis of Randomly Sampled Signals: Suppression of Aliasing and Sampler Jitter," *IEEE Trans. on Signal Processing*, vol.SP-52, pp.3324-3334, 2004.

[97] A. Tarczynski and D. Qu, "Optimal Random Sampling for Spectrum Estimation in DASP Applications," *International Journal of Applied Mathematics and Computer Science*, vol.15, pp.463-469, 2005.

[98] E. Masry, "Random Sampling of Deterministic Signals: Statistical Analysis of Fourier Transforms Estimates," *IEEE Trans. on Signal Processing*, vol.54, pp.1750-1761, 2006.

[99] M. H. Kalos and P. A. Whitlock, Monte Carlo Methods, Wiley-VCH, 2008.

[100] W. G. Cochran, Sampling Techniques, New York, John Willey & Sons, 1977.

[101] E. Masry, "Random Sampling Estimates of Fourier Transforms: Antithetical Stratified Monte Carlo," *IEEE Trans. Signal Processing*, vol. 57, pp.149-204, 2009.

[102] F. J. Beutler and O. A. Z. Leneman, "The Spectral Analysis of Impulse Processes," *Information and Control*, vol.12, pp.236-258, 1968.

[103] H. Urkowitz, Signal Theory and Random Processes, MA, USA, Artech House, 1983.

[104] E. Masry and M. C. Lui, "Discrete-Time Spectral Estimation of Continuous-Parameter Processes-A New Consistent Estimate," *IEEE Trans. on Information Theory*, vol.IT-22, pp.298-312, 1976.

[105] P. Stoica and R. L. Moses, Spectral Analysis of Signals, New Jersey, Pearson-Prentice Hall, 2005.

[106] P. Babu and P. Stoica, "Spectral Analysis of Nonuniformly Sampled Data - A Review," *Digital Signal Processing*, vol.20, pp.359-378, 2009.

[107] M. S. Bartlett, "Smoothing Periodograms from Time Series with Continuous Spectra," *Nature (London)*, vol.161, pp.686-687, 1948.

[108] P. Welch, "The Use of Fast Fourier Transform for the Estimation of Power Spectra: A Method Based on Time Averaging Over Short, Modified Periodograms," *IEEE Trans. on Audio and Electroacoustics*, vol.15, pp.70-73, 1967.

[109] F. J. Harris, "On the Use of Windows for Harmonic Analysis with the Discrete Fourier Transform," *Proceedings of the IEEE*, vol.66, pp.51-83, 1978.

[110] A. Antoniou, Digital Filters: Analysis, Design and Applications, New York, McGraw-Hill, 1993.

[111] D. J. Thomson, "Spectrum Estimation and Harmonic Analysis," *Proceedings of the IEEE*, vol.70, pp.1055-1096, 1982.

[112] P. Stoica, J. Li, and H. He, "Spectral Analysis of Nonuniformly Sampled Data: A New Approach Versus the Periodogram," *IEEE Trans. Signal Processing*, vol.57, pp.843-858, 2009.

[113] E. Masry, "Poisson Sampling and Spectral Estimation of Continuous-time Processes," *IEEE Trans. on Information Theory*, vol.IT-24, pp.173-183, 1978.

[114] R. Fantacci and A. Tani, "Performance Evaluation of a Spectrum Sensing Technique for Cognitive Radio Applications in B-VHF Communication Systems," *IEEE Trans. on Vehicular Technology*, vol.58, pp.1722-1730, 2009.

[115] M. Matinmikko, H. Sarvanko, M. Mustonen, and A. Mämmelä, "Performance of Spectrum Sensing Using Welch's Periodogram in Rayleigh Fading Channel," *proceedings of Int. Conf. on Cognitive Radio Oriented Wireless Networks and Communications (CROWNCOM '09)*, Hannover, 2009, pp.1-5.

[116] Z. Quan, S. Cui, A. H. Sayed, and H. V. Poor, "Optimal Multiband Joint Detection for Spectrum Sensing in Cognitive Radio Networks," *IEEE Trans. on Signal Processing*, vol.87, pp.1128-1140, 2009.

[117] Z. Chen, N. Guo, and R. C. Qiu, "Demonstration of Real-time Spectrum Sensing for Cognitive Radio," *IEEE Communications Letters*, vol.14, pp.915-917, 2010.

[118] T. H. Yu, S. Rodriguez-Parera, D. Markovic, and D. Cabric, "Cognitive Radio Wideband Spectrum Sensing Using Multitap Windowing and Power Detection with Threshold Adaptation," *proceedings of Int. Conf on Communications (ICC '10)*, Cape Town, 2010, pp.1-6.

[119] W. A. Gardner, "Common Pitfalls in the Application of Stationary Process Theory of Time-Sampled and Modulated Signals," *IEEE Trans. on Communications*, vol.COM-35, pp.529-534, 1987.

[120] W. A. Gardner, "Signal Interception: A Unifying Theoretical Framework for Feature Detection," *IEEE Trans. on Communications*, vol.36, pp.897-906, 1988.

[121] S. Baisch and G. H. R. Bokelmann, "Spectral Analysis with Incomplete Time Series: An Example from Seismology," *Computers and Geosciences*, vol.25, pp.739-750, 1999.

[122] Y. Wu, J. A. Stankovic , T. He, and S. Lin, "Realistic and Efficient Multi-channel Communications in Wireless Sensor Networks," *proceedings of IEEE 27th Conf. on Computer Communications* Arizona, April 2008, pp.1193 – 1201.

[123] P. Pawelczak, K. Nolan, L. Doyle, S. W. Oh, and D. Cabric, "Cognitive Radio: Ten Years of Experimentation and Development," *IEEE Communications Magazine*, vol.49, pp.90-100, 2011.

[124] S. M. Kay, Fundamentals of Statistical Signal Processing: Detection Theory, Upper Saddle River, NJ, Prentice-Hall, 1998.

[125] E. J. Candès and M. B. Wakin, "An Introduction to Compressive Sampling," *IEEE Signal Processing Magazine*, vol.25, pp.21-30, 2008.

[126] D. L. Donoho, "Compressed Sensing," *IEEE Trans. on Information Theory*, vol.52, pp.1289-1306, 2006.

[127] Y. Wang, A. Pandharipande, Y. L. Polo, and G. Leus, "Distributed Compressive Wide-band Spectrum Sensing," *proceedings of IEEE Information Theory and Applications Workshop*, 2009, pp.178-183.

[128] D. Sundman, S. Chatterjee, and M. Skoglund, "On the Use of Compressive Sampling for Wide-band Spectrum Sensing," *proceedings of IEEE International Symp. on Signal Processing and Information Technology*, 2010, pp.354-359.

[129] P. Kaligineedi and V. K. Bhargava, "Sensor Allocation and Quantization Schemes for Multi-Band Cognitive Radio Cooperative Sensing System," *IEEE Trans. on Wireless Communications*, vol.10, pp.284-293, 2011.

[130] B. I. Ahmad and A. Tarczynski, "A SARS Method for Reliable Spectrum Sensing in Multiband Communication Systems," *to appear in IEEE Trans. on Signal Processing*, 2011.

[131] B. I. Ahmad and A. Tarczynski, "The Effect of Cyclostationarity on A DASP-Based Spectrum Sensing Method," *proceedings of 9th Int. Conf. on Sampling Theory and its Applications (SAMPTA '11)*, Singapore, May 2011,

[132] A. DasGupta, Fundamentals of Probability: A First Course, New York, Springer, 2010.

[133] B. I. Ahmad and A. Tarczynski, "Reliable Wideband Multichannel Spectrum Sensing Using Randomized Sampling Schemes," *Signal Processing*, vol.90, pp.2232-2242, 2010.

[134] B. I. Ahmad and A. Tarczynski, "Wideband Spectrum Sensing Technique Based on Random Sampling on Grid: Achieving Lower Sampling Rates," *Digital Signal Processing*, vol.90, pp.466-476, 2011.

[135] R. Tandra and A. Sahai, "SNR Walls for Signal Detection," *IEEE Journal of Selected Topics in Signal Processing*, vol.2, pp.4-17, 2008.

[136] D. C. Oh and Y. H. Lee, "Energy Detection Based Spectrum Sensing for Sensing Error Minimization in Cognitive Radio Networks," *International Journal of Communication Networks and Information Security*, vol.1, 2009.

[137] F. Papenfuβ, Y. Artyukh, E. Boole, and D. Timmermann, "Nonuniform sampling driver design for optimal ADC utilization," *proceedings of IEEE Int. Symp. on Circuits and Systems (ISCAS '03)*, May 2003, pp.516-519.

[138] C. Rebai, M. Ben-Romdhane, P. Desgreys, P. Loumeau, and A. Ghazel, "Pseudorandom Signal Sampler for Relaxed Design of Multistandard Radio Receiver," *Microelectronics Journal*, vol.40, pp.991-999, 2009.

[139] E. Saramov and M. Georgieva, "Nonuniform Synchronous Sampling Analog Interface," *proceedings of 29th International Spring Seminar on Electronics Technology (ISSE '06)*, St. Marienthal, May 2006 pp.329-333.

[140] F. Papanfuss, Y. Artyukh, E. Boole, and D. Timmermann, "Optimal Sampling Functions in Nonuniform Sampling Driver Designs to Overcome the Nyquist Limit," *proceedings of* IEEE Conference on Acoustics, Speech and Signal Processing (ICASSP '03), April 2003, pp.257-260.

[141] J. Laska, S. Kirolos, Y. Massoud, R. Baraniuk, A. Gilbert, M. Iwen, and M. Strauss, "Random Sampling for Analog-to-information Conversion of Wideband Signals," *proceedings of IEEE Dallas Circuits and Systems Workshop*, 2007, pp.119-122.

[142] J. N. Laska, S. Kirolos, M. F. Duarte, T. S. Ragheb, R. G. Baraniuk, and Y. Massoud, "Theory and Implementation of an Analog-to-information Converter Using Random Demodulation," *proceedings of IEEE Int. Symp. on Circuits and Systems (ISCAS '07)*, 2007, pp.1959-1962.

[143] M. Mishali and Y. C. Eldar, "From Theory to Practice: Sub-Nyquist Sampling of Sparse Wideband Analog Signals," *IEEE Journal of Selected Topics in Signal Processing*, vol.4, pp.375-391, 2010.

[144] M. Mishali and Y. Eldar, "Wideband Spectrum Sensing at Sub-Nyquist Rates," *IEEE Signal Processing Magazine*, vol.28, pp.102-135, 2011.

[145] C. Cordeiro, K. Challapali, D. Birru, and S. Shankar, "IEEE 802.22: An Introduction to the First Wireless Standard Based on Cognitive Radios," *Journal of Communications*, vol.1, pp.38-47, 2006.

[146] J. J. Wojtiuk and R. Martin, "Random Sampling Enables Flexible Design for Multiband Carrier Signals," *IEEE Trans. on Signal Processing*, vol.49, pp.2438-2440, 2001.

[147] I. Bilinskis and G. Cain, "Digital Alias-free Signal Processing in the GHz Frequency Range," *proceedings of IEE Colloquium on Advanced Signal Processing for Microwave Applications* London, UK, November 1996, pp.1-6.

[148] M. Al-Ani, A. Tarczynski, and B. I. Ahmad, "A Novel Fourier Transform Estimation Method Using Random Sampling," *proceedings of 19th European Signal Processing Conference (EUSIPCO'11)*, Barcelona, 2011,

[149] W. Gardner, W. Brown, and C. K. Chen, "Spectral Correlation of Modulated Signals: Part II--Digital Modulation," *IEEE Trans. on Communications*, vol.35, pp.595-601, 1987.